

1. Introduction

1.1 Overview

The purpose of this research project under the Collaborative Science, Technology, and Applied Research (CSTAR) program is to better understand the relationship between large-scale circulation anomalies such as the North Atlantic Oscillation (NAO) and the Pacific/North American (PNA) pattern with precipitation events over the northeastern US. The tendency for large-scale circulation anomaly phase changes to be associated with the significant precipitation events over the Northeast will be established through the correlation of daily large-scale circulation anomaly indices and specific precipitation events. The relationship between large-scale circulation anomalies and research results from other CSTAR projects regarding mesoscale substructure and 500 hPa cutoff lows will also be presented.

1.2 Literature Review

1.2.1 Early Studies of Large-scale Circulation Anomalies

Early European explorers of Greenland were the first to note a difference in the severity of winter temperatures between Greenland and Europe. As summarized in van Loon and Rogers (1978), several explorers recorded their observations of the varying severity of winters. A table originally published by Gronau in 1811, and reproduced by Dannmeyer (1948), summarizes winter conditions for Greenland and Germany dating back to 1709. It indicates that temperature conditions in Greenland were often opposite

those in Germany. Other early observations of a seesaw of temperatures between Greenland and Europe mentioned by van Loon and Rogers (1978) include Crantz in his *History of Greenland* (1765), Dove (1839), Hann (1890), and diary entries by Hans Egede Saabye between 1770–78 as later edited and published by Ostermann (1942).

Among those who demonstrated an early understanding of the occurrence of observed temperature differences was Dove (1839), who as van Loon and Rogers (1978) mentions, reasoned that these seesaws in temperature only occur when the distances between two locations is greater than the width of an air current so that the two locations are on opposite sides of the current. During the early 20th century, work by scientists at the India meteorological department, including C. E. P. Brooks and Sir Gilbert Walker, focused on oscillations of sea level pressure (SLP) to describe the temperature seesaw between Greenland and Europe. A review of Walker (1924) by C. E. P. Brooks (1924) outlines areas of observed sea level pressure oscillations stating, “There is a swaying of pressure on a big scale backwards and forwards between the Indian Ocean and the Pacific Ocean, and there are swayings on a much smaller scale between the Azores and Iceland and between the areas of high and low pressure in the North Pacific.” Walker also set forth that the observed variations in temperature were a result of the pressure oscillations and were due in part to variations in the strength of the atmospheric circulation. Further work by Walker and Bliss (1932) reaffirmed Walker’s original findings, stating that the climatological winter pressure pattern in the North Atlantic, a low near Iceland and a high near the Azores, was “associated with high temperatures in north-west Europe and low temperatures off the Labrador coast.” Walker and Bliss (1932) also established a Southern Oscillation Index (SOI), dating back to 1875, for the

purpose of explaining oscillations in the surface pressure between Tahiti and Darwin. Walker's interest in the SOI stemmed from a perceived possible predictive relationship between the values of the SOI and precipitation anomalies during the Indian monsoon.

Following the pioneering research of Walker (1924) and Walker and Bliss (1932), new research focused on the relationship between changes in the general circulation and associated large-scale pressure and temperature oscillations. Most of the research focused on what became known as the North Atlantic Oscillation. A study of the NAO and the associated temperature anomaly patterns by Angstrom (1935) was the first to describe this associative relationship as a teleconnection. Other analyses of the temperature seesaw between Greenland and Europe included Loewe (1937), who refers to earlier work by Exner (1924) and Scherhag (1936) that had shown a high positive correlation between the surface pressure at Stykkisholmur, Iceland, and the pressure and temperature in western Greenland. Later, Loewe (1966) updated his work to include 100 years of data and calculated his own correlation coefficients to support the existence of the temperature seesaw between western Greenland and Europe. As with earlier work, he concluded that changes in the general circulation were a partial cause of these temperature seesaws.

1.2.2 Greenland/Europe Temperature Seesaw

After Loewe, research on the NAO and associated temperature oscillation was sparse until van Loon and Rogers (1978), Rogers and van Loon (1979), and Meehl and van Loon (1979) published a three part series on their work relating a variety of

atmospheric variables to the temperature seesaw between Greenland and Europe. In the first part, van Loon and Rogers (1978) summarized the temperature seesaw between Greenland and Europe and noted an associated correlation of temperature and pressure oscillations over North America, the Mediterranean and the Middle East. Temperature anomalies over Greenland were in phase with temperature anomalies over the Mediterranean, and western North and Central America. The opposing temperature anomalies over northern Europe were in phase with those over eastern North America south of 60°N. van Loon and Rogers (1978) also observed a negative correlation of sea-level pressure oscillations between the Icelandic low and the North Atlantic south of 50°N, the Mediterranean, Middle East and North Pacific. Finally, they noted that a specific phase of a circulation anomaly would dominate over the other on the order of several decades, and thus long-term regional trends in winter mean temperatures were considered a result of these circulation patterns.

In the second part of the series, Rogers and van Loon (1979) noted oceanic-atmospheric interactions associated with the NAO. In looking at the zonal geostrophic flow, strong westerlies over the Atlantic and accompanying weak trade winds were associated with winters dominated by below normal temperatures in Greenland. As a result, the strong westerlies were found to make the sea-surface temperatures (SST) over a majority of the North Atlantic Drift, a continuation of the Gulf Stream, warmer than normal, with cooler waters in the Canary, North Equatorial, and East and West Greenland currents. In looking at precipitation patterns, Rogers and van Loon (1979) found that during winters dominated by above normal temperatures in Greenland, areas such as Europe, the eastern Atlantic, extreme eastern North America and western

Greenland received more precipitation than during winters of the opposite temperature anomaly. According to Rogers and van Loon (1979), most of the northeast and continental US received more precipitation during winters dominated by positive Greenland temperature anomalies, while the extreme southeast and northwest US received less precipitation.

In the final part in the series, Meehl and van Loon (1979) looked at tropical teleconnections in relation to the temperature seesaw between Greenland and Europe. Identifying the intertropical convergence zone (ITCZ) as the band of heaviest precipitation, Meehl and van Loon (1979) noted that during winters dominated by below normal temperatures in Greenland, the ITCZ was positioned farther south than during winters with the opposite temperature anomaly. They also noted that the speed of the Gulf Stream between the US coast and Bermuda is slower during winters dominated by below normal temperatures in Greenland than during winters of the opposite anomaly. Variations in the speed of the Gulf Stream current will have an impact on the oceanic heat flux.

1.2.3 Large-scale Circulation Anomalies in the Midtroposphere

Shortly after this series of papers, an article by Wallace and Gutzler (1981) defined teleconnections as “contemporaneous correlations between geopotential heights on a given pressure surface at widely separated points on earth.” One of several key observations made by Wallace and Gutzler (1981) was the similarity between sea level pressure correlation maps and 500 hPa geopotential height correlation maps. This

observation matched findings by Blackmon *et al.* (1979), whose correlations between mean sea level pressure and 500 hPa geopotential height reached 0.95 in the North Atlantic. Based on these high correlations, Wallace and Gutzler (1981) identified and defined five Northern Hemisphere monthly averaged teleconnection patterns, including the NAO, with respect to mean sea-level pressure and midtropospheric geopotential heights. In their analysis of the sea-level pressure data and 500 geopotential height hPa data, Wallace and Gutzler (1981) noted that teleconnections at 500 hPa were more pronounced and complex than the same teleconnections at 1000 hPa. Thus, most of their discussion is dedicated to defining the five teleconnections at 500 hPa.

The five teleconnections identified by Wallace and Gutzler (1981) include the aforementioned NAO, which they break up into an West Atlantic Oscillation (WAO) and an East Atlantic Oscillation (EAO), having overlapping geography and a positive correlation between each other, and the North Pacific Oscillation (NPO). The NAO and NPO teleconnections were originally identified by Walker (1924) and Walker and Bliss (1932). Wallace and Gutzler (1981) also describe a Eurasian Oscillation (EO) extending from Scandinavia to Korea, a zonally symmetric seesaw of sea level pressures as originally noted by Lorenz (1951), and finally the Pacific/North American (PNA) pattern, which has two centers of action located over the Pacific, a third one over western North America and a fourth one over the southeast US. Previous work that had identified the properties of the PNA pattern prior to Wallace and Gutzler (1981) include Allen *et al.* (1940), Namias (1951), Klein (1952), Martin (1953), Klein et al. (1960), Klein (1965), O'Conner (1969), Dickson and Namias (1976), Dickson (1977), and Namias (1978). Wallace and Gutzler's (1981) definition of the PNA was an expansion

of the results presented by Dickson (1977), who used composite anomaly charts of 700 hPa height, 1000–700 hPa thickness, and SLP for five winters (1960–61, 1962–63, 1967–68, 1969–70 and 1976–77) in order to compare circulation statistics of the selected winters. The research for this study incorporates the teleconnection definitions of the NAO and PNA based on 500 hPa geopotential heights as described by Wallace and Gutzler (1981).

The results published by Wallace and Gutzler (1981) led to numerous studies on teleconnections including Horel (1981), Rogers (1981), Barnston and Livezey (1987), Nakamura *et al.* (1987), and Glowienka-Hense (1990), all of whom examined the statistical aspects of the NAO. Horel (1981) was able to identify the teleconnection patterns outlined by Wallace and Gutzler (1981) after linearly transforming the principal components they had derived. Using an eigenvector analysis, Rogers (1981) found that while the spring and autumn SLP and 500 hPa geopotential height eigenvectors have the same sign and configuration, the correlation between summer eigenvectors of these variables is weaker. Barnston and Livezey's (1987) work confirmed the existence of the low-frequency circulation patterns defined by Wallace and Gutzler (1981) and identified less obvious patterns. They also identified the NAO as the strongest intraannual low frequency circulation, identifiable in all seasons. Nakamura *et al.* (1987) separated four Northern Hemisphere teleconnection patterns into two groups based on speculations about how kinetic energy sources maintained these patterns. The EAO and PNA patterns were lumped into one group as Nakamura *et al.* (1987) suggested that these patterns are partially maintained by the barotropic instability in jet-exit regions. The WAO and West Pacific Oscillation (WPO) patterns were lumped into a second group,

given that Nakamura *et al.* (1987) hypothesized that their proximity to storm track entrance regions over the western ocean basins was a possible source of kinetic energy. Glowienka-Hense (1990) performed an eigenvector analysis of SLP, concluding that the NAO pattern is defined by the first eigenvector for January through July, and September, and the NAO is defined by the second eigenvector for the remaining months. The large-scale pattern associated with both eigenvectors is centered around a node at 55°N. The first eigenvector is represented by two anomaly centers at 65°N, 30°W and 40°N, 20–30°W. The second eigenvector is represented by two anomaly centers at 65°N, 10–20°W and 40°N, 0–30°W.

Work by, for example, DeWeaver and Nigam (2000a,b), and Wallace *et al.* (2000) examined the zonal-mean circulation with respect to the NAO. DeWeaver and Nigam (2000a,b) concluded that the stationary waves, which define the NAO, are maintained by altering the latitudinal tilt of the North Atlantic jet through changes of the zonal-mean flow anomalies. Wallace *et al.* (2000) also concluded that the dynamics of the zonally symmetric flow determine the planetary wave structures that define Northern Hemisphere teleconnections.

Other subsequent research on the NAO includes Esbensen (1984), who compared intermonthly and interannual teleconnection signals at 700 hPa and Wallace *et al.* (1993), who compared the interannual and interdecadal variability of 500 hPa geopotential height, sea-level pressure and 1000–500 hPa thickness fields. Esbensen (1984) found that of the five teleconnections identified by Wallace and Gutzler (1981) only the PNA pattern was distinctly visible in the intermonthly and interannual temporal bands. Wallace *et al.* (1993) concluded that teleconnections such as the PNA were more

prominent during the winter than summer and that the PNA exhibits a large amount of interdecadal variability. A study by Renwick and Wallace (1995) on the interaction of the Southern Oscillation (SO) with the PNA concluded that during the warm phase of the El Niño-Southern Oscillation (ENSO) there is an increase in the frequency of occurrence of the positive PNA pattern. Rogers (1984) investigated the relationship between the SO and NAO, finding an intermediate frequency of covariance between the SO and NAO with a period of 5–6 years.

Concepts pertinent to this research are the understanding of the 500 hPa geopotential height patterns associated with the positive and negative phases of the NAO and PNA teleconnections and typical atmospheric features associated with the NAO and PNA anomaly patterns. Studies that have explored these concepts include Dole (1986) who noted that numerous dissimilar 500 hPa flow patterns can occur for a specific Northern Hemisphere teleconnection pattern. However, he found that the 500 hPa flow for one phase of Northern Hemisphere NAO and PNA teleconnection patterns was typically associated with blocking, while the other phase was typically associated with an intense area of zonal flow. In later work on the evolution of persistent anomaly patterns, Dole (1989) concluded that the onset and initial development as well as the breakdown of the 500 hPa geopotential height anomalies can be rapid, and can come with little warning. He also noted that associated anomaly centers can develop and intensify downstream from the initial anomaly center.

1.2.4 Large-scale Circulation Anomalies and Synoptic-scale Events

The relationship between the rearrangement of 500 hPa geopotential height patterns, which define the teleconnection anomalies, and major synoptic-scale events, including rapid cyclogenesis, is relatively unknown. Recent studies have examined the relationship between teleconnection anomalies and the extent of North Atlantic storminess. Nakamura and Wallace (1990) noted that a negative NAO regime results in increased 500 hPa baroclinic wave activity in the upstream storm track. Serreze *et al.* (1997) found an increase in the cold season surface cyclone events from Labrador to Portugal during extreme negative NAO patterns. Looking at just the positive NAO, Rogers (1997) found it to be indirectly linked to storm track variation in the far eastern Atlantic.

Hart and Grumm (2001) found a weak correlation of large East Coast storms to the SOI, PNA, and NAO. They compared monthly teleconnection indices to a 21-day running mean of four atmospheric variables including geopotential height, temperature, wind, and moisture, and a fifth variable (M_{TOTAL}), which was the average of the previous four. They found a slight correlation between M_{TOTAL} and the NAO and SOI with correlation values of -0.21 and -0.22 , respectively. Hart and Grumm (2001) thus concluded that large-scale circulation anomalies account for roughly 5% of the variance of their daily M_{TOTAL} variable. However, Hart and Grumm's (2001) comparison of the 21-day running mean of atmospheric variables to monthly teleconnection indices instead of daily teleconnection indices could be considered a factor in the non-correlation of their results.

1.2.5 Temperature and Precipitation Patterns of NAO/PNA

Temperature anomalies associated with the NAO have been well documented over Greenland and Europe. van Loon and Rogers (1978) noted that during the positive phase of the NAO the temperature anomaly over Greenland, northern North America, the southern Mediterranean, the Middle East, Central America, western North America and Alaska is negative, while the temperature anomaly over Europe and North America south of 60°N is positive. Leathers *et al.* (1991) found a negative (positive) correlation between the PNA index and temperature over the southeast (northwest) US. Outside of the continental US, a positive PNA pattern is associated positive temperature anomalies over Alaska and negative temperature anomalies over far-east Asia.

Precipitation anomaly patterns have also been associated with teleconnections. A positive NAO pattern is usually associated with above normal precipitation over northern Europe and Scandinavia, and below normal precipitation over southern Europe and Greenland, with the opposite being true for a negative NAO (e.g., Rogers and vanLoon 1979; Hurrell 1995). Leathers *et al.* (1991) found that the highest correlations between precipitation over the US and the PNA occurred during winter and early spring. From November through March, a negative correlation between precipitation and the PNA exists over the Ohio Valley, Great Lakes, Rocky Mountains, and Pacific Northwest. During these same months the only consistent positive correlation is located over the extreme southeast US. Lamb and Pepler (1987) found that Moroccan precipitation was inversely related to the sign of the NAO, where a high negative NAO would lead to high Moroccan precipitation amounts. The same negative correlation was

found by Herrera *et al.* (2001) in their study of the NAO and its influence on precipitation on the Canary Islands. Through the study of ice core samples, Appenzeller *et al.* (1998) also found that western Greenland observed decreases (increases) in net precipitation during positive (negative) NAO patterns. Hurrell (1995) and Hurrell and van Loon (1997) found a decline in the precipitation rate over much of the Greenland Ice Sheet, central and southern Europe and the Mediterranean during a positive NAO pattern, with the opposing case apparent over an area stretching from Iceland to Scandinavia during a negative NAO pattern.

1.2.6 Arctic Oscillation

Thompson and Wallace (1998, 2000, 2001), and Thompson *et al.* (2000), have recently identified the Arctic Oscillation (AO), or Northern Hemisphere annular mode, as an important contributor to atmospheric circulation variability over the Northern Hemisphere. In describing the AO, Thompson and Wallace (1998) define it as a “seesaw of atmospheric mass between the Arctic and midlatitudes.” They use the leading Empirical Orthogonal Function (EOF) of the Northern Hemisphere wintertime SLP anomalies poleward of 20°N to identify the AO. Thompson and Wallace (1998) also calculated correlation statistics between monthly surface air temperatures (SAT) and monthly NAO and AO index values. The results reveal higher correlation values between the AO and SATs than between the NAO and SATs. In the first article of a two-part series, Thompson and Wallace (2000) suggest that the zonally symmetric monthly variability in the geopotential height field is primarily due to the AO while in

the second article, Thompson *et al.* (2000) conclude that the active season for the AO is January through March when fluctuations in the AO are observed in the lower stratosphere. Thompson *et al.* (2000) also state their preference of the AO to the NAO. The reasons Thompson *et al.* (2000) prefer the AO include: (1) the AO has a Southern Hemisphere counterpart, (2) the AO can be connected to stratospheric dynamical processes, (3) intraseasonal and interannual variability can be better explained by the AO, while an entire winter season of the NAO has to be averaged in order to obtain a representation of corresponding planetary-scale circulation anomalies, (4) the AO shows a greater positive index trend than the NAO, or a more substantiate warming of the Northern Hemisphere climate, and (5) a larger number of the Northern Hemisphere climate trends are more similar to the AO index than the NAO index.

Thompson and Wallace (2001) explored the North Atlantic component of the AO in greater detail using daily NCEP/NCAR Reanalysis data. They concluded that a low index of the AO (equivalent of a negative NAO in the North Atlantic basin) correlated with a greater frequency of 500 hPa blocking patterns over Alaska and the North Atlantic, a higher frequency of cold outbreaks over North America, Europe, Siberia, and Asia, and a higher frequency of “Nor’easters” than a high index of the AO. As in previous work on the AO, Thompson and Wallace (2001) noted that tropospheric and stratospheric circulations are coupled during January through March. On a more regional scale, Ambaum and Hoskins (2002) suggest that the NAO has a stratospheric connection. They conclude that wave propagation and geostrophic and hydrostatic adjustments are key links in the interaction between the troposphere and stratosphere. To help the scientific community reach a consensus on which teleconnection is more

appropriate, Wallace (2000) presented facts concerning the specific attributes of the NAO and AO, and suggested that numerical experiments be performed to explore the effects of the NAO and AO on regional climates.

Other studies concerning comparisons of the AO and NAO include Deser (2000) and Ambaum *et al.* (2001). Deser (2000) examined the annular symmetry of the AO as defined by Thompson and Wallace (1998). Deser (2000) concluded that the Arctic center of action is dominant over the Atlantic and Pacific centers, and thus accounts for the annular characteristic of the AO. Ambaum *et al.* (2001) advocate using the NAO and PNA patterns. Their conclusions suggest that the NAO better represents the Northern Hemisphere variability than the AO. The temporal and especially the spatial aspects of this study, which involve daily variations over the Northeast US and the fact that the NAO and PNA are well documented, have lead to the selection of the NAO and PNA for this research instead of the AO.

Few studies have focused on daily teleconnection indices and their relationship to atmospheric variables such as temperature and precipitation. Blackmon *et al.* (1984) filtered 500 hPa geopotential height fluctuations into long, intermediate, and small time scales of greater than 30 days, 10–30 days, and 2.5–6 days, respectively. They focused on the long and intermediate time scales, stating that one-point correlation 500 hPa geopotential height maps for long periods resembled the teleconnection patterns. The 500 hPa geopotential height fluctuations for short periods resembled wave trains poleward and downstream of climatological mean jets. Recently, daily values (observed and forecast) of teleconnection indices such as the NAO and PNA have become available online from the Climate Diagnostics Center (CDC; www.cdc.noaa.gov) and the

Climate Prediction Center (CPC; www.cpc.noaa.gov). The availability of these daily teleconnection indices has facilitated research and forecast studies. As an example, Stephenson (2001) has explored the predictability of the NAO through the long-range persistence of the daily NAO index.

1.3 Study Goals

As has been discussed, previous literature has defined the NAO and PNA teleconnections in terms of large-scale circulation flow patterns and anomalies that are present at both the surface and midtroposphere. These large-scale circulation flow patterns and anomalies are associated with temperature and precipitation anomalies throughout the Northern Hemisphere, including North America, Greenland, and Europe. Although previous studies have also noted the differing frequency of storm activity in the North Atlantic basin in association with the teleconnections, they have focused mainly on the monthly or seasonal timescales, with little attention to the interaction between daily large-scale circulation anomalies and synoptic-scale weather systems. The main objective interest of this research is to expand the understanding of the relationship between northeast US precipitation events and the daily NAO and PNA indices. This objective will be addressed by exploring the relationship of the 500 hPa geopotential height field, within the defined domain of the teleconnection patterns, to synoptic-scale precipitation events through several case studies of memorable events such as the Superstorm of 1993 (e.g., Kocin *et al.* 1995; Uccellini *et al.* 1995; Bosart *et al.* 1996; Dickinson *et al.* 1997). A tendency for the transition of the NAO and PNA

teleconnection indices in association with major synoptic-scale events over the Northeast also will be explored.

The thesis is organized as follows: Section 2 will cover the data sources and analysis methods. Section 3 will present the key research findings. Section 4 will discuss the results presented in section 3, and section 5 will conclude the thesis with suggestions for future research topics.

2. Data and Methodology

2.1 Data

The National Centers for Environmental Prediction (NCEP)/ National Center for Atmospheric Research (NCAR) reanalysis dataset (Kalnay *et al.* 1996; Kistler *et al.* 2001) was used to obtain the data for this research. The NCEP/NCAR gridded reanalysis data have a global resolution of $2.5^{\circ} \times 2.5^{\circ}$ and are available on 17 isobaric levels from 1000 hPa to 10 hPa. Data are available from January 1948 through the present. This project used the twice daily (0000 and 1200 UTC) gridded 500 hPa geopotential heights at 12 h intervals from January 1953 through December 2000.

Daily precipitation data for this project were taken from the Unified Precipitation Dataset (UPD). This dataset incorporates the National Oceanic and Atmospheric Administration (NOAA) first order station precipitation measurements, daily cooperative observation measurements, and River Forecast Center data, representing over 13,000 stations in the US after 1992. Radar-derived precipitation estimates from the WSR-88D operational Doppler radar network have been incorporated into the UPD in recent years and allow for precipitation estimates in the immediate coastal waters. The dataset has a $0.25^{\circ} \times 0.25^{\circ}$ resolution extending from $60^{\circ}\text{--}140^{\circ}\text{W}$ and $20^{\circ}\text{--}60^{\circ}\text{N}$. The UPD is available from January 1948 through December 1998, with 24 h precipitation amounts recorded from 1200 UTC to 1200 UTC (www.cpc.ncep.noaa.gov/products/outreach/atlas.html 2002).

2.2 Methodology

To best represent regional-scale flow associated with large-scale circulation anomalies, such as the NAO, the original emphasis on NAO indices in terms of sea-level pressure was abandoned in favor of an NAO index calculated from gridded 500 hPa geopotential height data using the procedure defined by Wallace and Gutzler (1981). A Fortran program was used to calculate the NAO and PNA indices from 500 hPa geopotential height data. The twice daily 500 hPa geopotential heights were averaged at each grid point along and within the boundaries of the domains described in sections 2.2.1 and 2.2.2 to get the daily average 500 hPa geopotential height as shown in section 2.2.4. The daily average 500 hPa geopotential height values for each grid point were then summed and divided by the total number of grid points in the boxes defined in sections 2.2.1 and 2.2.2. Specific calculations of the teleconnection indices are discussed in section 2.2.4.

2.2.1 NAO Analysis

Two 500 hPa zonal domains, an Azores domain (35–45°N, 70–10°W) and an Iceland domain (55–70°N, 70–10°W), are used to define the NAO index (Fig. 2.1). This definition matches that of the Climate Diagnostics Center (CDC). Daily NAO indices were computed by taking the difference of domain averaged 500 hPa geopotential heights between the Azores domain and Iceland domain.

2.2.2 PNA Analysis

Four 500 hPa zonal domains, a Hawaiian domain (15–25°N, 140–180°W), an Alaskan domain (40–50°N, 140–180°W), a Pacific Northwest domain (45–60°N, 105–125°W) and a Southeast US domain (25–35°N, 70–90°W), are used to define the PNA index (Fig. 2.2). This definition also matches that of the CDC. Daily PNA indices were computed by adding the difference between the Hawaiian domain and Alaskan domain to the difference between the Pacific Northwest domain and the Southeast US domain.

2.2.3 Precipitation Analysis

Precipitation data from the UPD were analyzed over a northeast US domain (Fig. 2.3). Within the continental US the domain borders extend east and north from 38°N and 80°W near the West Virginia, Virginia border. Along the northeast US coast and US/Canada border the data boundary marks the last grid point at which the annual precipitation amount according to the UPD was greater than 76.2 cm. The precipitation data were normalized as described in section 2.2.4.

2.3 Calculations

The daily NAO and PNA indices, along with the daily precipitation indices, were calculated and standardized according to the following definition (e.g., Wilks 1995):

$$Z = \frac{x' - \bar{x}}{s}$$

Here Z is the index anomaly, x' is the average daily 500 hPa geopotential height or precipitation amount, \bar{x} is the long-term average 500 hPa geopotential height or precipitation amount, and s is the long-term standard deviation. The precipitation was standardized to eliminate seasonal and regional variability. A daily value of Z was calculated at each grid point along the borders and within each index domain. The long-term average 500 hPa geopotential height and long-term standard deviation were based on the 48 years of available data (1953–2000). To filter out subsynoptic-scale influences on the indices, a five-day running mean was applied to the daily values. To check the validity of the daily values, monthly NAO and PNA indices from (<http://www.cgd.ucar.edu/~jhurrell>) and (<http://www.cpc.ncep.noaa.gov/products/precip/CWlink/pna>), respectively, were compared to monthly indices as calculated from the daily indices.

Linear regression equations are used to determine correlations between daily PNA and NAO indices and daily precipitation data. These correlations were calculated on monthly and seasonal (SON, DJF, MAM) timescales using daily data. Villani (2001) established the validity of the statistical platform Microsoft Excel, which was used to calculate the linear regression equations and the associated correlation values for this research.

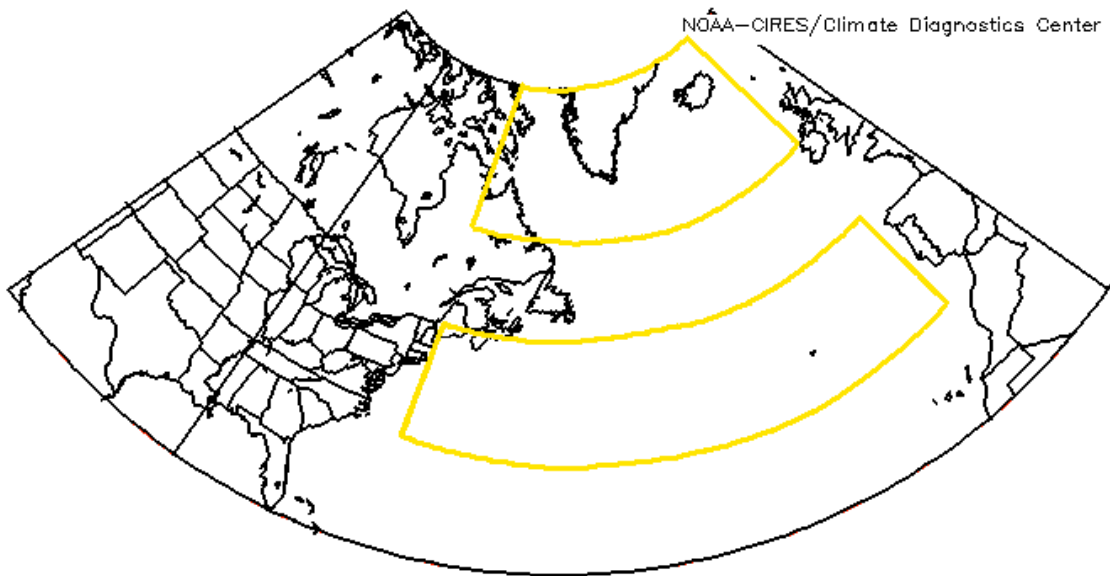


Fig. 2.1. NAO domain as defined by the Climate Diagnostics Center (CDC).

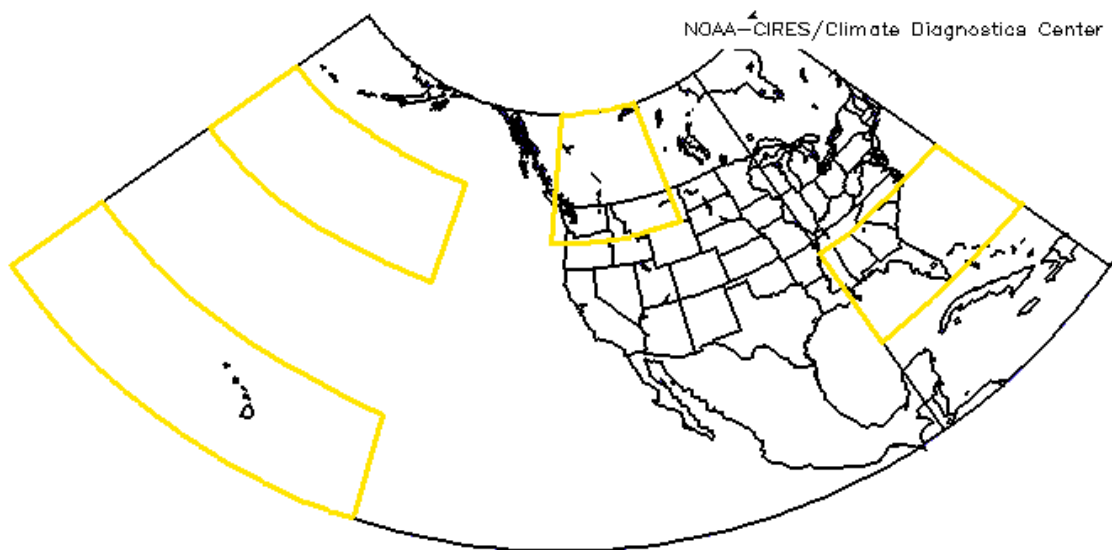


Fig. 2.2. PNA domain as defined by the Climate Diagnostics Center (CDC).

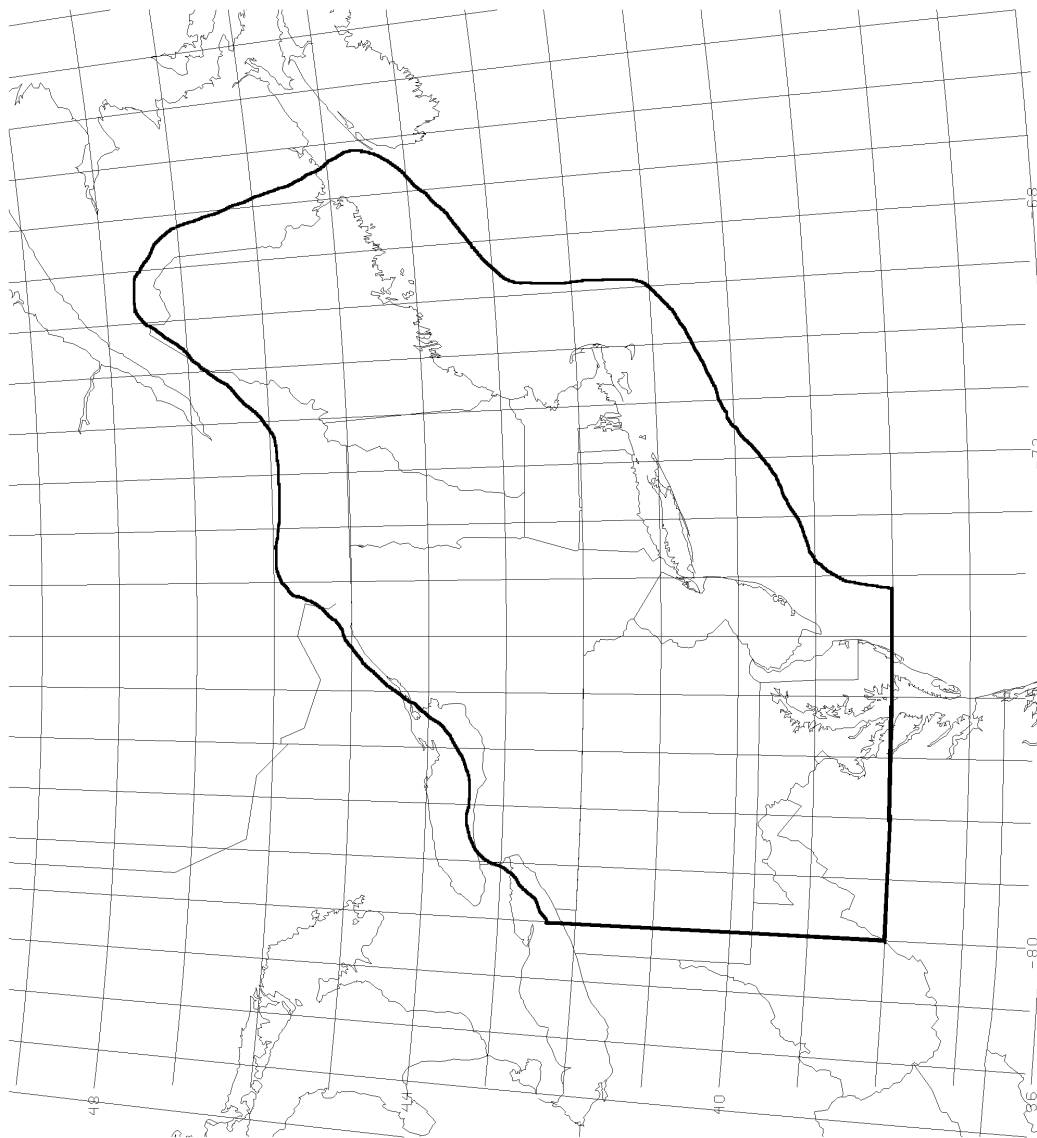


Fig. 2.3 Northeast US domain, where the black line represents the 756 mm annual isoheyt.

3. Results

3.1 Overview

In this section, results of the statistical analysis between daily large-scale circulation anomalies and northeast US precipitation amounts, NAO and PNA transitions, and the examination of four recent northeast US precipitation events are presented. First, the statistical analysis will examine the correlation between precipitation amount over a northeast US domain outlined in section 2.2.3 and daily NAO and PNA indices. Second, results from work on NAO transitions will include statistics concerning the relationship between northeast US precipitation events and transitions of the NAO index. Finally, the 12–14 March 1993 “Superstorm,” 24–26 January 2000 “Surprise” storm, 18–20 January 1996 “Meltdown,” and 5–9 January 1998 ice storm are discussed as examples of precipitation events coinciding with NAO transitions.

3.2 Statistics

The square of the correlation coefficient, or R^2 value, was calculated between the daily precipitation amount over a northeast US domain (Fig. 2.3), and daily large-scale circulation anomaly indices. The R^2 values were calculated for three seasons (SON, DJF, MAM) over the period of 1954 through 1998. The daily NAO and PNA indices are correlated with DPI values of greater than zero, one, two, three, and four, or daily

domain average precipitation values of 2.5 mm, 6.3 mm, 8.2 mm, and 10.1mm respectively. The relationship between northeast US precipitation events and the transition of the NAO (from positive to negative or negative to positive) is also discussed.

3.2.1 Daily NAO/Precipitation Correlations

Results for the three seasonal calculations of the square of the correlation coefficients (R^2 values) between daily NAO indices and daily northeast US domain averaged precipitation were essentially zero for DPI values both greater than zero and two. For the fall season (SON) the R^2 values for DPI values of greater than zero, one, two, three, and four are 0.0017, 0.0001, 0.0006, 0.0055 and 0.0661, respectively (Figs. 3.1–3.5). The R^2 values for the winter season (DJF) for daily precipitation indices greater than zero, one, two, and three are 0.0049, 0.0012, 0.0048, and 0.0192, respectively (Figs. 3.6–3.9). Finally R^2 values for the spring season (MAM) for daily precipitation indices greater than zero, one, two and three were 0.0014, 0.00001, 0.0088, and 0.4767, respectively (Figs. 3.10–3.13). A discussion of these results will be presented in chapter 4.

3.2.2 Daily PNA/Precipitation Correlations

The R^2 values for the correlation between DPI values and daily PNA indices were similar to the results for daily the NAO indices. The R^2 values representing the fall

season for daily precipitation indices greater than zero, one, two, three, and four were 0.0226, 0.0015, 0.0002, 0.047, and 0.0059, respectively (Figs. 3.14–3.18). For the winter season the R^2 value for daily precipitation indices greater than zero, one, two, and three were 0.0076, 0.0122, 0.0169, and 0.0017, respectively (Figs. 3.19–3.22). The spring season R^2 values for daily precipitation indices greater zero, one, two, and three were 0.0104, 0.0124, 0.0021, and 0.009, respectively (Figs. 3.23–3.26). For both the NAO and PNA nearly 60 percent of the cool season precipitation events were between DPI values of zero and one.

3.2.3 NAO transitions

While a correlation between precipitation amount and large-scale circulation anomaly indices does not exist, the occurrence of precipitation events just prior to and during NAO transitions was observed when coordinating the daily time series of the cool-season NAO index with precipitation data, as is seen for the 1993–1994 cool season (Fig. 3.27). The classification of a large-scale circulation index transition is as follows. First, the index must change sign from either positive to negative, or negative to positive. Second, the resulting phase change must last for at least five days, and finally the magnitude of the phase change must be at least one standard deviation centered on an index value of zero. A precipitation event is defined as at least one day with a DPI value greater than or equal to zero. The association of these precipitation events with NAO transitions focused on a four-day period that included the two days prior to the transition as well as the two days encompassing the transition.

Using these criteria, the study of 18 cool seasons (1968 to 1973, 1983 to 1988, and 1993 to 1998) netted 127 transitions of the NAO (Table 1). Seventy-six of the 127 or roughly 60% of the transitions had a precipitation event within the four-day NAO transition period considered. In separating the transitions into a phase change pattern of positive to negative or negative to positive, 69 of the 127 NAO transitions were from positive to negative and 58 were from negative to positive. Forty-nine of the 69 or 71% of the positive to negative NAO phase transitions had an associated precipitation event within the four-day NAO transition period. Twenty-seven of the 58 or 47% of the negative to positive NAO transitions had an associated precipitation event within the four-day NAO transition period. Besides these preliminary results, primary evidence of NAO transitions in association with precipitation events over the northeast US can be seen through the study of specific cases.

3.3 Case Studies

The case studies presented in this research are grouped according to the associated NAO transition with the negative-to-positive transition storms first, followed by the positive-to-negative transition storms second. The 12–14 March 1993 “Superstorm”, and 24–26 January 2000 “Surprise” storm are in the first group, and the 18–20 January 1996 “Meltdown”, and 5–9 January 1998 ice storm in the second group. Each case study will include the daily PNA and NAO time series encompassing the event, an analysis of SLP, storm total precipitation, mean and anomaly maps of 850 hPa

height and temperature, 300 hPa winds, and an analysis of the NAO phase change with 500 hPa geopotential height and anomaly fields.

3.3.1 12–14 March 1993

The 12–14 March 1993 “Superstorm” paralyzed the eastern US from the Gulf Coast to the Northeast. The storm was directly responsible for 79 deaths, more than 600 injuries, and 2 billion dollars in damage spread across 20 states (<http://www.noaanews.noaa.gov/stories/s334c.htm>). Nearly 50 percent of the US population was affected by the storm (<http://hpccsun.unl.edu/nebraska/stuproj/ametf99/sherman>). Synoptic and dynamic analyses of the storm include Kocin *et al.* (1995), who presented a synoptic overview of the storm. Uccellini *et al.* (1995) touted the success of the forecasters in predicting the storm, as they noted the storm was forecast up to five days in advance. One of several results reached in Bosart *et al.* (1996) noted the formation of a positive PNA pattern (Fig. 3.28b) during cyclogenesis from analysis of the 500 hPa geopotential height and anomaly fields. They also noted the presence of a central and eastern Atlantic blocking pattern, which supports the negative NAO indices as seen in Fig. 3.28a. Finally, Dickinson *et al.* (1997) studied the cyclogenesis and medium-range forecasting aspects of the 12–14 March event. They concluded that the initial cyclogenesis of the storm was due to the interaction of multiple potential vorticity (PV) maxima and the convectively unstable environment. Dickinson *et al.* (1997) also noted the 12-14 March “Superstorm”

to be the deepest extratropical cyclone observed in the Gulf of Mexico from 1957 through 1996.

3.3.1a Synoptic Analysis

The time-mean SLP map for 12-14 March 1993 (Fig. 3.29a) shows a broad surface anticyclone over the central Atlantic and cyclone with an associated trough over the eastern North Atlantic. The track of the 12-14 March “Superstorm” surface low is easily discernible by the weak trough paralleling the East coast. Behind the storm a surface anticyclone is centered over the Midwest. Negative SLP anomalies (Fig. 3.29b) in the eastern North Atlantic suggest an anomalously strong trough over the region. Positive anomalies over the surface anticyclone in the central US coupled with the negative anomalies associated with the storm along the east coast imply strong surface cold air advection behind the storm as it moved up the East Coast. Precipitation totals greater than 40 mm stretched the length of the East coast, with numerous areas, including Washington, DC; Philadelphia; New York; and Boston receiving 50–70 mm of precipitation (Fig. 3.30).

The 850 hPa geopotential height (Figs. 3.31a,b) and temperature fields (Fig. 3.32a) during the 12-14 March “Superstorm” show that a strong cold air advection pattern has brought anomalously cold air (Fig. 3.32b) to the entire Gulf Coast. The 850 hPa temperatures (Fig. 3.32a) have dropped well below zero across the entire eastern US. An “S” shape in the -5°C 850 hPa contour off the Northeast coast (Fig. 3.32a) reflects the strong cyclogenesis and warm air advection that occurred with this storm.

At 300 hPa (Fig. 3.33a) a deep trough was positioned over the eastern US with a jet positioned on the downstream side. The mean position of the jet streak between 12 and 14 March was along the east coast in an orientation matching the track of the surface low. The three-day average west-southwest vector wind speed of the 300 hPa jet was 45 m s^{-1} , which related to an anomalous southerly vector wind speed on the order of 30 m s^{-1} (Fig. 3.33b).

3.3.1b NAO/PNA Analysis

The 12-14 March 1993 “Superstorm” matched up with a negative to positive change in the NAO (Fig. 3.28a) and PNA (Fig. 3.28b). In analysis of the NAO, the large-scale 500 hPa geopotential height and anomaly pattern prior to the Superstorm for 9–11 March 1993 (Figs. 3.34a,b) shows a large area of negative 500 hPa geopotential height anomalies associated with a trough over the North Atlantic bounded on the north by an area of positive 500 hPa geopotential height anomalies associated with a short-wave ridge over Iceland. The positive-north and negative-south anomaly pattern (Fig. 3.34b) is characteristic of the negative NAO values in Figure 3.28a for this period. Between 9 and 11 March the PNA index had just undergone a positive-to-negative transition. The 500 hPa geopotential height field closely resembled a positive PNA pattern with a trough-ridge-trough pattern extending from the Gulf of Alaska to the eastern US (Fig. 3.35a). Figures 3.35a,b show that a short wave ridge was positioned upstream of the trough over the Gulf of Alaska. This short wave ridge was positioned directly over the Gulf of Alaska domain of the PNA, which was consequently dominated

by positive 500 hPa geopotential height anomalies. The presence of the Gulf of Alaska trough is more visible over the central North Pacific as negative 500 hPa geopotential height anomalies lay over the Hawaiian domain (Figs. 3.35a,b). Over North America a ridge over the Pacific Northwest and a trough in the East were the most representative of a positive PNA pattern. In North America positive 500 hPa geopotential height anomalies over the Pacific Northwest domain were associated with the western North America ridge, while the core of the negative 500 hPa geopotential height anomalies associated with the trough over eastern North America were centered north of the southeast US PNA domain. Thus, the negative PNA index observed in Fig. 3.28b is due to the dominating influence of the North Pacific PNA domains.

Explosive cyclogenesis that occurred during 12–14 March coincided with a negative-to-positive transition of the NAO (Fig. 3.28a). Bosart *et al.* (1996) and Dickinson *et al.* (1997) showed that a strong downstream jet and ridge developed in conjunction with the Superstorm cyclogenesis. Development of a sharp downstream ridge over the NAO domain and the resulting intensification of the North Atlantic jet are indications of a strengthening positive NAO (Figs. 3.36a,b). For the 12-14 March period the PNA index remained weakly negative (Fig. 3.28b). The 500 hPa geopotential height field still resembled a positive PNA pattern with a trough-ridge-trough pattern from the North Pacific to eastern North America (Fig. 3.37a). Analysis of the 500 hPa geopotential height anomaly field, however, shows that the anomaly dipole over the Pacific resembled a negative PNA index pattern with positive anomalies in the Gulf of Alaska domain and negative anomalies in the Hawaiian domain (Fig. 3.37b). Downstream, the ridge over western North America is weak, and displaced from the

Pacific Northwest PNA domain. Farther downstream the trough associated with the Superstorm dominates the southeast US PNA domain. The weak PNA index values are a result of the strong negative PNA signal from the Pacific domains being partially canceled by the effects of the Superstorm over the eastern US.

From 15–17 March the remnant storm moved towards Greenland, as the 500 hPa downstream ridge and associated positive geopotential height anomalies reached western Europe (Figs. 3.38a,b). The 500 hPa geopotential height anomaly analysis shows a negative-over-positive 500 hPa geopotential height anomaly dipole that is characteristic of a positive NAO regime (Fig. 3.38b). During the same period the PNA index was beginning a negative-to-positive transition (Fig. 3.28b). The 500 hPa geopotential height ridge-over-trough pattern in the North Pacific was still in place, while the downstream ridge-trough pattern had flattened (Fig. 3.39a). The flattening 500 hPa geopotential height pattern resulted in weakening the North Pacific 500 hPa geopotential height anomalies and displacing the eastern North American 500 hPa geopotential height anomalies farther north (Fig. 3.39b). Though negative anomalies are now over the Pacific Northwest domain, the weakening North Pacific anomaly centers keep the PNA index near zero.

3.3.2 24–26 January 2000

The 24–26 January 2000 “Surprise” storm was so labeled as it caught many people in the Northeast off guard. Snow accumulations of over 150 mm fell in a band from South Carolina to Vermont. Areas around Raleigh, North Carolina, received the

greatest amounts with accumulations of over 500 mm. A fresh snow pack and cold air behind the system led to numerous record lows in the days following the storm (<http://www.ems.psu.edu/WeatherWorld/summaries/sum1.00.html>). Recent studies of the event have focused on the inability of the short- and medium-range models to correctly forecast the storm track. In a study of the short- and medium-range model output, Langland *et al.* (2002) concluded that the upper-air pattern over the North Pacific prior to the storm led to substantial error growth rates in certain initialized fields. They further narrowed the forecast difficulties of short-range models to ridging in the Gulf of Alaska and eastern North Pacific. Zhang *et al.* (2002) also noted error growth from inaccurate initial conditions as causes for the models inexact storm track forecast.

3.3.2a Synoptic Analysis

A large area of high pressure over the North Atlantic dominated the time-mean SLP field between 24 and 26 January (Fig. 3.40a). This area seemed to be a key feature in determining the storm track, which can be identified by the elongated area of low pressure paralleling the East coast, or along the western periphery of the surface high. As can be seen in Fig. 3.40b, the broad area of high pressure over the North Atlantic is anomalously strong.

Similar features could be found at 850 hPa with a strong anticyclone oriented north/south over the central North Atlantic and an elongated trough along the East coast (Fig. 3.41a). A slight “S” shape in the 850 hPa geopotential height contours along the northeast US coast identified the mean position of the storm during this period. The 850

geopotential hPa height anomaly field (Fig. 3.41b) showed the strength of the North Atlantic ridging. A comparison of the 850 hPa temperature (Figs. 3.42a,b) and height fields (Figs. 3.41a,b) show cold air advection behind the storm over the Ohio Valley and southeast US, and warm air advection just off the East coast.

At 300 hPa (Fig. 3.43a) a trough-ridge pattern was in position over the eastern US and western North Atlantic. In the 300 hPa flow, the left exit region of a jet streak was positioned in the base of the trough over the Gulf Coast. The jet-induced ageostrophic circulation typical of the left exit region of a jet streak would have contributed to the development of the 24-26 January storm. Once the storm had begun development further analysis of the surface (Fig. 3.40a,b), 850 hPa (Fig. 3.41a,b), and 300 hPa (Fig. 3.43a,b) revealed that the coastal track of the 24-26 January storm was due mainly to the anticyclonic circulation present at all levels over the North Atlantic.

3.3.2b NAO/PNA Analysis

The 24-26 January 2000 storm occurred during a negative-to-positive transition of the NAO (Fig. 3.44a) and PNA (Fig. 3.44b). Analysis of the 500 hPa geopotential height over the NAO domains from 21-23 January shows a highly amplified trough-ridge pattern (Fig. 3.45a). A positive 500 hPa geopotential height anomaly center is positioned over the northern NAO domain, with a negative 500 hPa geopotential height anomaly over the western boundary of the southern NAO domain (Fig. 3.44b). The positive-over-negative anomaly pattern is consistent with a negative NAO. A negative PNA index weakened during the period prior to the storm (Fig. 3.45b). The most

prominent features in the 500 hPa geopotential height field stemmed from a split flow pattern located in the diffluent exit region of the North Pacific jet. A positively tilted ridge-trough couplet was positioned over the eastern North Pacific and western North America. Downstream, a broad trough was located over eastern North America (Fig. 3.46a). Positive 500 hPa geopotential height anomalies over the Gulf of Alaska PNA domain dominated the PNA index, as the three remaining PNA domains were minimally influenced by 500 hPa flow pattern (Fig. 3.46b).

A trough-ridge system remained in place over eastern North America and the North Atlantic during 24-26 January (Fig. 3.47a). The trough over eastern North America had narrowed with its axis paralleling the East coast. Cyclogenesis along the eastern US seaboard had led to the downstream ridge development over the western Atlantic that extended a positively tilted ridge axis from the central North Atlantic into England. Positive 500 hPa geopotential height anomalies associated with the 500 hPa ridge over the North Atlantic are present in both NAO domains (Fig. 3.47b). Negative 500 hPa geopotential height anomalies associated with the storm on the East Coast and with a trough over the eastern North Atlantic were both within the southern domain. However the expansion of positive 500 hPa geopotential height anomalies within the southern domain is responsible for the weakening negative NAO index. By 24-26 January the PNA index had transitioned from negative to positive (Fig. 3.44b). The positively tilted ridge-trough couplet in the last period had reorganized as a ridge-over-trough split flow feature and progressed eastward ahead of a deep 500 hPa upstream cutoff cyclone entering the western Gulf of Alaska PNA domain (Fig. 3.48a). Rapid coastal cyclogenesis was associated with a deepening trough off the eastern US. The

500 hPa cutoff cyclone over the Bering Strait, downstream high latitude ridge associated with split flow, and deep trough over the eastern US constituted a positive PNA through a negative-positive-negative 500 hPa geopotential height anomaly pattern (Fig. 3.48b).

Between 27 and 29 January the storm lifted northeast towards Greenland while the downstream ridge-trough system over the North Atlantic became further amplified (Fig. 3.49a). The southern extent of a polar vortex had moved over Greenland and Iceland during this period. Positive 500 hPa geopotential height anomalies over the sharp North Atlantic ridge were present in both domains, with the positive anomaly center centered between the two domains (Fig. 3.49b). Negative 500 hPa geopotential height anomalies over the two North Atlantic troughs were located along the boundaries of the southern NAO domain. Negative 500 hPa geopotential height anomalies with the southern fringes of the polar vortex were concentrated over the high latitudes of the northern NAO domain. The tightening of the 500 hPa geopotential height contours suggested the strengthening of the North Atlantic Jet, a property associated with a positive NAO index. The PNA index leveled off between 27 and 29 January (Fig. 3.44b). A deep 500 hPa cutoff cyclone had nosed into the western Gulf of Alaska, and was mirrored by a strong 500hPa anticyclone west of Hawaii (Fig. 3.50a). A ridge-trough pattern was in place over North America, although the trough associated with the storm had mostly lifted out, leaving the ridge as the dominant feature. The time-mean 500 hPa geopotential height anomaly pattern had a negative-over-positive anomaly dipole in the North Pacific (Fig. 3.50b). An expansive positive 500 hPa geopotential height anomaly covered much of North America, including the Pacific Northwest PNA

domain. The signature of a strong central North Pacific jet and western North American ridging is indicative of the positive PNA indices observed for this period.

3.3.3 18–20 January 1996

Prior to the 18–20 January 1996 “Meltdown”, three successive storms dumped significant snow accumulations in parts of the northeast US. The biggest storm to contribute to the Northeast snowpack was the blizzard of 1996, which dumped upwards of four feet of snow over the higher elevations of western Virginia and West Virginia. The 18–20 January 1996 storm brought warm air and heavy rains (Fig. 3.52) on top of the deep snowpack over the northeast US. In 24 h, areas of northeast Pennsylvania received over 75 mm of precipitation, which fell on a snowpack with snow water equivalents of 75 to 150 mm. The result was devastating flooding that killed 30 and caused an estimated \$1.5 billion in damage (Leathers *et al.* 1998).

3.3.3a Synoptic Analysis

The 18-20 January 1996 storm took an inland track, which can be seen by the elongated trough over the Great Lakes in the time-mean SLP analysis (Fig. 3.51a). A possible reason for the more inland track of the surface cyclone is the strong surface anticyclone off the northeast US coast during this period. The anticyclonic flow around the anomalously strong surface high (Fig. 3.51b) funneled warm moist air northward ahead of the storm. Warm surface temperatures coupled with moderate to heavy

precipitation totals (Fig. 3.52), especially over elevated regions that had the largest snowpacks, contributed to devastating floods.

The 850 hPa geopotential height pattern (Fig. 3.53a) mirrors the SLP pattern (Fig. 3.51a) with a large anticyclone off the northeast US coast and a trough axis cutting through the Great Lakes. Both 850 hPa features were anomalously strong (Fig. 3.53b), and the resultant height gradient between the two features suggests the presence of a southerly low-level jet. The strong southerly jet (Fig. 3.53a,b) coupled with the anomalously warm mean 850 hPa temperature field (Fig. 3.54a,b) for this period, showed a warm air advection pattern along the entire US East coast.

The 300 hPa flow (Fig. 3.55a) navigates through a trough in the eastern US and an anticyclone over the North Atlantic. Jet streaks are located in the base of the trough and farther downstream on the northwest fringes of the North Atlantic anticyclone. The Great Lakes region is under the influence of the left exit region, and right entrance region of the 50 m s^{-1} jet streaks. As seen in Figure (3.55b) the flow associated with the jet streak over Canada is anomalously strong.

3.3.3b NAO/PNA Analysis

Unlike the previous two cases, the 18-20 January 1996 “Meltdown” occurred with positive-to-negative transition of the NAO (Fig. 3.56a) and PNA (Fig. 3.56b). From 15-17 January, a 500 hPa polar low was located over the Davis Strait and bounded to the east by a 500 hPa ridge axis that stretched from the Azores into central Europe (Fig. 3.57a). A tight 500 hPa potential height gradient between the two features is

indicative of a strong North Atlantic jet and positive NAO. The 500 hPa geopotential height anomaly field illustrates a positive NAO with a negative-over-positive anomaly dipole (Fig. 3.57b). During the same period the PNA was in the middle of a positive-to-negative transition (Fig. 3.56b). A visible remnant of the positive PNA pattern is the presence of a North Pacific 500 hPa height gradient or the implied existence of a North Pacific jet (Fig. 3.58a). Features that hint at the forthcoming negative PNA include a positively tilted trough axis that cuts through the Pacific Northwest and a short wave ridge in the Gulf of Alaska. The 500 hPa geopotential height anomaly field (Fig. 3.58b) shows that a positive PNA dipole exists in the two North Pacific domains, while a negative PNA dipole is visible in the two North American domains. The PNA transition for this case looks to have worked its way upstream.

During the storm, from 18 to 20 January, the positive NAO rapidly weakened (Fig. 3.56a). A 500 hPa ridge that formed downstream of the storm forced its way northward into the 500 hPa polar low. The core of the polar low retreated poleward and was replaced by a trough-ridge-trough pattern that stretched from North America to Europe (Fig. 3.59a). The positive NAO anomaly dipole prior to the storm had been replaced with a latitudinally oriented anomaly dipole, with a positive anomaly center in the western Atlantic and negative anomaly center in the eastern Atlantic (Fig. 3.59b). Between 18 and 20 January the magnitude of the negative PNA grew. Key features in the 500 hPa geopotential height field included the zonal flow over the North Pacific that had weakened and retreated northward, and a trough axis that extended south from a polar low centered north of Hudson Bay (Fig. 3.60a). Negative 500 hPa geopotential height anomalies covered western North America with the exception of Alaska (Fig.

3.60b). Positive 500 hPa geopotential height anomalies straddled the negative anomaly to the east and west. A negative PNA dipole was now present in the Pacific and North American domains.

As the storm moved into the North Atlantic between 22 and 24 January, the 500 hPa polar low had relocated to just north of Hudson Bay (Fig. 3.61a). The 500 hPa ridge over the central North Atlantic had broken off a part of the polar low as the ridge pushed into northern Europe. The leftover 500 hPa cutoff was centered over northern Spain and Portugal. Positive 500 hPa geopotential height anomalies now dominated the northern NAO domain, and negative anomalies dominated the southern NAO domain (Fig. 3.61b). The negative PNA was nearing a peak in magnitude during 22-24 January (Fig. 3.56b). Over the North Pacific a negatively tilted 500 hPa ridge axis extended from the Bering Strait to east of Hawaii (Fig. 3.62a). A 500 hPa short wave had deepened and moved onshore over the western US. The 500 hPa geopotential height anomaly field exemplified a negative PNA pattern in three of the four domains, with the Hawaiian domain remaining neutral (Fig. 3.62b). A positive-negative-positive pattern is configured over the Gulf of Alaska domain, Pacific Northwest domain, and southeast US domain, respectively.

3.3.4 5–9 January 1998

The early January 1998 ice storm crippled the northeast US and southern Ontario Canada. As reviewed by Gyakum and Roebber (2001), the storm resulted in 56 fatalities, caused over \$4 billion in damage, and left over 3 million utility customers

without power. Observed radial ice loads were as high as 125 mm. In their analysis of the storm, Gyakum and Roebber (2001) state that the area of maximum precipitation occurred under a deformation zone separating a cold surface anticyclone on the poleward side from a surface trough axis stretching from the Gulf of Mexico to the Great Lakes on the equatorward side.

3.3.4a Synoptic Analysis

As also mentioned in Gyakum and Roebber (2001), the key features in the time-mean SLP field for 5-9 January (Fig. 3.63a) include a zonally oriented ridge axis over northern Canada, and an inverted trough extending north from the Gulf of Mexico into the northeast US. The time-mean SLP associated with the ridge axis across Canada was anomalously strong (Fig. 3.63b). Surface flow across the northeast US and southern Canada was easterly, channeling moist air inland off the Atlantic. This flow pattern allowed for a six day precipitation total (Fig. 3.64) of greater than 40 mm over all of New England and extreme southern Quebec. Many areas of upstate New York, Vermont, New Hampshire, and Maine received over 70 mm of precipitation, most of which fell in the form of freezing rain.

A key feature in the 850 hPa geopotential height field (Fig. 3.65a,b) is the anticyclone centered off of the East Coast. Southerly flow on the west side of the anticyclone brought warm, moist air from the south into the northeast US. Closely packed east/west oriented 850 hPa temperature isotherms (Fig. 3.66a) across the northeast US and Quebec was approximately orthogonal to the 850 hPa flow.

Anomalously warm 850 hPa temperatures for January (Fig. 3.66b) are evidenced by the 0°C isotherm, which stretched from southern Quebec through northern Maine.

The presence of a 300 hPa jet streak over northeastern Canada was critical in enhancing precipitation totals over the northeast US and southeastern Canada (Figs. 3.67a,b). The ageostrophic circulation typically associated with right entrance region of this jet may have helped enhance the vertical motion.

3.3.4b NAO/PNA Analysis

Both the NAO and PNA indexes changed sign during the 5-9 January 1998 ice storm. The NAO (Fig. 3.68a) flipped from positive to negative, while the PNA (Fig. 3.68b) changed from negative to positive. The entire regime change of the NAO consisted of two phases. The first phase included a change from positive to weakly negative NAO values. The weak negative NAO regime lasted for nearly two weeks before becoming more strongly negative. The absence of deep cyclogenesis during the first phase suggests that this process is not a factor in the initial NAO regime change.

Prior to the ice storm, 2-4 January, an elongated 500 hPa polar low stretched from far northern Canada to Scandinavia, and a subtropical 500 hPa North Atlantic high was located south of the Azores. Between these two features there was a very large 500 hPa geopotential height gradient with an associated jet (Fig. 3.69a). This 500 hPa geopotential height pattern was reflected in a textbook positive NAO pattern in the 500 hPa height anomaly field (Fig. 3.69b). From 2-4 January the negative PNA index was increasing in magnitude, or becoming more negative (Fig. 3.68b). A sharp 500 hPa

ridge-trough pattern was present over the North Pacific with a flat ridge visible downstream over the southeastern US (Fig. 3.70a). The 500 hPa geopotential height anomaly field shows a positive-negative-positive pattern over the Gulf of Alaska domain, Pacific Northwest domain, and southeast US domain, respectively (Fig. 3.70b). Three of the four PNA domains had contributed to the quickly intensifying negative PNA index.

Over the period 5–9 January, a 500 hPa short wave dug into the southeastern US, which resulted in the downstream development of a 500 hPa ridge-trough system (Fig. 3.71a). This evolution of the large-scale pattern broke down the positive NAO regime in place prior to the event. Positive 500 hPa height anomalies for this pattern (Fig. 3.71b) were in the ridge, with negative anomalies in the trough. The meridional orientation of the anomaly dipole resulted in a weak negative NAO signature. The PNA index was transitioning from negative to positive between 5 and 9 January 1998 (Fig. 3.68a). During that period a mean 500 hPa trough-ridge pattern was in place over the North Pacific, with a similar trough-ridge pattern over North America and the western Atlantic (Fig. 3.72a). Negative 500 hPa geopotential height anomalies were associated with the North Pacific and western North American troughs (Fig. 3.72b). Positive 500 hPa geopotential height anomalies were present over the eastern third of North America. The North American PNA domains were the last to contribute to the fading negative PNA.

From 10–13 January, a deep trough resided over the eastern Atlantic with zonal flow upstream (Fig. 3.73a). The associated 500 hPa geopotential height anomalies were negative in the trough and positive in the zonal flow (Fig. 3.73b). The anomaly dipole

retained a meridional orientation, consistent with a weak negative NAO. During the same period a 500 hPa cutoff low had moved over the Aleutians and pinched the eastern North Pacific 500 hPa ridge between the Aleutian low and a retreating North American polar low (Fig. 3.74a). Negative 500 hPa geopotential height anomaly centers positioned over the Aleutians and western Canada were the only 500 hPa geopotential height anomalies within PNA domains (Fig. 3.74b). The increasing positive PNA index during this period suggested that the negative anomalies over the Gulf of Alaska domain were dominant.

By 13–15 January (Figs. 3.75a,b), the 500 hPa trough over the eastern Atlantic has been replaced by a cutoff low east of Labrador and a downstream high-amplitude ridge. The resulting 500 hPa height anomaly pattern features a large positive anomaly center in the northern domain over the Davis Strait, and weak negative and positive height anomalies over the southern domain. In the North Pacific, a tight 500 hPa geopotential height gradient between the Aleutian low and subtropical Pacific high implies a strong North Pacific jet and positive PNA pattern (Fig. 3.76a). A split flow in the diffluent exit region of the North Pacific jet had led to a downstream ridge-over-trough pattern positioned over western North America. The 500 hPa geopotential height anomaly field showed a negative-over-positive anomaly dipole in the North Pacific PNA domains (Fig. 3.76b). This dipole pattern was the dominant mode of the growing positive PNA index.

From 16–18 January the Labrador 500 hPa cutoff and associated high-amplitude ridge moved eastwards. A weak high-latitude ridge associated with a negatively tilted short wave in the northern branch has built in behind the cutoff. The two ridges on

either side of the cutoff show up as a southwest–northeast elongated positive 500 hPa height anomaly (Figs. 3.77a,b). Farther upstream the 500 hPa Aleutian low remained in place with a downstream ridge–trough pattern over North America (Fig. 3.78a). Negative 500 hPa geopotential height anomalies were in place over the Aleutians, Gulf of Alaska, and southeast US (Fig. 3.78b). Positive 500 hPa geopotential height anomalies stretched from Hawaii to California. A negative-over-positive anomaly dipole remained in the North Pacific during this period. In North American PNA dipole the 500 hPa geopotential height anomalies were nonexistent in the Pacific Northwest domain, and weakly negative over the southeast US domain. Both anomaly dipoles made a positive contribution to the positive PNA index during this period.

By 19–22 January (Figs. 3.79a,b), the easternmost cutoff low has moved out of the domain and a negatively tilted trough had moved off of the East Coast. The formation of the 500 hPa cutoff low allows a sharp downstream ridge–trough pattern to develop. The ridge and upstream cutoff are reflected as a positive-over-negative 500 hPa geopotential height anomaly pattern, suggesting an increase in the magnitude of the negative value of the NAO index (Fig. 3.68a). During this period the positive PNA index falls slightly towards zero (Fig 3.68b). The 500 hPa Aleutian low and downstream Pacific Northwest ridge remained in place, though the low had weakened and ridge had built farther north (Fig. 3.80a). The trough over the southeast US had moved out over the North Atlantic. Again, the North Pacific PNA anomaly dipole was negative over positive (Fig 3.80b). For this period the positive 500 hPa anomalies over the Pacific Northwest domain controlled the North American PNA anomaly dipole, because the southeast US domain was devoid of 500 hPa geopotential height anomalies.

Finally, by 23–25 January a Rex-type blocking pattern is in place with a cutoff anticyclone (cyclone) situated over England (Spain) (Figs. 3.81a,b). This pattern arose as the high-latitude ridge near Greenland shifted eastward while a short-wave trough undercut the ridge, resulting in a strongly negative NAO pattern. From 23-25 January the positive PNA index increased in magnitude (Fig. 3.68b). The 500 hPa Aleutian cyclone had deepened and extended farther southeastward towards the North American coast (Fig. 3.82a). The ridge lingered over the Pacific Northwest. With the resurgence of the Aleutian cyclone, the negative-over-positive North Pacific 500 hPa geopotential height anomaly dipole remained through the 23-25 January period (Fig 3.82b). The North Pacific anomaly dipole was a consistent feature throughout the post 5-9 January ice storm period. As in previous periods after the ice storm, the North American anomaly dipole was nearly absent of 500 hPa geopotential height anomalies. The strengthening positive PNA index for this period is a direct consequence of the strengthening North Pacific 500 hPa features.

3.4 Summary

The research presented in this chapter focused on the relationship between daily large-scale circulation anomaly indices and precipitation over the northeast US. In sections 3.1.1 and 3.1.2 it was shown that a correlation does not exist between daily precipitation amount in the Northeast, and daily NAO and PNA values. A transition of the NAO index was defined and a preliminary relationship between NAO transitions and northeast US precipitation events was established. The study of 18 cool seasons

revealed the tendency for northeast US precipitation events having a DPI greater than zero to occur within a four-day period just prior to and during a transition in the NAO index. Nearly 71% of the NAO transitions that occurred with an associated precipitation event in the Northeast were positive-to-negative transitions.

In section 3.2 four precipitation events that occurred with transitions in the NAO were analyzed. For each event a synoptic discussion as well as an analysis of the relationship between the large-scale midtropospheric circulation patterns and the NAO and PNA indices was presented. The NAO transitions associated with the four northeast US precipitation events were dependent on the magnitude of the downstream 500 hPa pattern rearrangement. A greater amplification of the downstream 500 hPa geopotential height pattern occurred prior to and during the two events associated with positive-to-negative transitions than with the two events associated with the negative-to-positive transitions. Due to the large geographical area that defines the PNA index, it is unclear at this time what role large precipitation events over the northeast US play in transitions of the PNA index. However, analysis of the four northeast US precipitation events may suggest that large precipitation events along the East Coast could either be the final phase of a PNA transition that started upstream or the first phase of a PNA transition that moves upstream. Discussion of these results will be presented in Chapter 4.

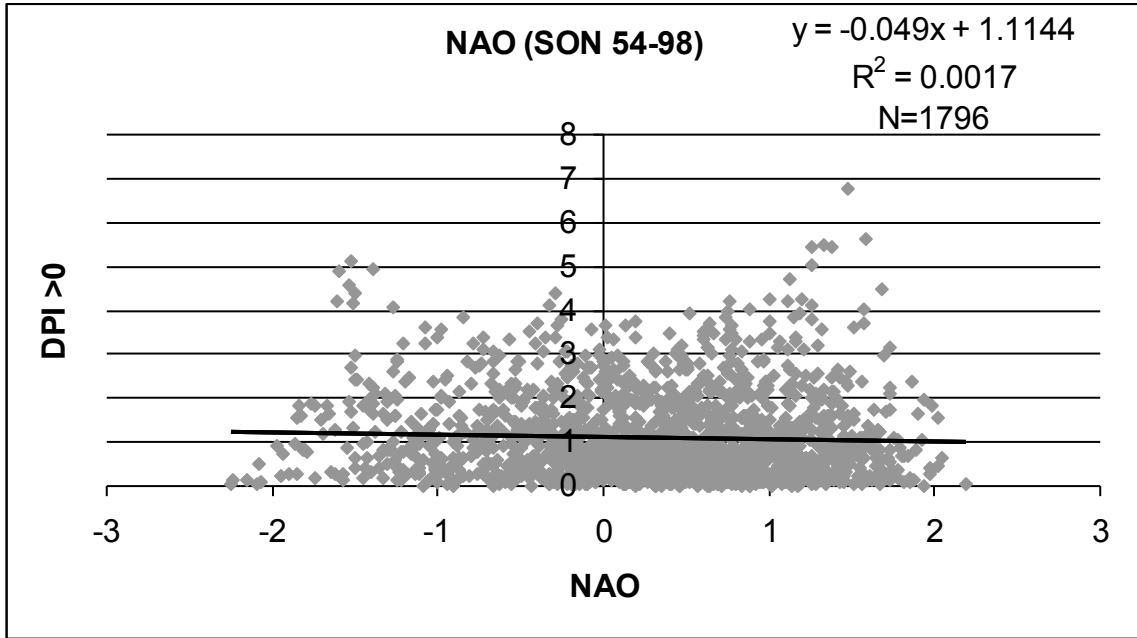


Fig. 3.1. Correlation between the daily NAO and a domain-average precipitation greater than 2.5 mm (DPI > 0) for the fall seasons between 1954 and 1998.

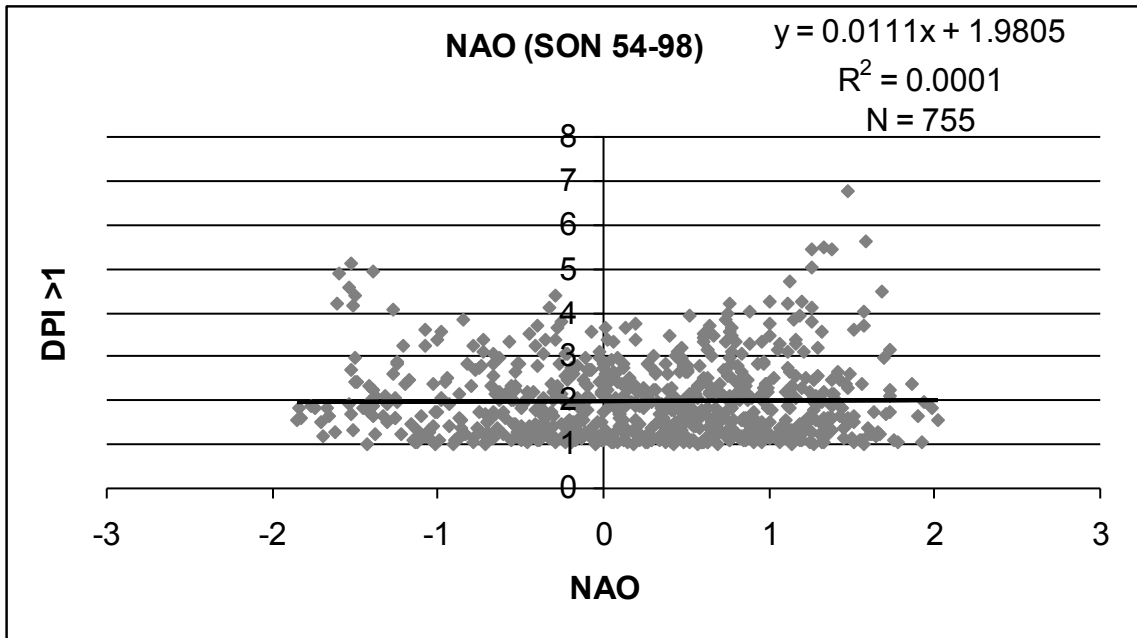


Fig. 3.2. Correlation between the daily NAO and a domain-average precipitation greater than 4.4 mm (DPI > 1) for the fall seasons between 1954 and 1998.

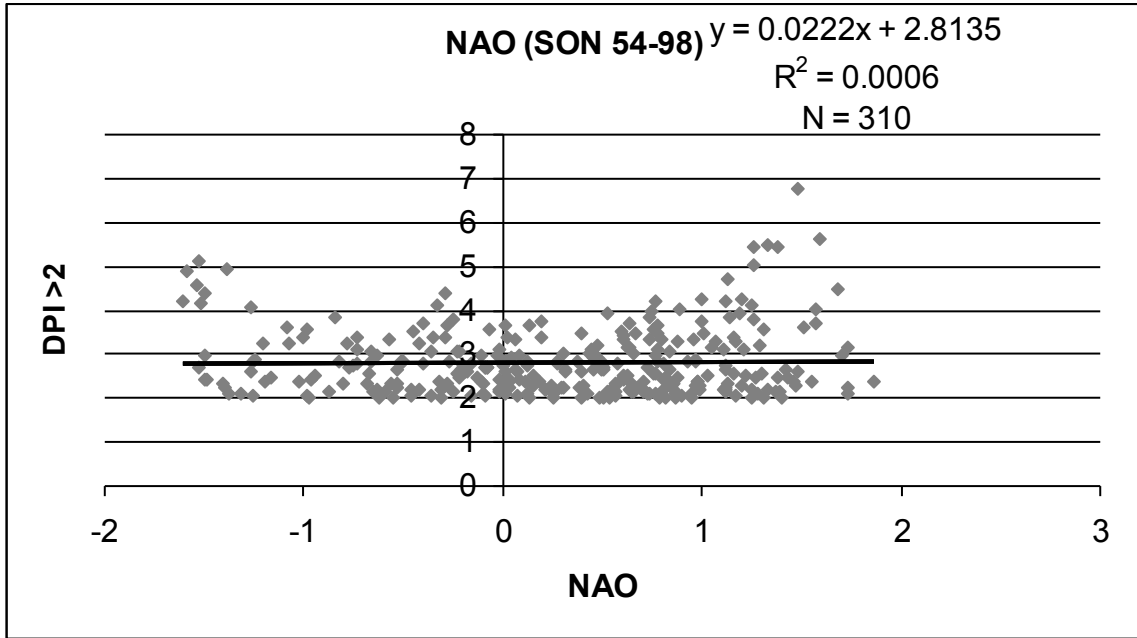


Fig. 3.3. Correlation between the daily NAO and a domain-average precipitation greater than 6.3 mm (DPI > 2) for the fall seasons between 1954 and 1998.

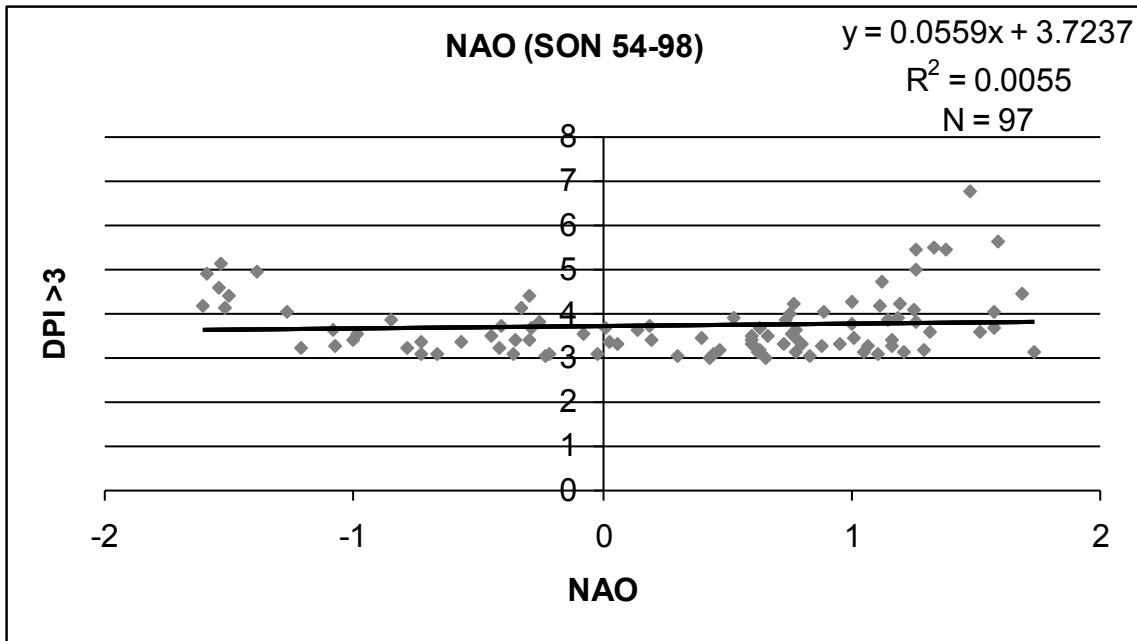


Fig. 3.4. Correlation between the daily NAO and a domain-average precipitation greater than 8.2 mm (DPI > 3) for the fall seasons between 1954 and 1998.

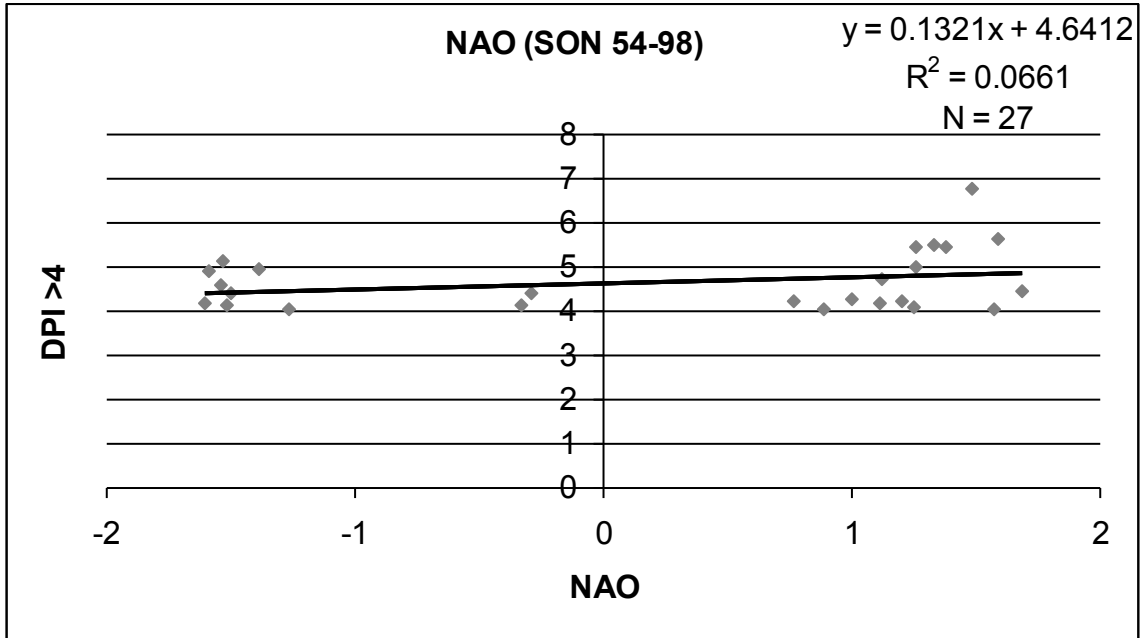


Fig. 3.5. Correlation between the daily NAO and a domain-average precipitation greater than 10.1 mm (DPI > 4) for the fall seasons between 1954 and 1998.

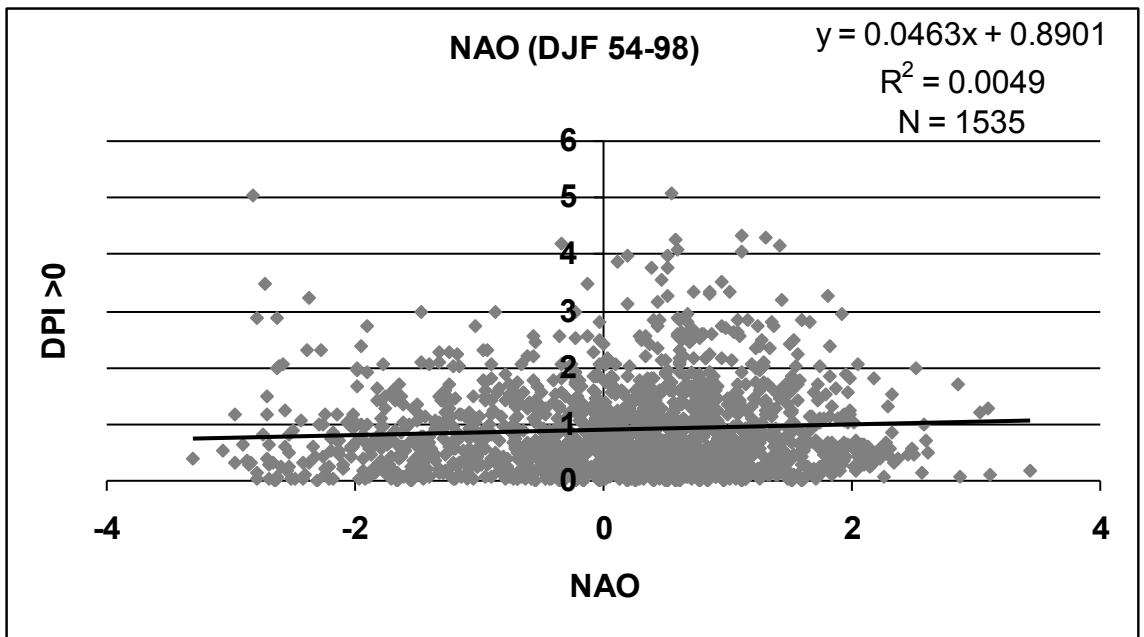


Fig. 3.6. Correlation between the daily NAO and a domain-average precipitation greater than 2.5 mm (DPI > 0) for the winter seasons between 1954 and 1998.

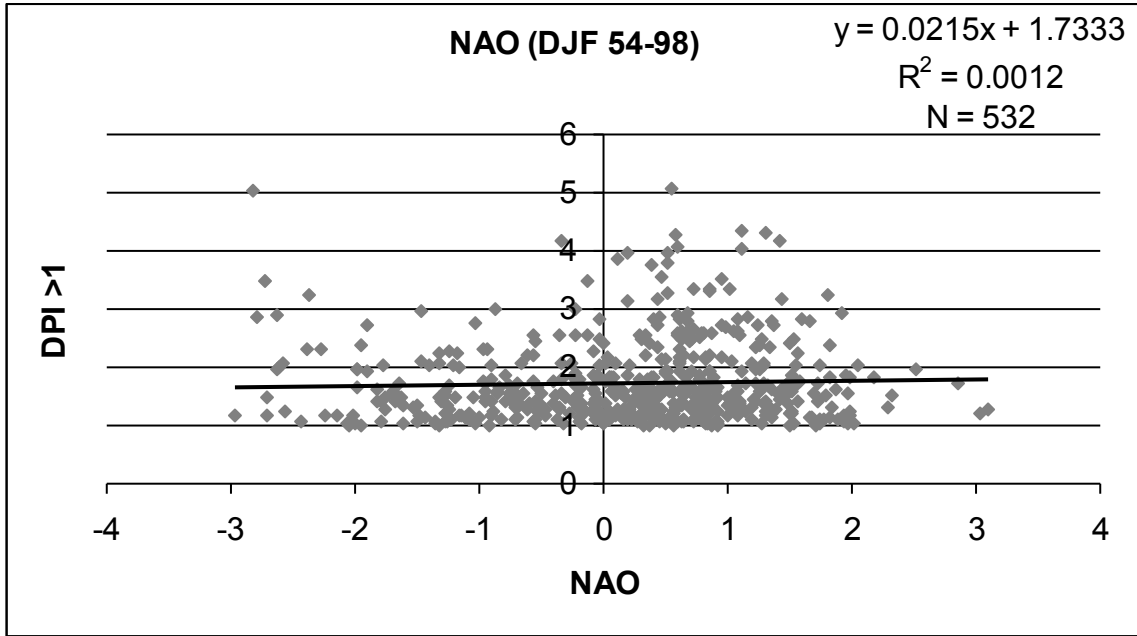


Fig. 3.7. Correlation between the daily NAO and a domain-average precipitation greater than 4.4 mm (DPI > 1) for the winter seasons between 1954 and 1998.

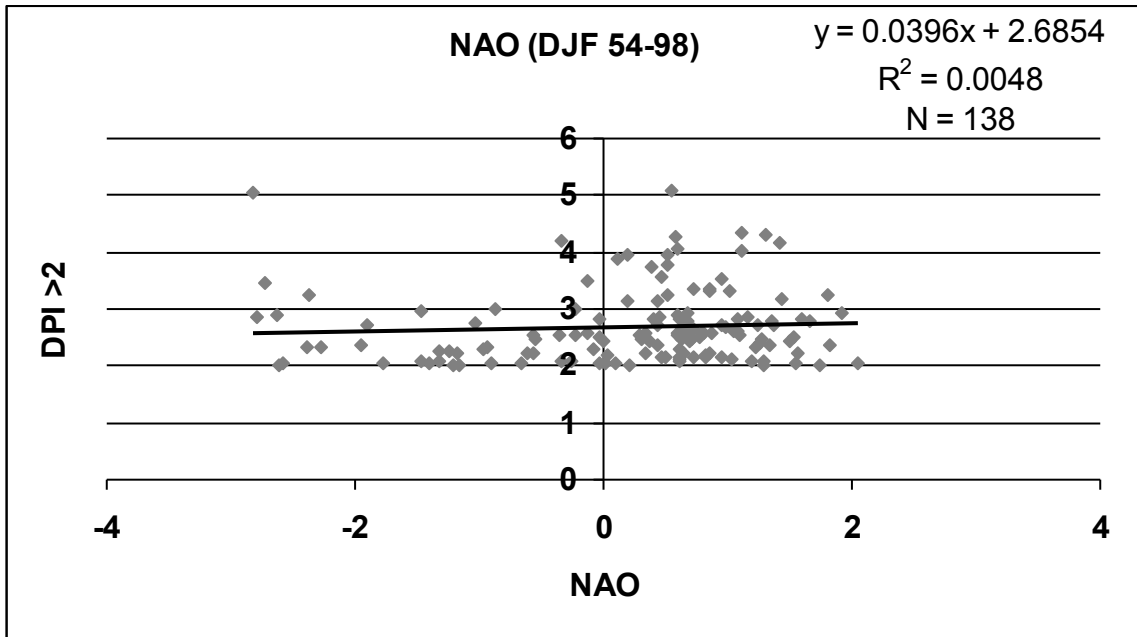


Fig. 3.8. Correlation between the daily NAO and a domain-average precipitation greater than 6.3 mm (DPI > 2) for the winter seasons between 1954 and 1998.

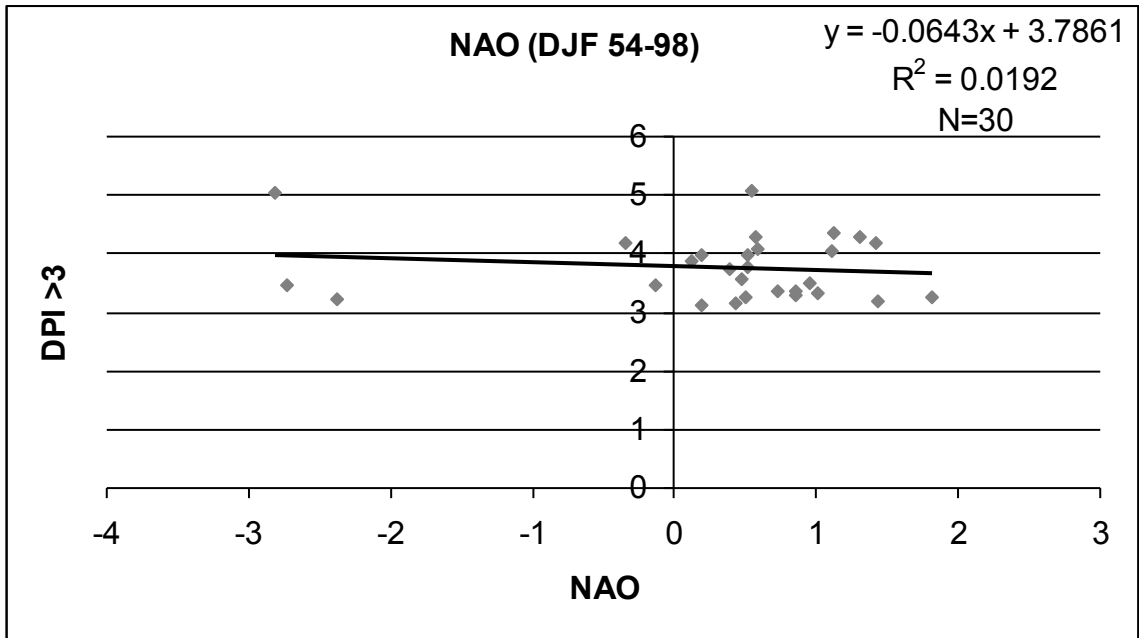


Fig. 3.9. Correlation between the daily NAO and a domain-average precipitation greater than 8.2 mm (DPI > 3) for the winter seasons between 1954 and 1998.

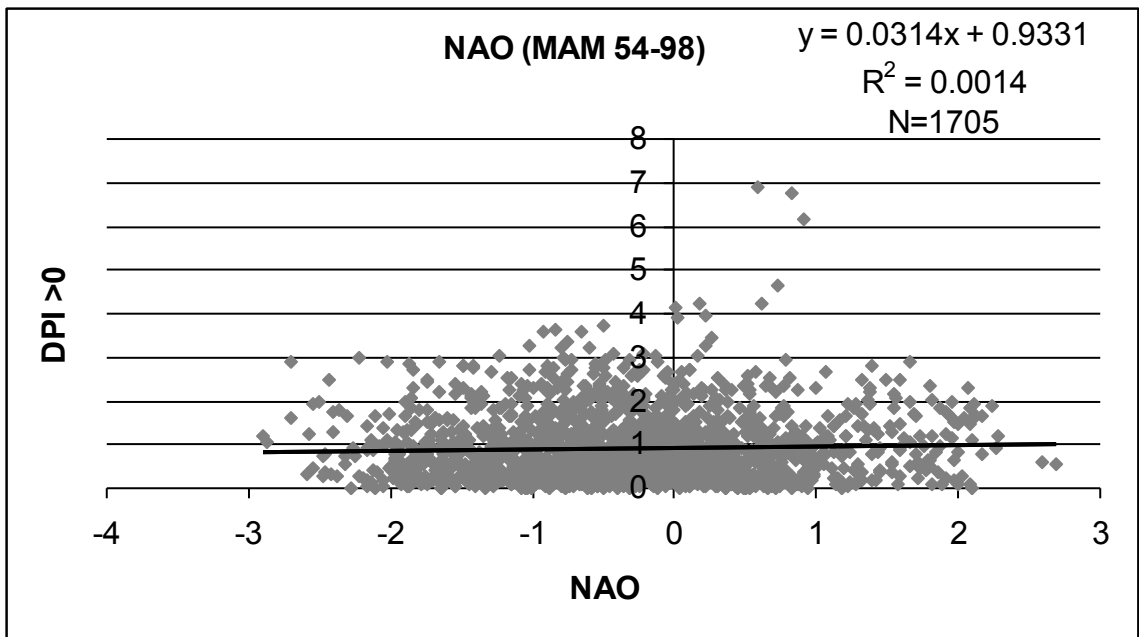


Fig. 3.10. Correlation between the daily NAO and a domain-average precipitation greater than 2.5 mm (DPI > 0) for the spring seasons between 1954 and 1998.

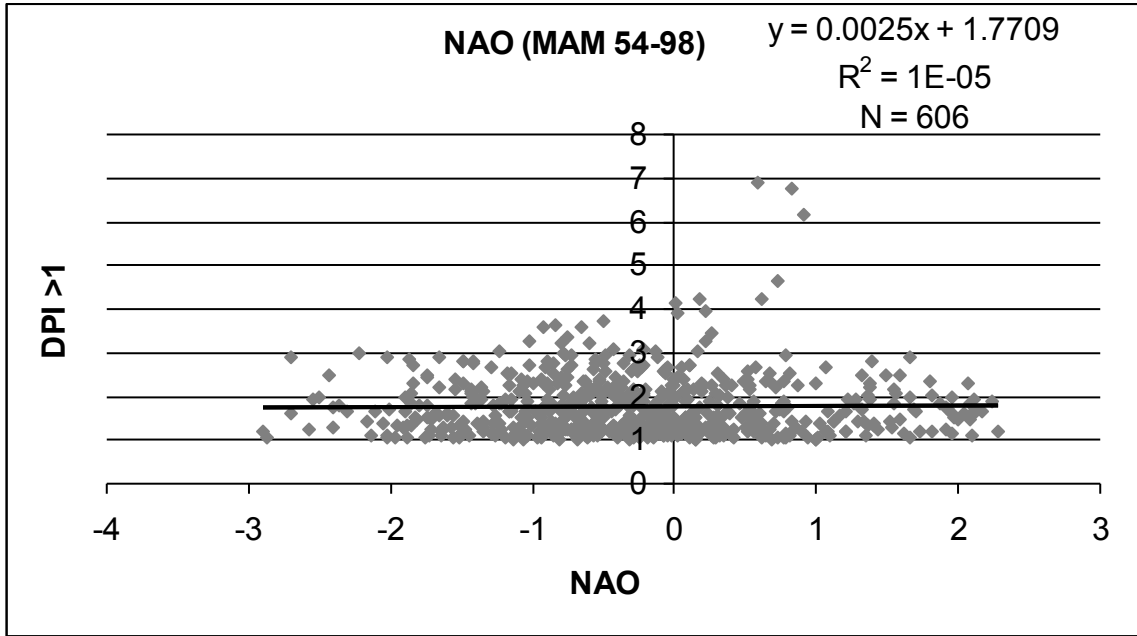


Fig. 3.11. Correlation between the daily NAO and a domain-average precipitation greater than 4.4 mm (DPI > 1) for the spring seasons between 1954 and 1998.

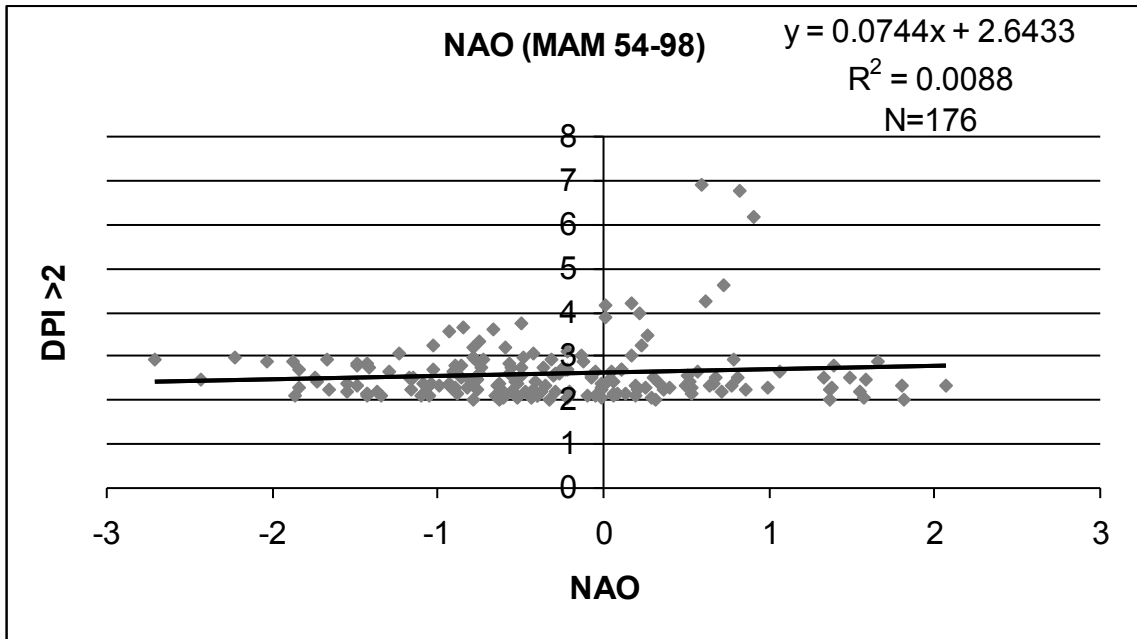


Fig. 3.12. Correlation between the daily NAO and a domain-average precipitation greater than 6.3 mm (DPI > 2) for the spring seasons between 1954 and 1998.

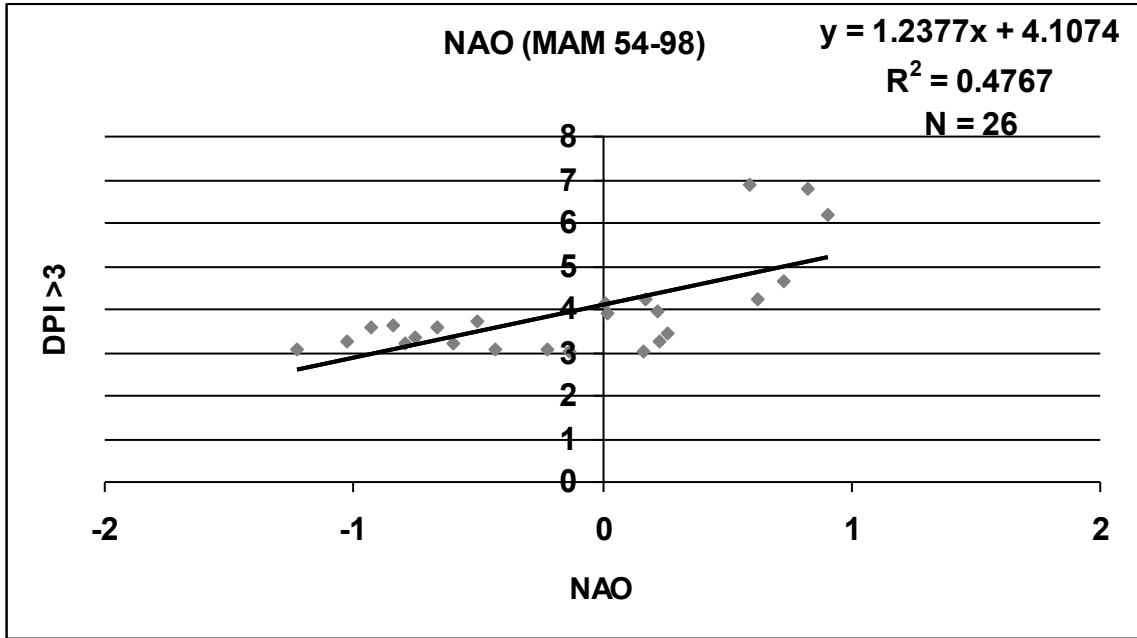


Fig. 3.13. Correlation between the daily NAO and a domain-average precipitation greater than 8.2 mm (DPI > 3) for the spring seasons between 1954 and 1998.

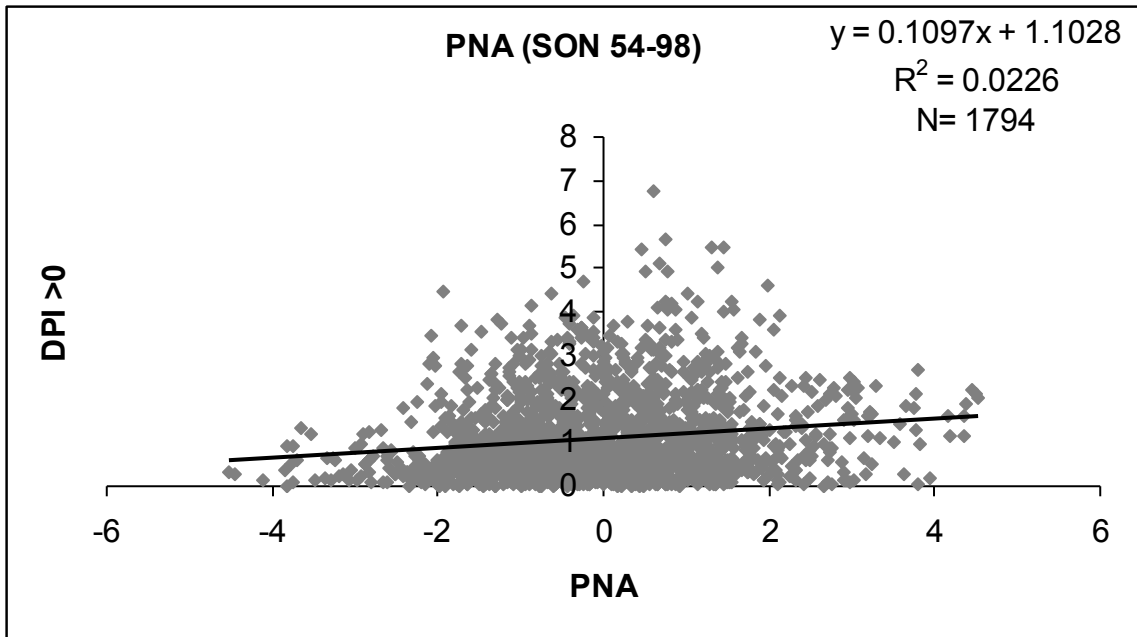


Fig. 3.14. Correlation between the daily PNA and a domain-average precipitation greater than 2.5 mm (DPI > 0) for the fall seasons between 1954 and 1998.

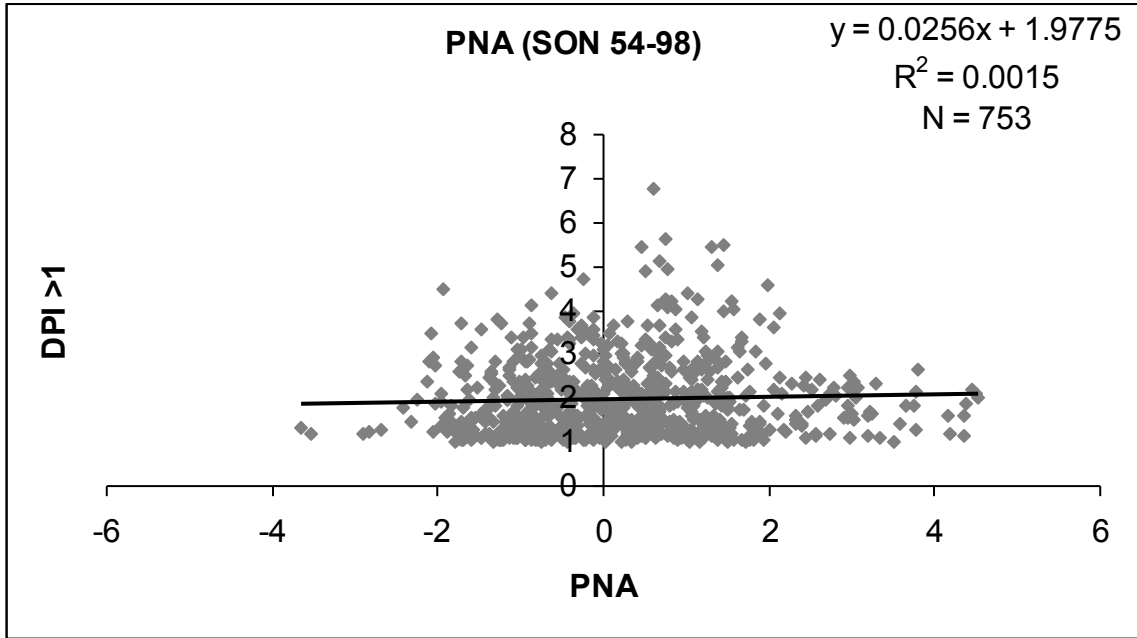


Fig. 3.15. Correlation between the daily PNA and a domain-average precipitation greater than 4.4 mm (DPI > 1) for the fall seasons between 1954 and 1998.

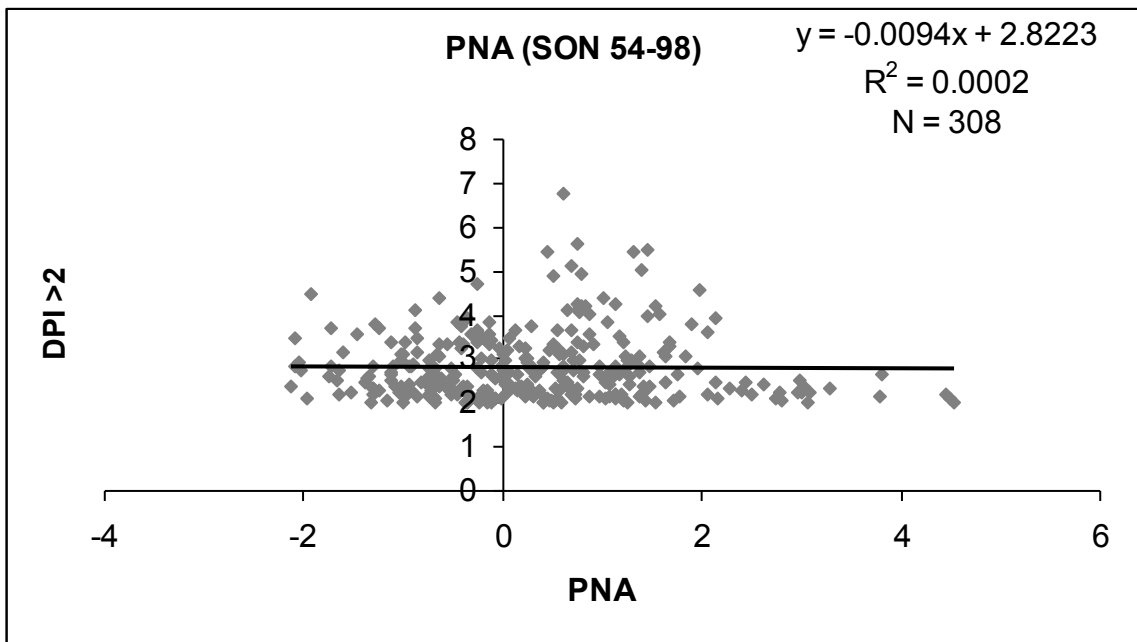


Fig. 3.16. Correlation between the daily PNA and a domain-average precipitation greater than 6.3 mm (DPI > 2) for the fall seasons between 1954 and 1998.

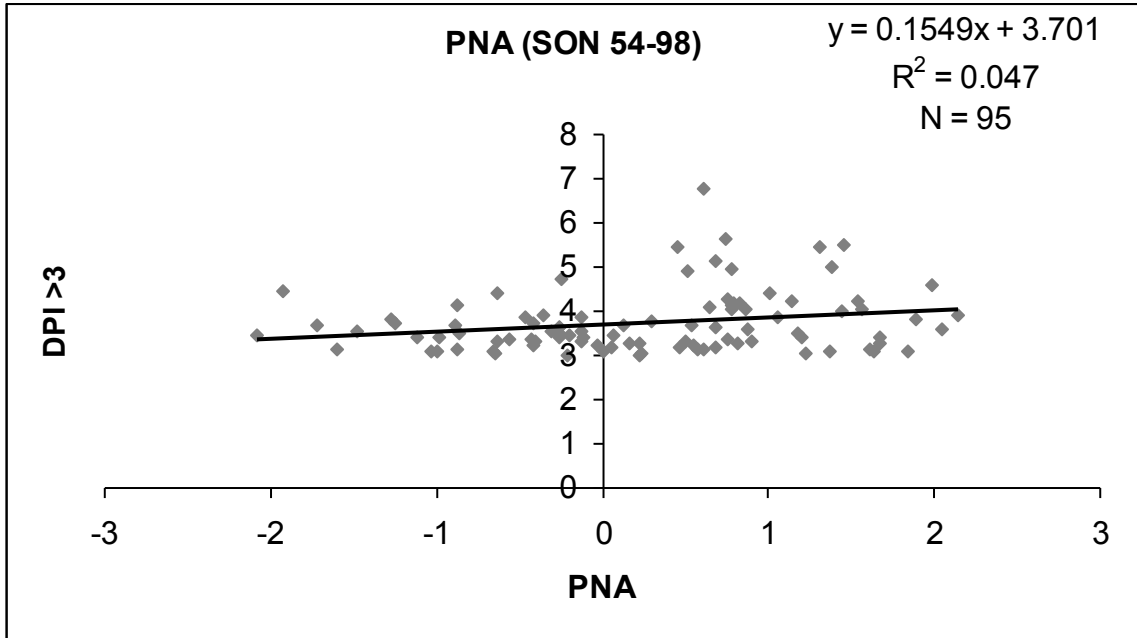


Fig. 3.17. Correlation between the daily PNA and a domain-average precipitation greater than 8.2 mm (DPI > 3) for the fall seasons between 1954 and 1998.

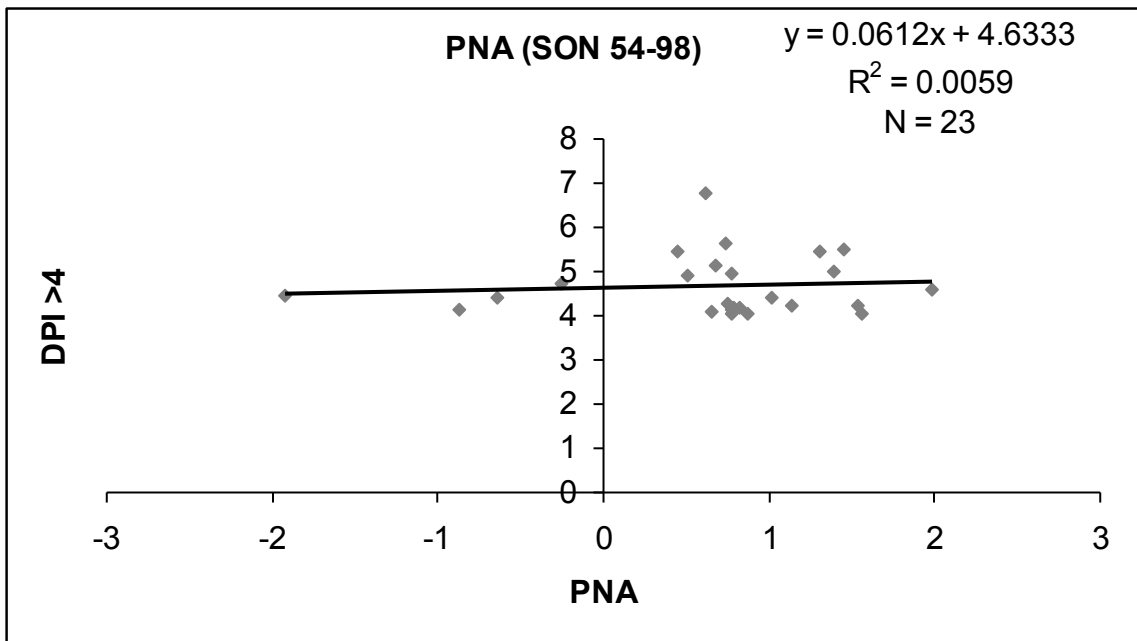


Fig. 3.18. Correlation between the daily PNA and a domain-average precipitation greater than 10.1 mm (DPI > 4) for the fall seasons between 1954 and 1998.

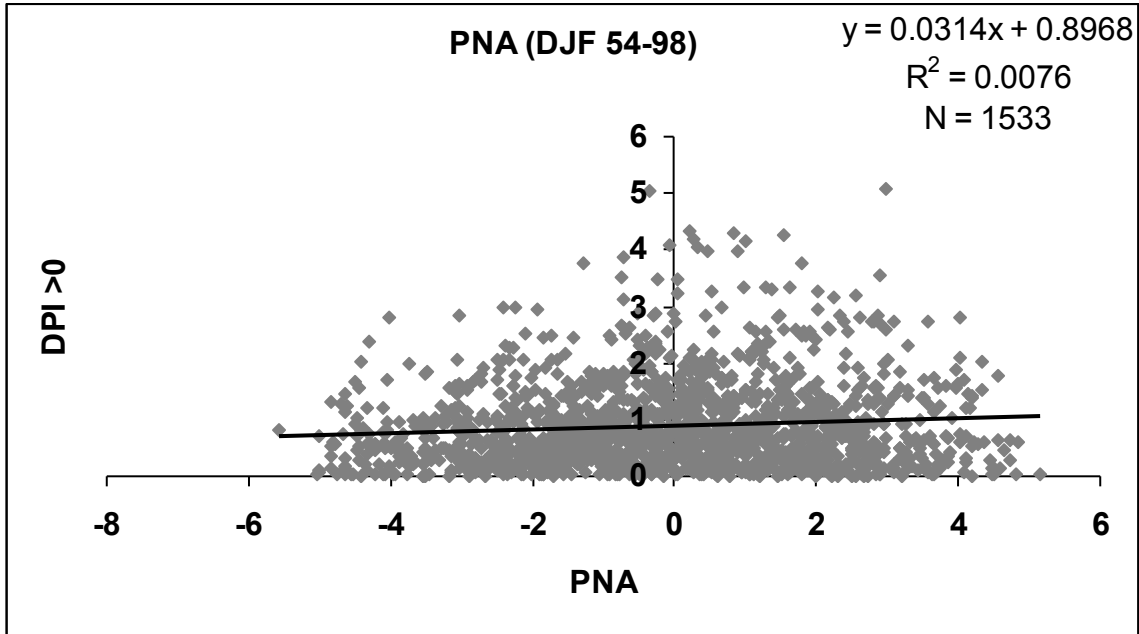


Fig. 3.19. Correlation between the daily PNA and a domain-average precipitation greater than 2.5 mm (DPI > 0) for the winter seasons between 1954 and 1998.

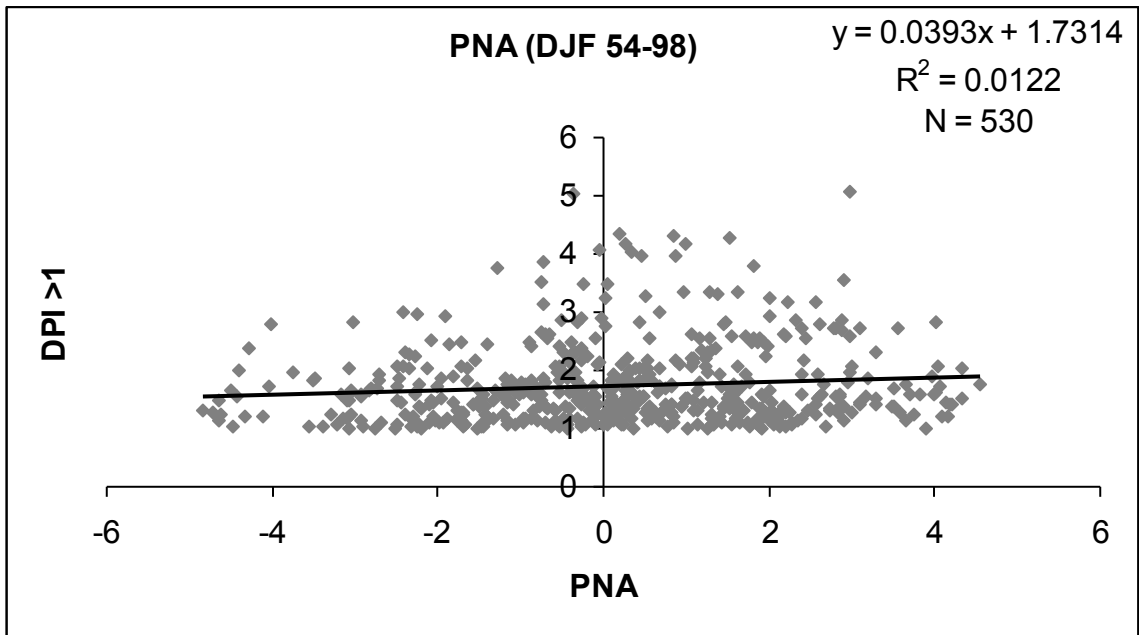


Fig. 3.20. Correlation between the daily PNA and a domain-average precipitation greater than 4.4 mm (DPI > 1) for the winter seasons between 1954 and 1998.

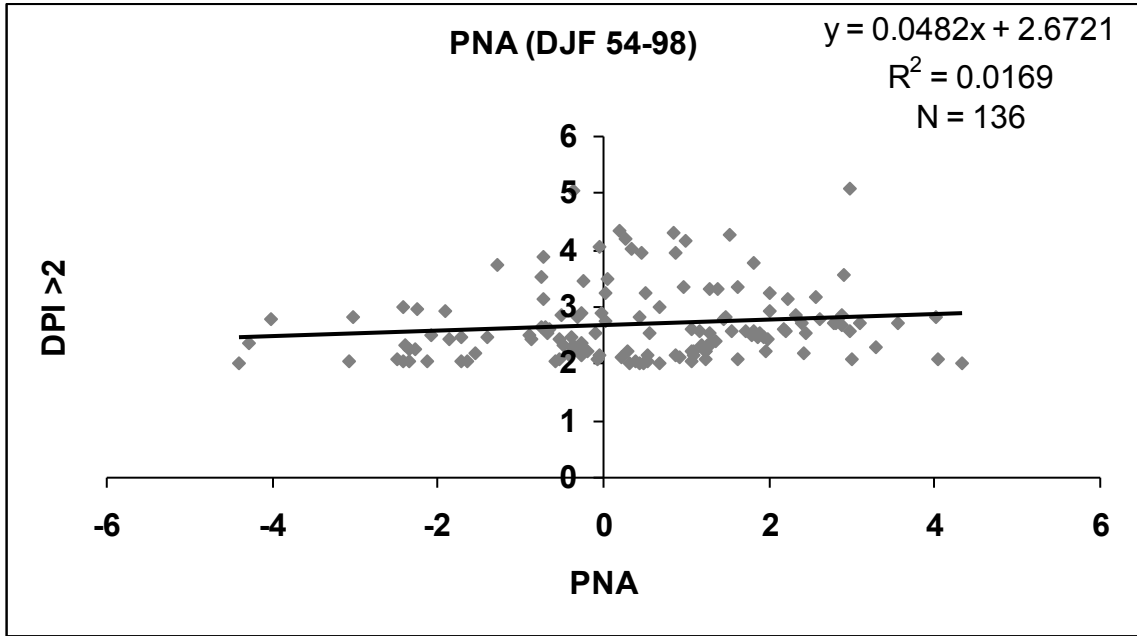


Fig. 3.21. Correlation between the daily PNA and a domain-average precipitation greater than 6.3 mm (DPI > 2) for the winter seasons between 1954 and 1998.

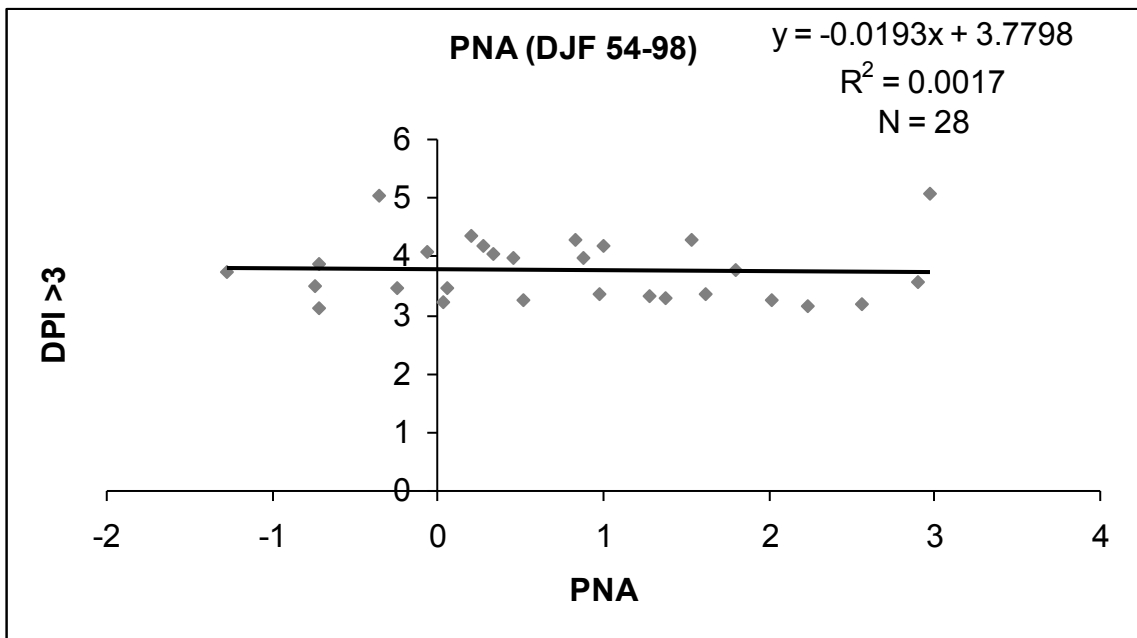


Fig. 3.22. Correlation between the daily PNA and a domain-average precipitation greater than 8.2 mm (DPI > 3) for the winter seasons between 1954 and 1998.

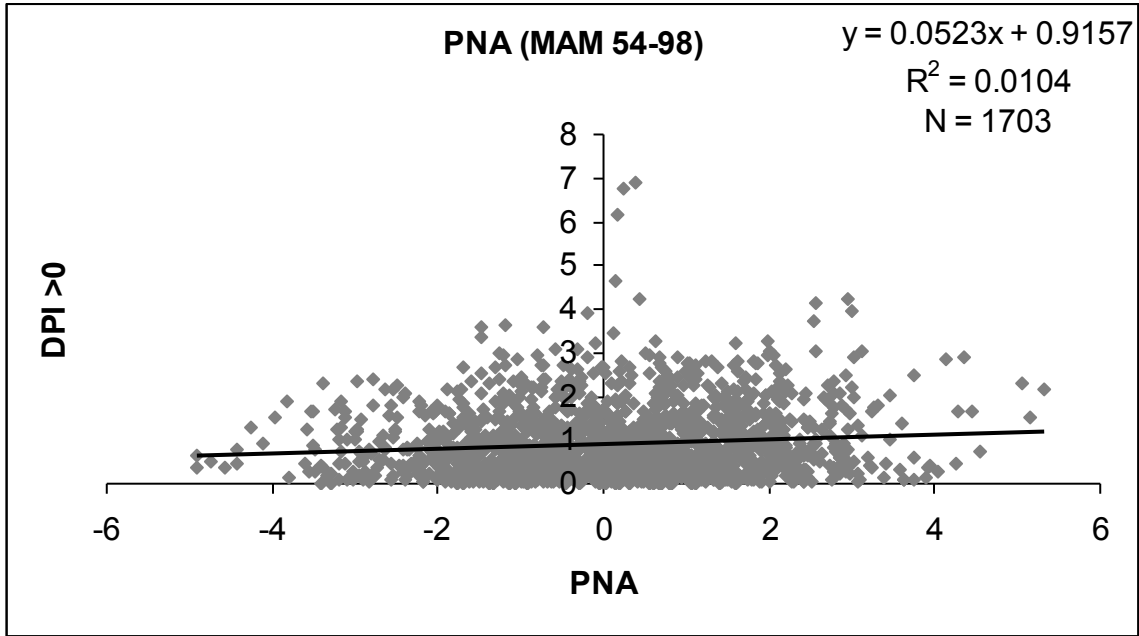


Fig. 3.23. Correlation between the daily PNA and a domain-average precipitation greater than 2.5 mm (DPI > 0) for the spring seasons between 1954 and 1998.

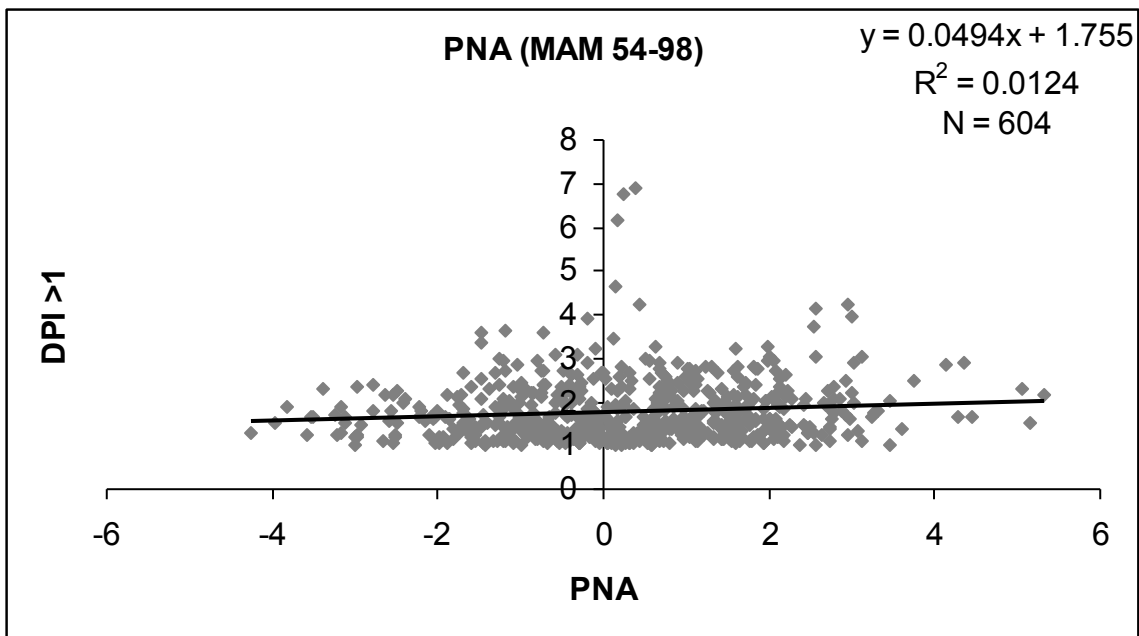


Fig. 3.24. Correlation between the daily PNA and a domain-average precipitation greater than 4.4 mm (DPI > 1) for the spring seasons between 1954 and 1998.

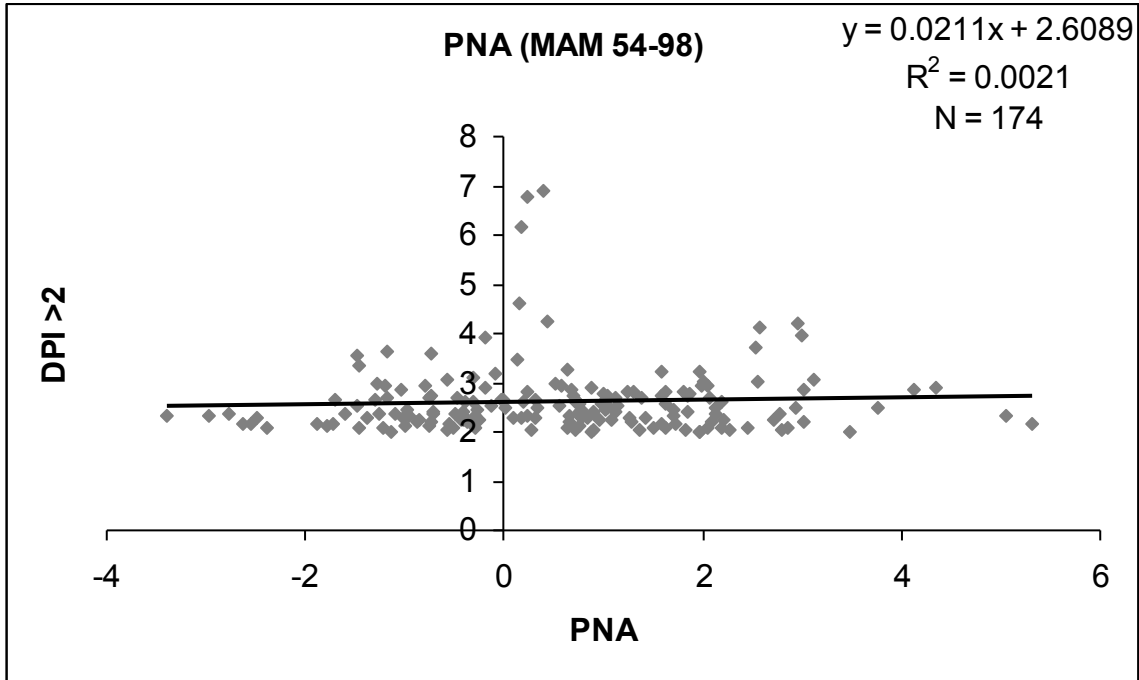


Fig. 3.25. Correlation between the daily PNA and a domain-average precipitation greater than 6.3 mm (DPI > 2) for the spring seasons between 1954 and 1998.

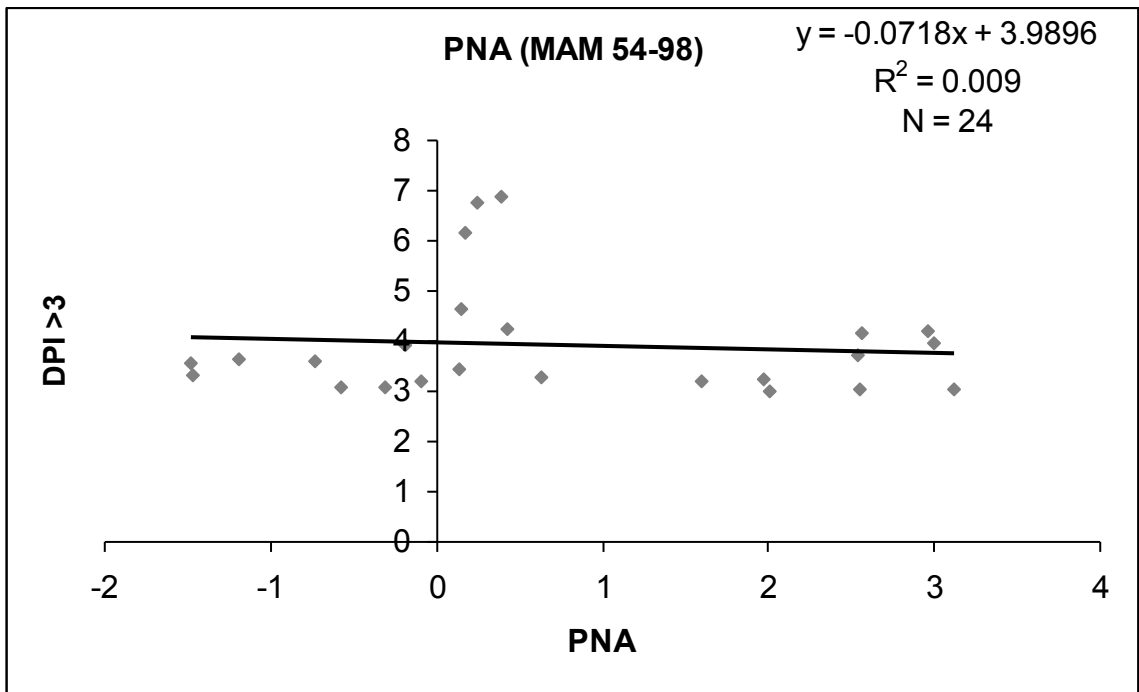


Fig. 3.26. Correlation between the daily PNA and a domain-average precipitation greater than 8.2 mm (DPI > 3) for the spring seasons between 1954 and 1998.

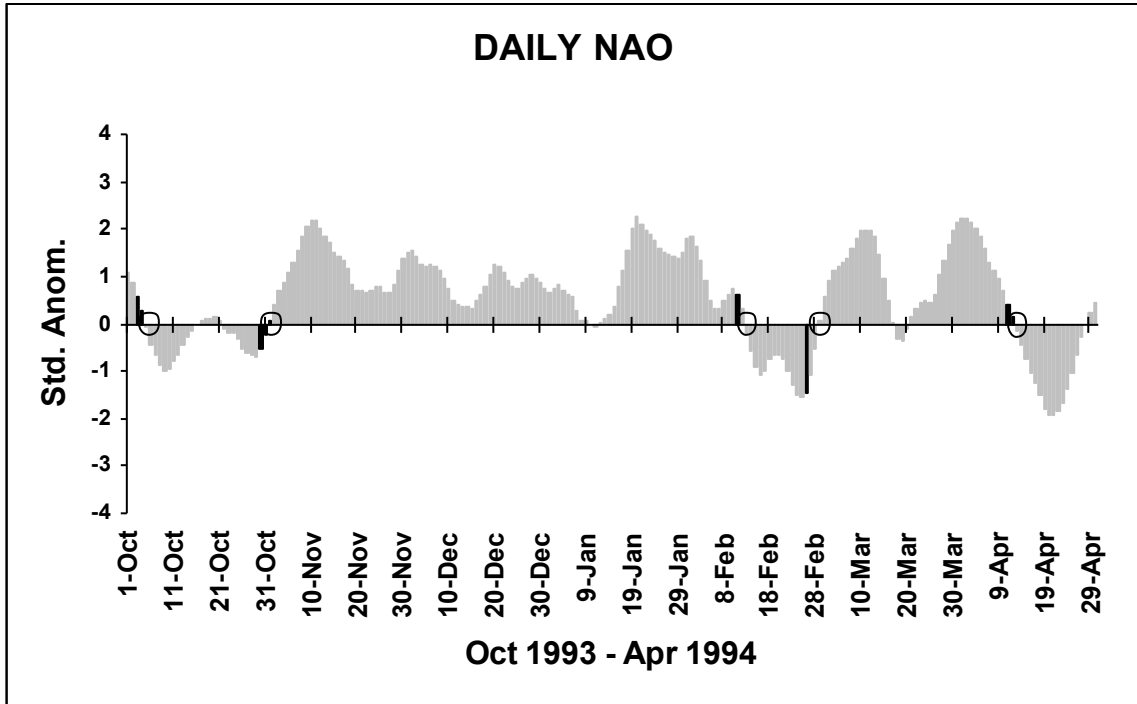


Fig. 3.27. Daily NAO index during 1993–1994 cool season with transitions circled in black and days with a daily domain-average precipitation greater than 2.5 mm ($DPI > 0$) highlighted in black.

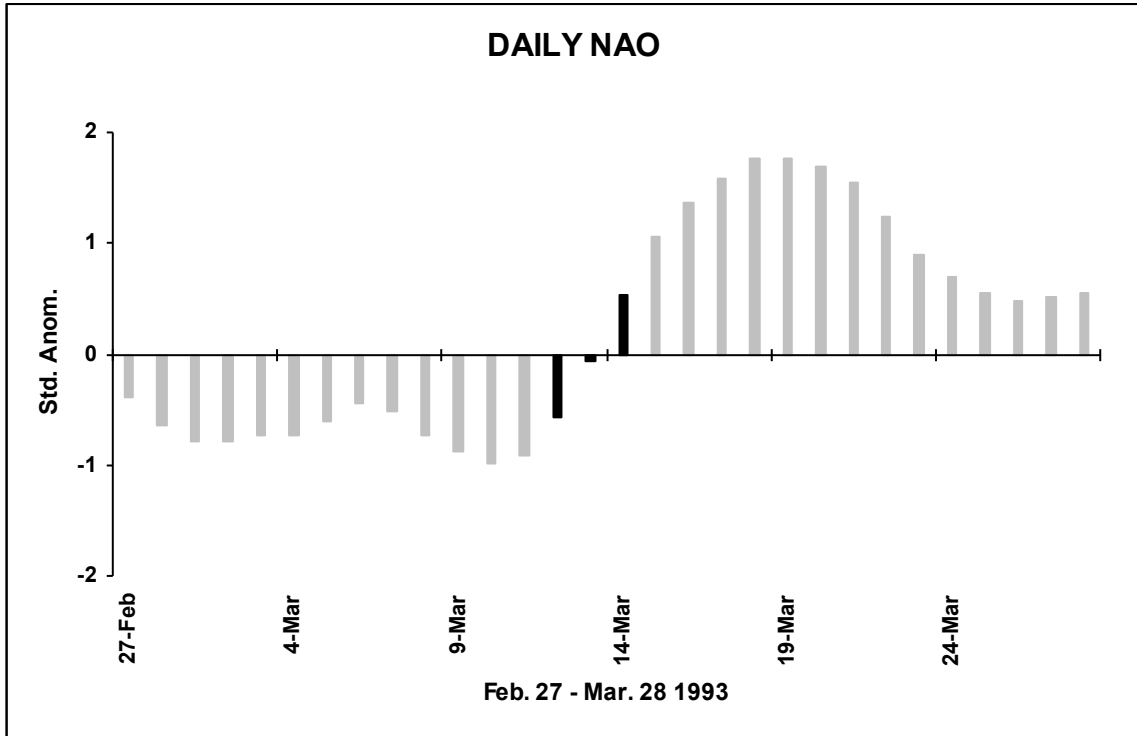


Fig. 3.28a. Daily NAO index with the 12–14 March 1993 “Superstorm” highlighted in black.

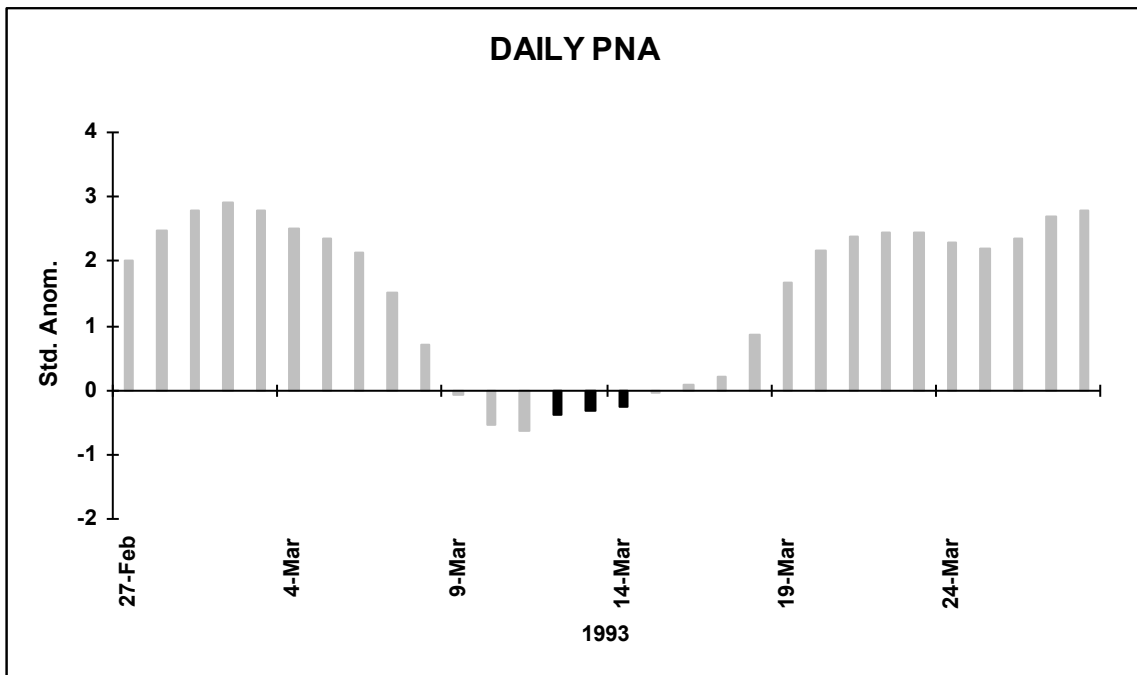


Fig. 3.28b. Daily PNA index with the 12–14 March 1993 “Superstorm” highlighted in black.

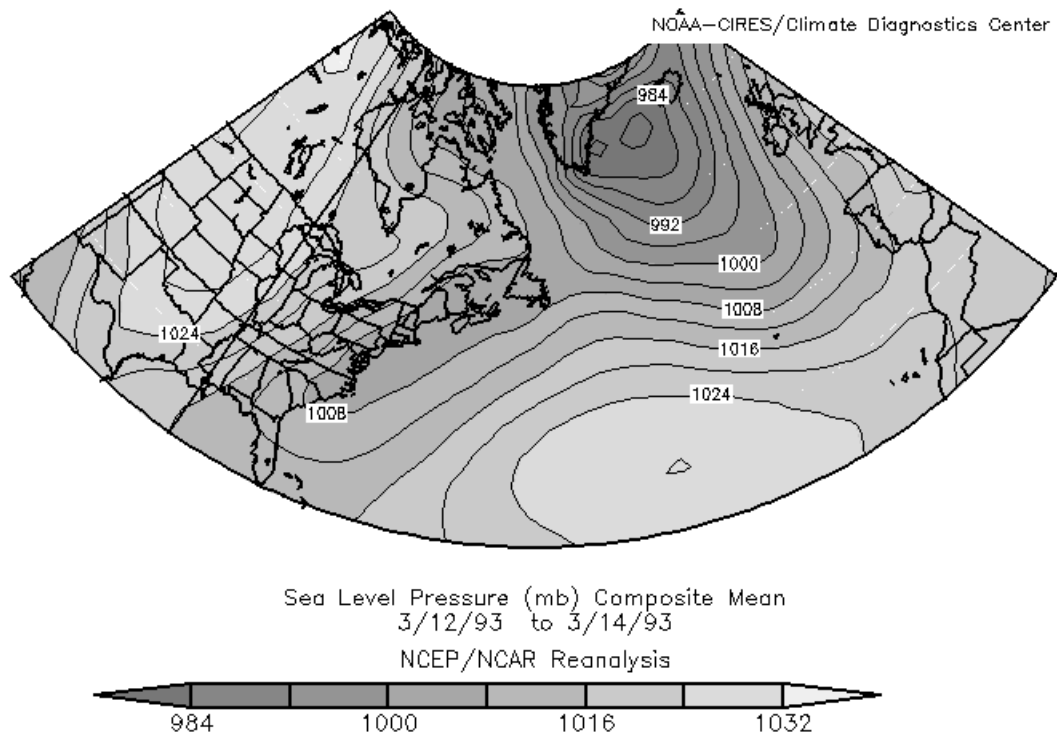


Fig. 3.29a. Sea-level pressure map (mb) for the 12–14 March 1993 “Superstorm.”

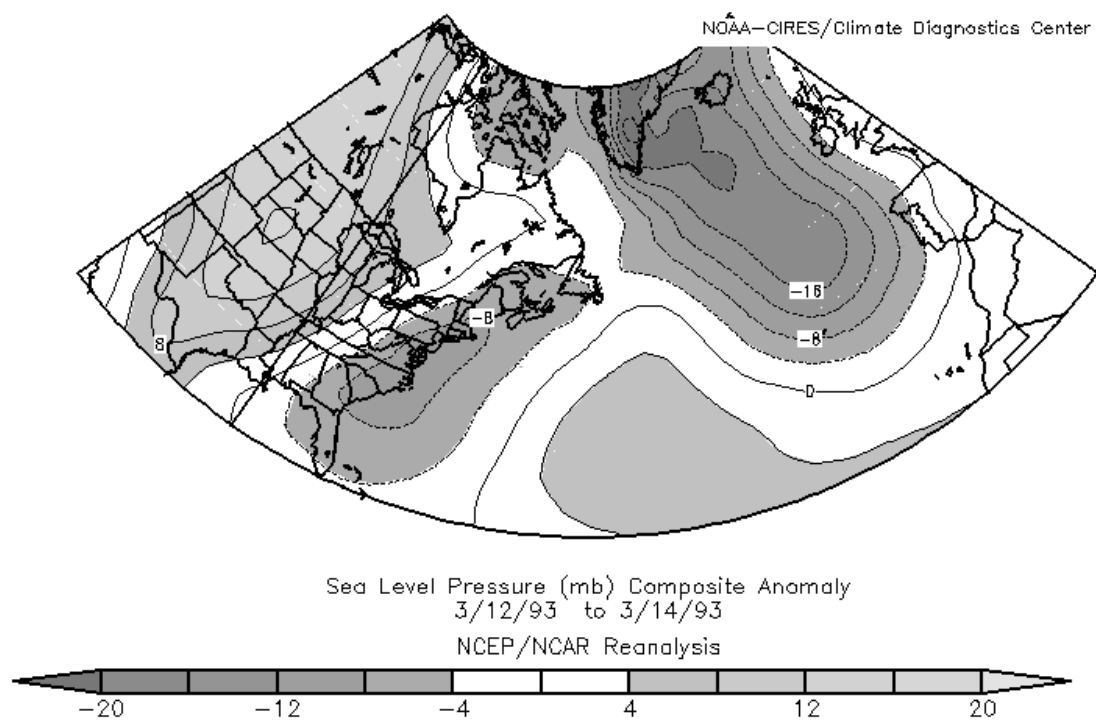


Fig. 3.29b. Sea-level pressure anomaly map (mb) for the 12–14 March 1993 “Superstorm”.

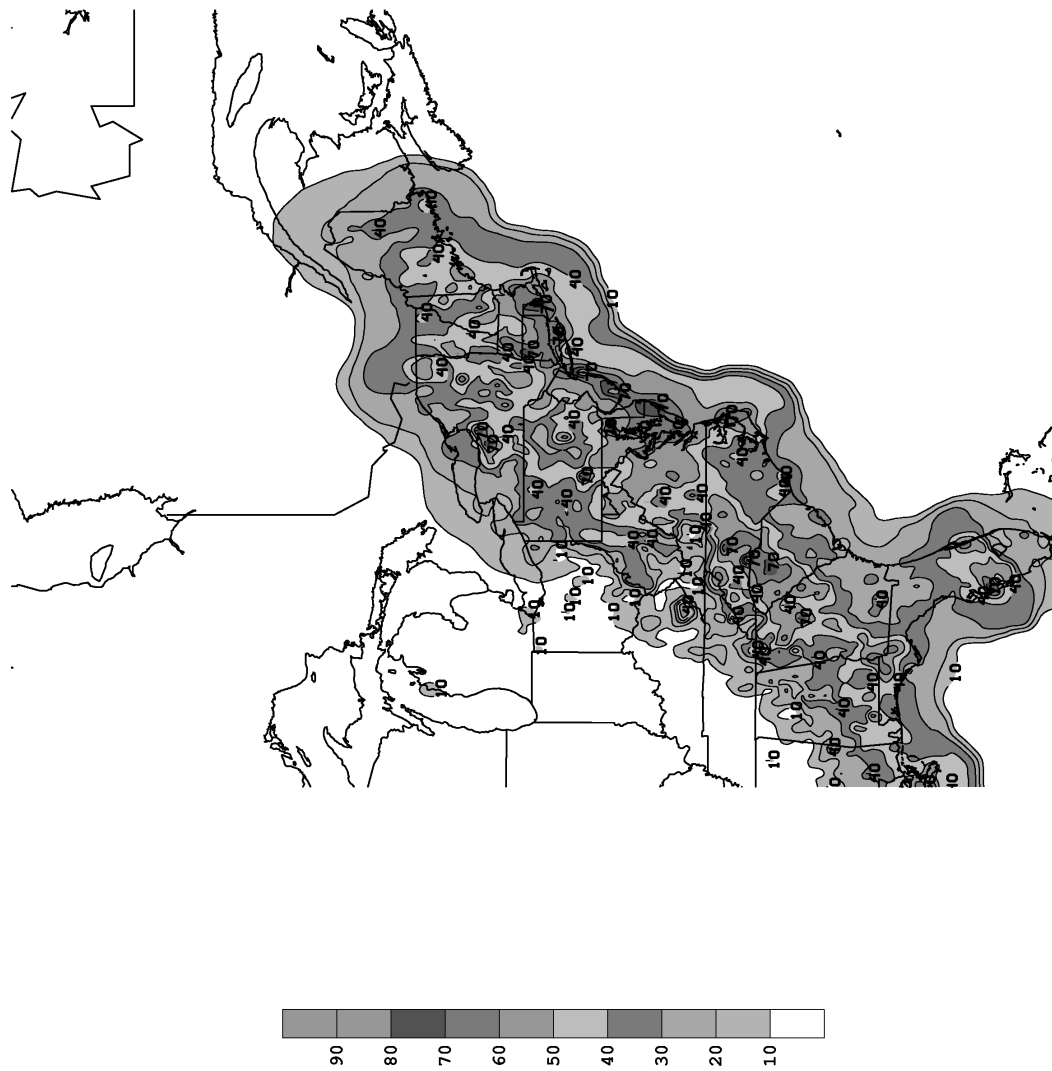


Fig. 3.30. Precipitation total (mm) starting at 1200 UTC on 12 March and ending at 1200 UTC on 15 March 1993.

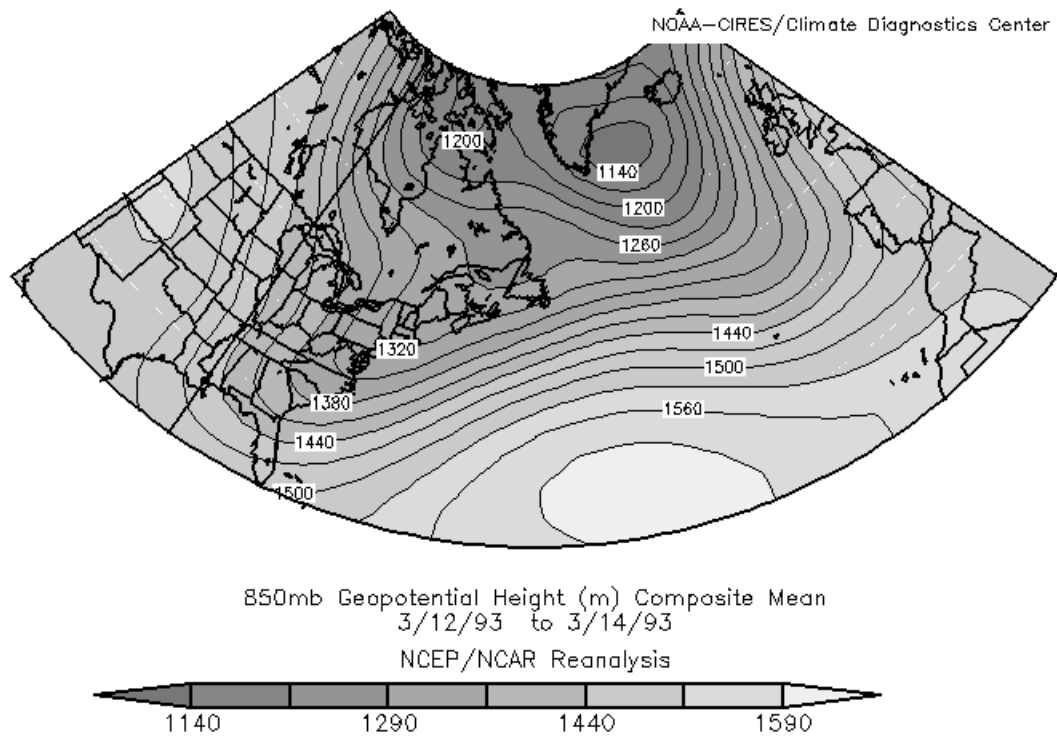


Fig. 3.31a. 850 mb geopotential height map (m) for the 12–14 March 1993 “Superstorm.”

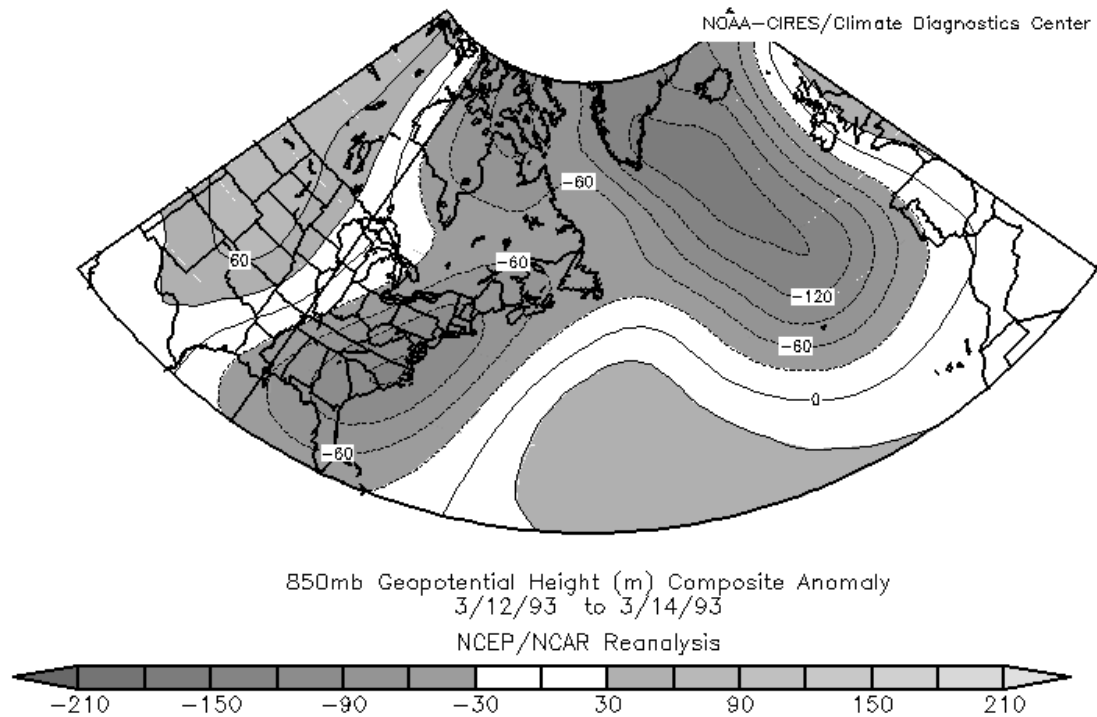


Fig. 3.31b. 850 mb geopotential height anomaly map (m) for the 12–14 March 1993 “Superstorm.”

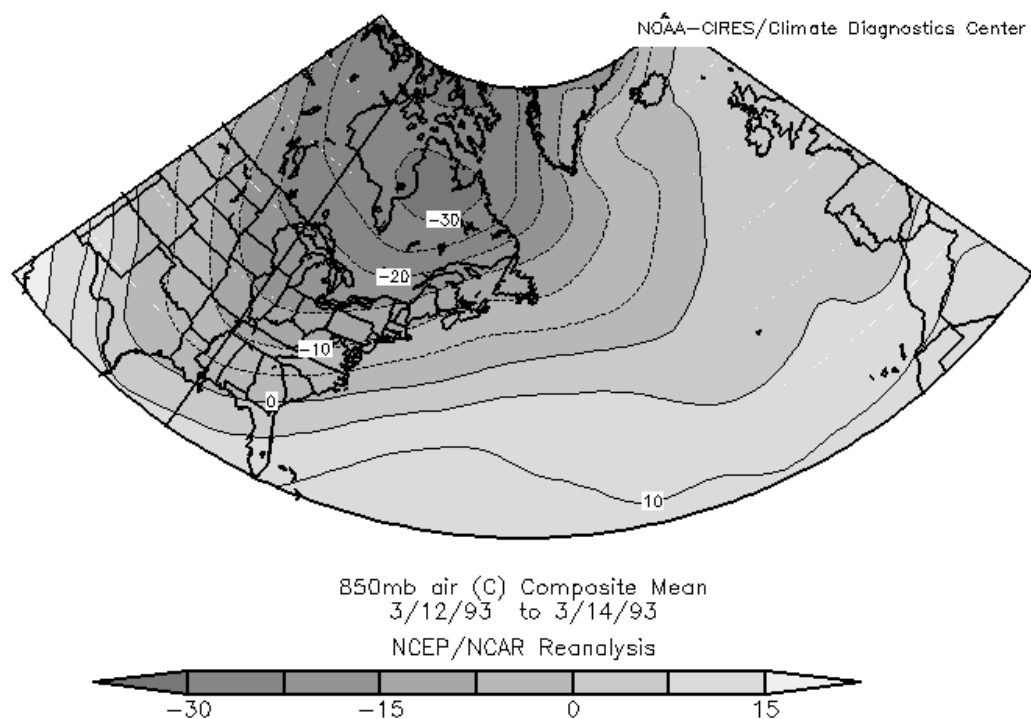


Fig. 3.32a. 850 mb temperature map (°C) for the 12–14 March 1993 “Superstorm.”

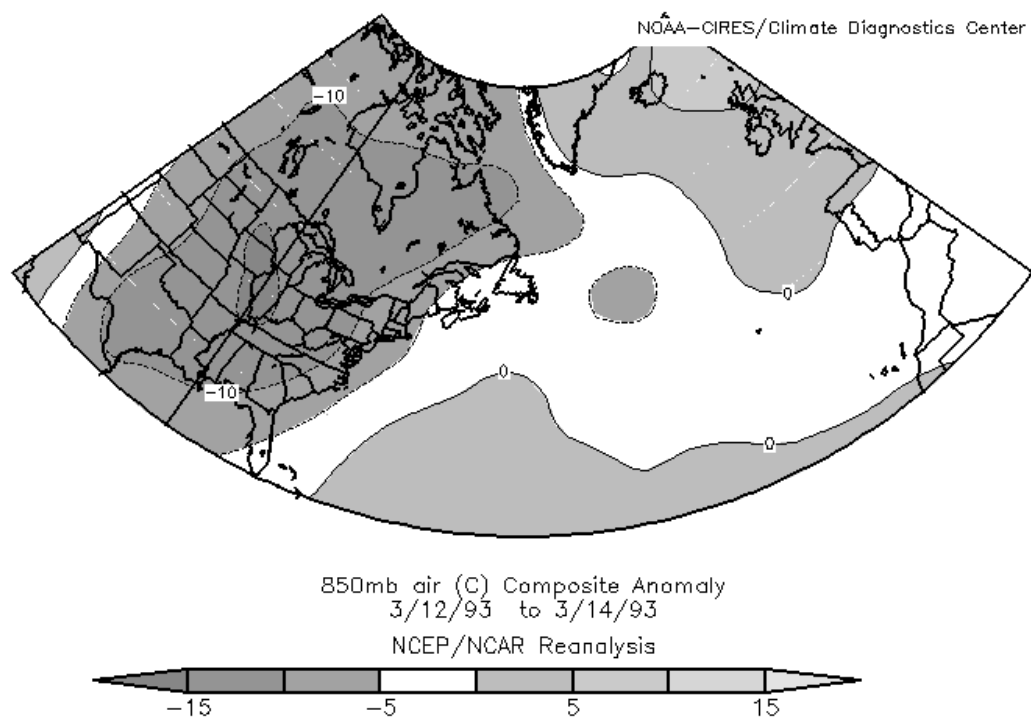


Fig. 3.32b. 850 mb temperature anomaly map (°C) for the 12–14 March 1993 “Superstorm.”

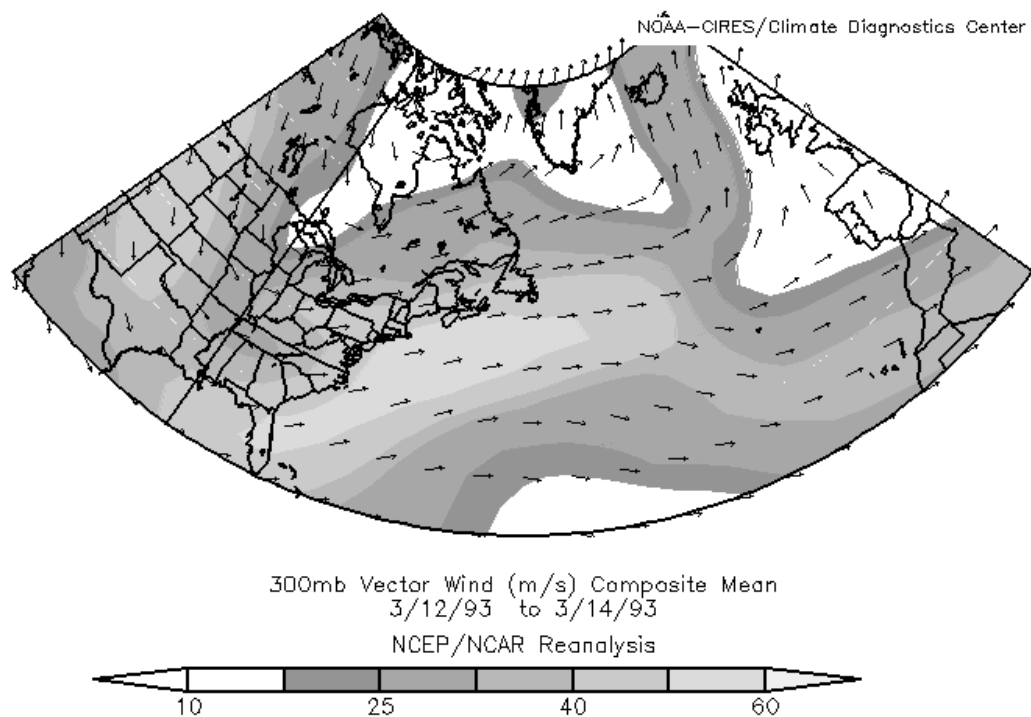


Fig. 3.33a. 300 mb vector wind map (m s^{-1}) for the 12–14 March 1993 “Superstorm.”

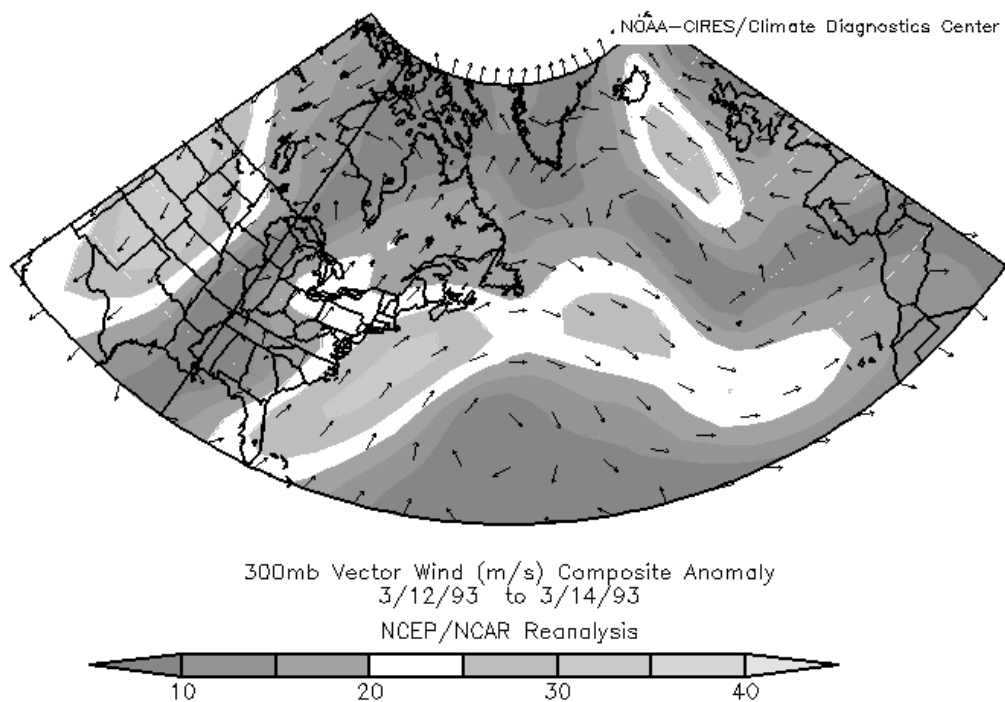


Fig. 3.33b. 300 mb vector wind map (m s^{-1}) for the 12–14 March 1993 “Superstorm.”

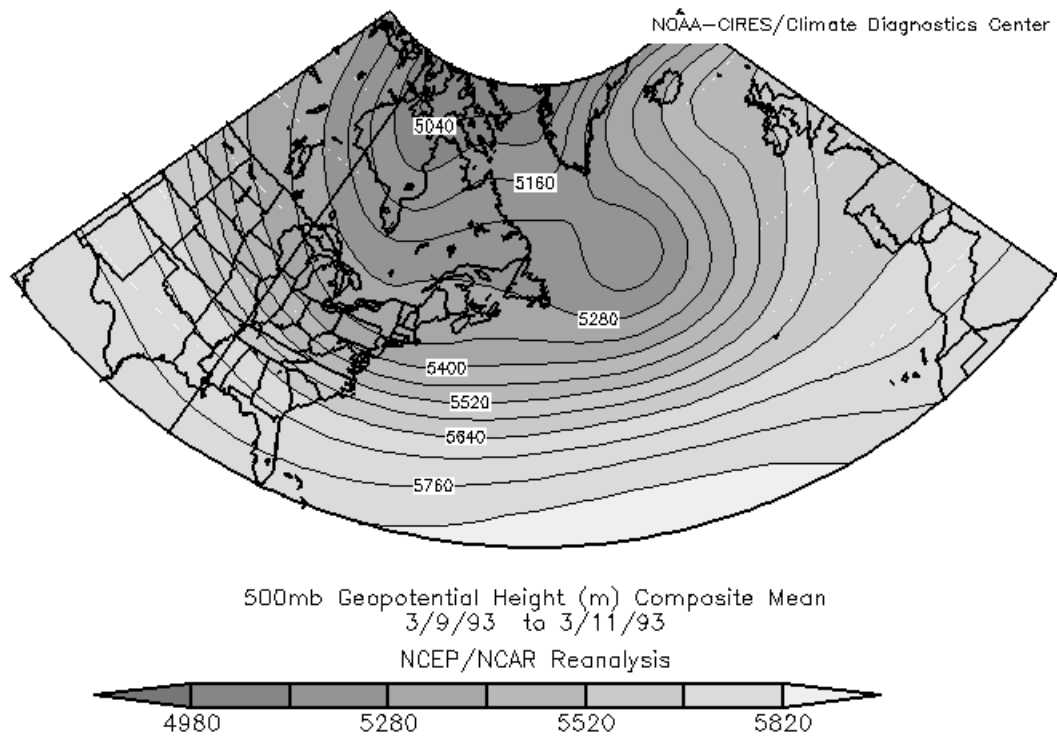


Fig. 3.34a. 500 mb geopotential height map (m) covering the two NAO domains prior to the 12–14 March 1993 “Superstorm.”

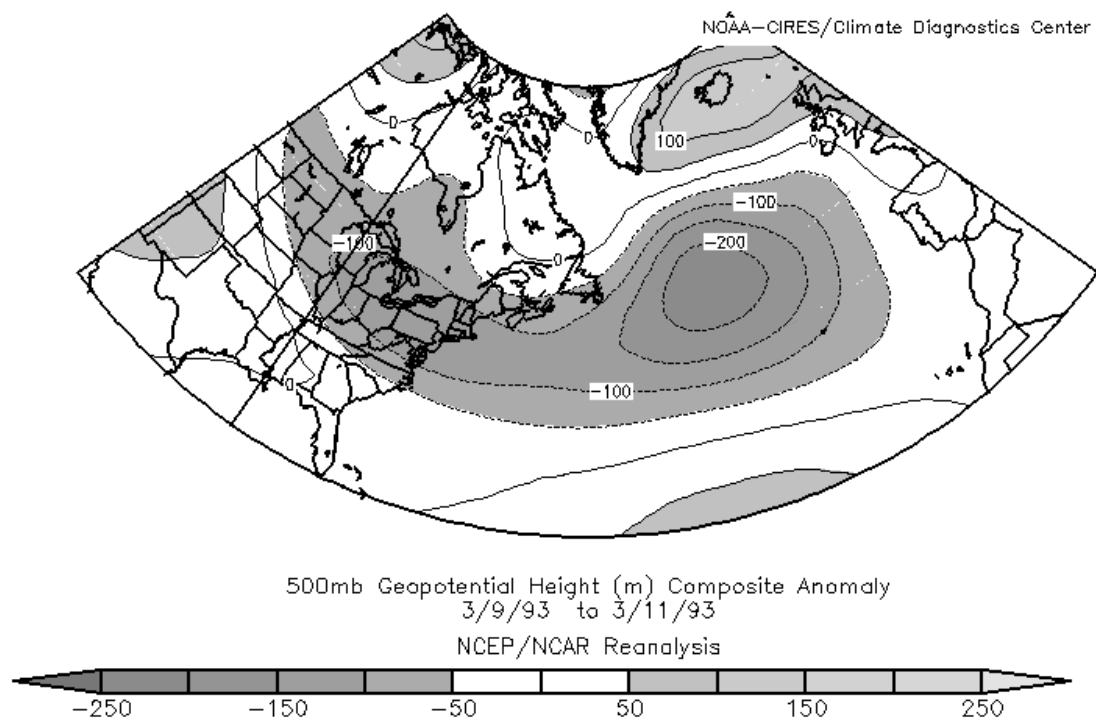
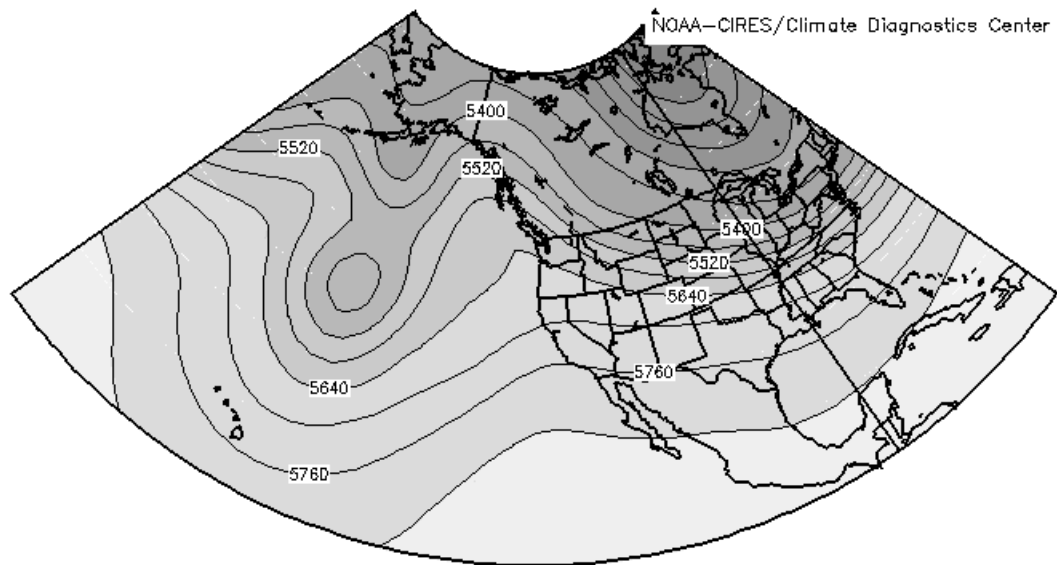


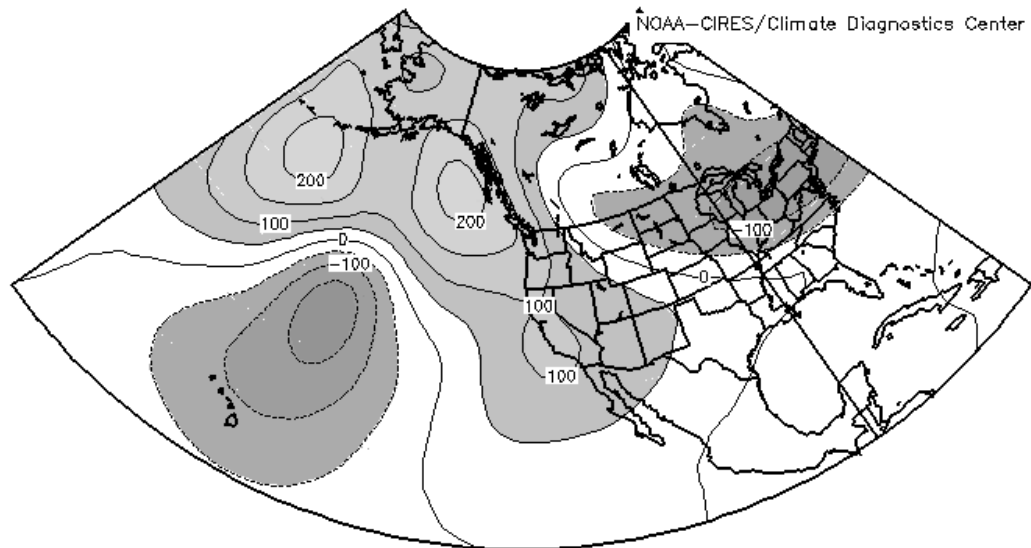
Fig. 3.34b. 500 mb geopotential height anomaly map (m) covering the two NAO domains prior to the 12–14 March 1993 “Superstorm.”



500mb Geopotential Height (m) Composite Mean
3/9/93 to 3/11/93
NCEP/NCAR Reanalysis



Fig. 3.35a. 500 mb geopotential height map (m) covering the four PNA domains prior to the 12–14 March 1993 “Superstorm.”



500mb Geopotential Height (m) Composite Anomaly
3/9/93 to 3/11/93
NCEP/NCAR Reanalysis

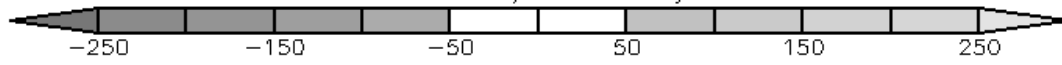


Fig. 3.35b. 500 mb geopotential height anomaly map (m) covering the four PNA domains prior to the 12–14 March 1993 “Superstorm.”

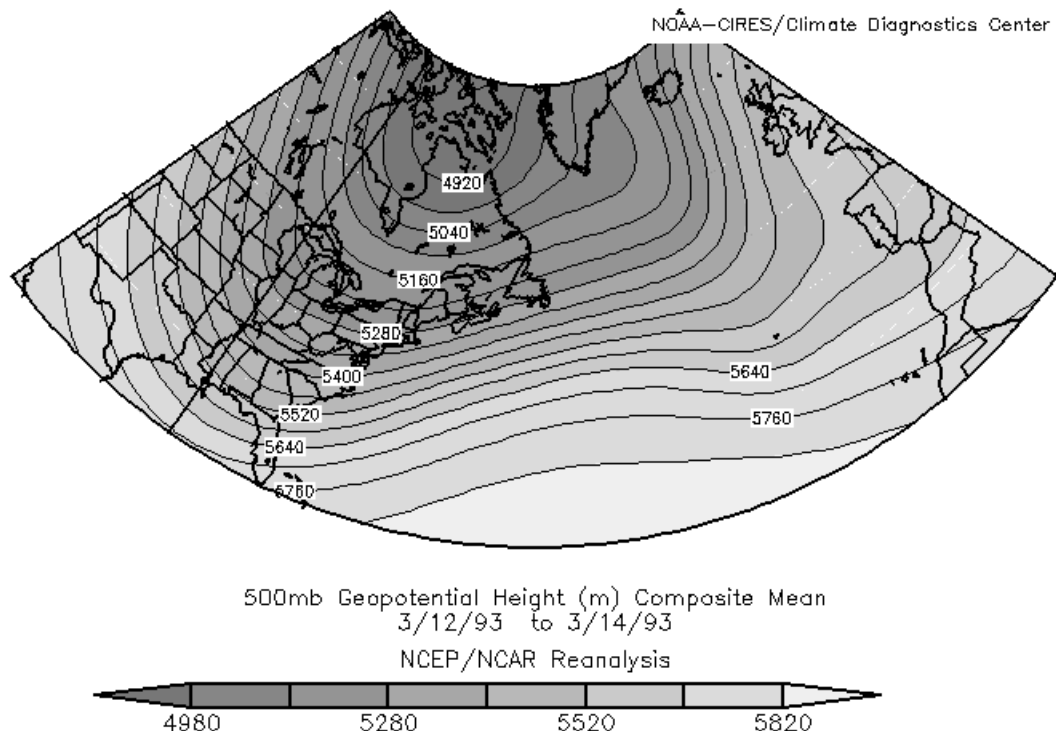


Fig. 3.36a. 500 mb geopotential height map (m) covering the two NAO domains during the 12–14 March 1993 “Superstorm.”

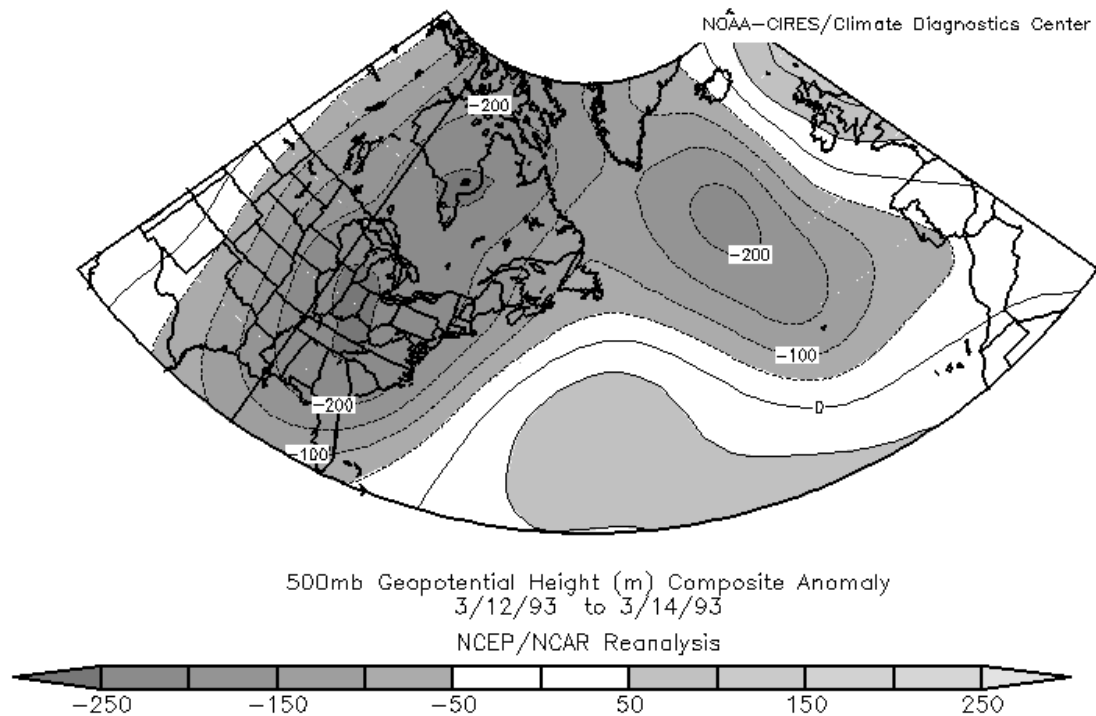


Fig. 3.36b. 500 mb geopotential height anomaly map (m) covering the two NAO domains during the 12–14 March 1993 “Superstorm.”

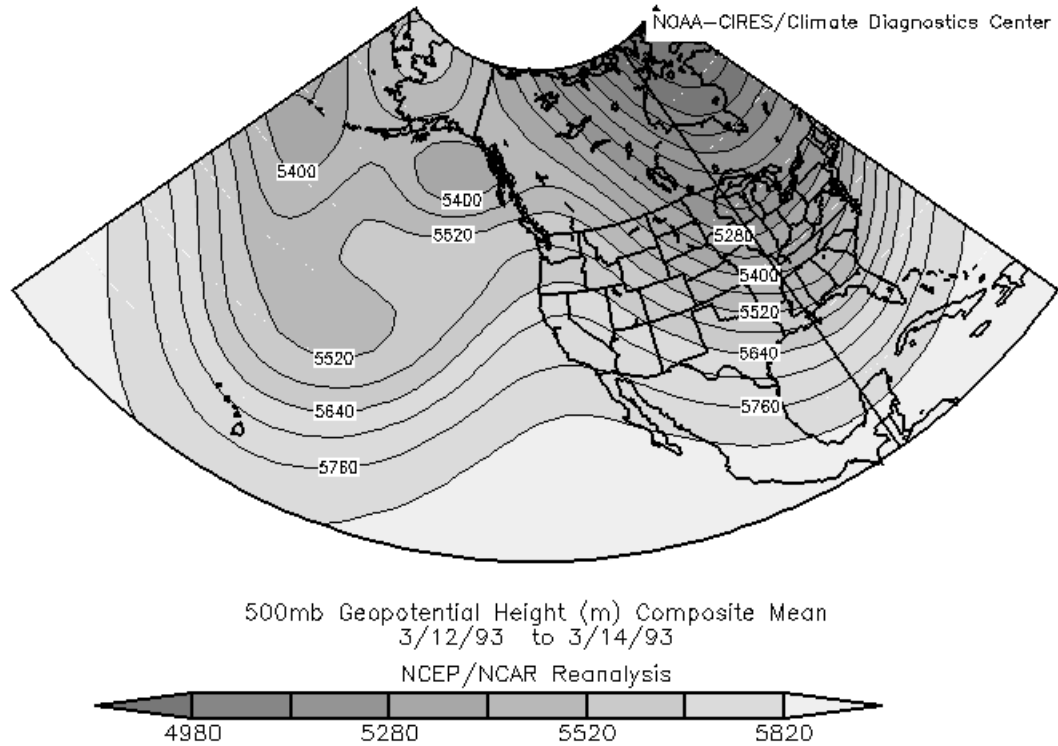


Fig. 3.37b. 500 mb geopotential height anomaly map (m) covering the four PNA domains during the 12–14 March 1993 “Superstorm.”

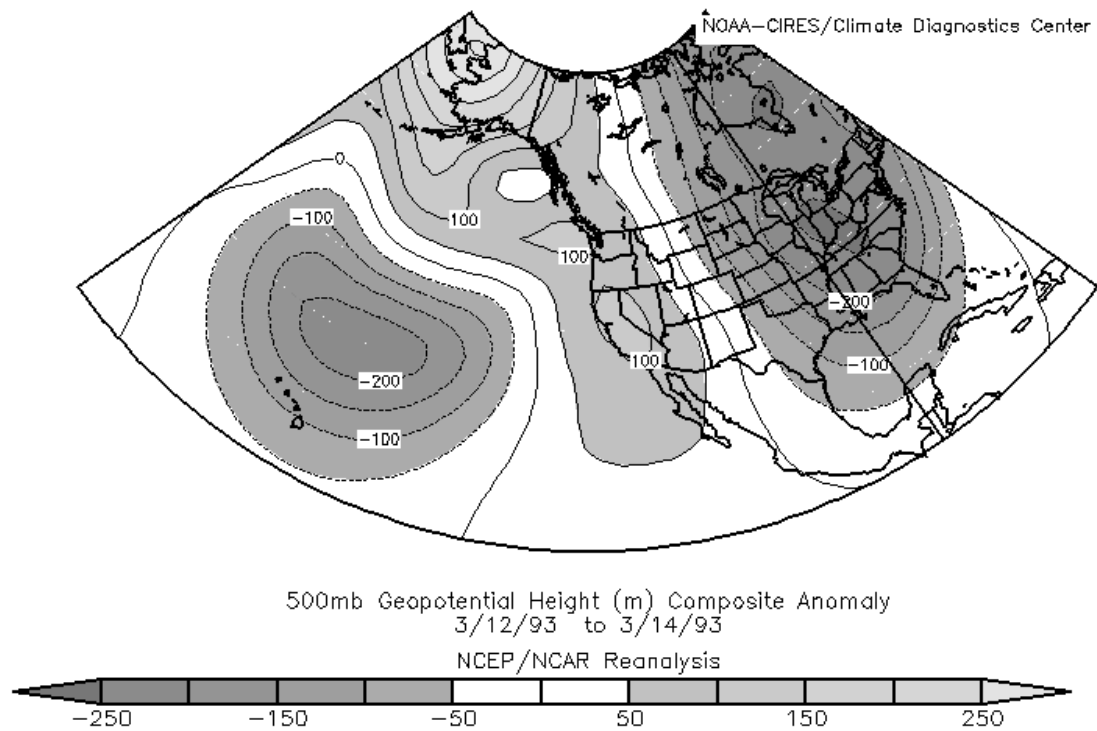


Fig. 3.37b. 500 mb geopotential height anomaly map (m) covering the four PNA domains during the 12–14 March 1993 “Superstorm.”

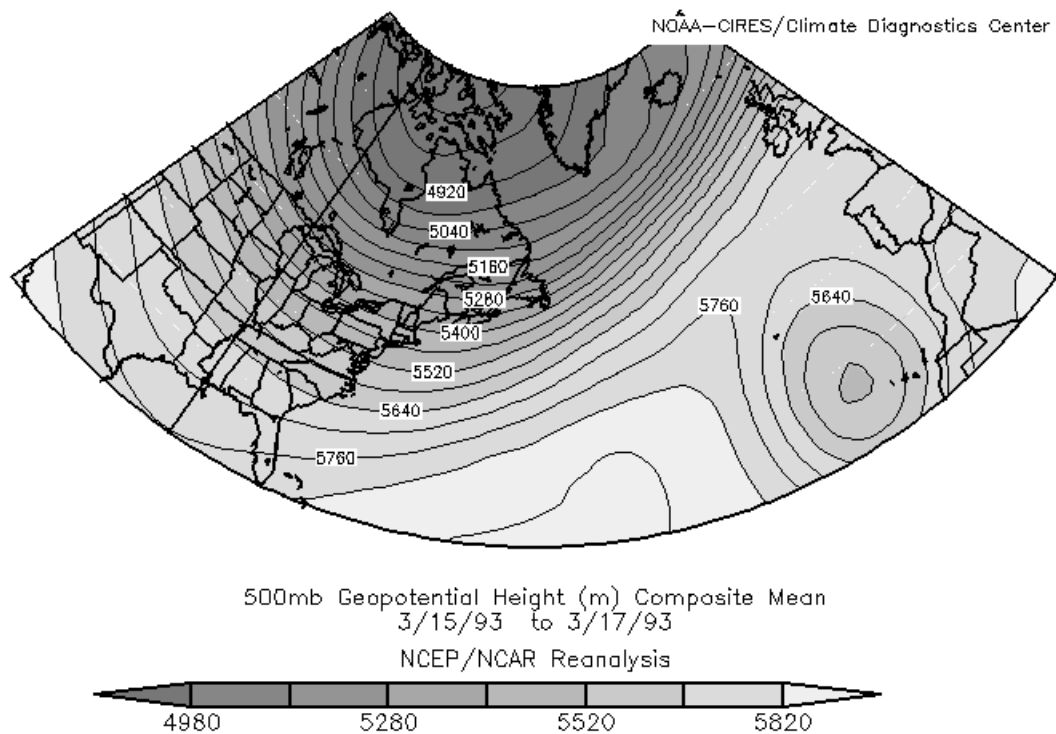


Fig. 3.38a. 500 mb geopotential height map (m) covering the two NAO domains after the 12–14 March 1993 “Superstorm.”

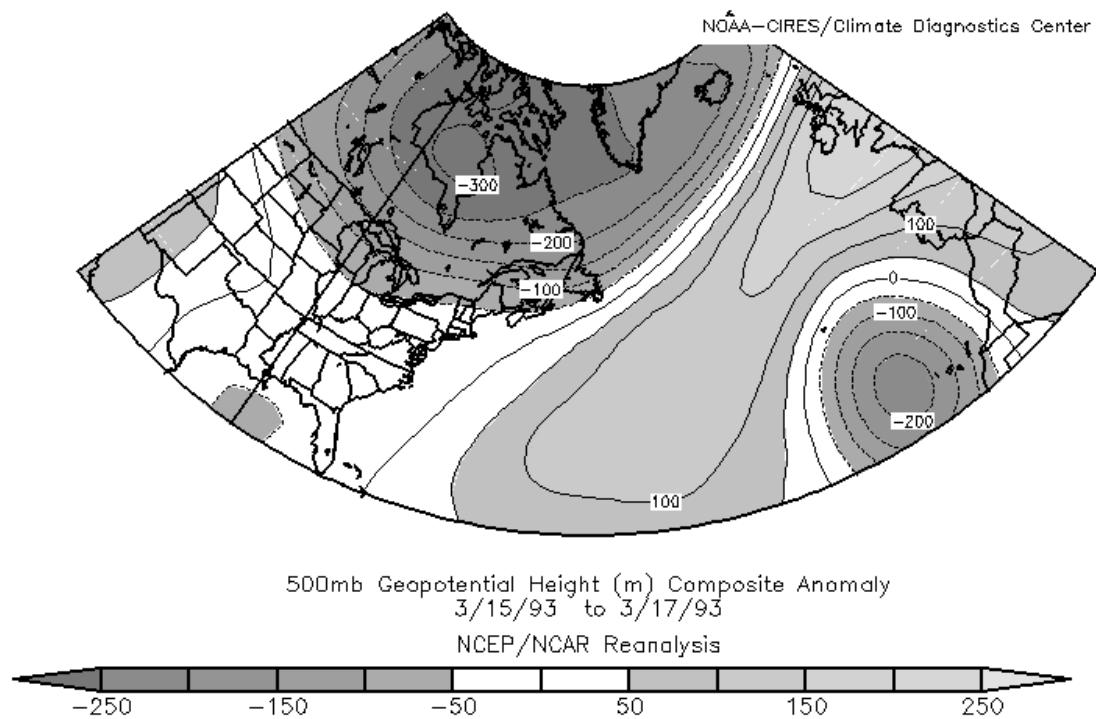


Fig. 3.38b. 500 mb geopotential height anomaly map (m) covering the two NAO domains after the 12–14 March 1993 “Superstorm.”

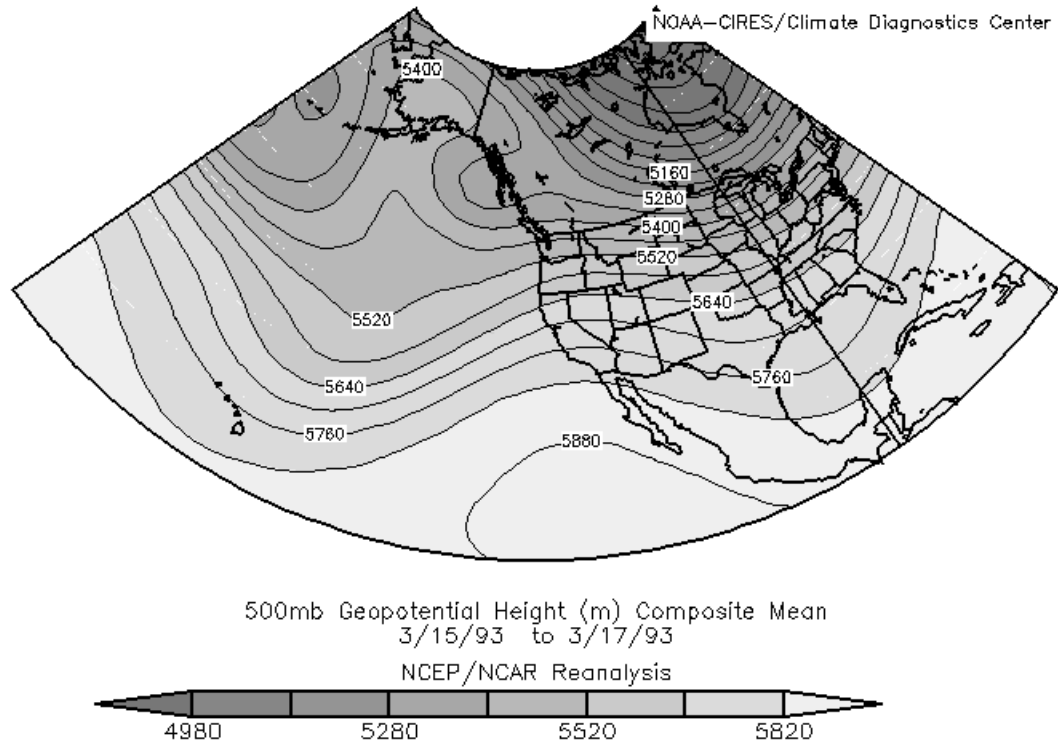


Fig. 3.39a. 500 mb geopotential height map (m) covering the four PNA domains after the 12–14 March 1993 “Superstorm.”

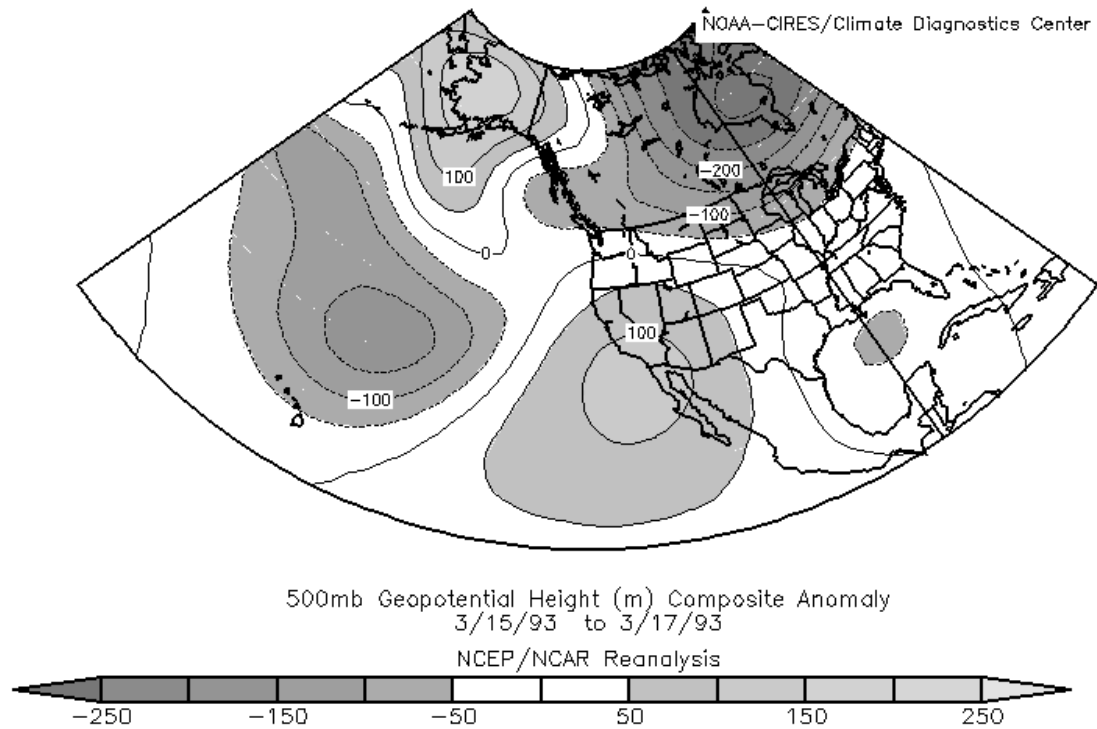


Fig. 3.39b. 500 mb geopotential height anomaly map (m) covering the four PNA domains after the 12–14 March 1993 “Superstorm.”

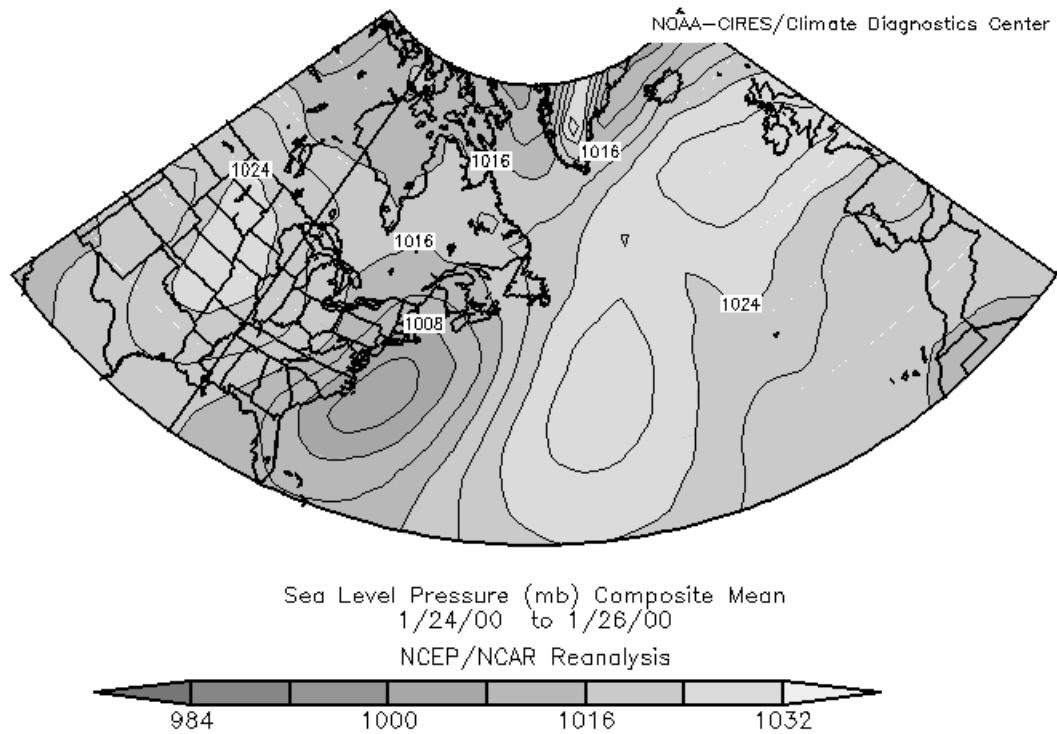


Fig. 3.40a. Sea-level pressure map (mb) for the 24–26 January 2000 storm.

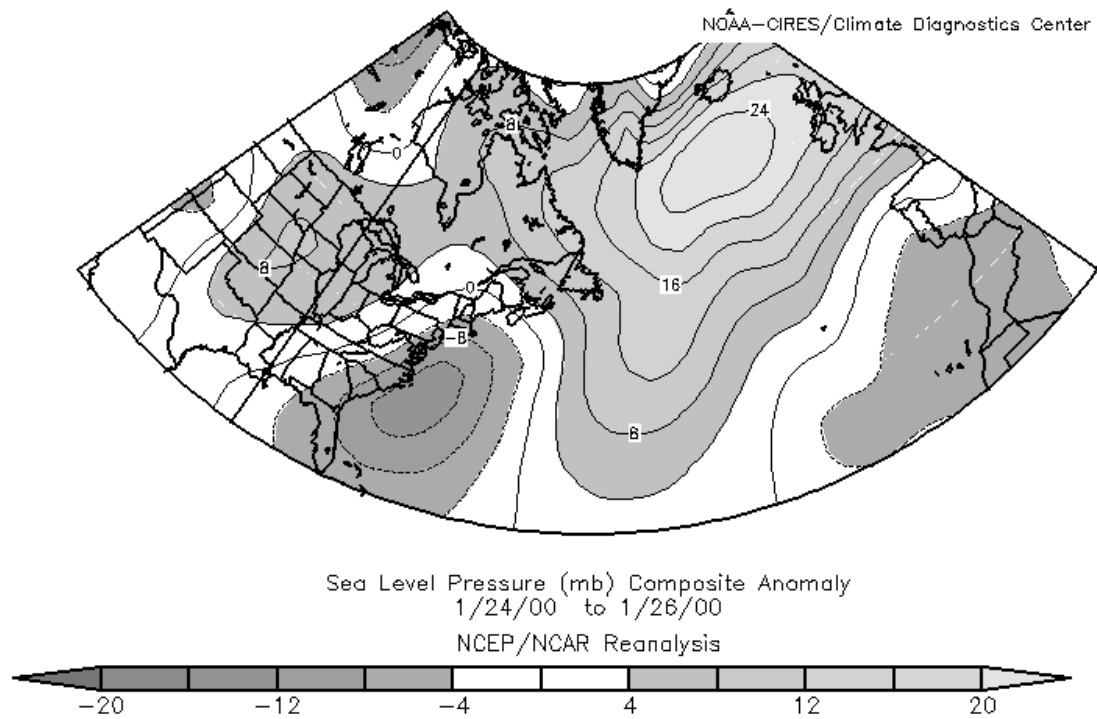


Fig. 3.40b. Sea-level pressure anomaly map (mb) for the 24–26 January 2000 storm.

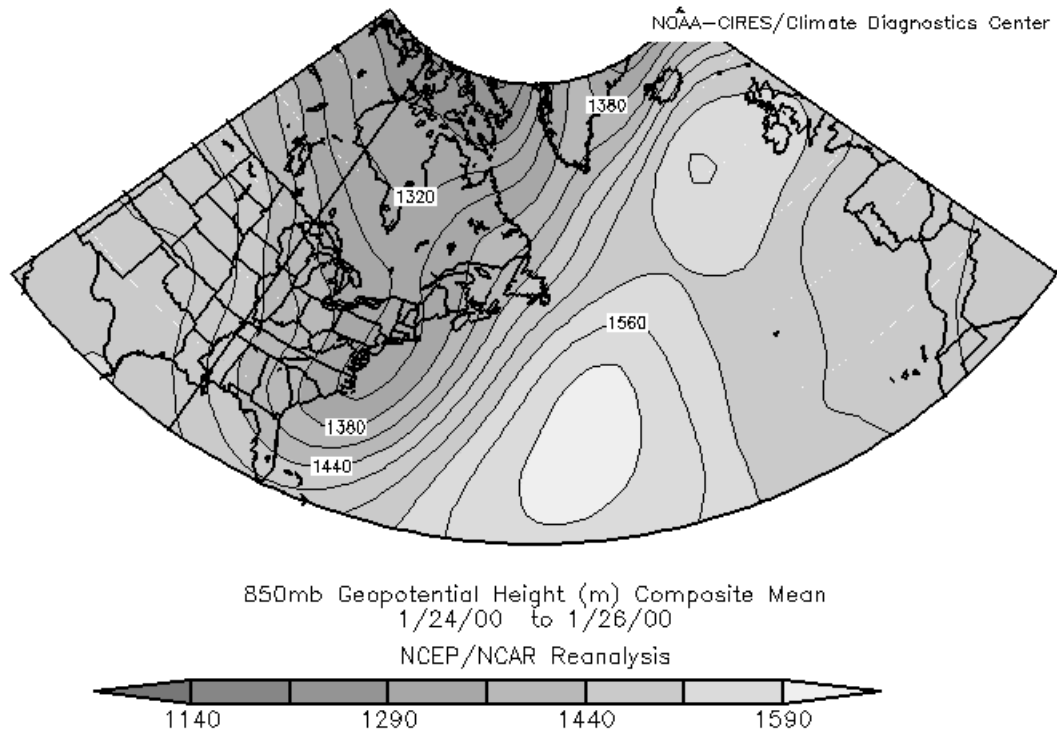


Fig 3.41a. 850 mb geopotential height map (m) for the 24–26 January 2000 storm.

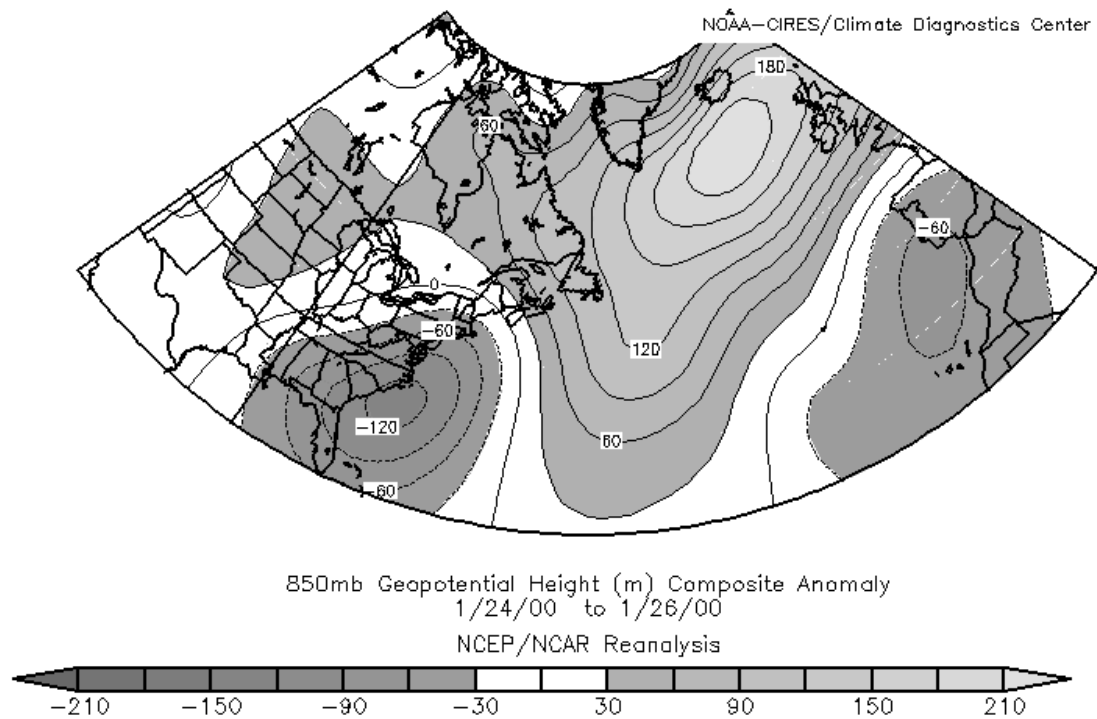


Fig 3.41b. 850 mb geopotential height anomaly map (m) for the 24–26 January 2000 storm.

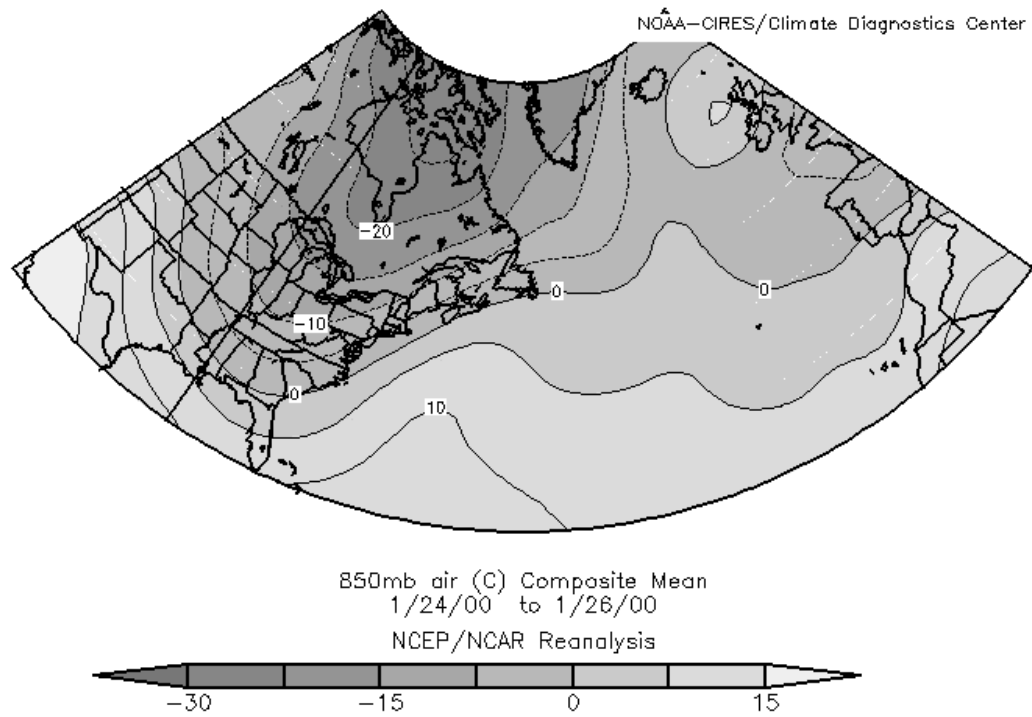


Fig. 3.42a. 850 mb temperature map (°C) for the 24–26 January 2000 storm.

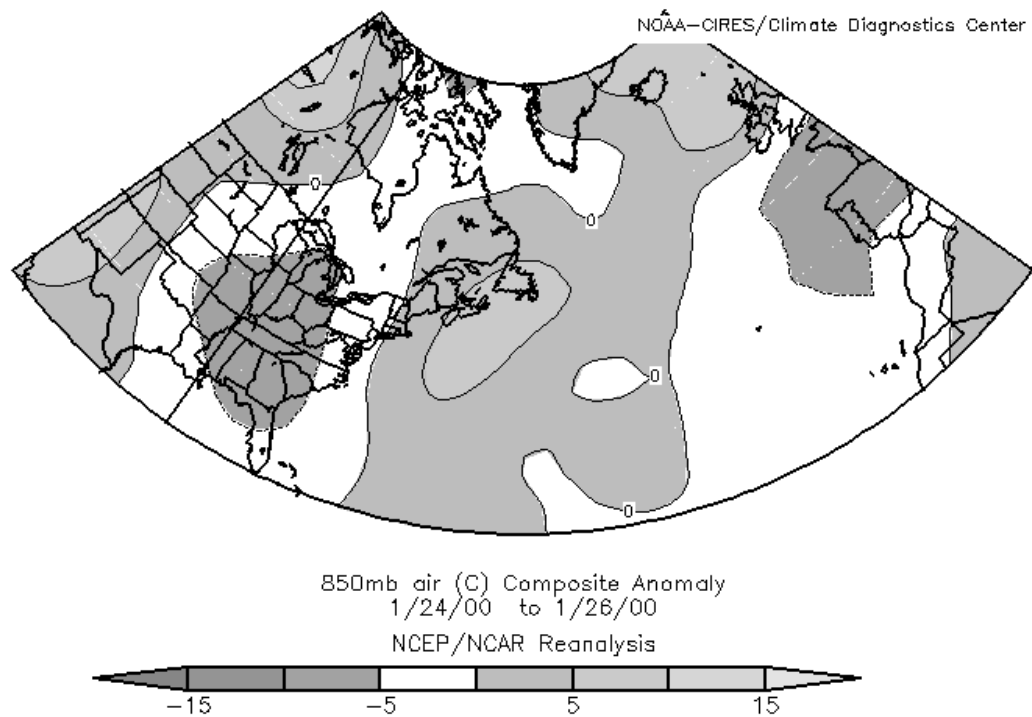


Fig. 3.42b. 850 mb temperature anomaly map (°C) for the 24–26 January 2000 storm.

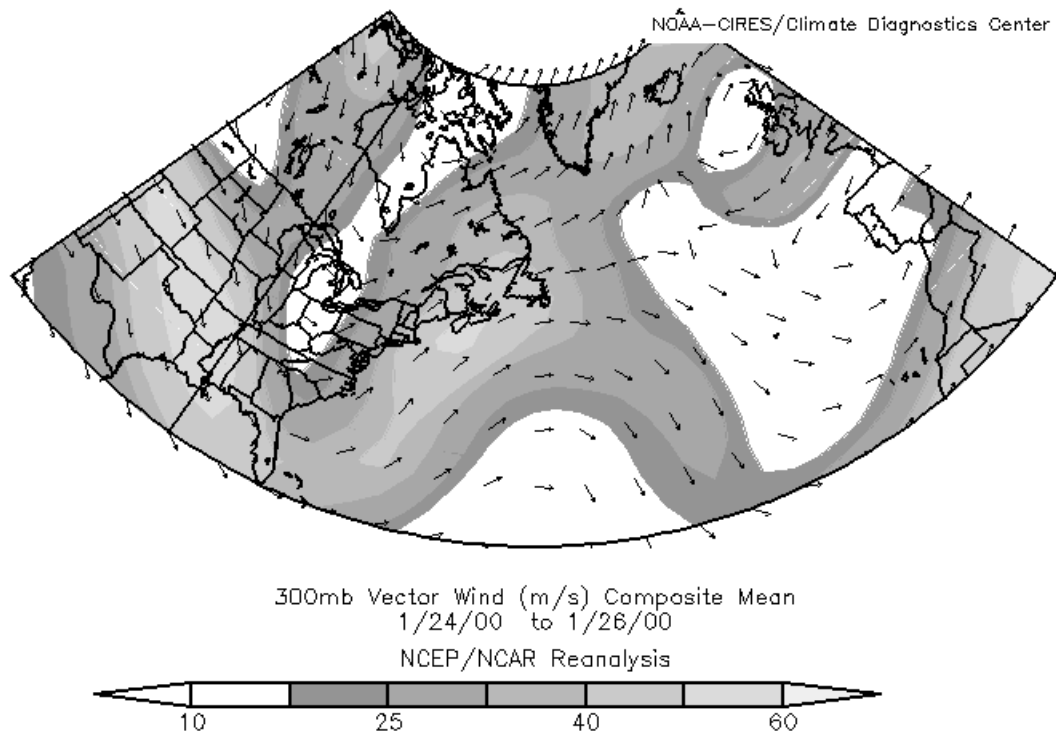


Fig 3.43a. 300 mb vector wind map (m s^{-1}) for the 24–26 January 2000 storm.

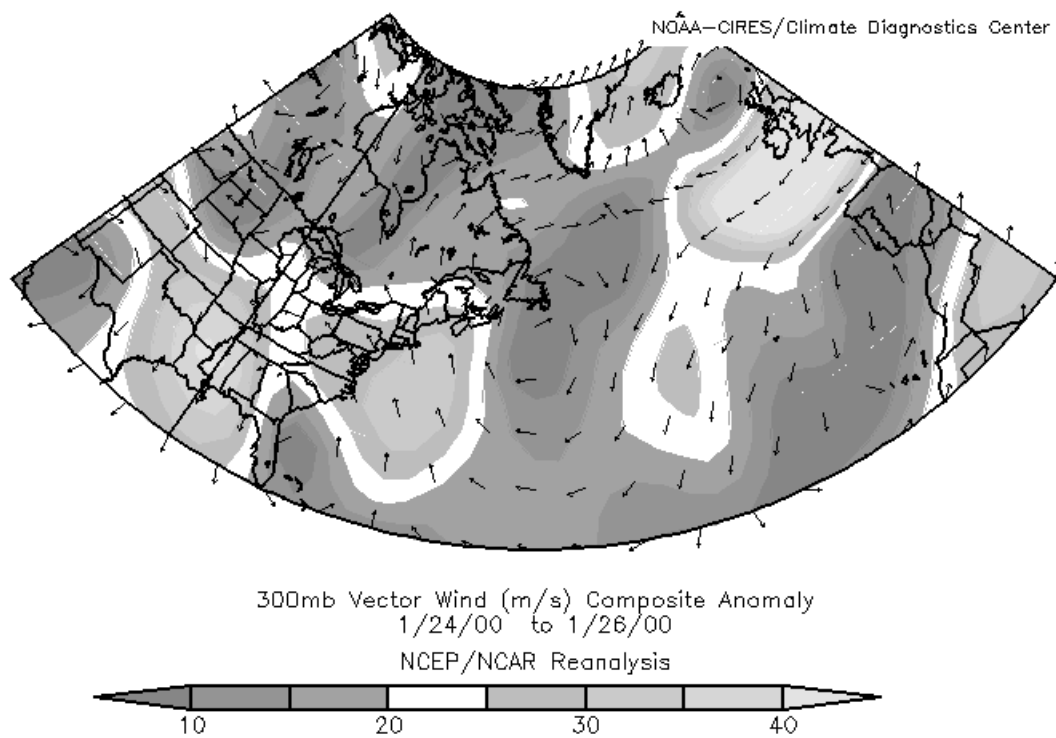


Fig 3.43b 300 mb vector wind anomaly map (m s^{-1}) for the 24–26 January 2000 storm.

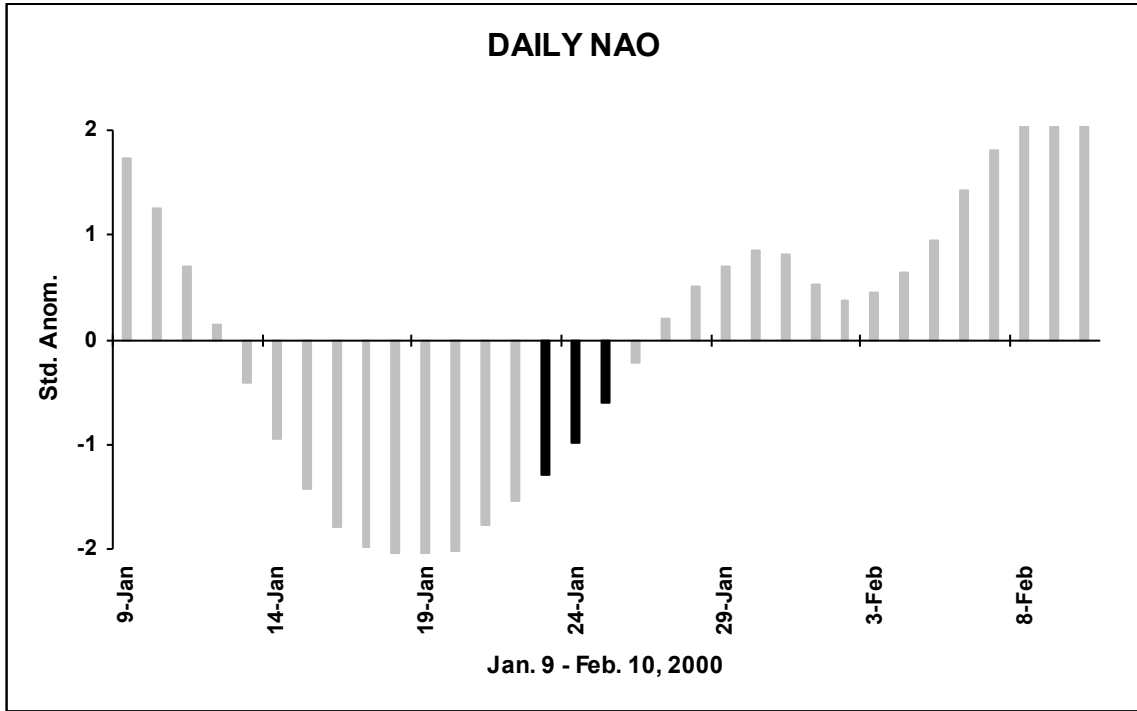


Fig. 3.44a. Daily NAO index with the 24–26 January 2000 storm highlighted in black.

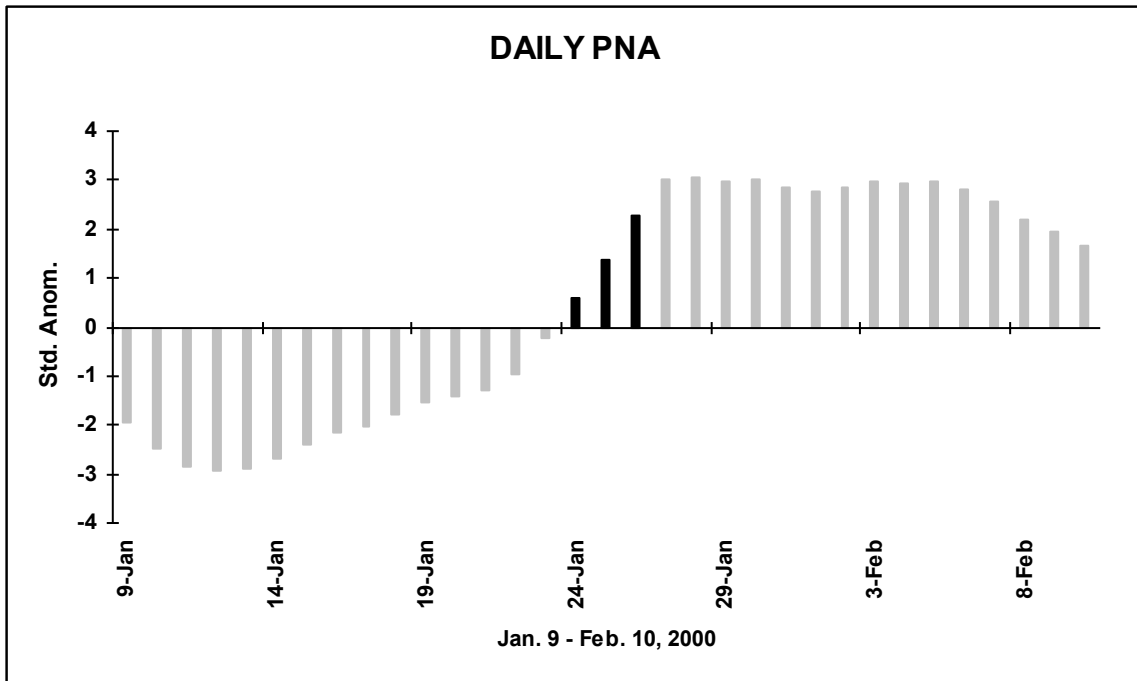


Fig. 3.44b. Daily PNA index with the 24–26 January 2000 storm highlighted in black.

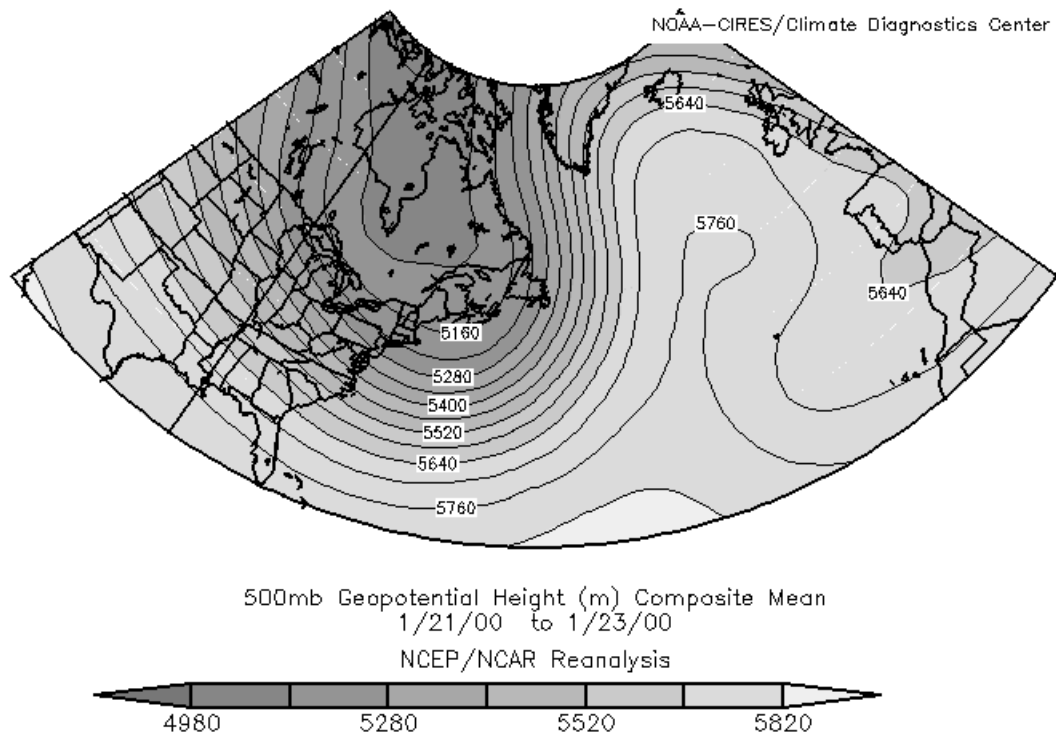


Fig. 3.45a. 500 mb geopotential height map (m) covering the two NAO domains prior to the 24–26 January 2000 storm.

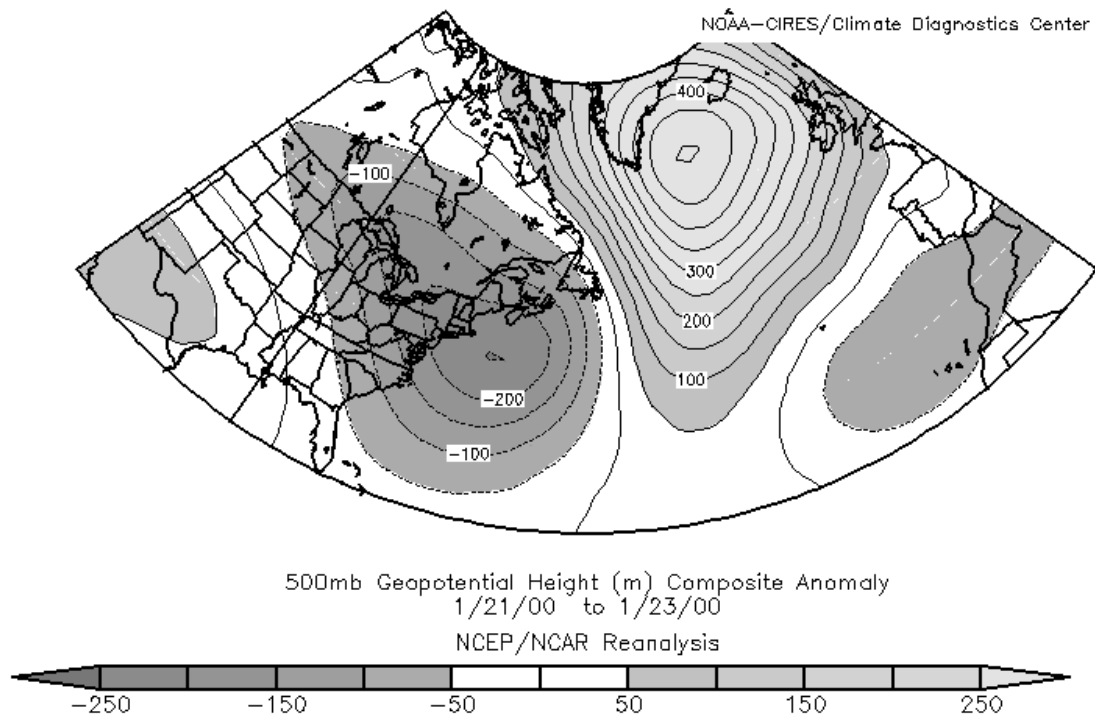


Fig. 3.45b. 500 mb geopotential height anomaly map (m) covering the two NAO domains prior to the 24–26 January 2000 storm.

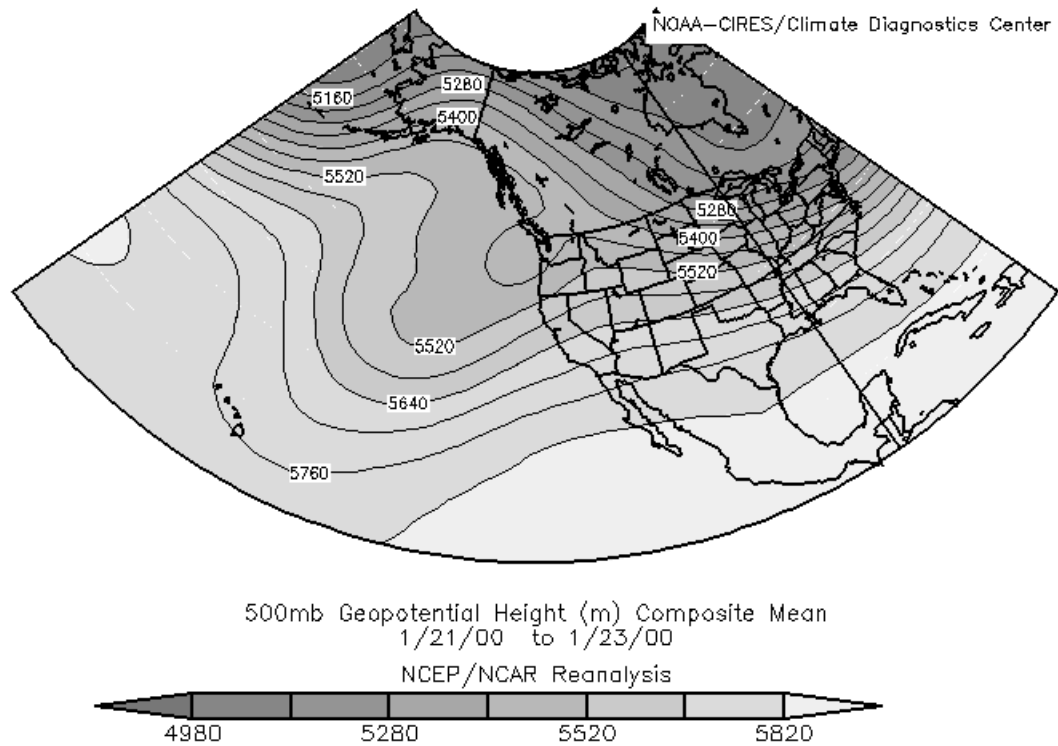


Fig. 3.46a. 500 mb geopotential height map (m) covering the four PNA domains prior to the 24–26 January 2000 storm.

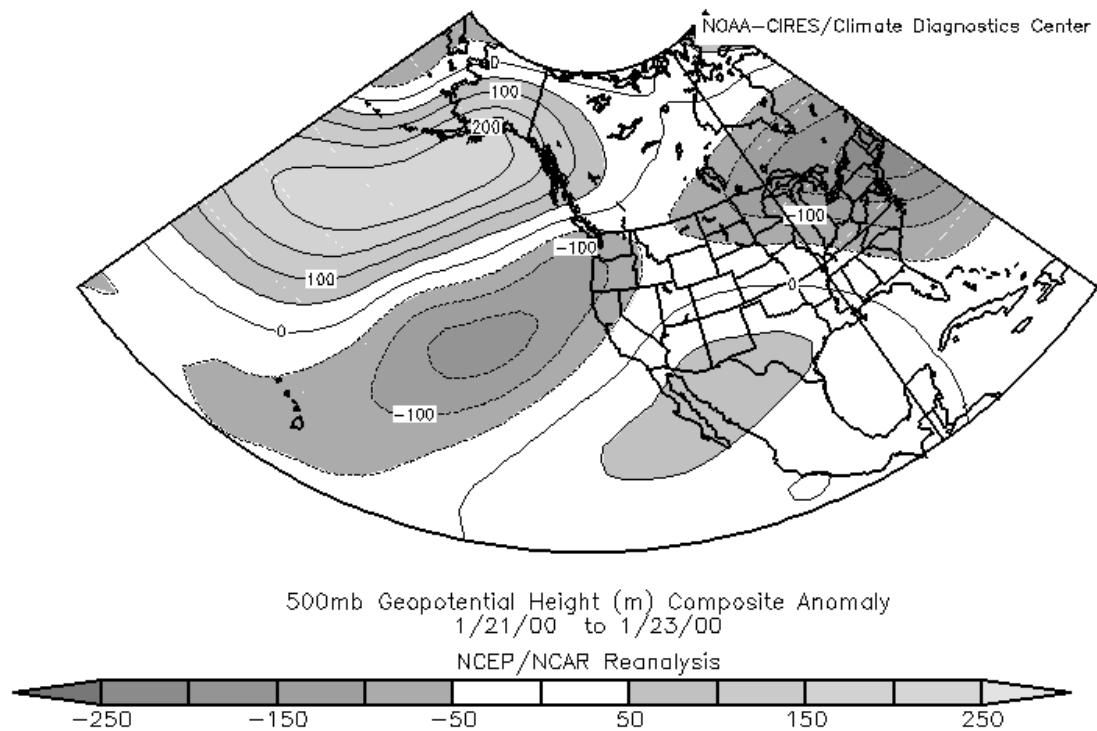


Fig. 3.46b. 500 mb geopotential height anomaly map (m) covering the four PNA domains prior to the 24–26 January 2000 storm.

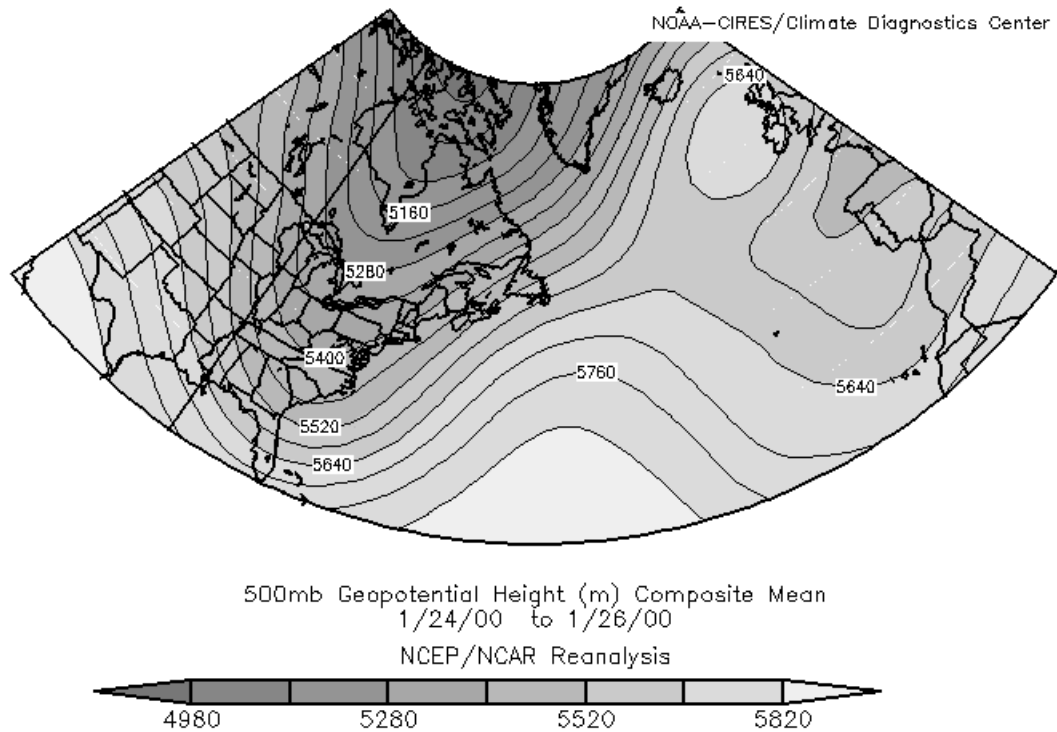


Fig. 3.47a. 500 mb geopotential height map (m) covering the two NAO domains during the 24–26 January 2000 storm.

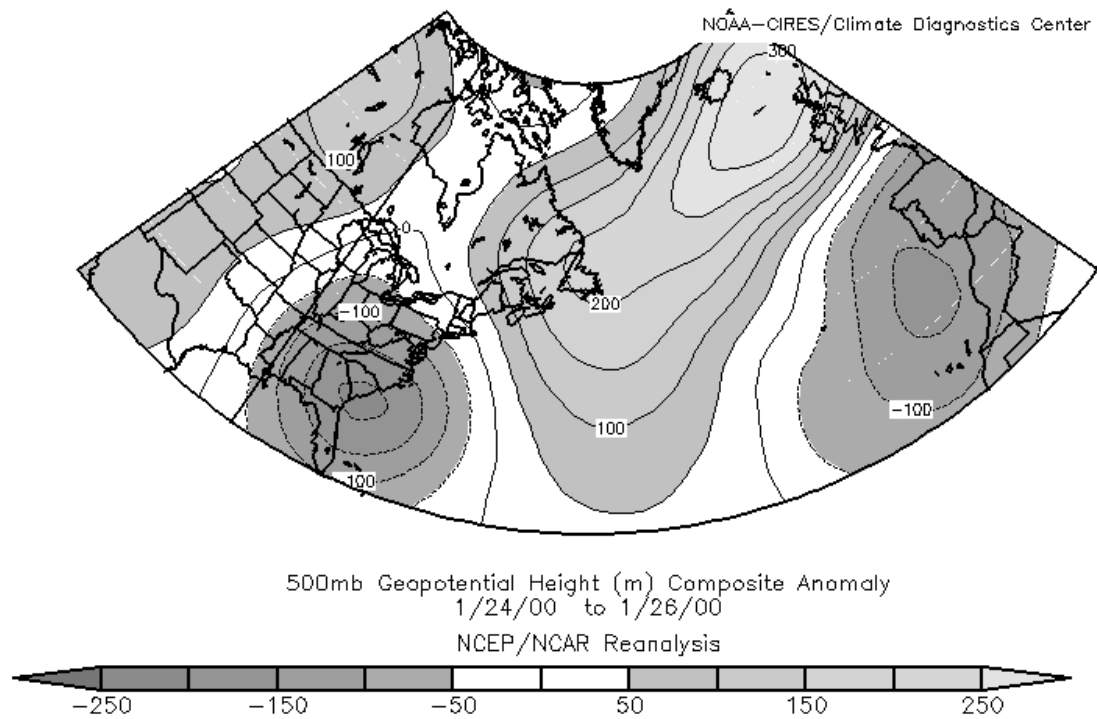


Fig. 3.47b. 500 mb geopotential height anomaly map (m) covering the two NAO domains during the 24–26 January 2000 storm.

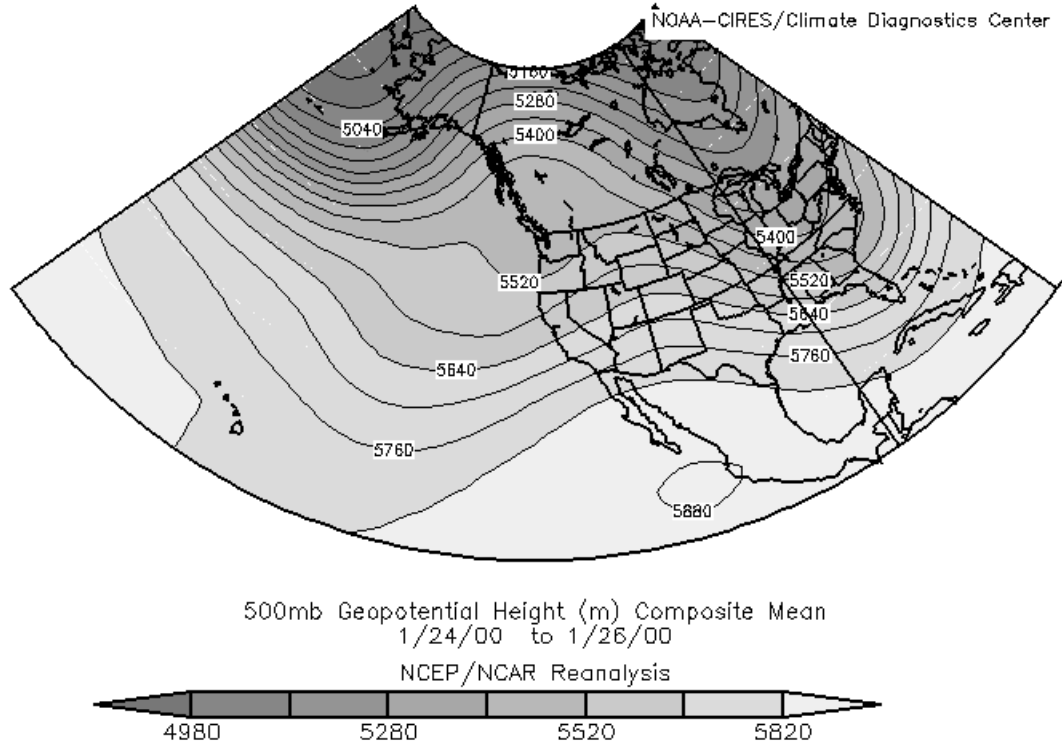


Fig 3.48a. 500 mb geopotential height map (m) covering the four PNA domains during the 24–26 January 2000 storm.

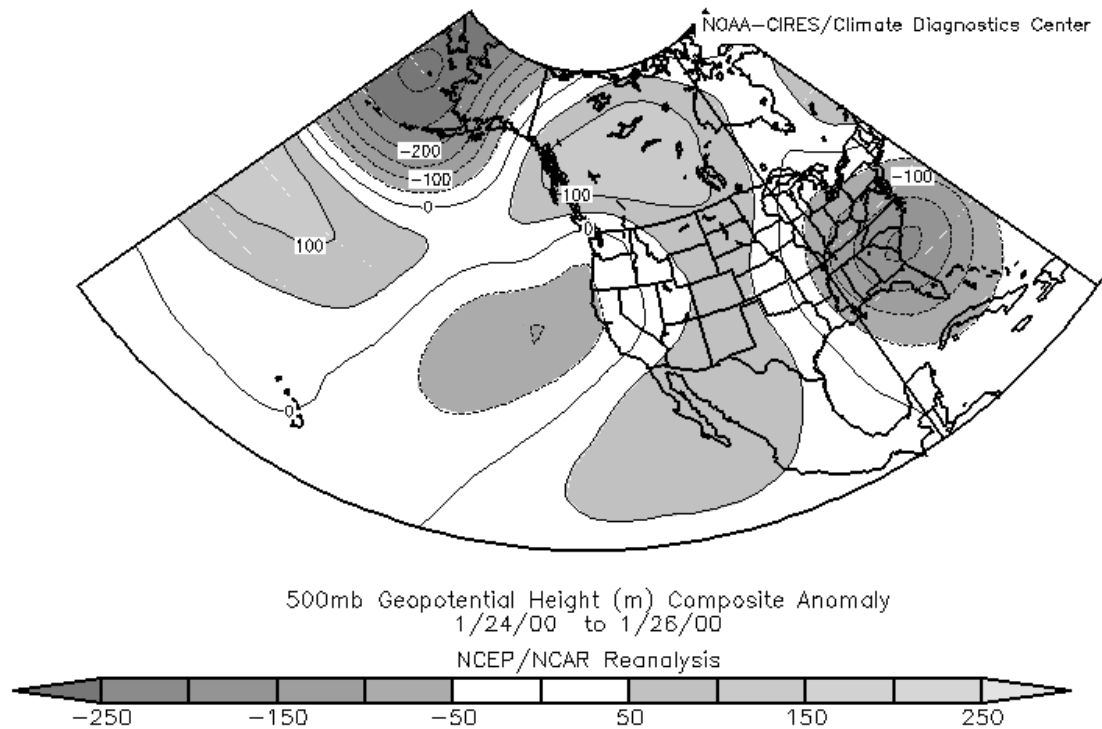


Fig 3.48b. 500 mb geopotential height anomaly map (m) covering the four PNA domains during the 24–26 January 2000 storm.

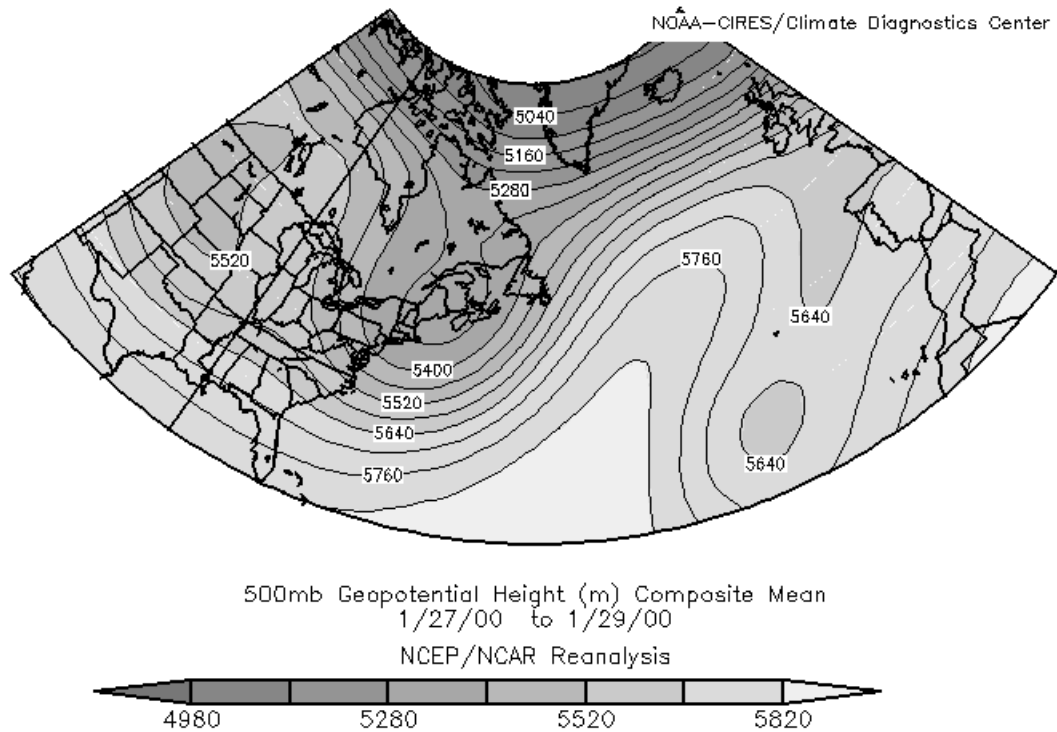


Fig. 3.49a. 500 mb geopotential height map (m) covering the two NAO domains after the 24–26 January 2000 storm.

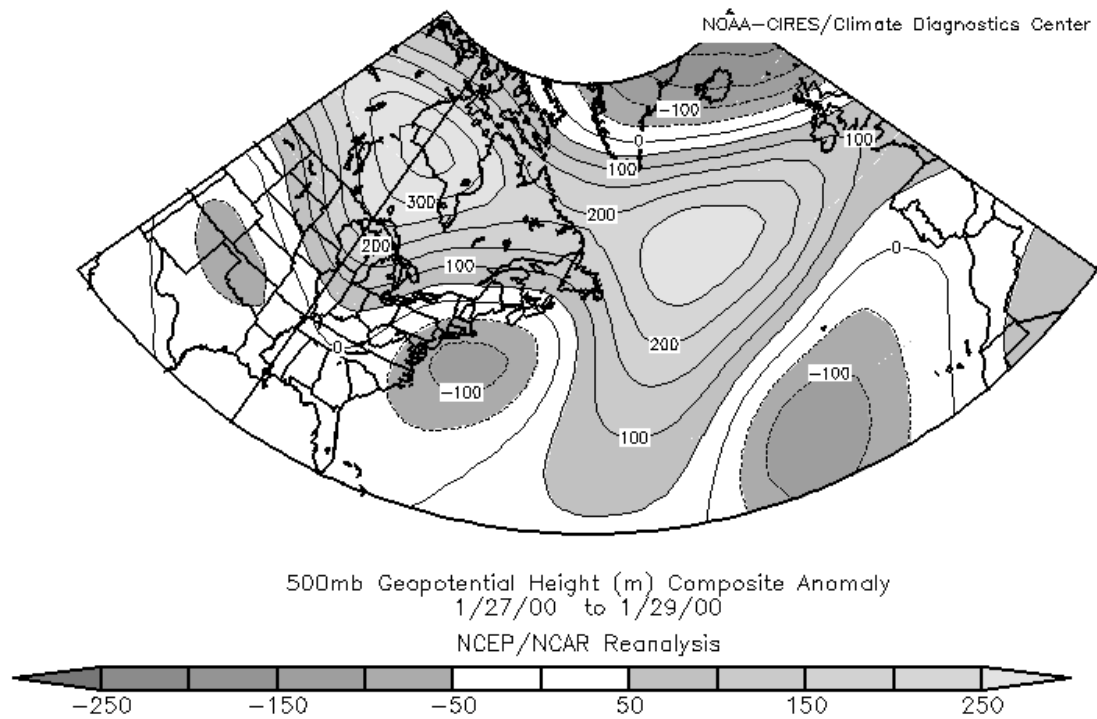


Fig. 3.49b. 500 mb geopotential height anomaly map (m) covering the two NAO domains after the 24–26 January 2000 storm.

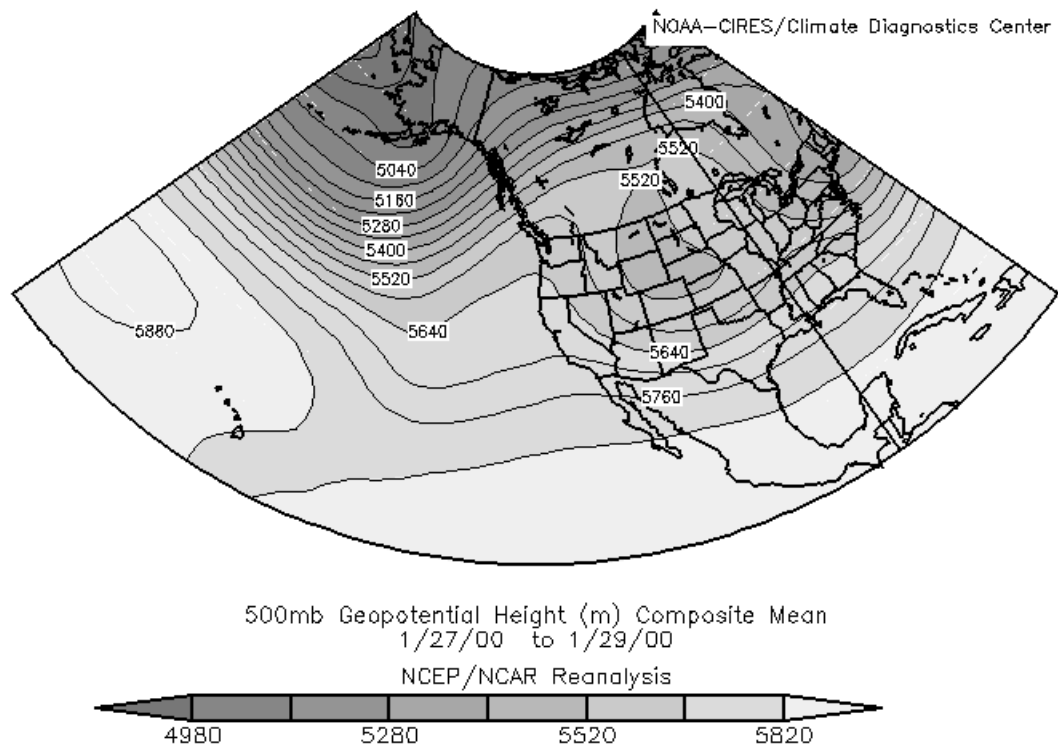


Fig 3.50a. 500 mb geopotential height map (m) covering the four PNA domains after the 24–26 January 2000 storm.

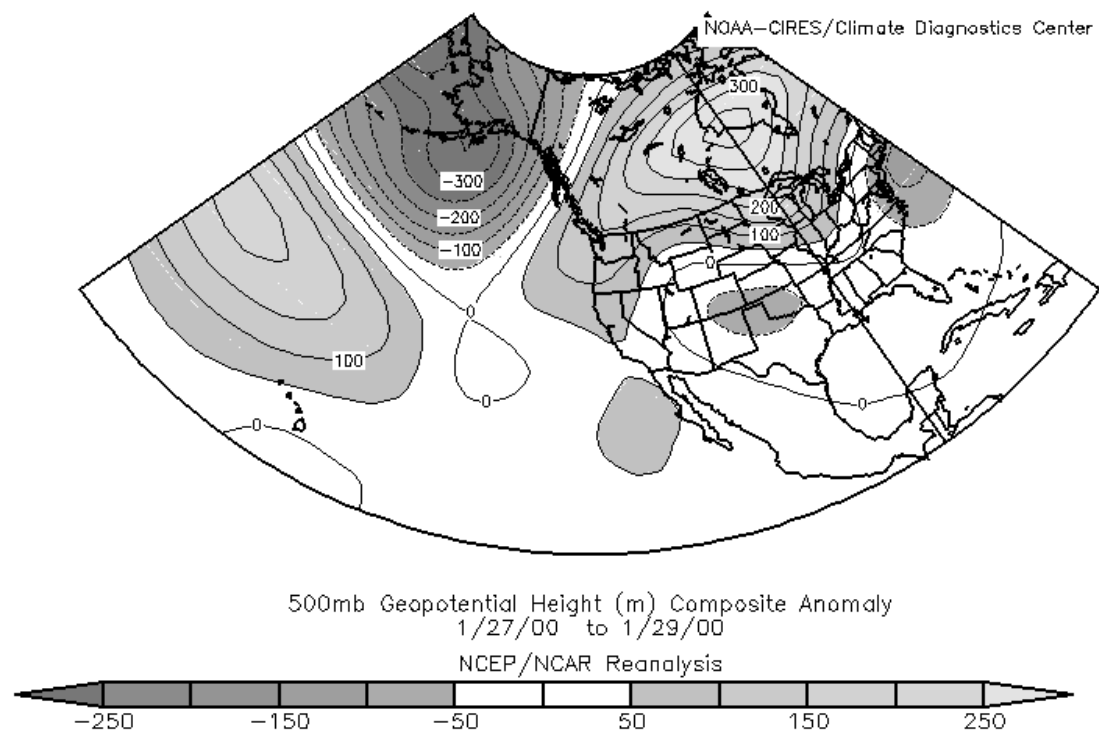


Fig 3.50b. 500 mb geopotential height anomaly map (m) covering the four PNA domains after the 24–26 January 2000 storm.

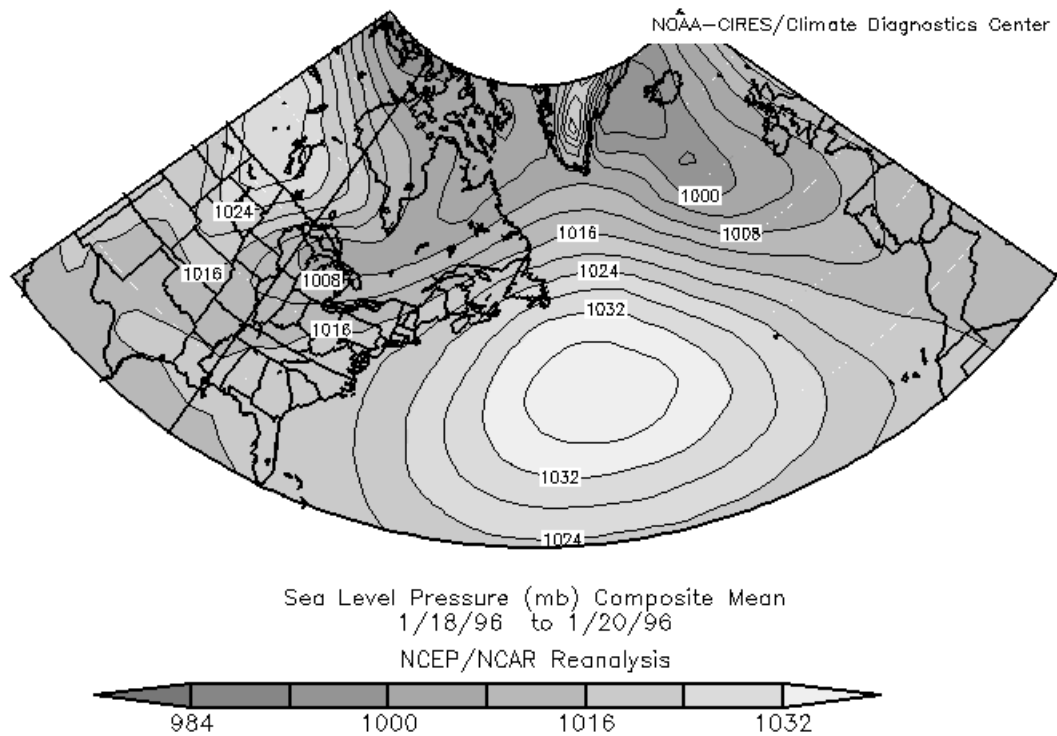


Fig. 3.51a. Sea-level pressure map (mb) for the 18–20 January 1996 storm.

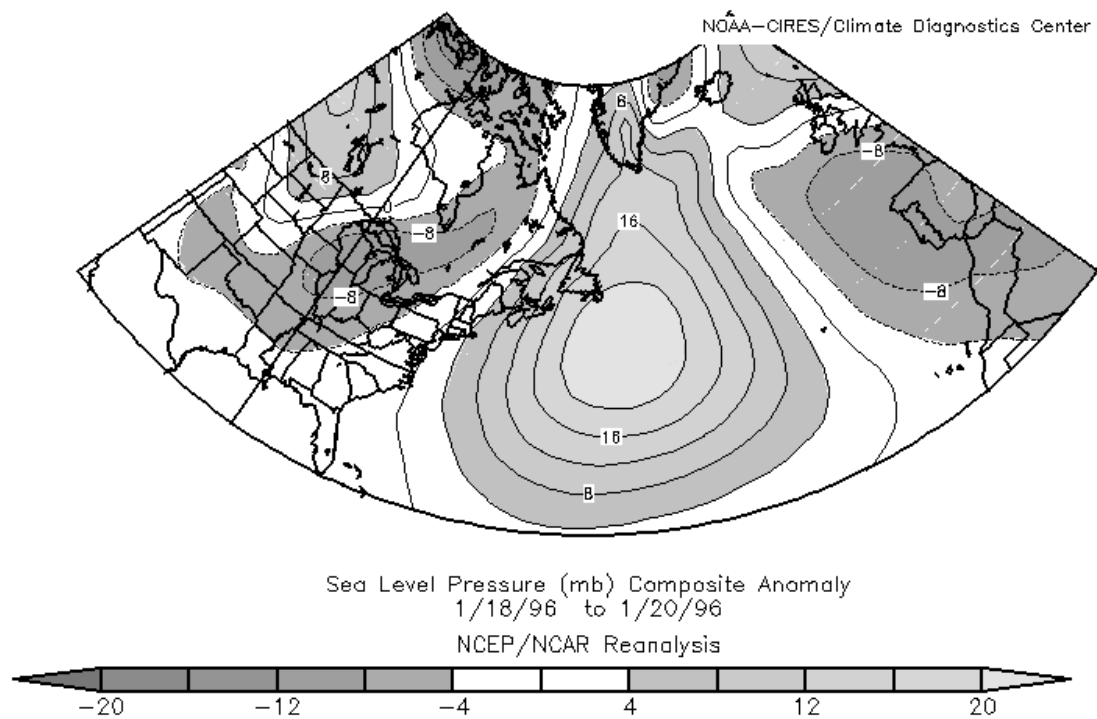


Fig. 3.51b. Sea-level pressure anomaly map (mb) for the 18–20 January 1996 storm.

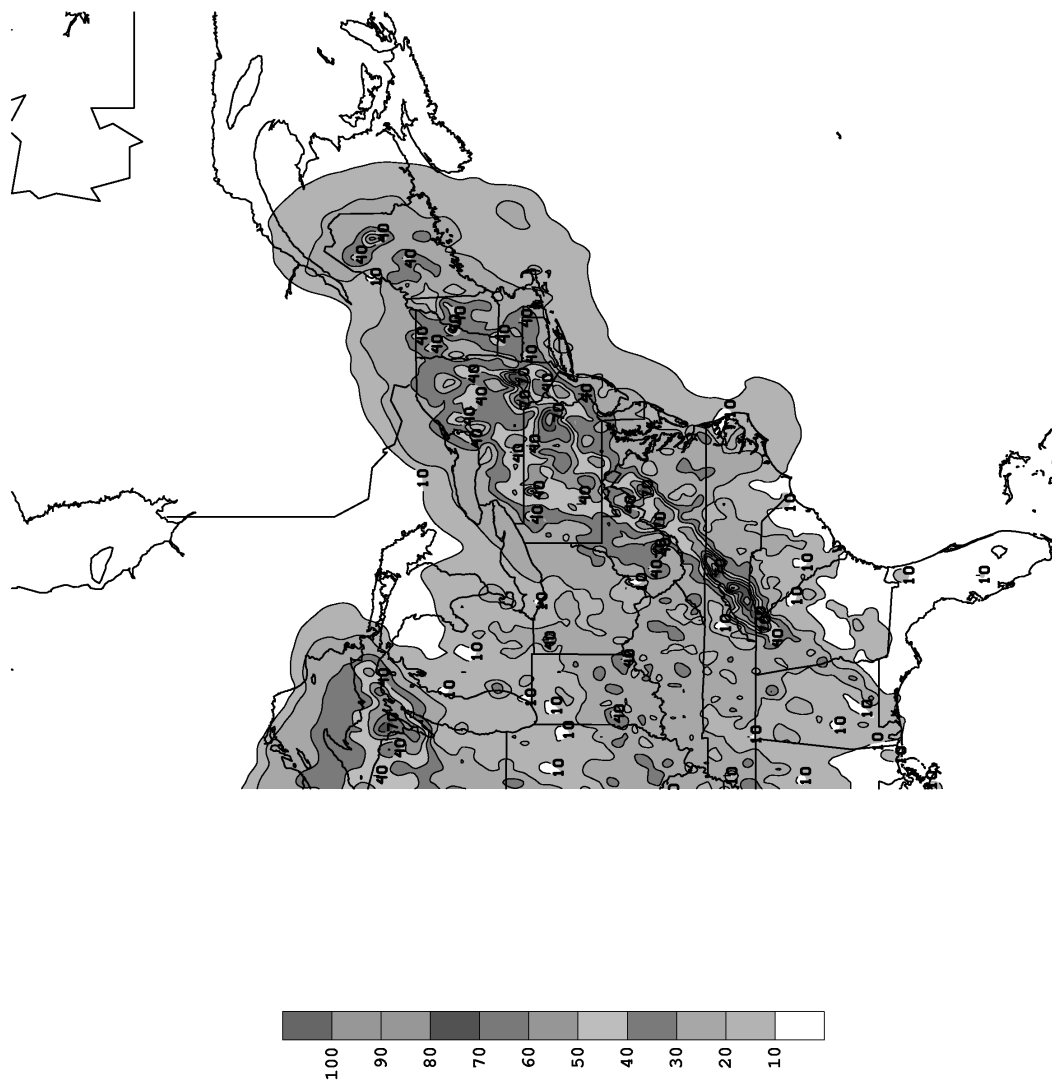


Fig. 3.52. Precipitation total (mm) starting at 1200 UTC on 18 January and ending at 1200 UTC on 21 January 1996.

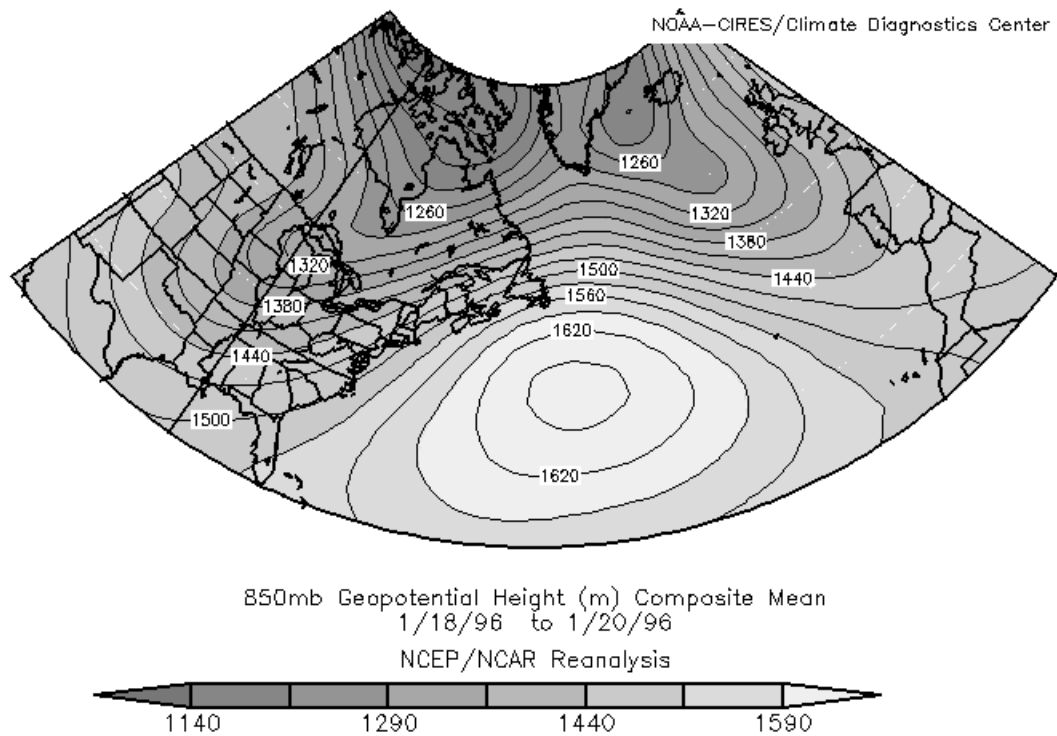


Fig. 3.53a. 850 mb geopotential height map (mb) for the 18–20 January 1996 storm.

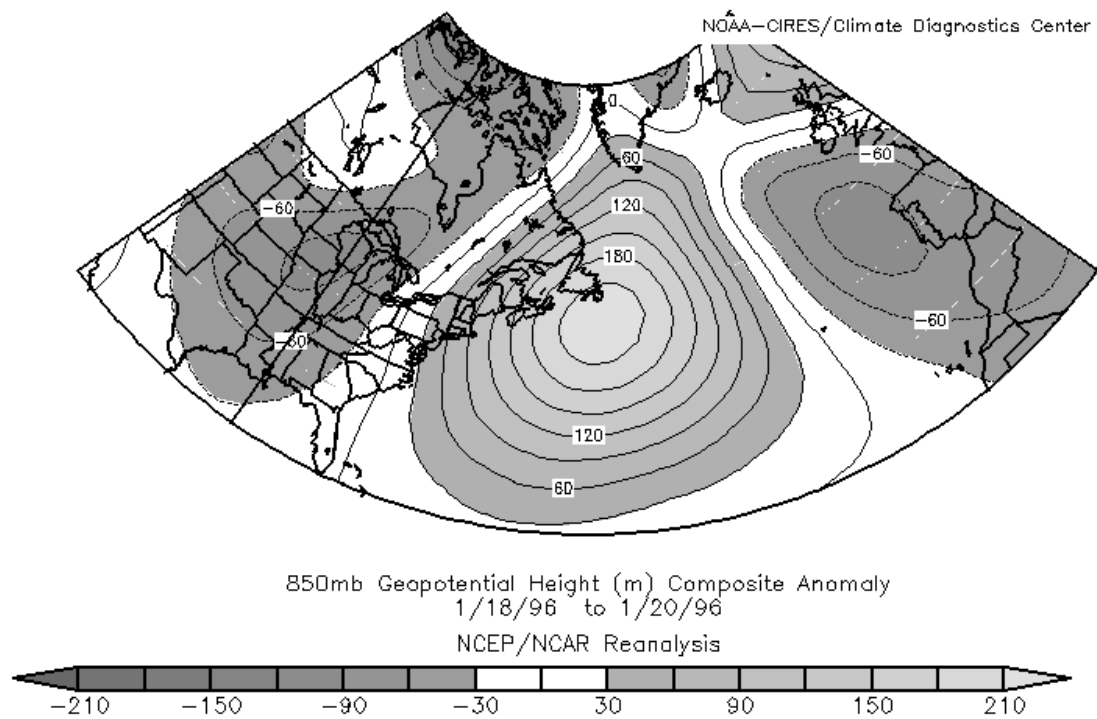


Fig. 3.53b. 850 mb geopotential height anomaly map (mb) for the 18–20 January 1996 storm.

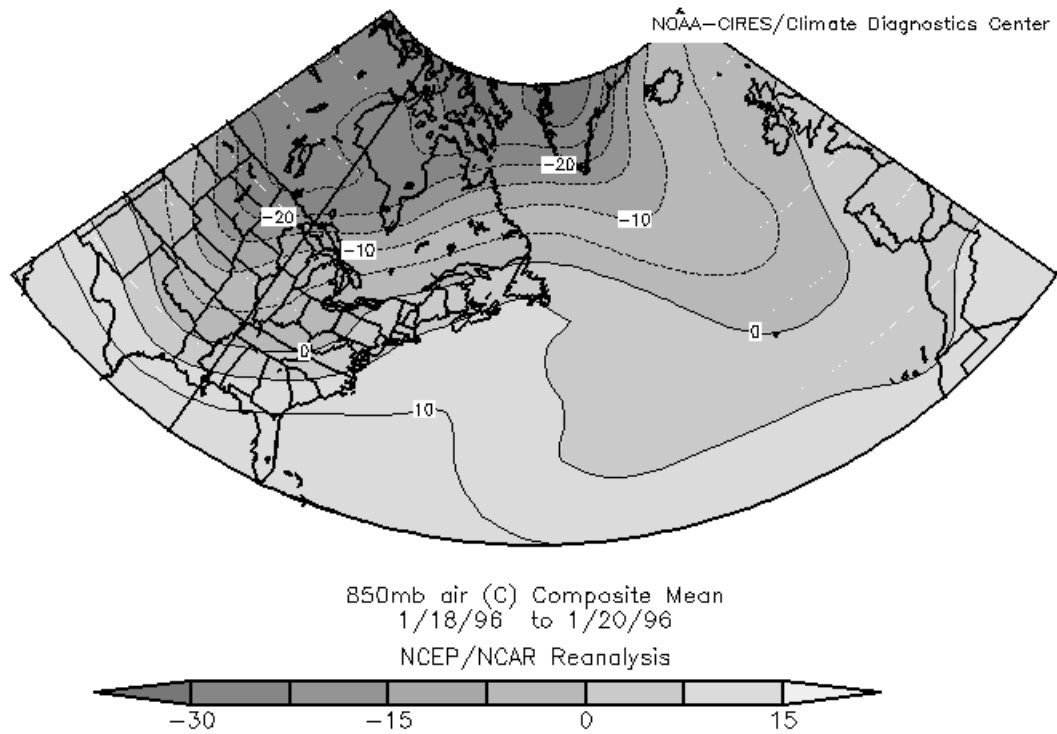


Fig. 3.54a. 850 mb temperature map ($^{\circ}\text{C}$) for the 18–20 January 1996 storm.

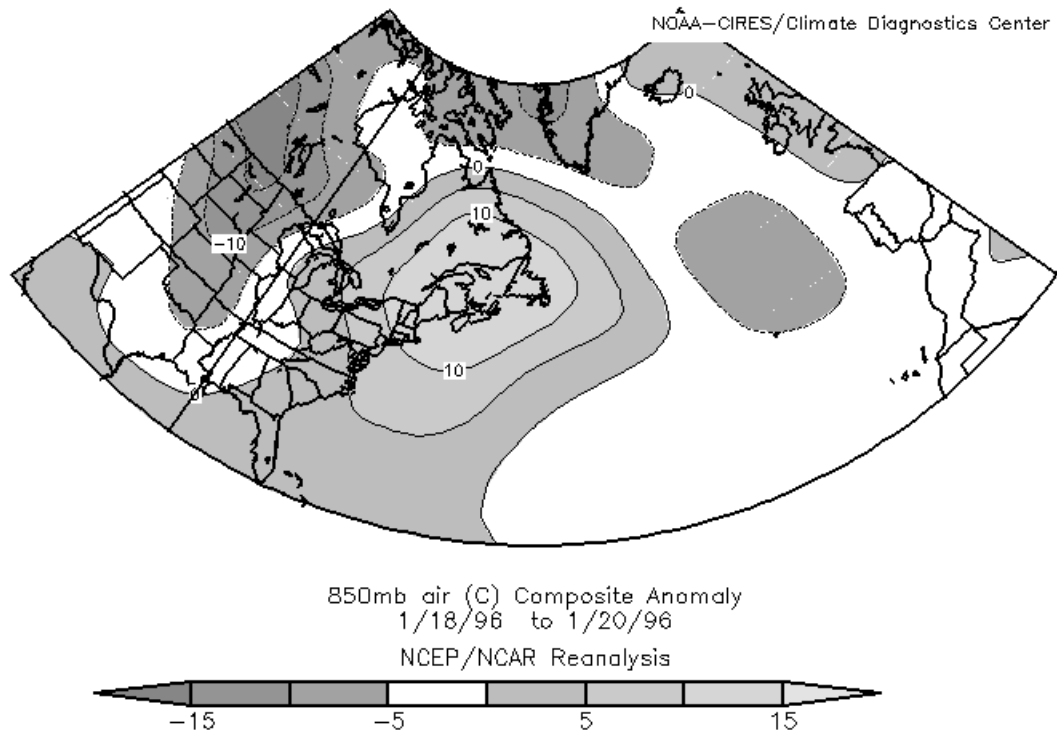


Fig. 3.54b. 850 mb temperature anomaly map ($^{\circ}\text{C}$) for the 18–20 January 1996 storm.

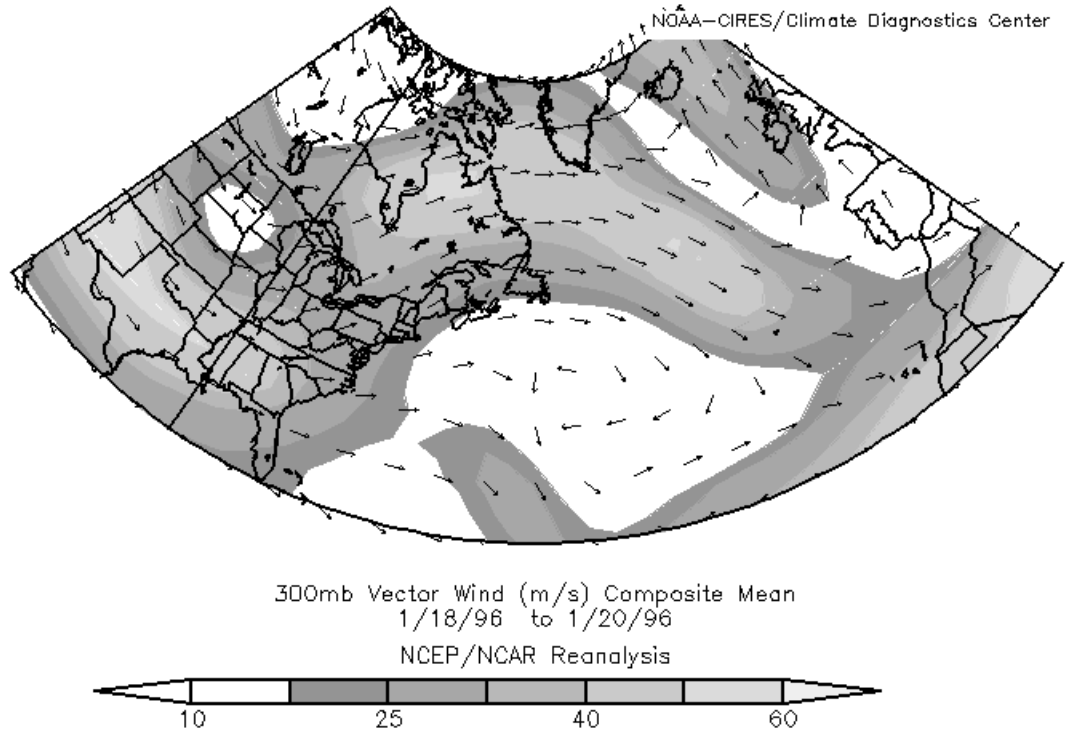


Fig. 3.55a. 300 mb vector wind map (m s^{-1}) for the 18–20 January 1996 storm.

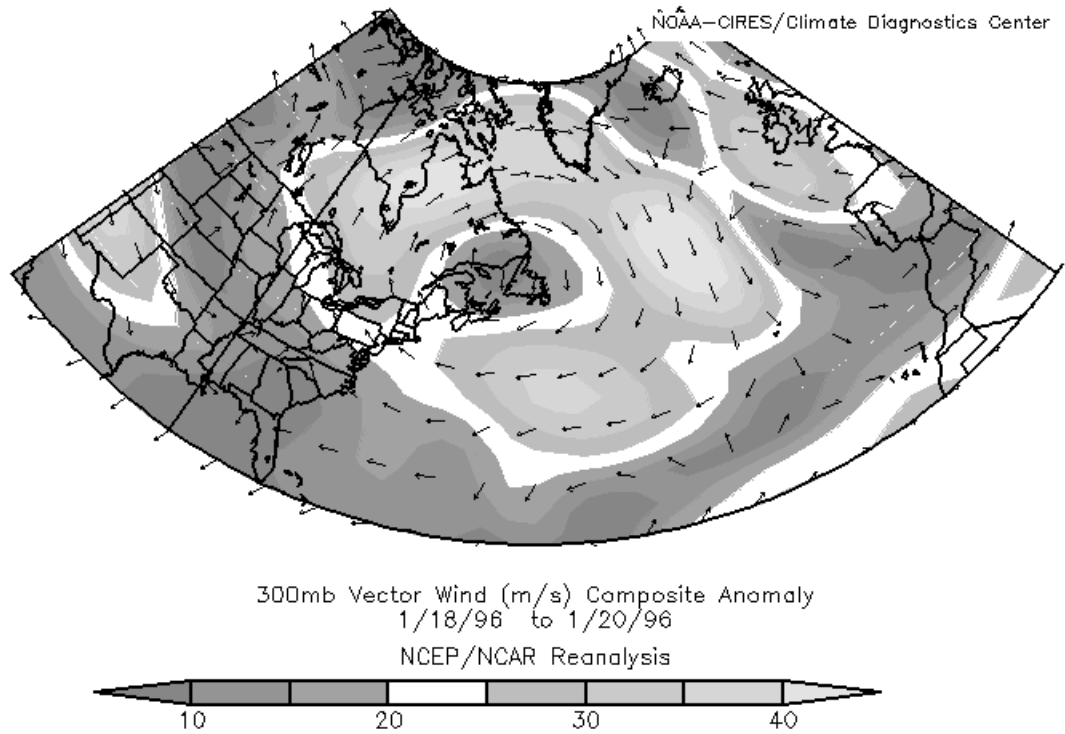


Fig. 3.55b. 300 mb vector wind anomaly map (m s^{-1}) for the 18–20 January 1996 storm.

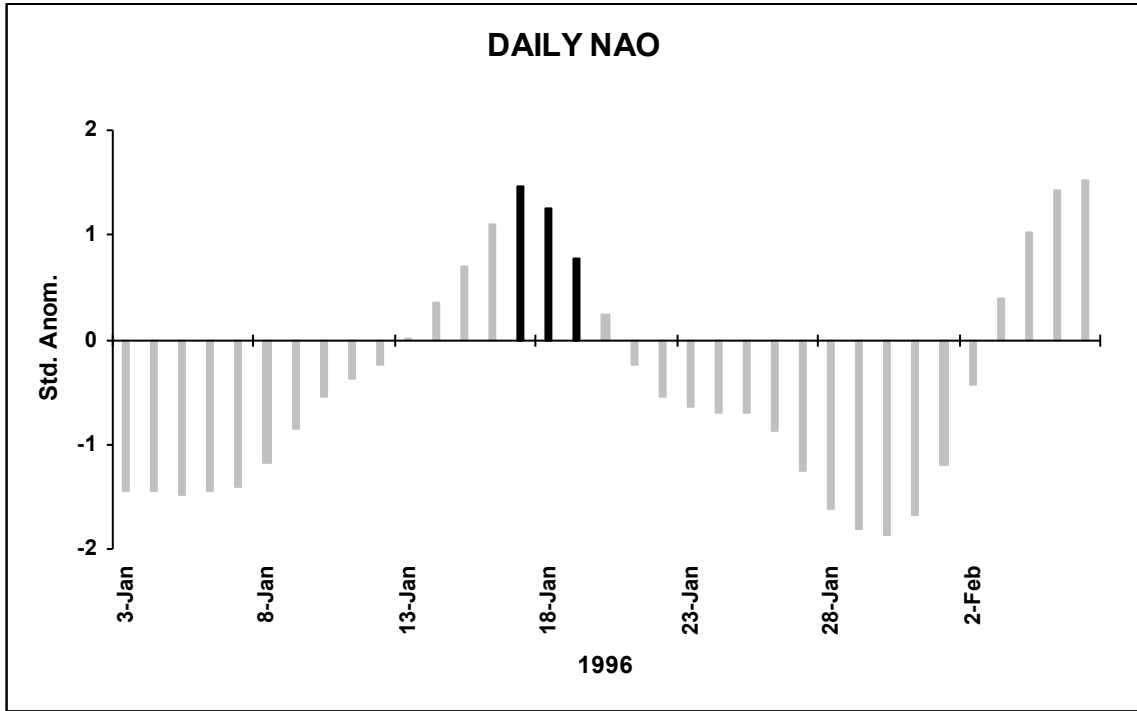


Fig. 3.56a. Daily NAO index with the 18–20 January 1996 storm highlighted in black.

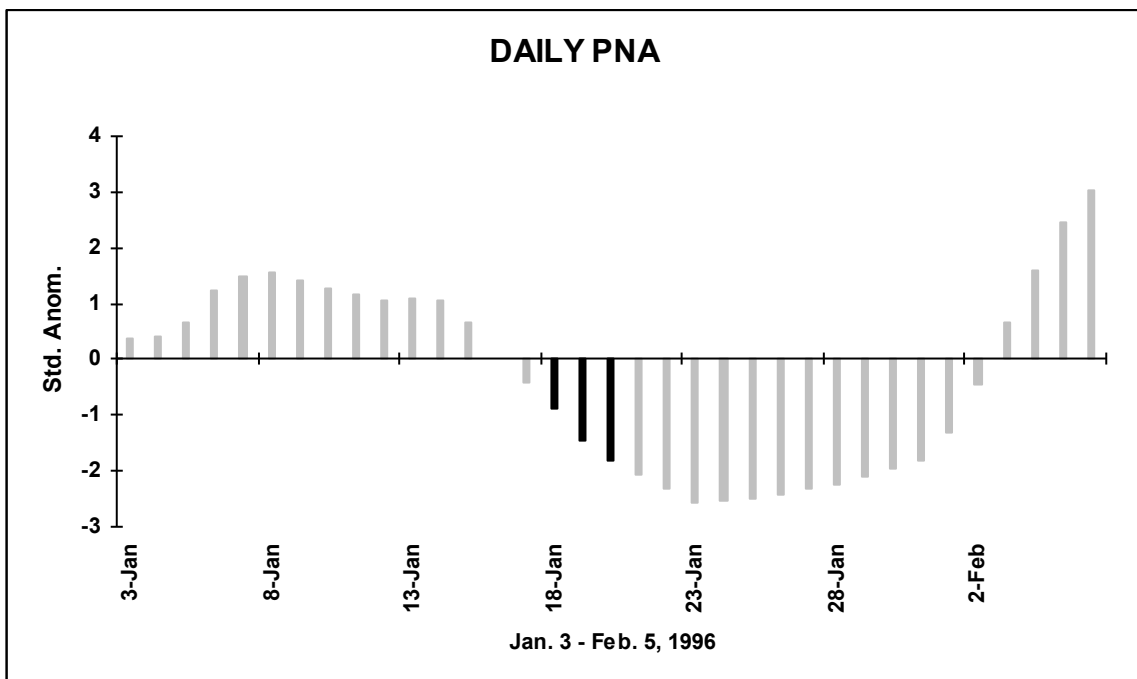


Fig. 3.56b. Daily PNA index with the 18–20 January 1996 storm highlighted in black.

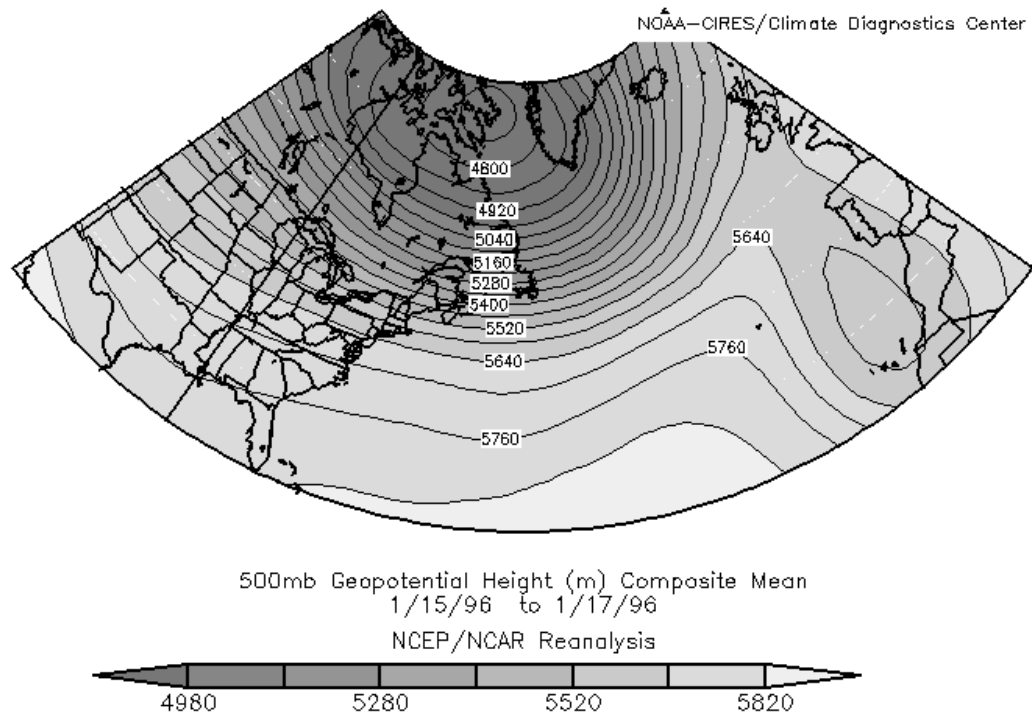


Fig. 3.57a. 500 mb geopotential height map (m) covering the two NAO domains prior to the 18–20 January 1996 storm.

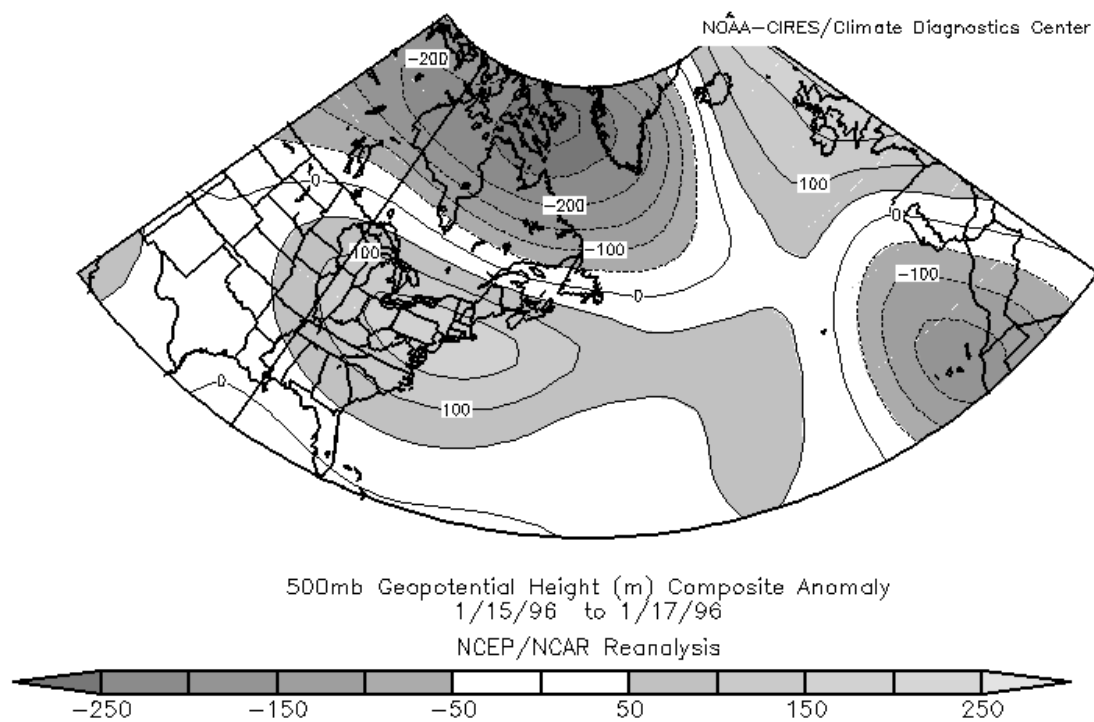


Fig. 3.57b. 500 mb geopotential height anomaly map (m) covering the two NAO domains prior to the 18–20 January 1996 storm.

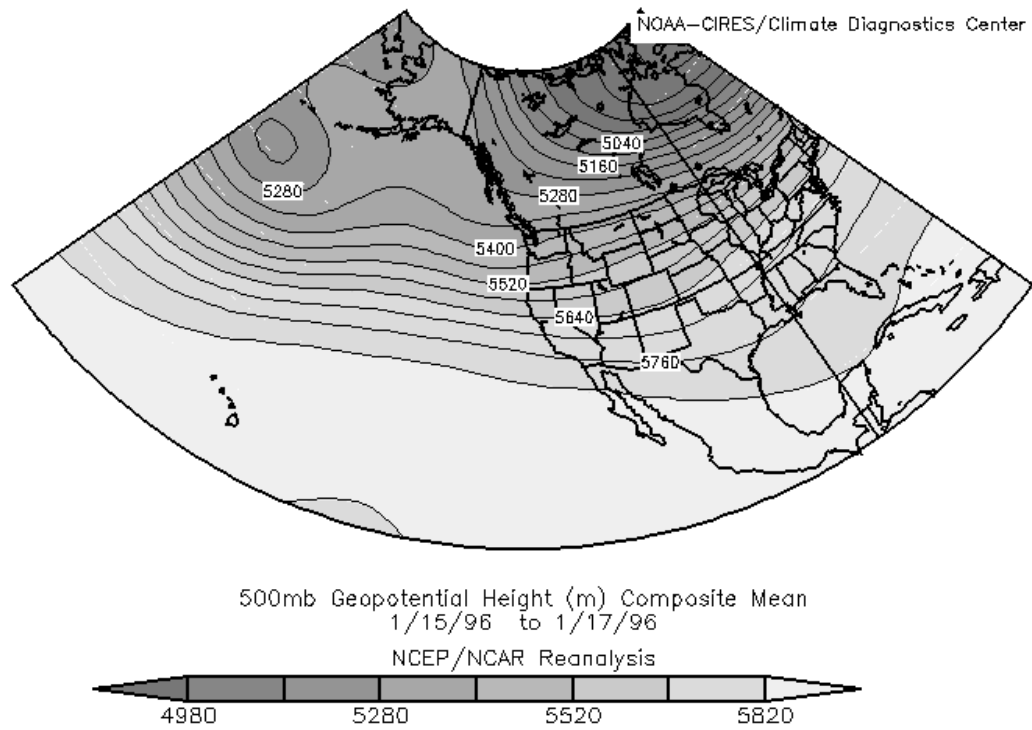


Fig. 3.58a. 500 mb geopotential height map (m) covering the four PNA domains prior to the 18–20 January 1996 storm.

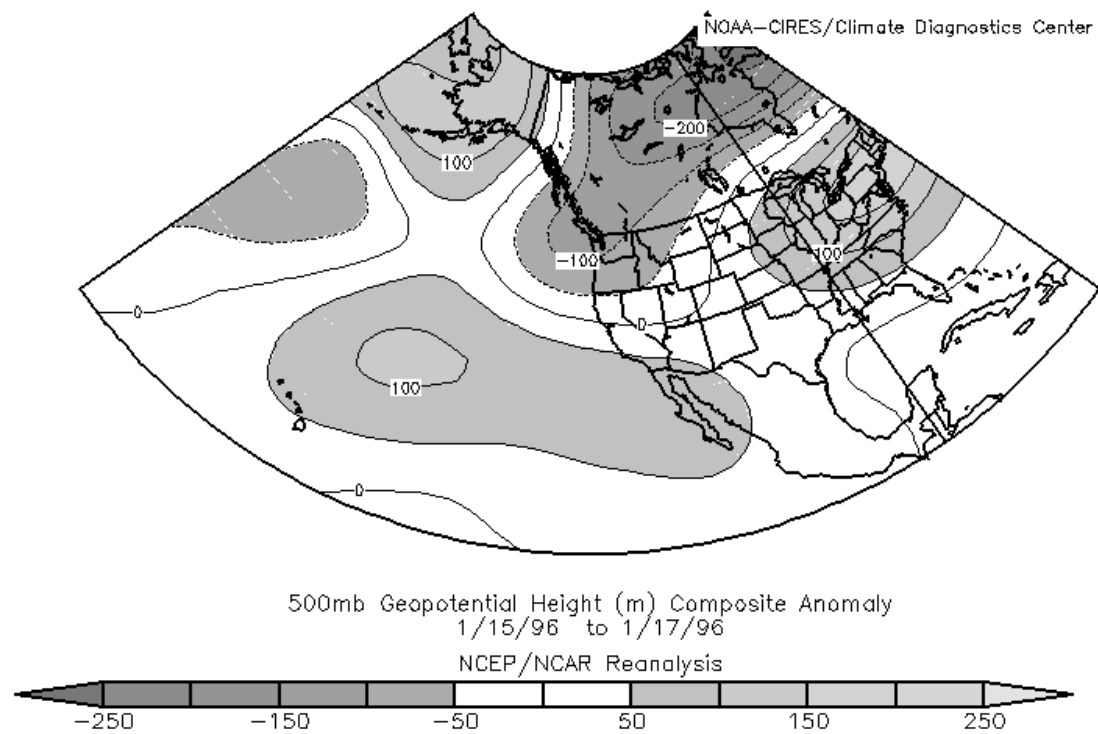


Fig. 3.58b. 500 mb geopotential height anomaly map (m) covering the four PNA domains prior to the 18–20 January 1996 storm.

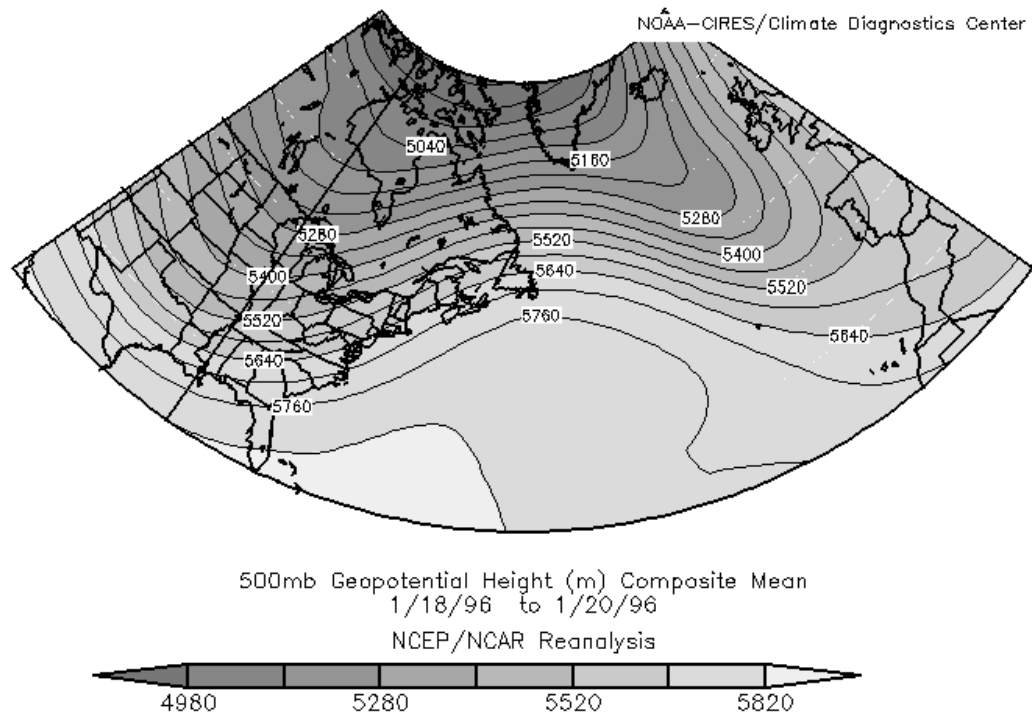


Fig. 3.59a. 500 mb geopotential height map (m) covering the two NAO domains during the 18–20 January 1996 storm.

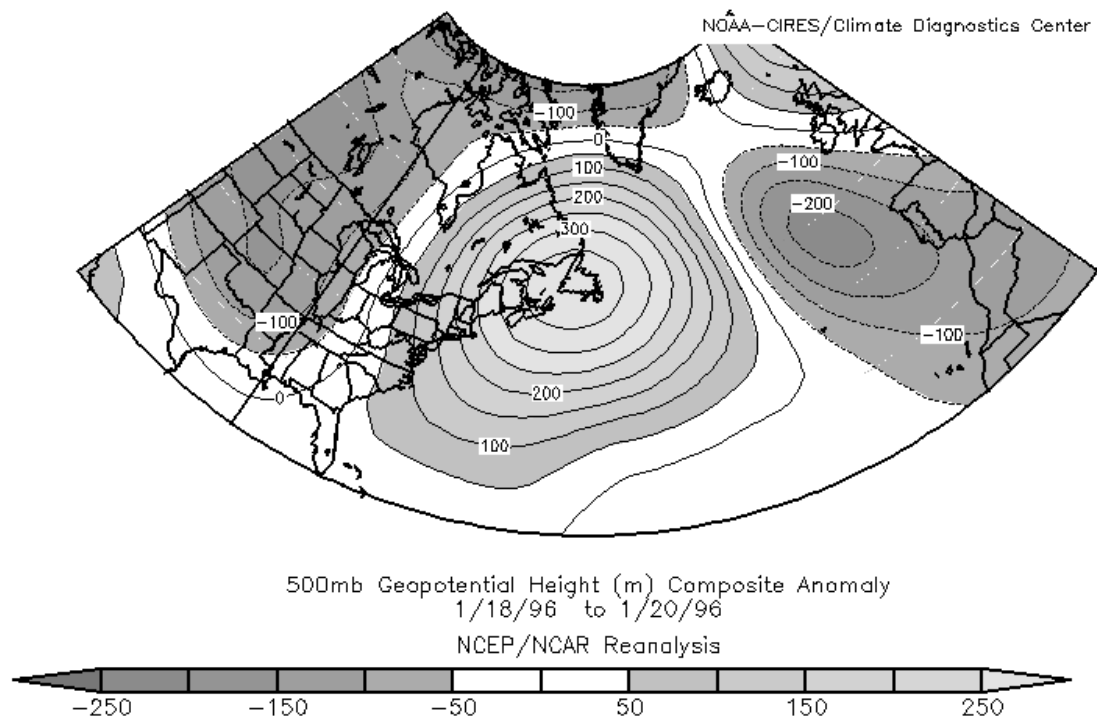


Fig. 3.59b. 500 mb geopotential height anomaly map (m) covering the two NAO domains during the 18–20 January 1996 storm.

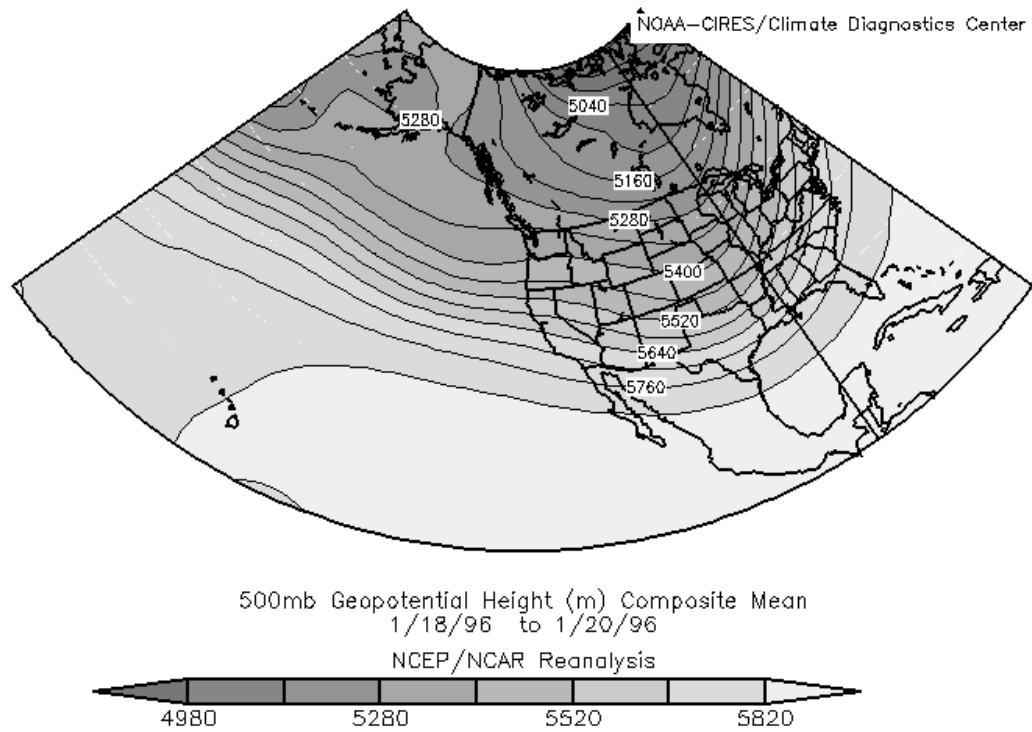


Fig. 3.60a. 500 mb geopotential height map (m) covering the four PNA domains during the 18–20 January 1996 storm.

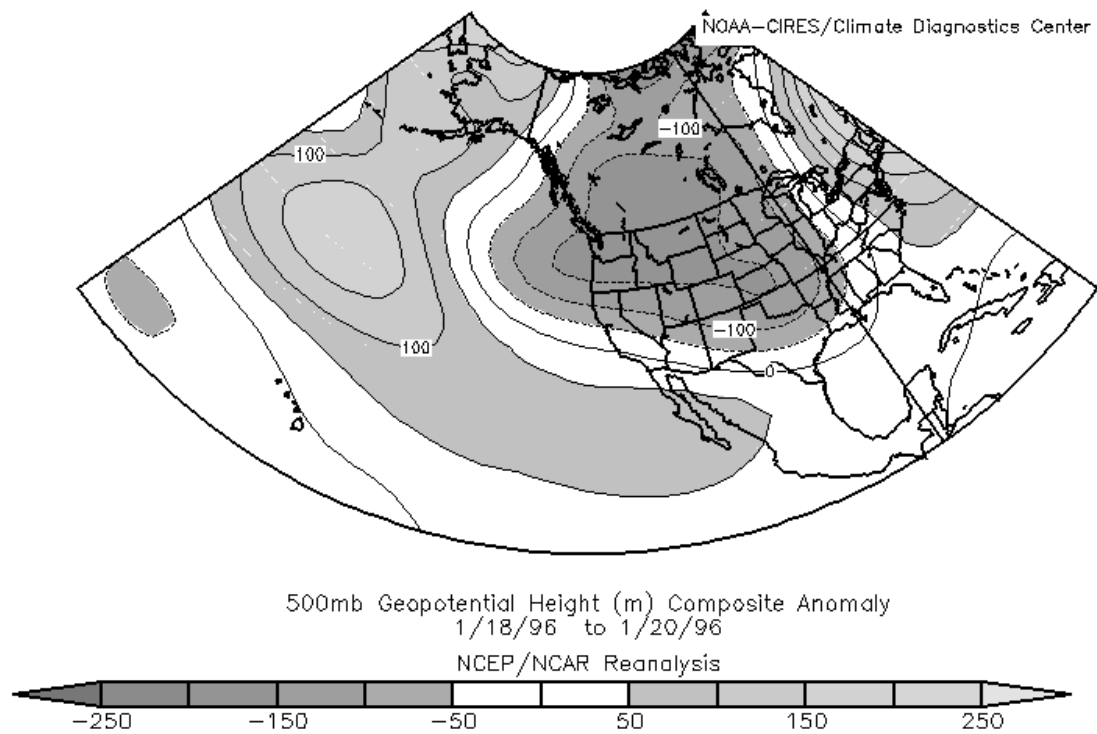


Fig. 3.60b. 500 mb geopotential height anomaly map (m) covering the four PNA domains during the 18–20 January 1996 storm.

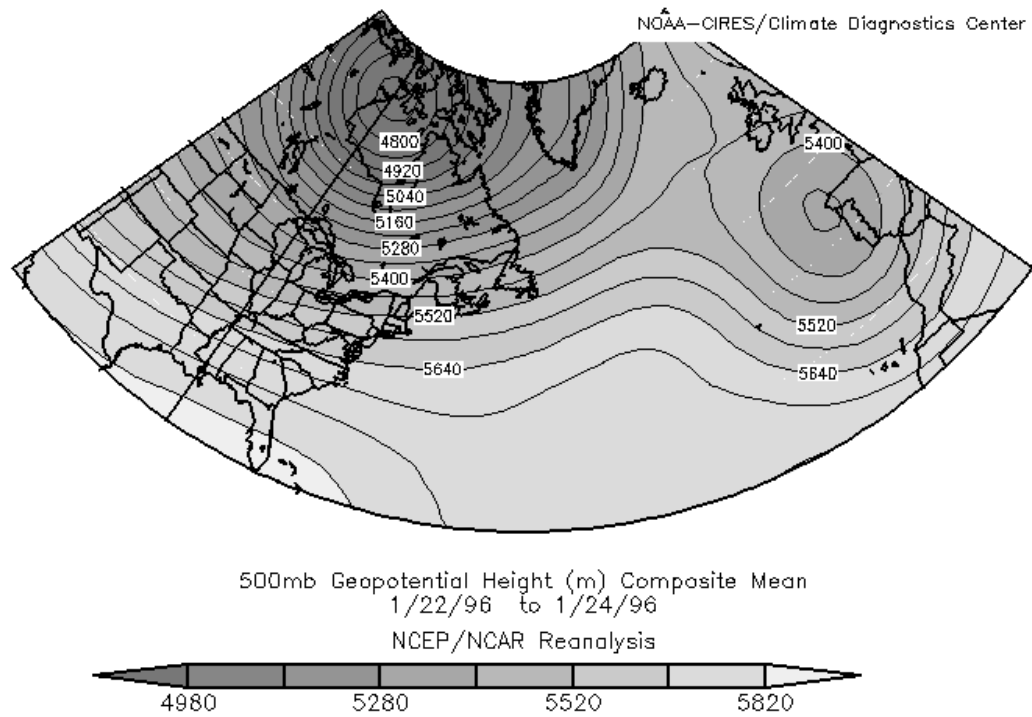


Fig. 3.61a. 500 mb geopotential height map (m) covering the two NAO domains after the 18–20 January 1996 storm.

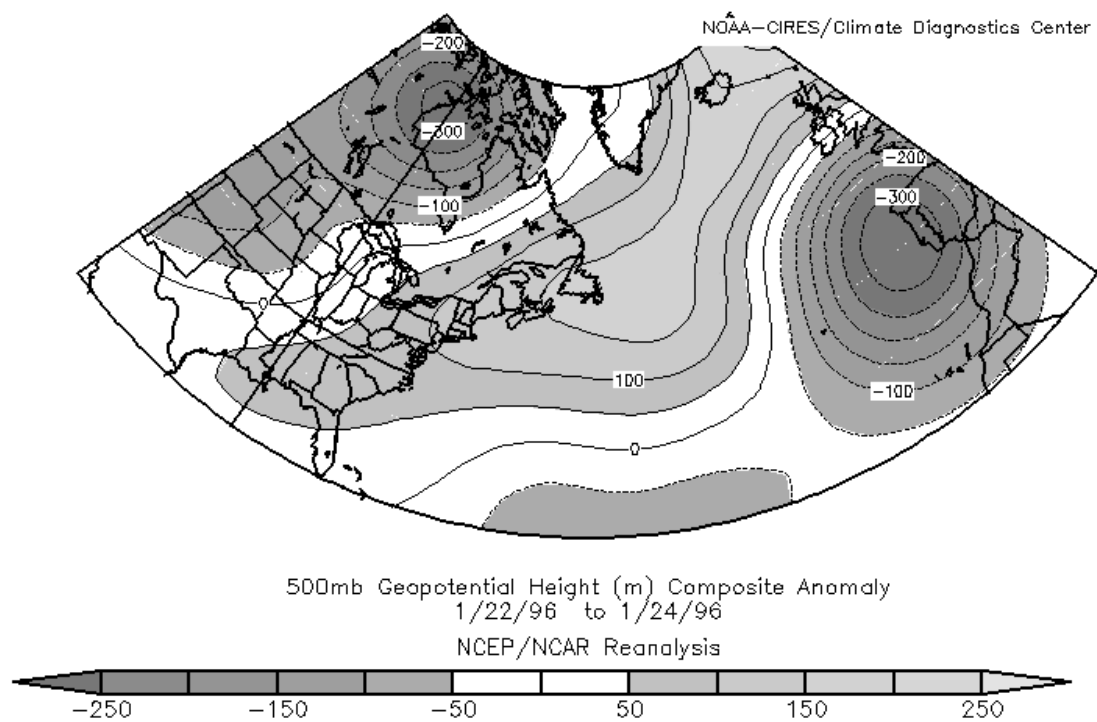


Fig. 3.61b. 500 mb geopotential height anomaly map (m) covering the two NAO domains after the 18–20 January 1996 storm.

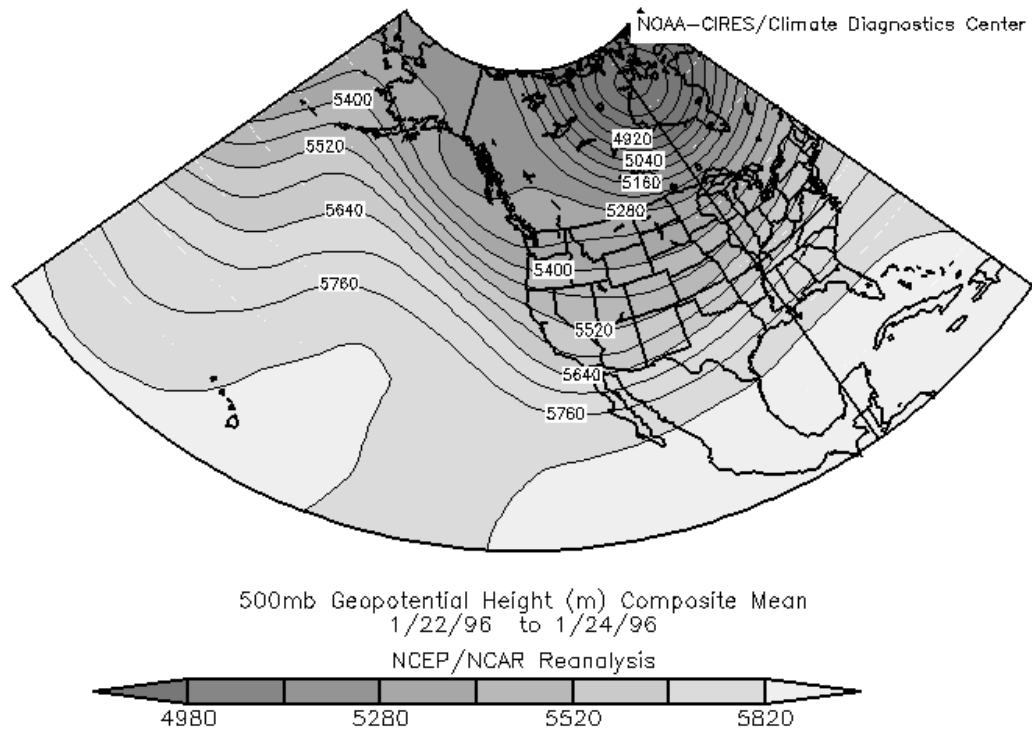


Fig. 3.62a. 500 mb geopotential height map (m) covering the four PNA domains after the 18–20 January 1996 storm.

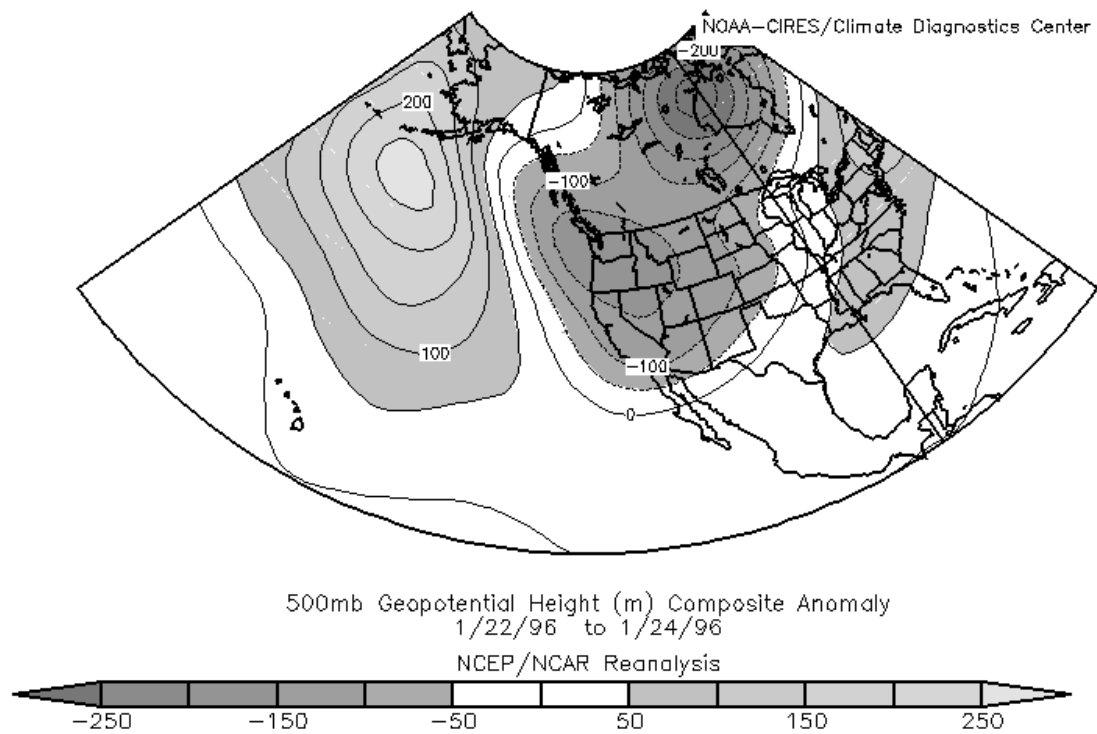


Fig. 3.62b. 500 mb geopotential height anomaly map (m) covering the four PNA domains after the 18–20 January 1996 storm.

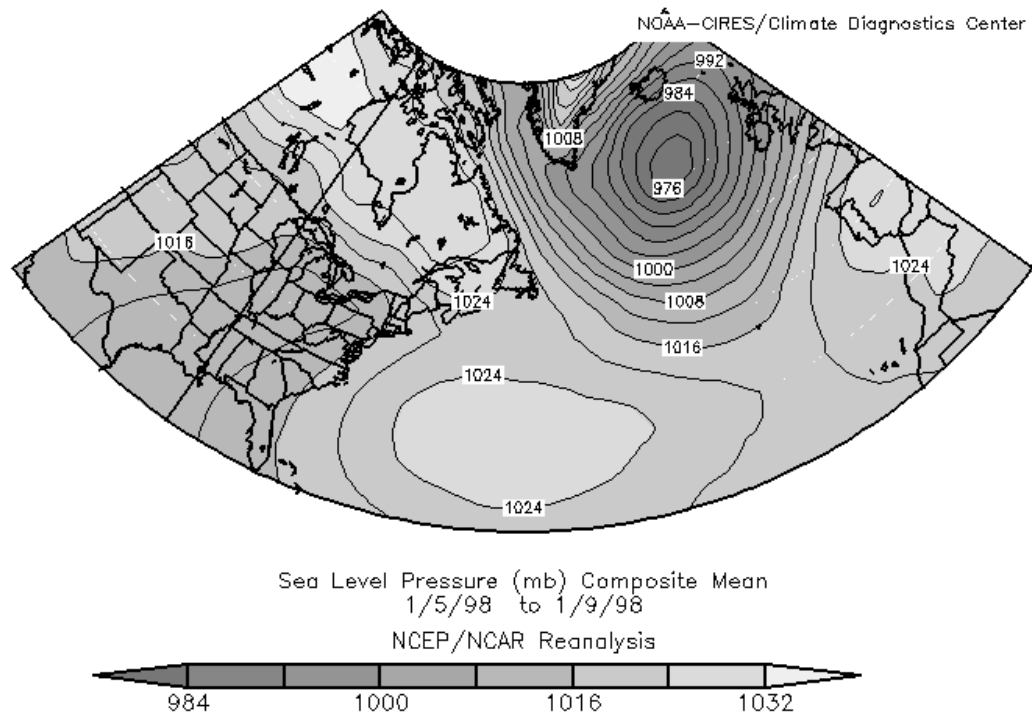


Fig. 3.63a. Sea-level pressure map (mb) for the 5–9 January 1998 ice storm.

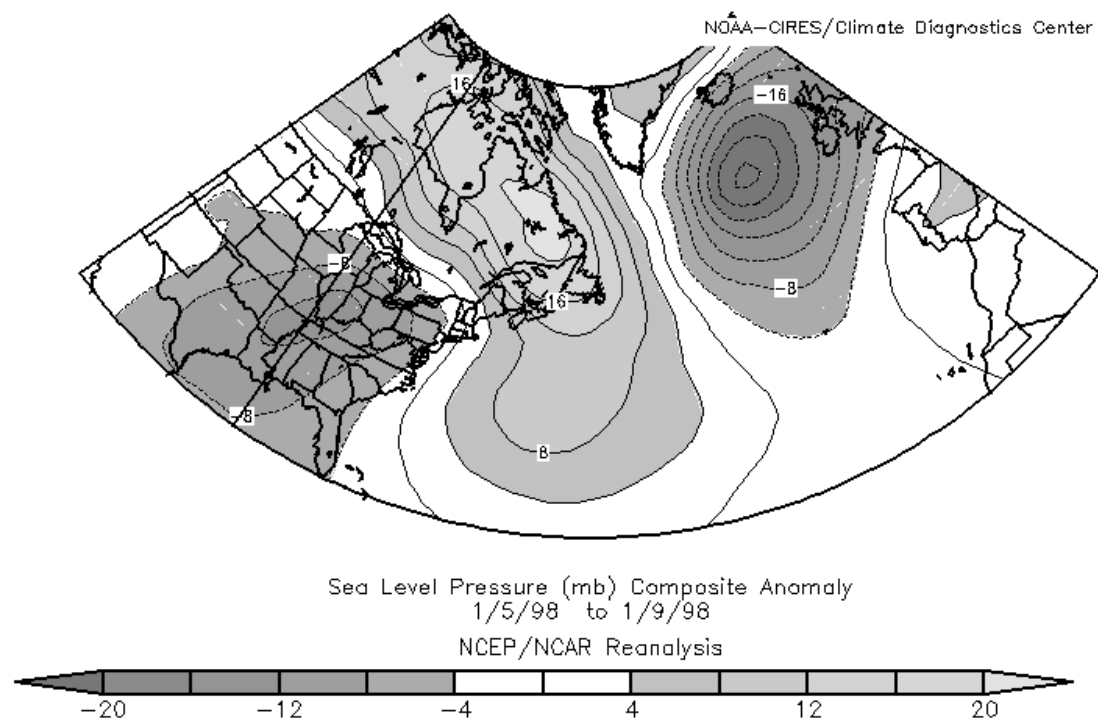


Fig. 3.63b. Sea-level pressure anomaly map (mb) for the 5–9 January 1998 ice storm.

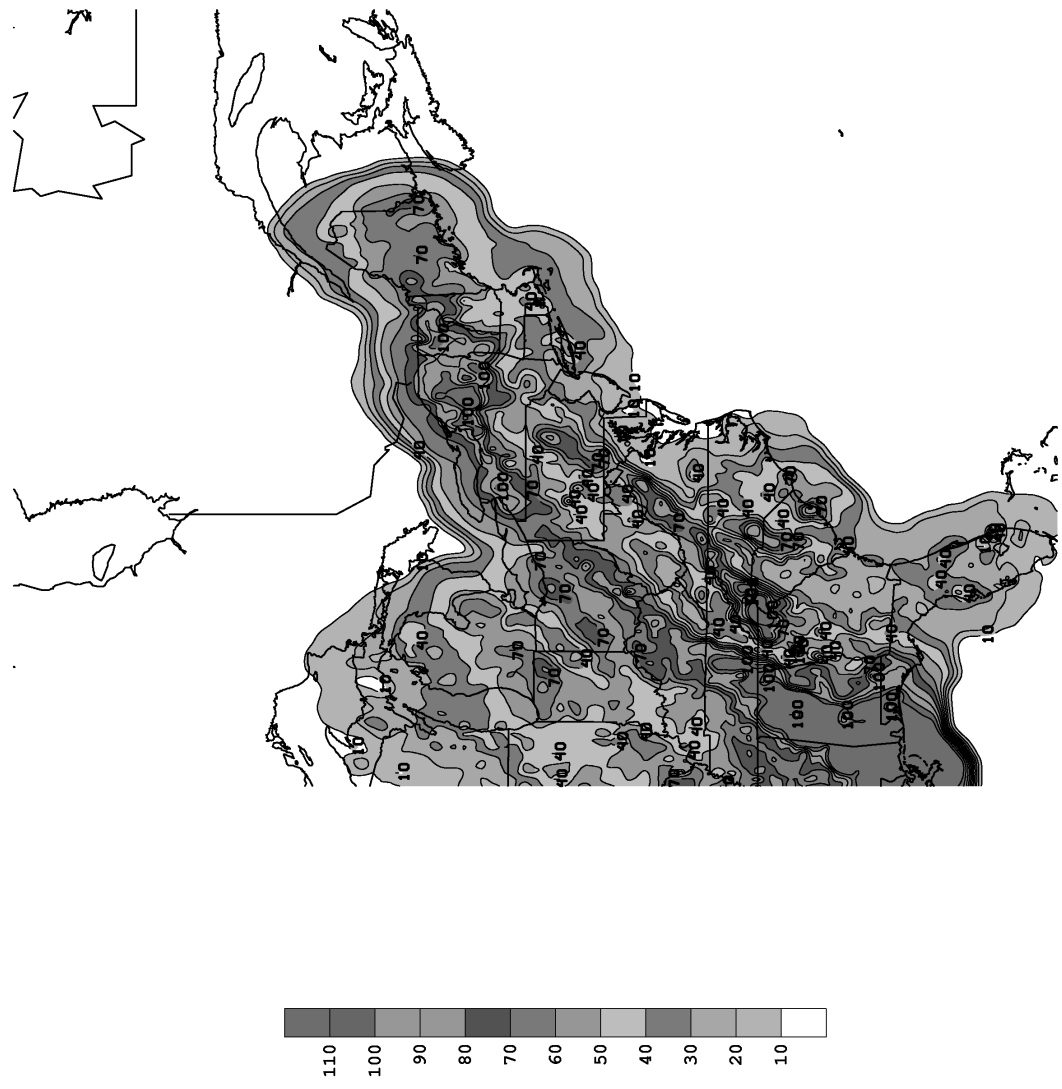


Fig. 3.64. Precipitation total (mm) starting at 1200 UTC on 5 January and ending at 1200 UTC on 9 January 1998.

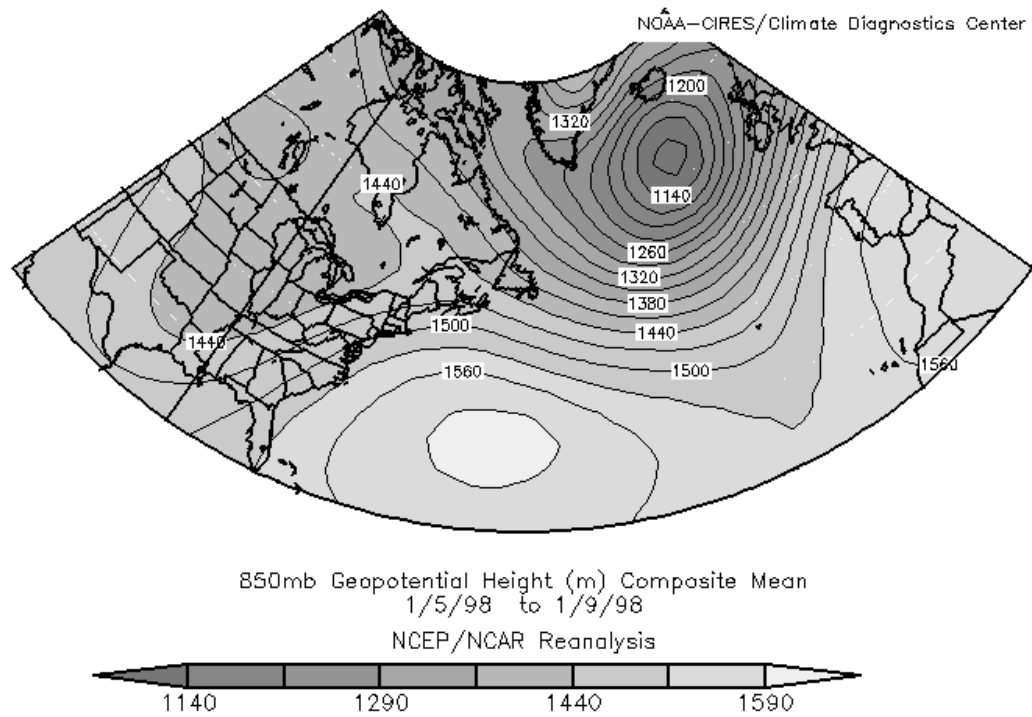


Fig. 3.65a. 850 mb geopotential height map for the 5–9 January 1998 ice storm.

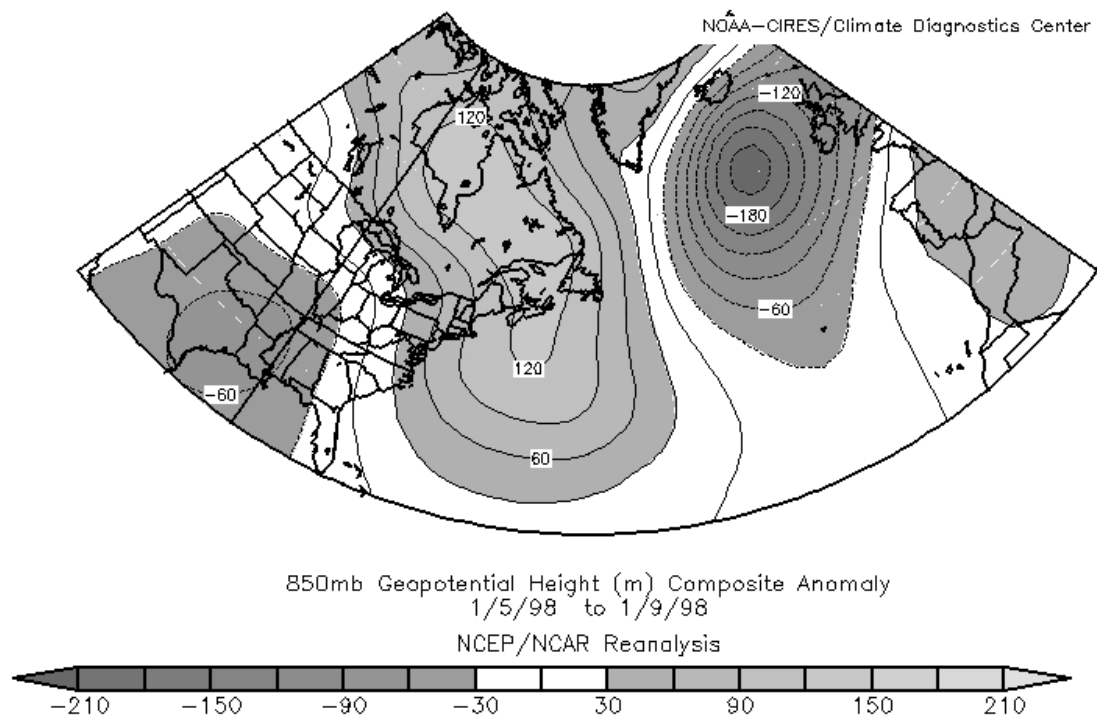


Fig. 3.65b. 850 mb geopotential height anomaly map for the 5–9 January 1998 ice storm.

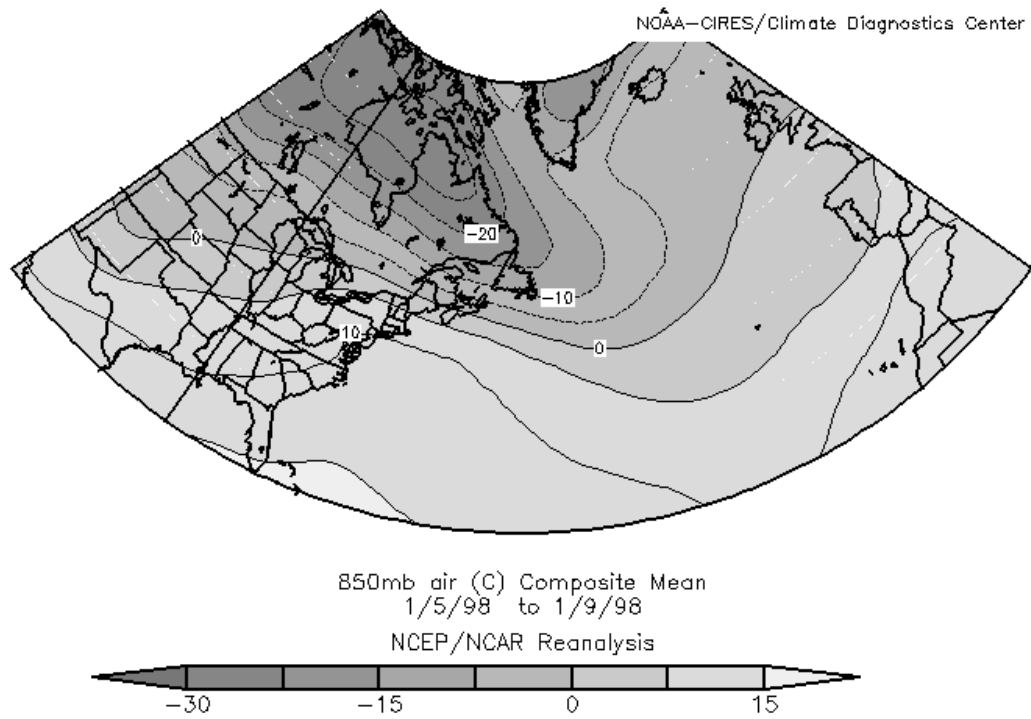


Fig. 3.66a. 850 mb temperature map (°C) for the 5–9 January 1998 ice storm.

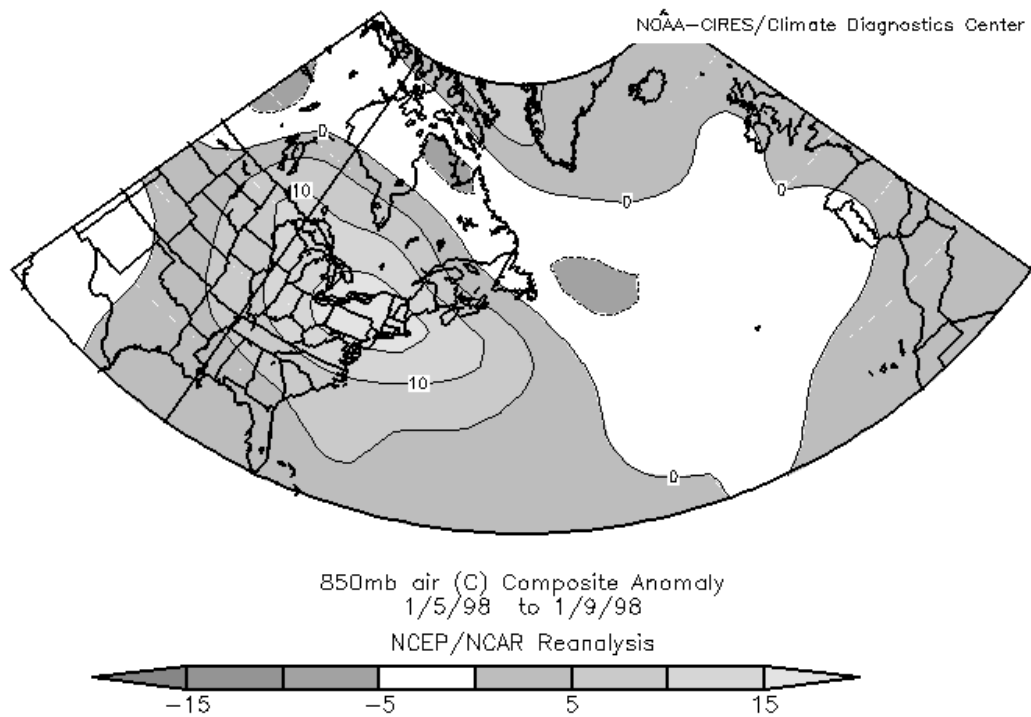


Fig. 3.66b. 850 mb temperature anomaly map (°C) for the 5–9 January 1998 ice storm.

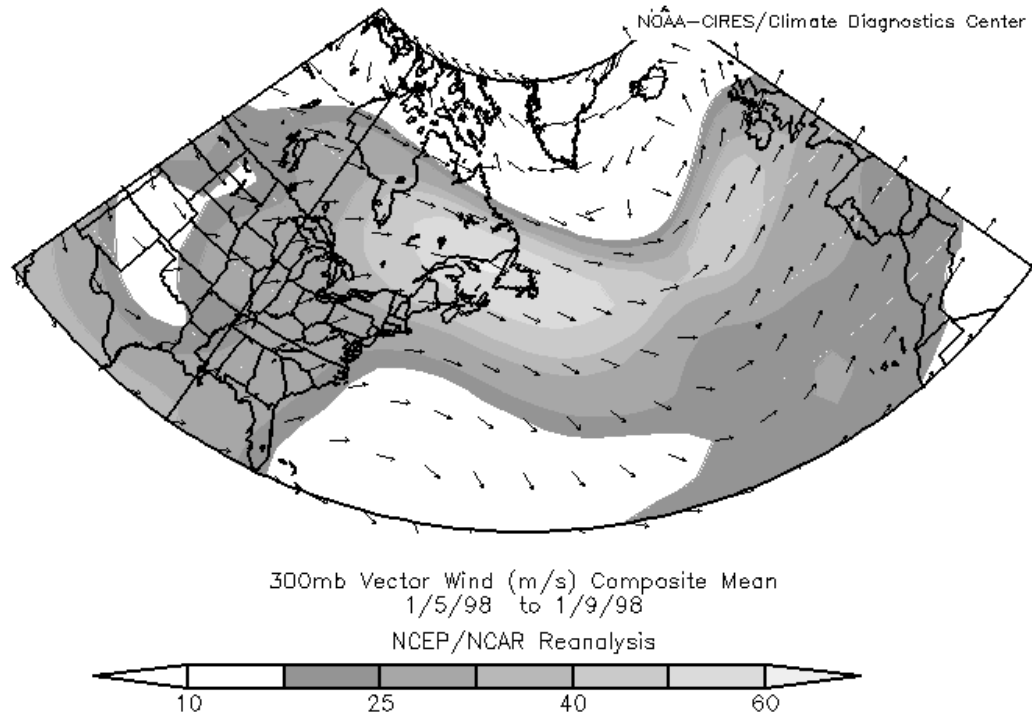


Fig. 3.67a. 300 mb vector wind map (m s^{-1}) for 5–9 January 1998 ice storm.

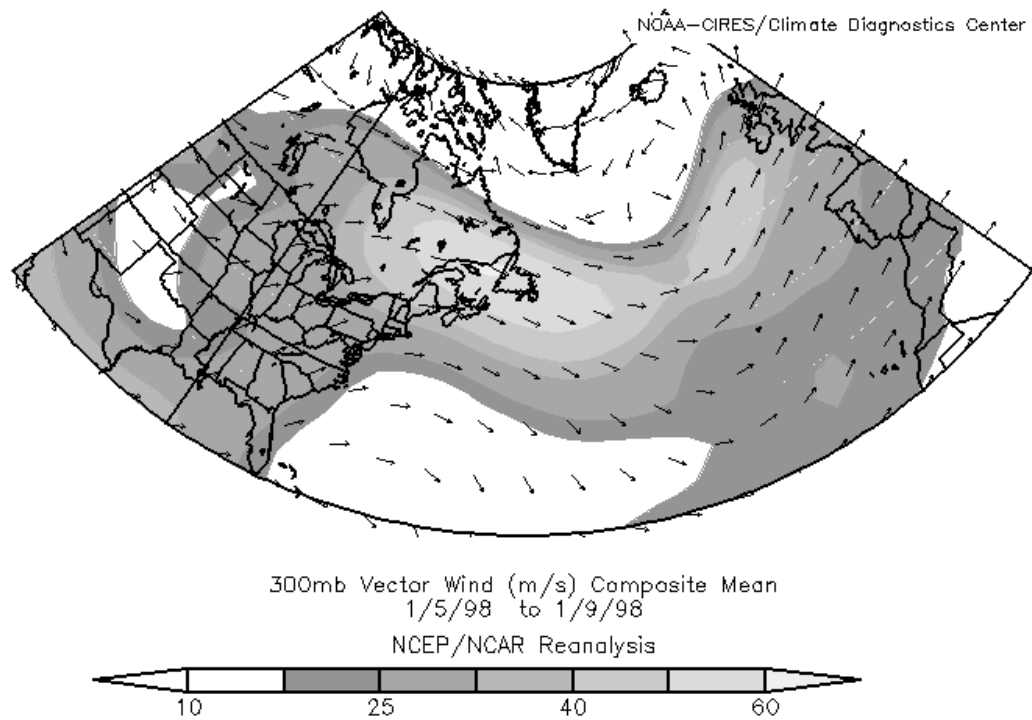


Fig. 3.67b. 300 mb vector wind anomaly map (m s^{-1}) for 5–9 January 1998 ice storm.

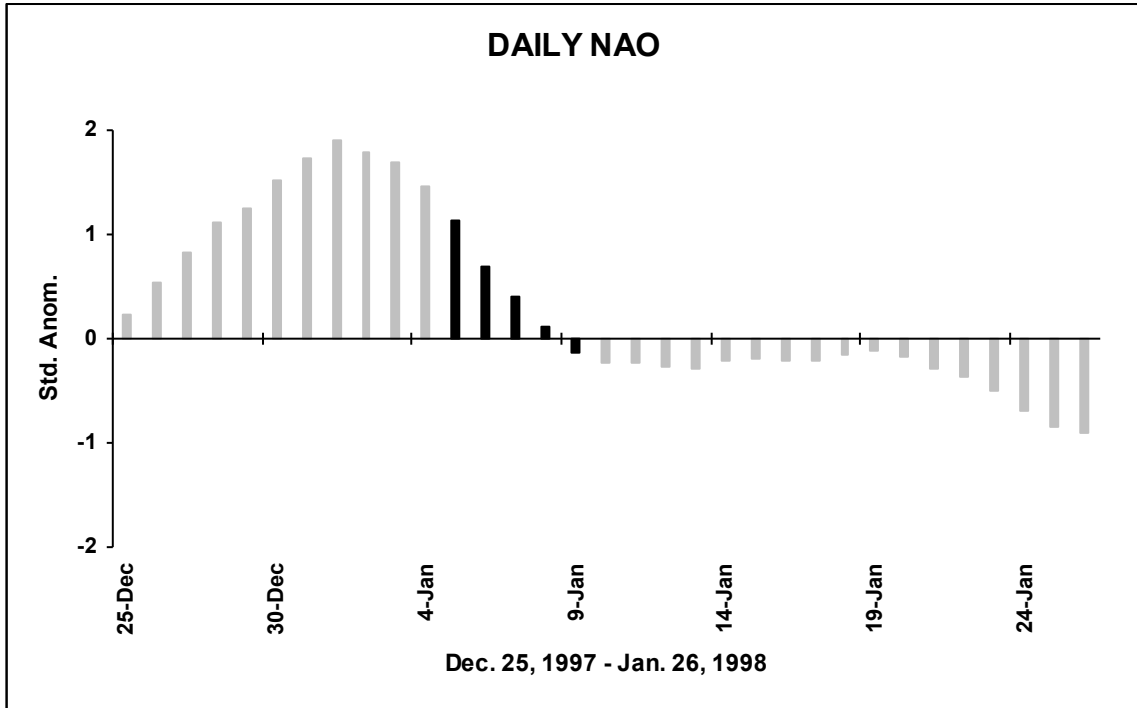


Fig. 3.68a. Daily NAO index, with the 5–9 January 1998 ice storm highlighted in black.

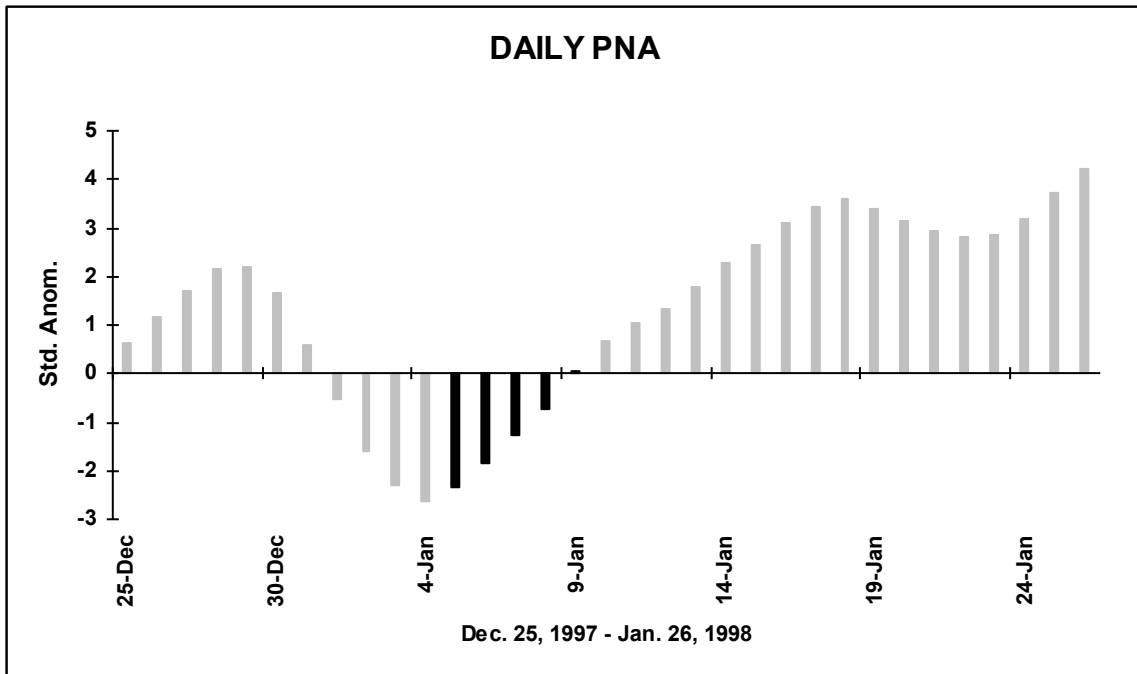


Fig. 3.68b. Daily PNA index, with the 5–9 January 1998 ice storm highlighted in black.

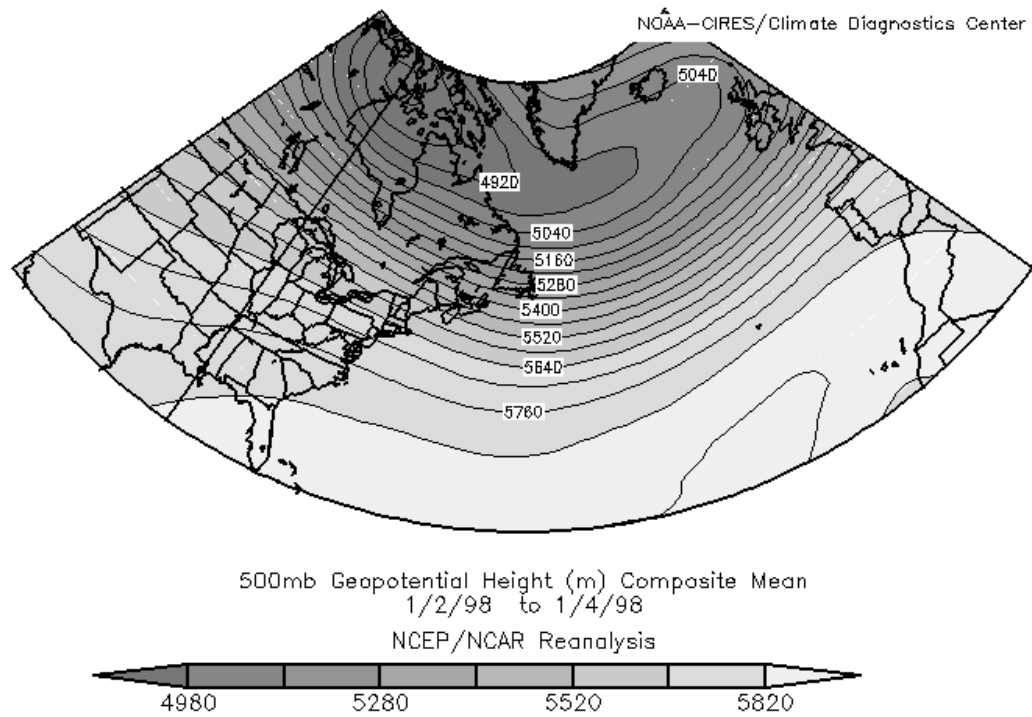


Fig. 3.69a. 500 mb geopotential height map (m) covering the two NAO domains prior to the 5–9 January 1998 ice storm.

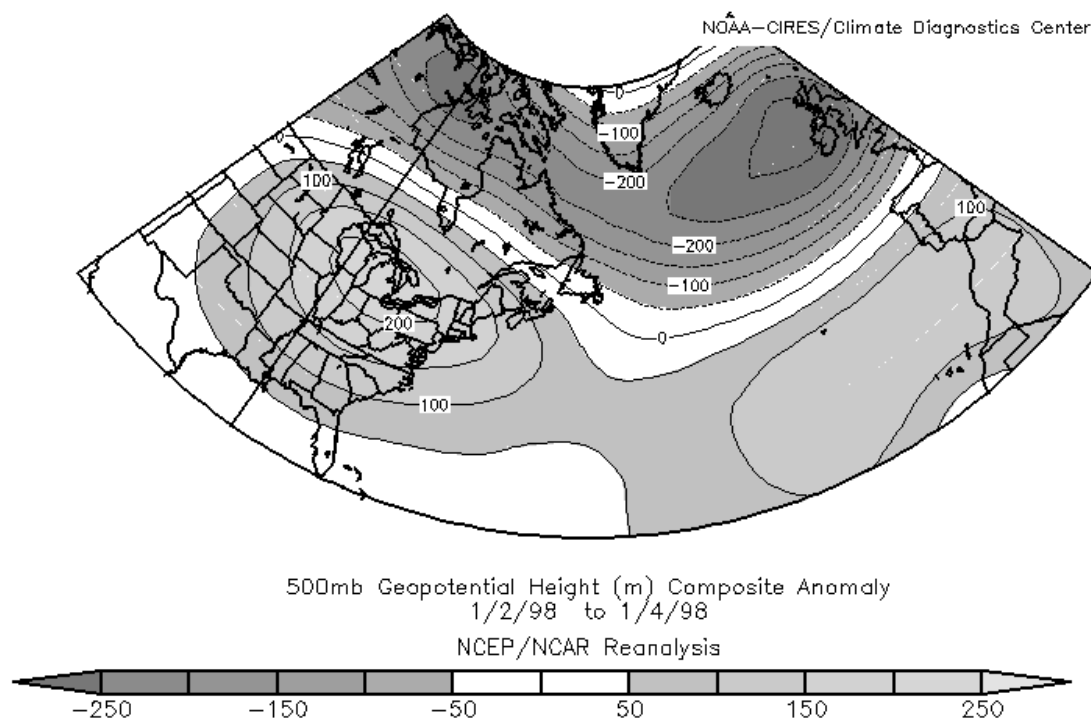


Fig. 3.69b. 500 mb geopotential height anomaly map (m) covering the two NAO domains prior to the 5–9 January 1998 ice storm.

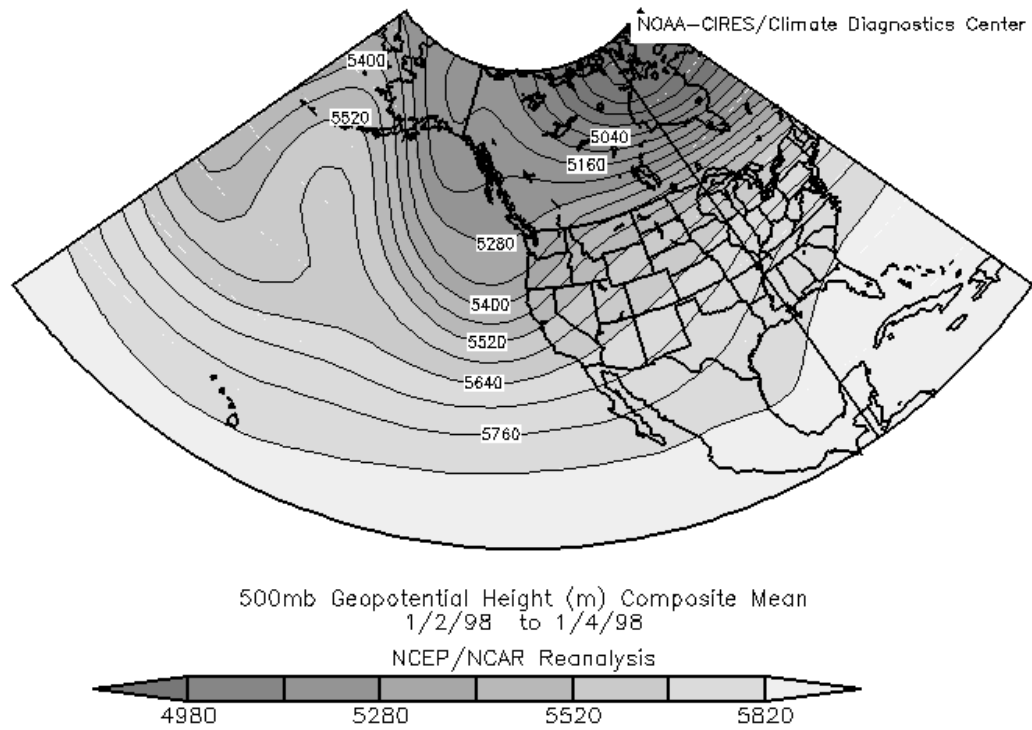


Fig. 3.70a. 500 mb geopotential height map (m) covering the four PNA domains prior to the 5–9 January 1998 ice storm.

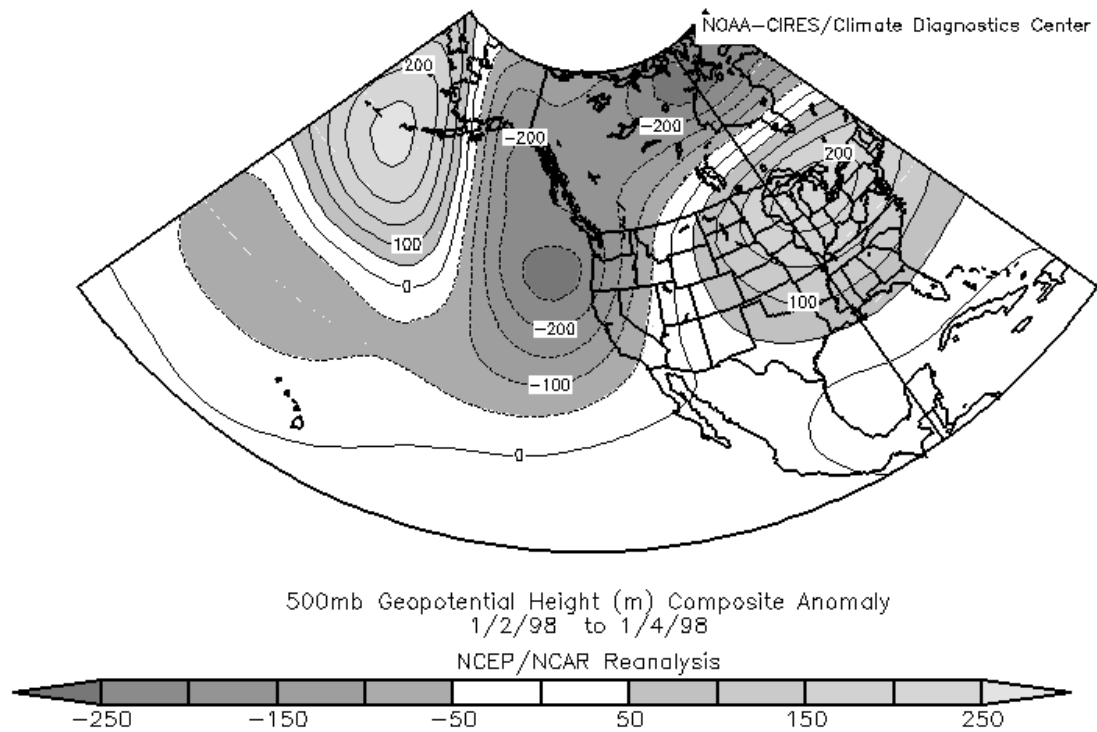


Fig. 3.70b. 500 mb geopotential height anomaly map (m) covering the four PNA domains prior to the 5–9 January 1998 ice storm.

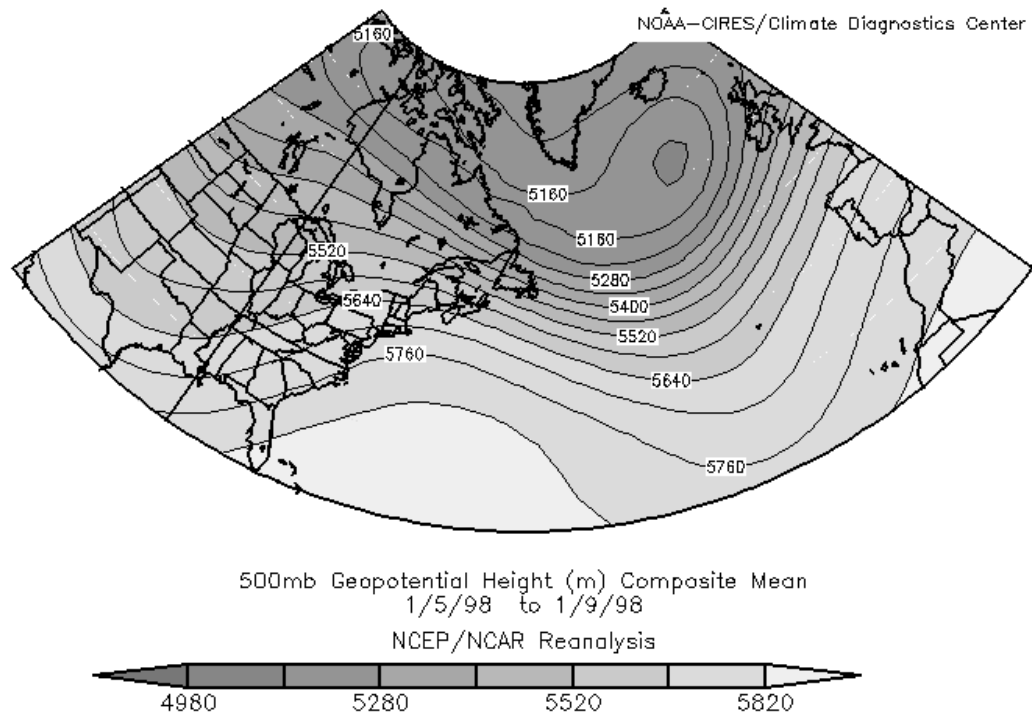


Fig. 3.71a. 500 mb geopotential height map (m) covering the two NAO domains during the 5–9 January 1998 ice storm.

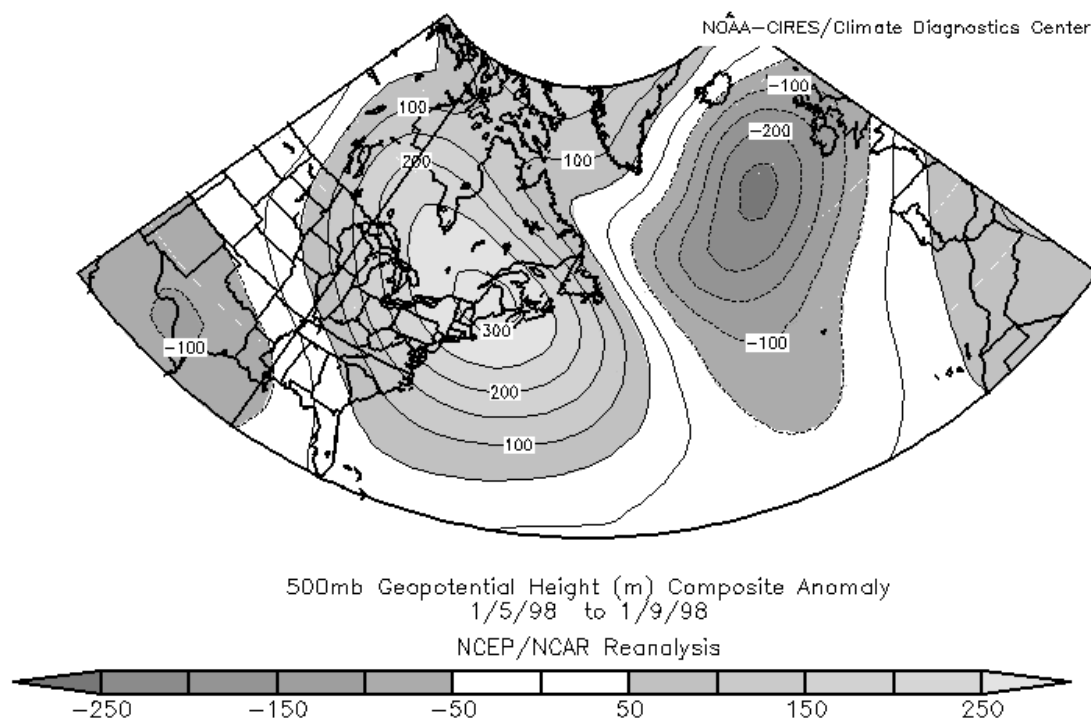


Fig. 3.71b. 500 mb geopotential height anomaly map (m) covering the two NAO domains during the 5–9 January 1998 ice storm.

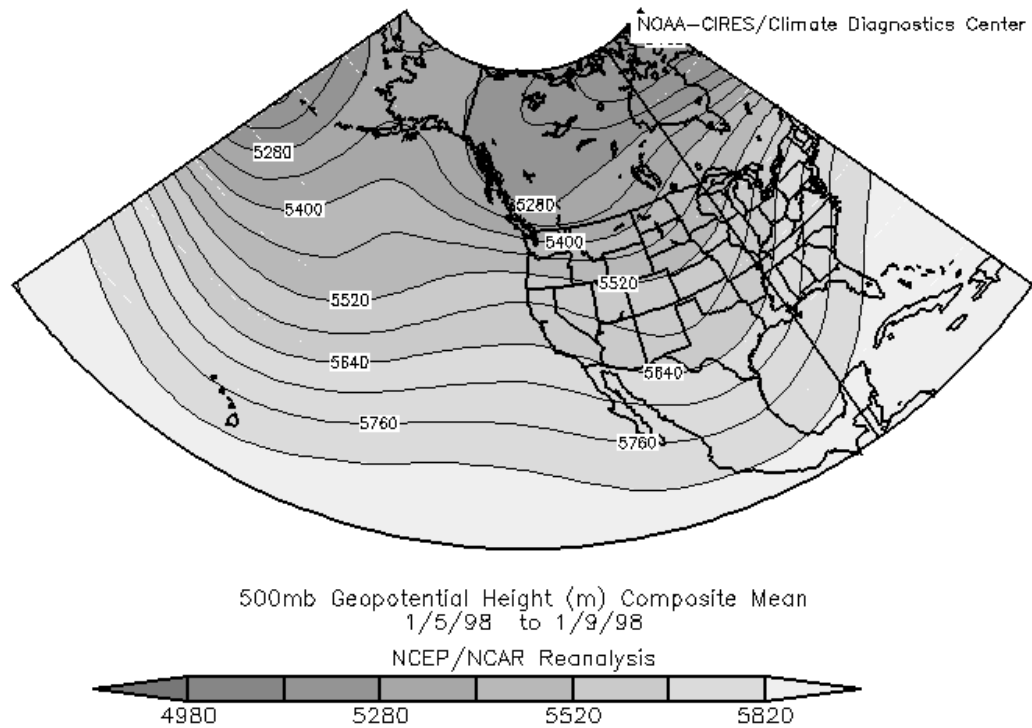


Fig. 3.72a. 500 mb geopotential height map (m) covering the four PNA domains during the 5–9 January 1998 ice storm.

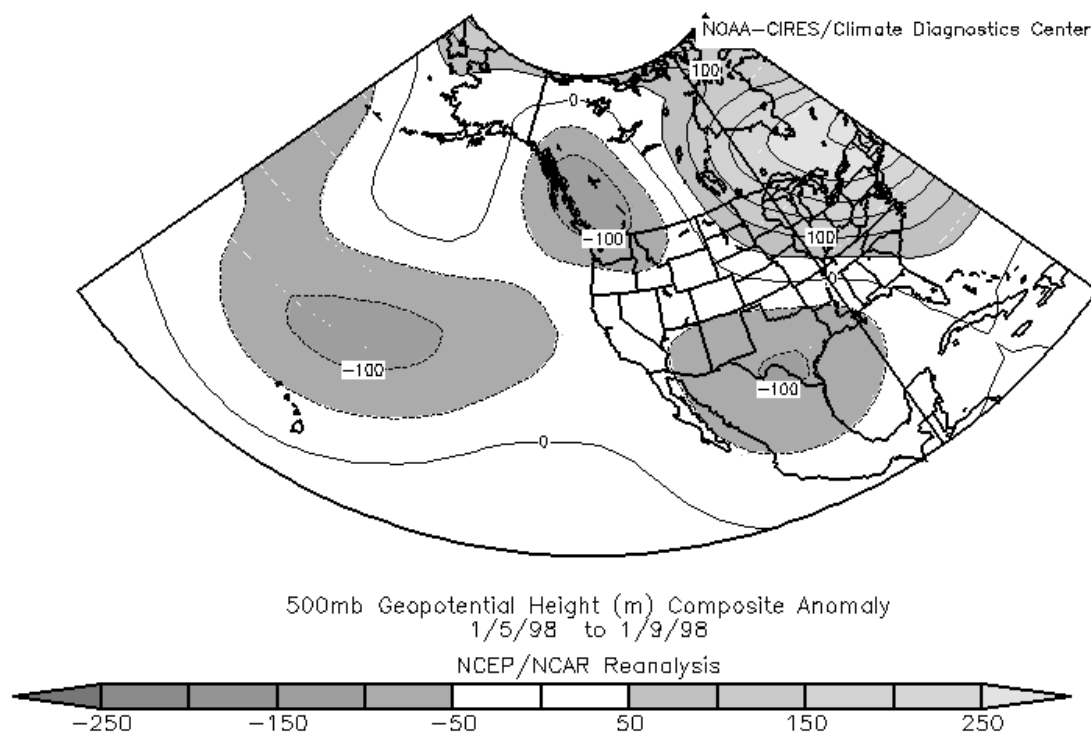


Fig. 3.72b. 500 mb geopotential height anomaly map (m) covering the four PNA domains during the 5–9 January 1998 ice storm.

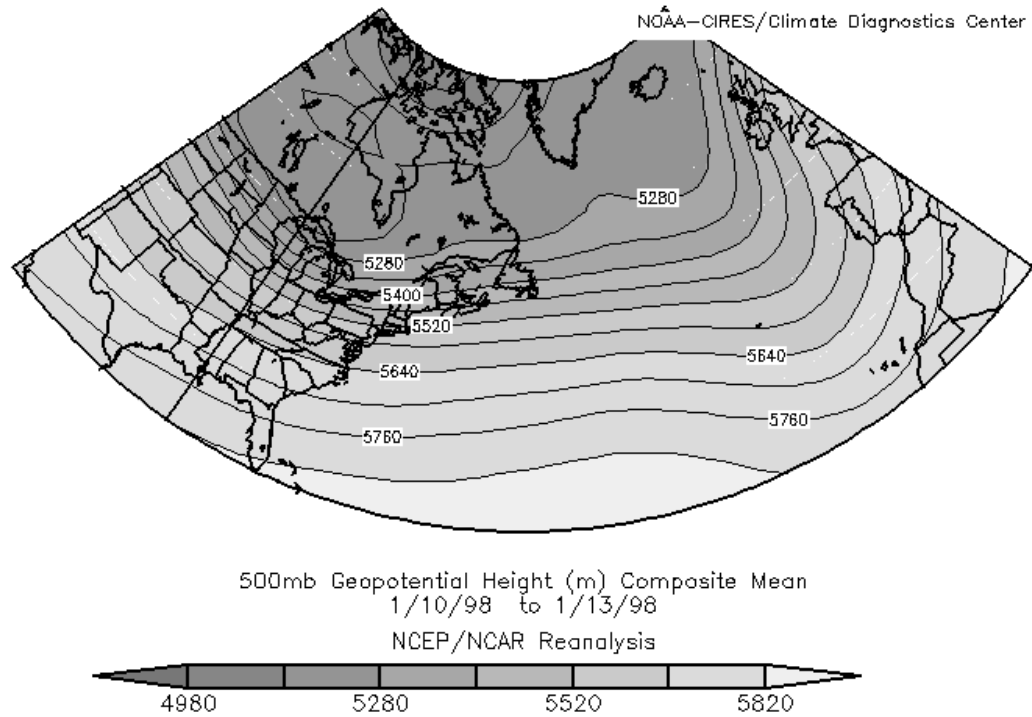


Fig. 3.73a. 500 mb geopotential height map (m) covering the two NAO domains after the 5–9 January 1998 ice storm.

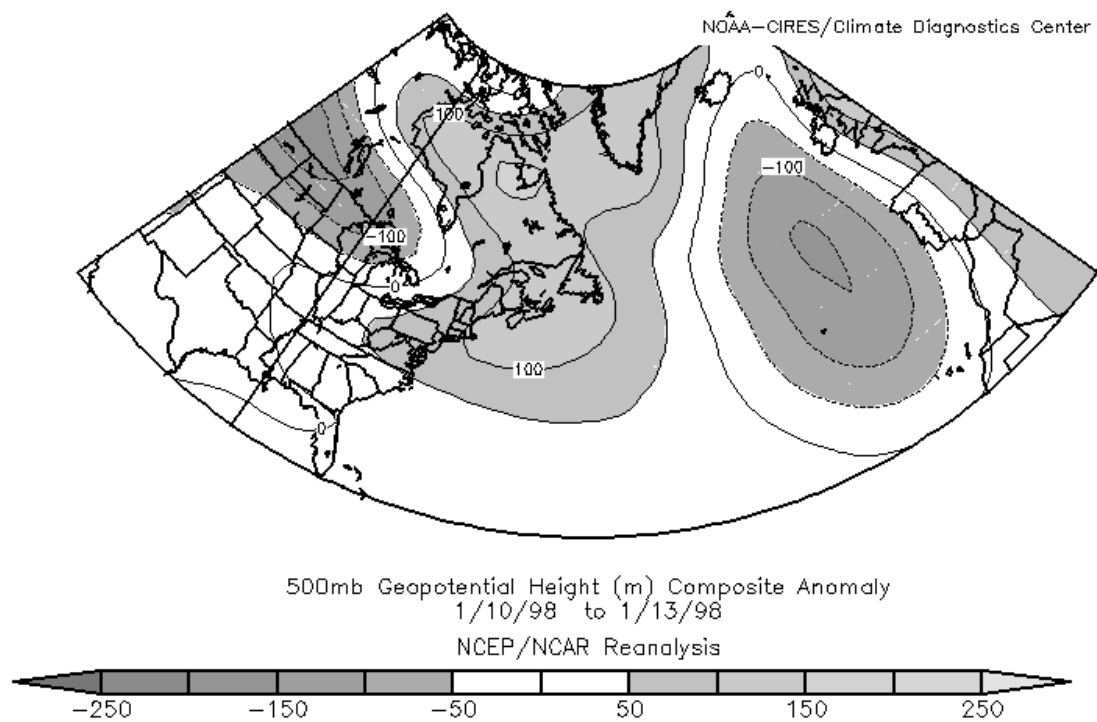


Fig. 3.73b. 500 mb geopotential height anomaly map (m) covering the two NAO domains after the 5–9 January 1998 ice storm.

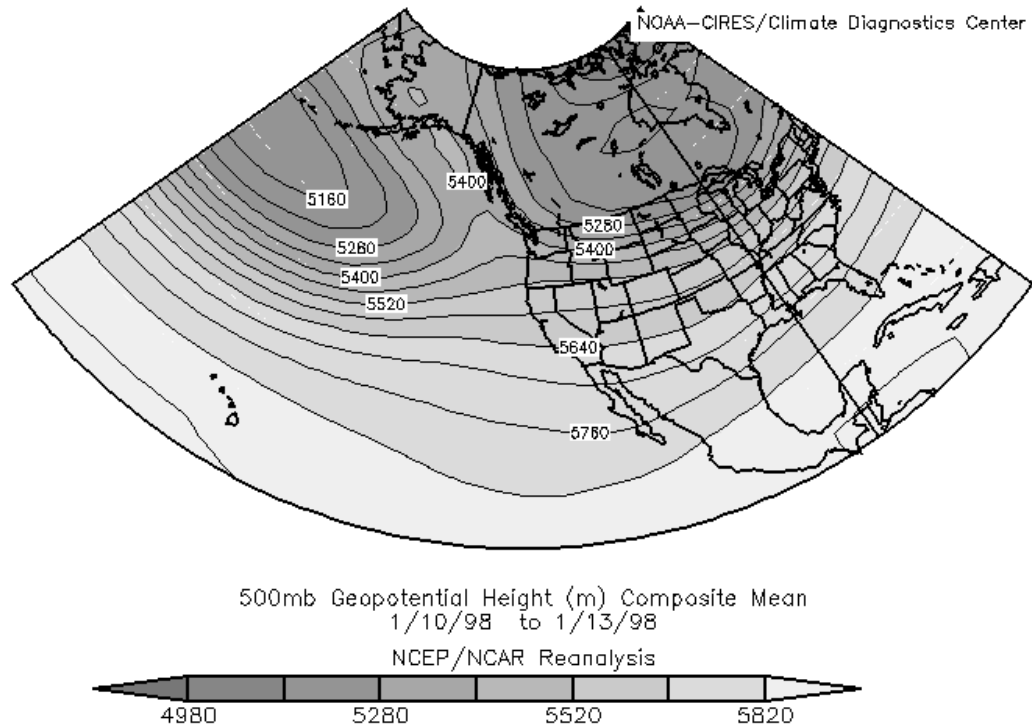


Fig. 3.74a. 500 mb geopotential height map (m) covering the four PNA domains after the 5–9 January 1998 ice storm.

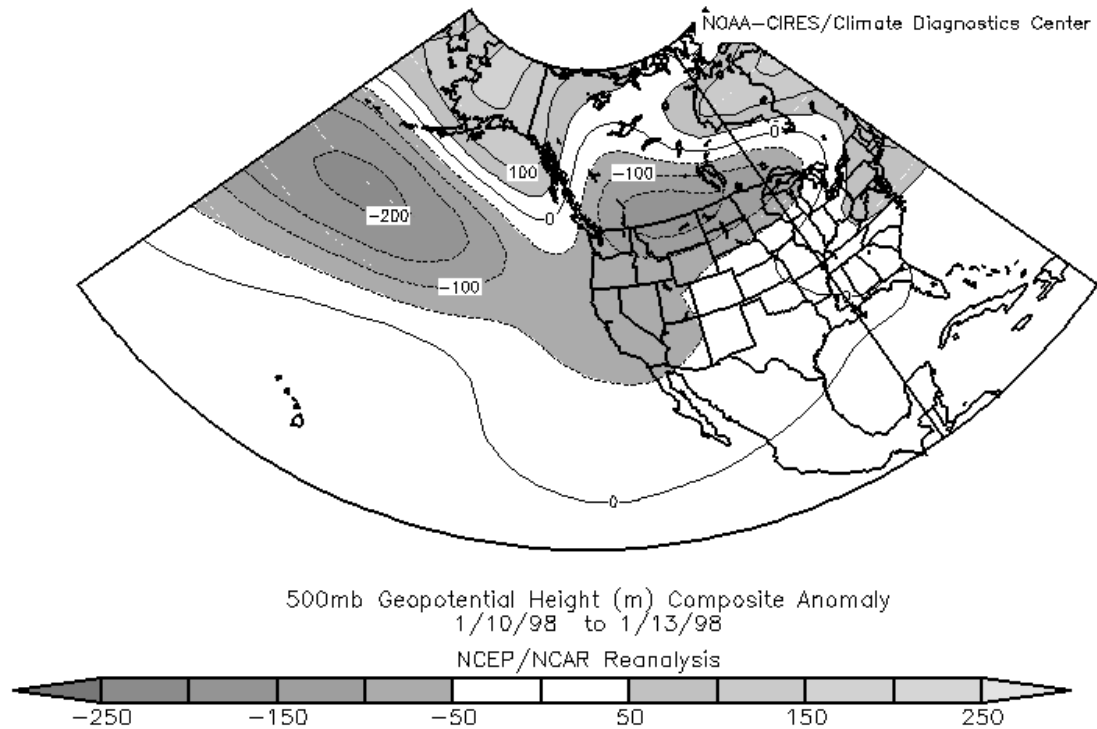


Fig. 3.74b. 500 mb geopotential height anomaly map (m) covering the four PNA domains after the 5–9 January 1998 ice storm.

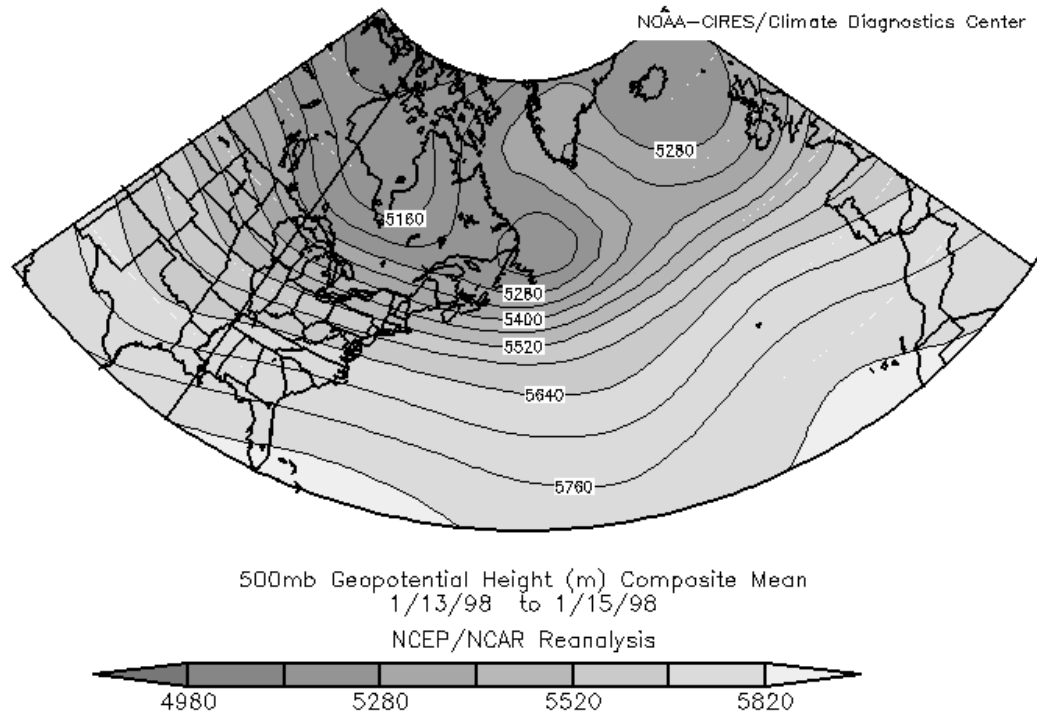


Fig. 3.75a. 500 mb geopotential height map (m) covering the two NAO domains after the 5–9 January 1998 ice storm.

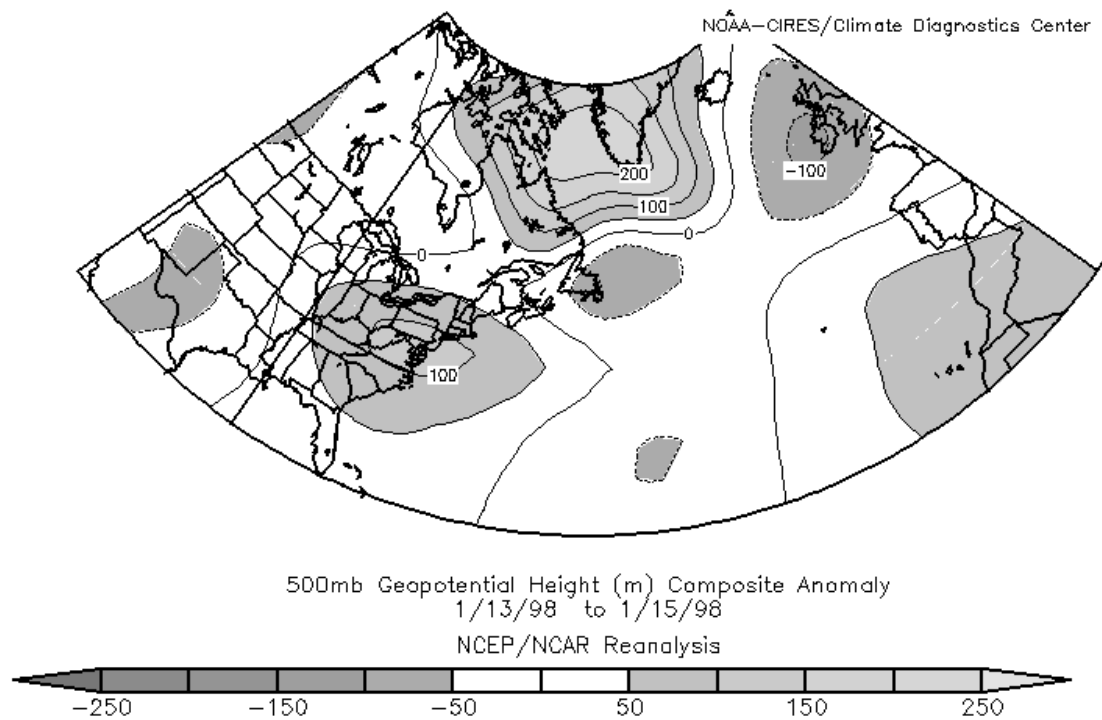


Fig. 3.75b. 500 mb geopotential height anomaly map (m) covering the two NAO domains after the 5–9 January 1998 ice storm.

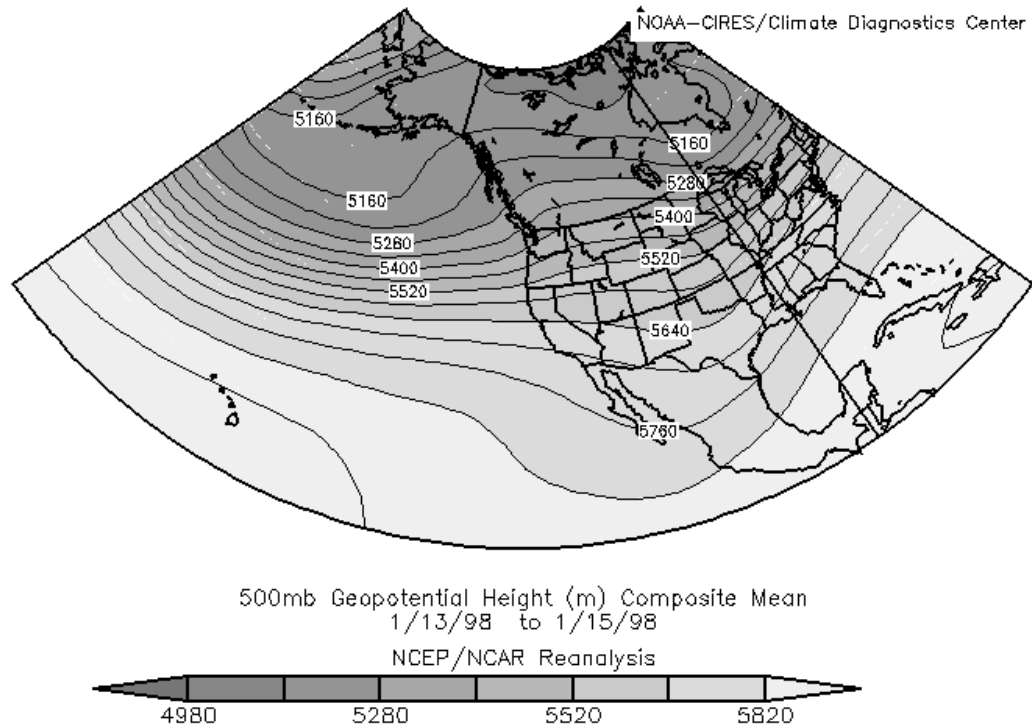


Fig. 3.76a. 500 mb geopotential height map (m) covering the four PNA domains after the 5–9 January 1998 ice storm.

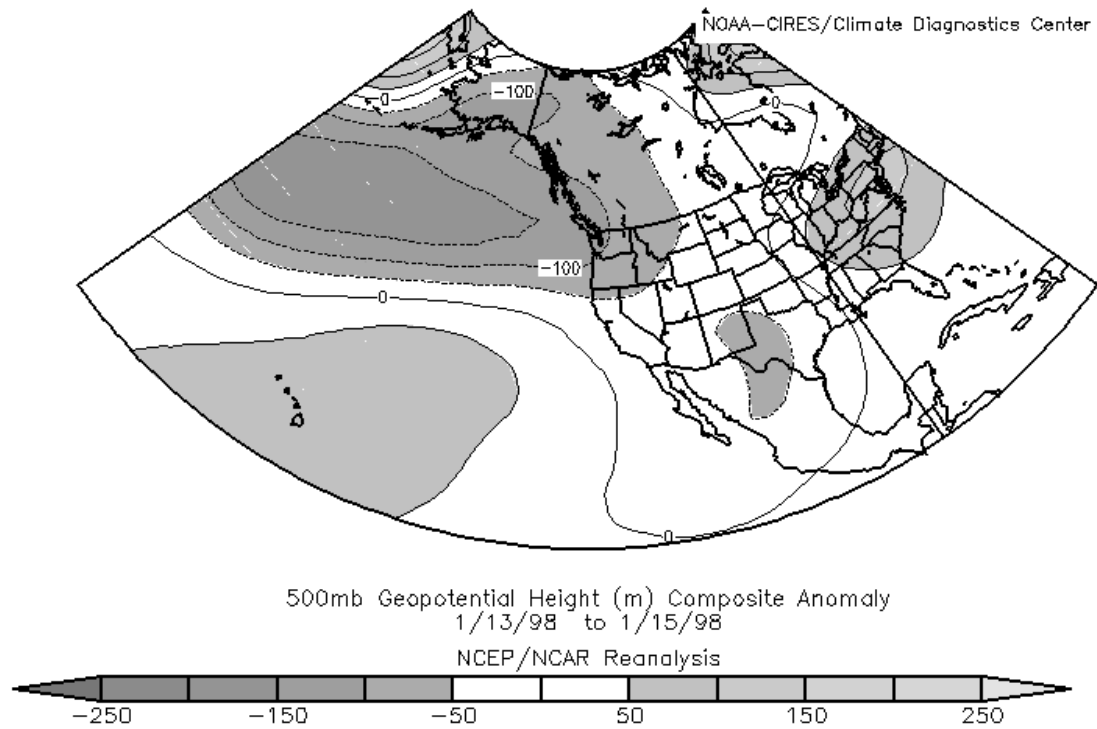


Fig. 3.76b. 500 mb geopotential height map (m) covering the four PNA domains after the 5–9 January 1998 ice storm.

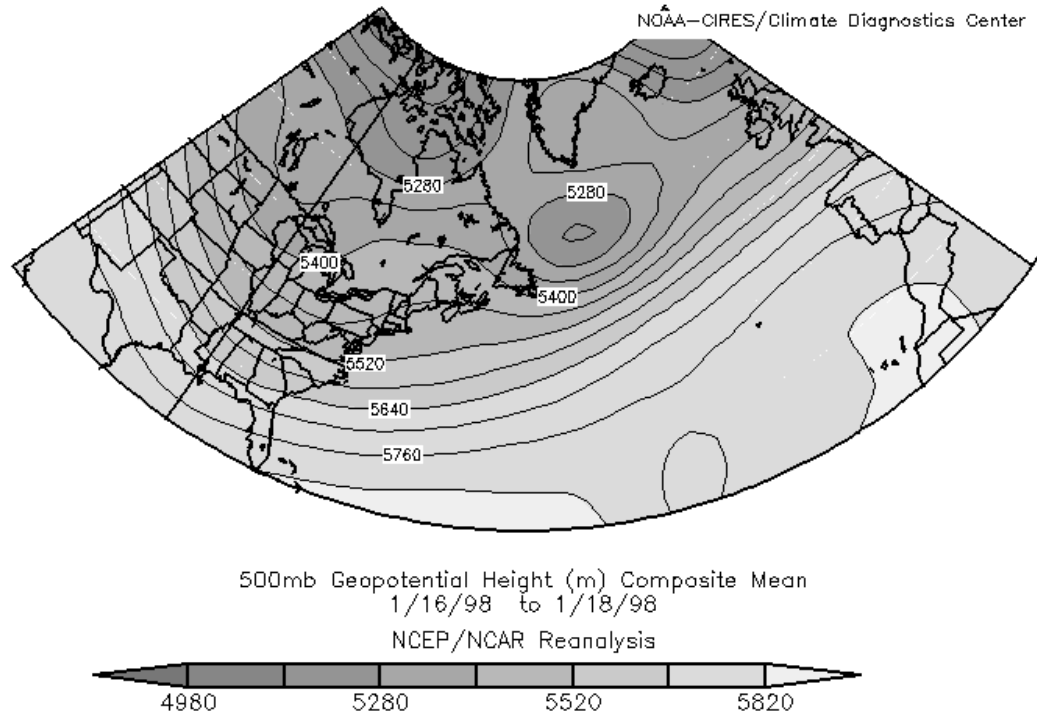


Fig. 3.77a. 500 mb geopotential height map (m) covering the two NAO domains after the 5–9 January 1998 ice storm.

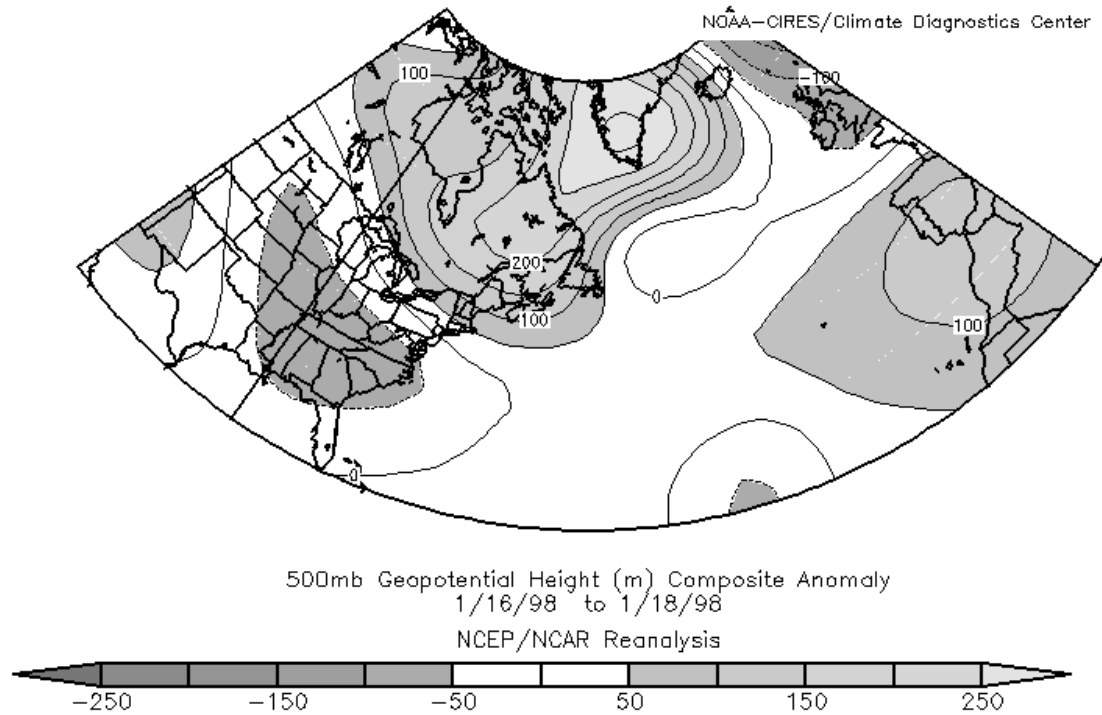


Fig. 3.77b. 500 mb geopotential height anomaly map (m) covering the two NAO domains after the 5–9 January 1998 ice storm.

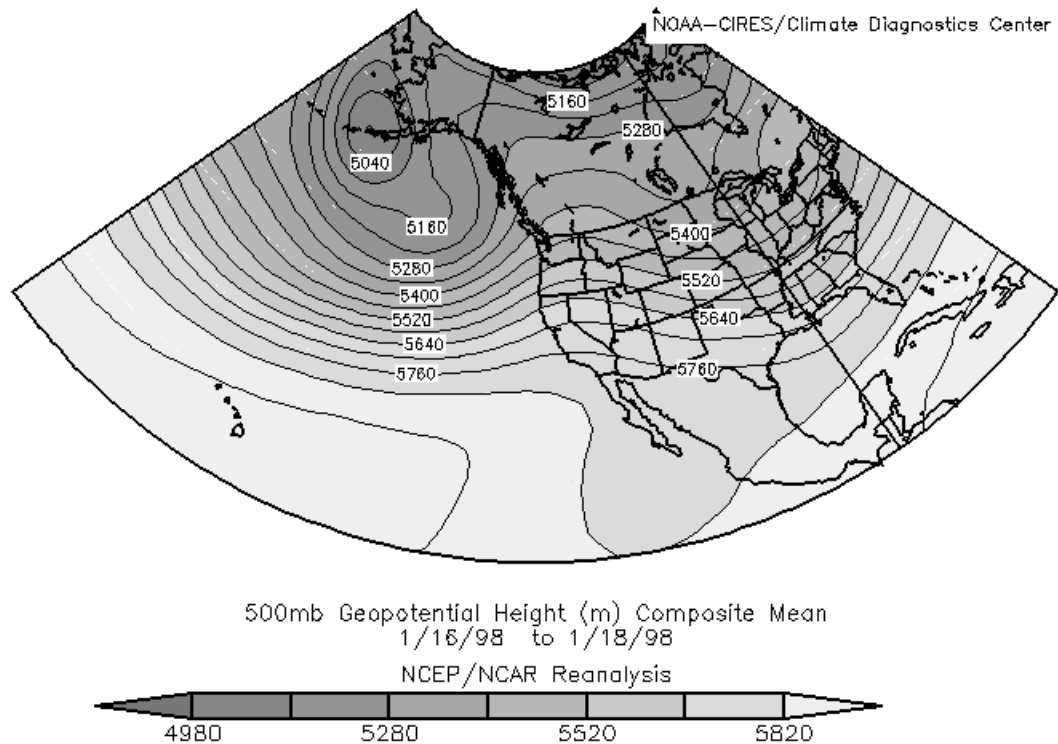


Fig. 3.78a. 500 mb geopotential height map (m) covering the four PNA domains after the 5–9 January 1998 ice storm.

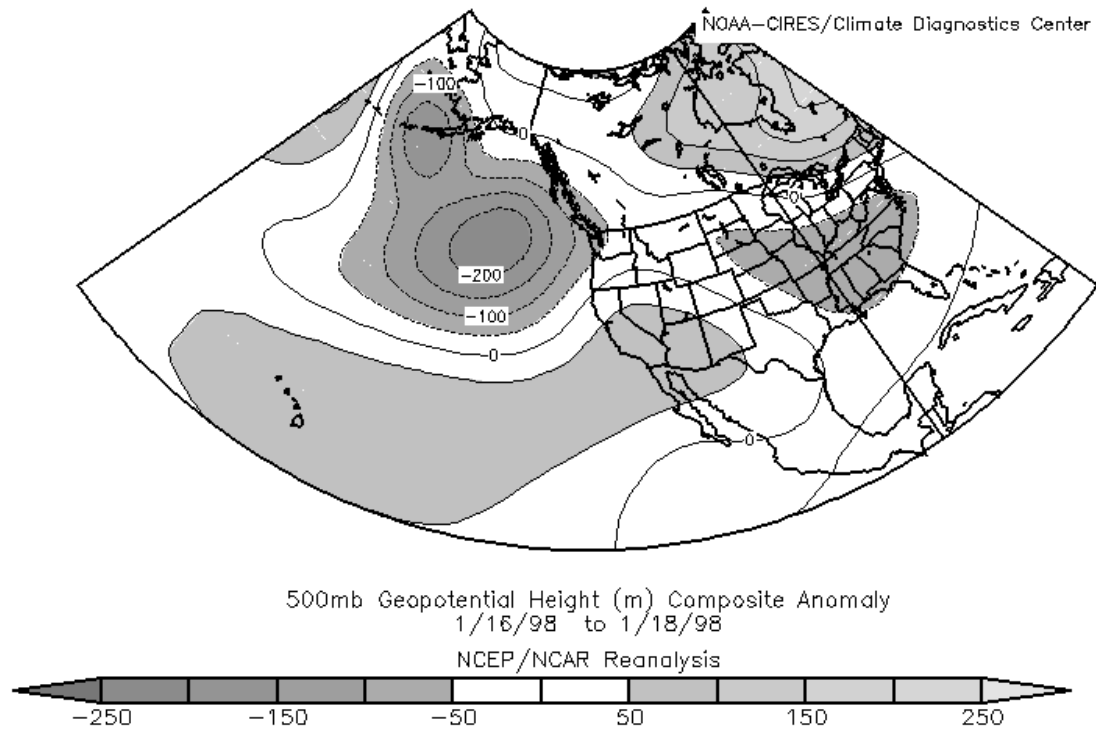


Fig. 3.78b. 500 mb geopotential height anomaly map (m) covering the four PNA domains after the 5–9 January 1998 ice storm.

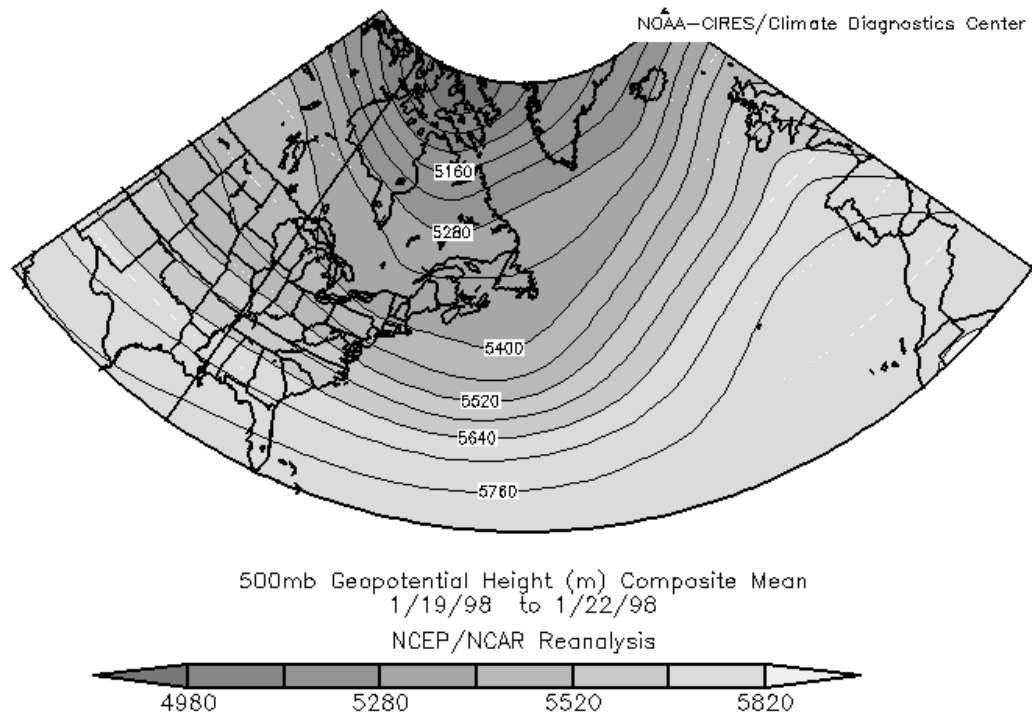


Fig. 3.79a. 500 mb geopotential height map (m) covering the two NAO domains after the 5–9 January 1998 ice storm.

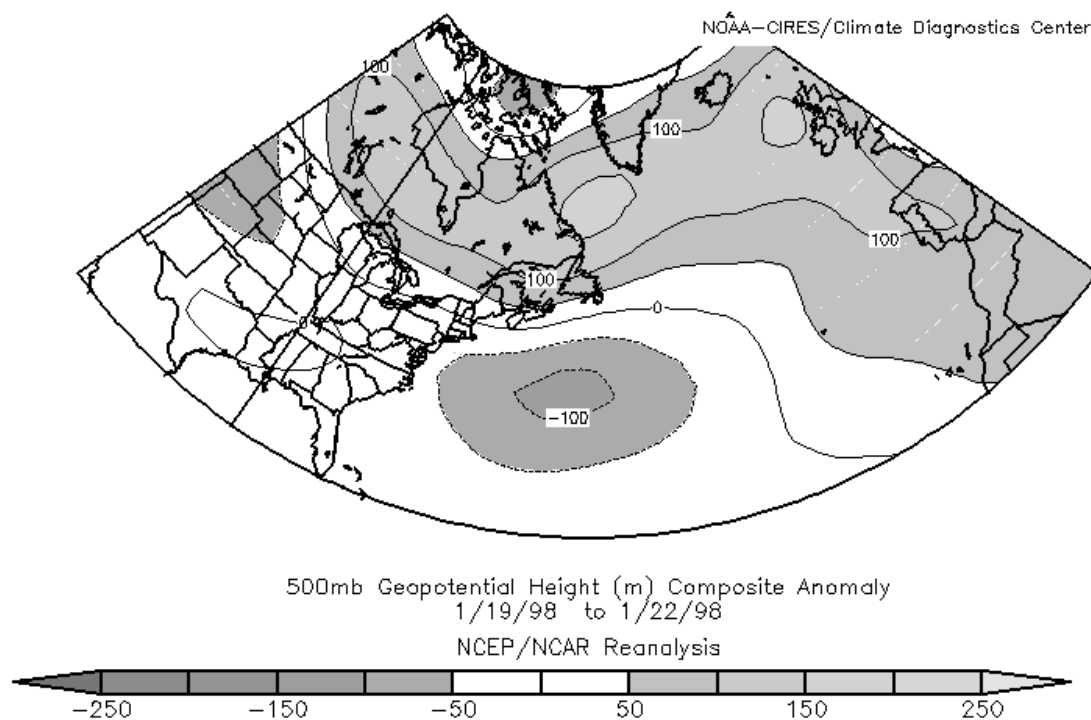


Fig. 3.79b. 500 mb geopotential height anomaly map (m) covering the two NAO domains after the 5–9 January 1998 ice storm.

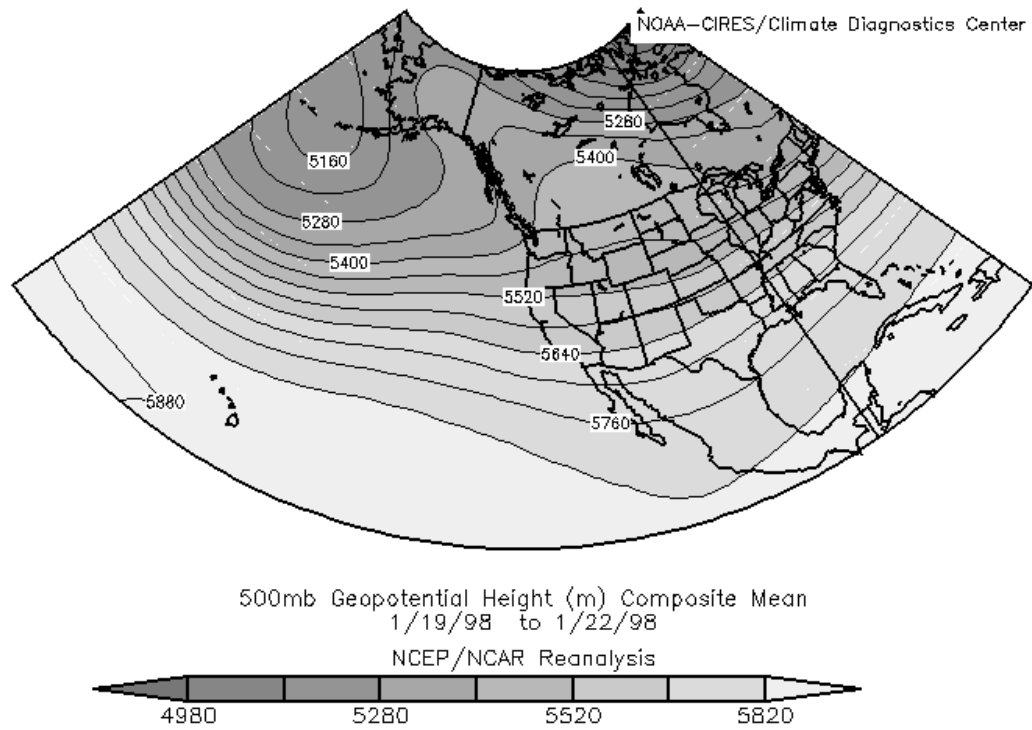


Fig. 3.80a. 500 mb geopotential height map (m) covering the four PNA domains after the 5–9 January 1998 ice storm.

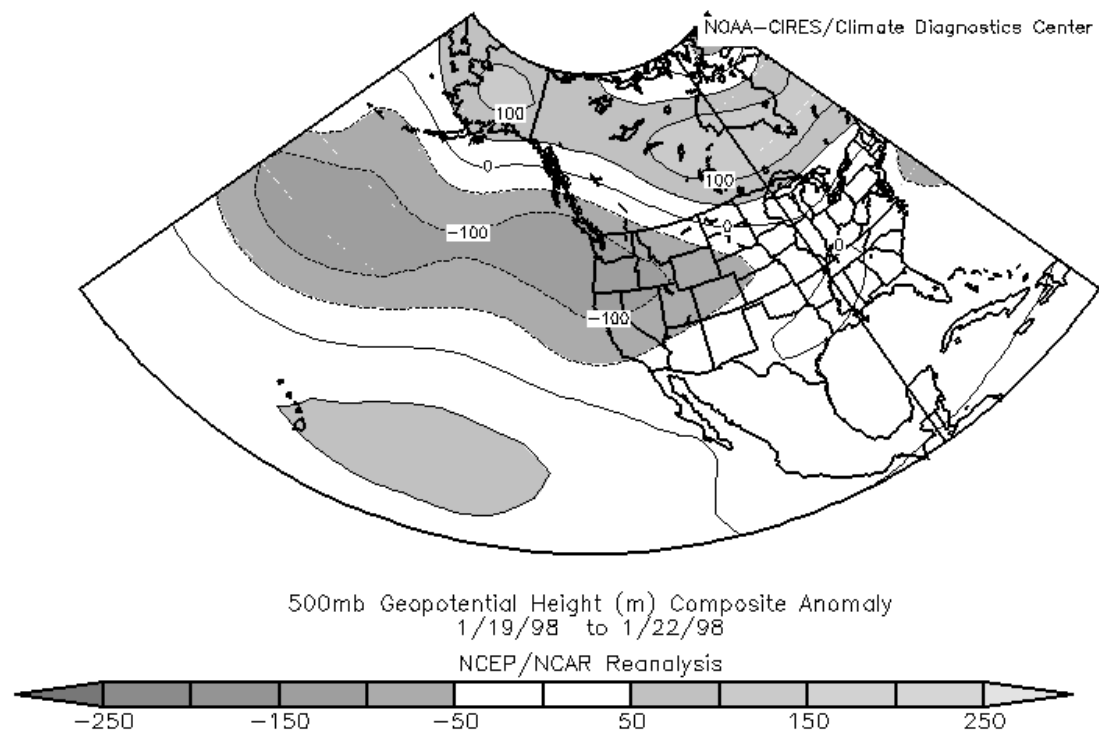


Fig. 3.80b. 500 mb geopotential height anomaly map (m) covering the four PNA domains after the 5–9 January 1998 ice storm.

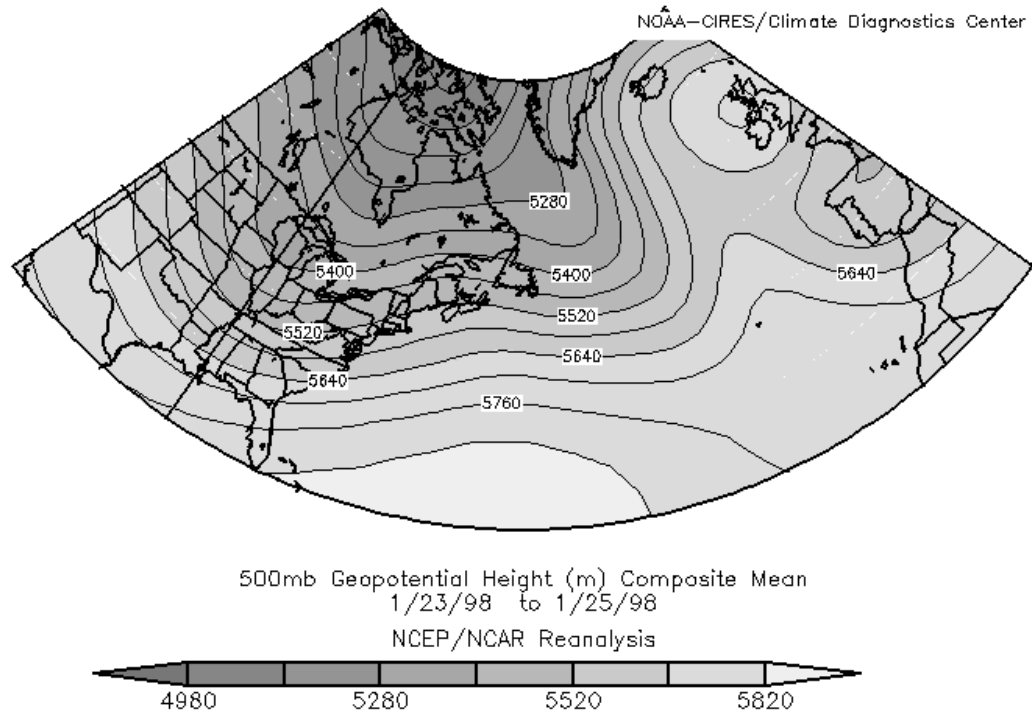


Fig. 3.81a. 500 mb geopotential height map (m) covering the two NAO domains after the 5–9 January 1998 ice storm.

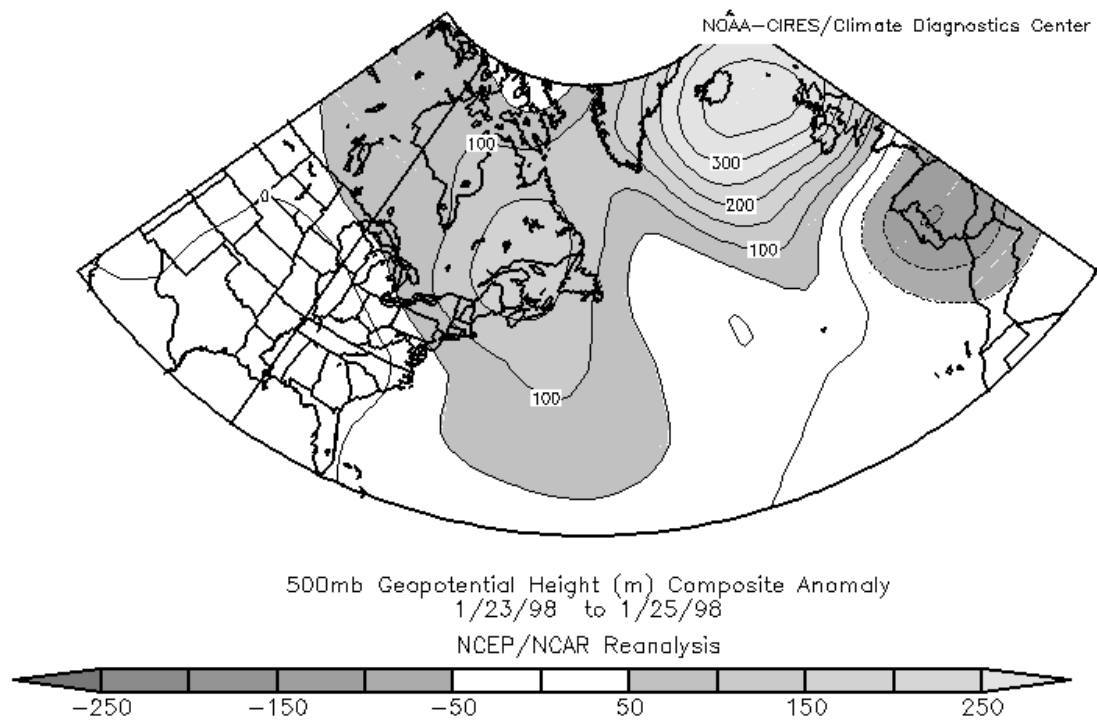


Fig. 3.81b. 500 mb geopotential height anomaly map (m) covering the two NAO domains after the 5–9 January 1998 ice storm.

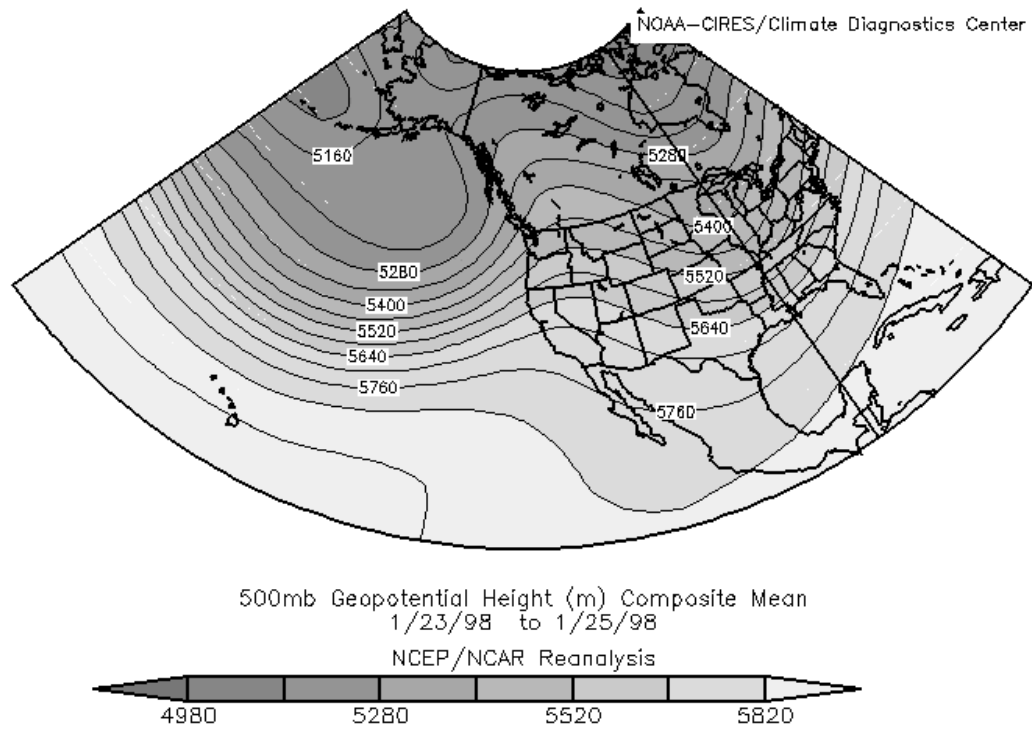


Fig. 3.82a. 500 mb geopotential height map (m) covering the four PNA domains after the 5–9 January 1998 ice storm.

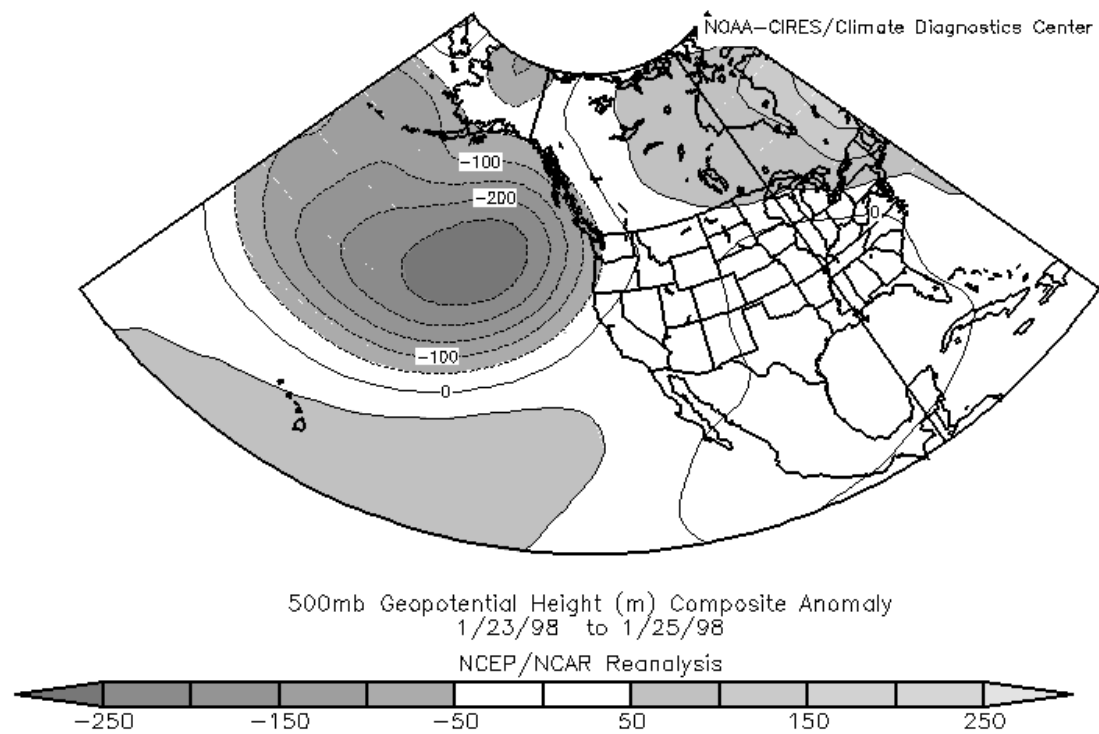


Fig. 3.82b. 500 mb geopotential height anomaly map (m) covering the four PNA domains after the 5–9 January 1998 ice storm.

Table 1: Occurrence of NAO Transitions with Northeast US Precipitation Events

<p>18 cool seasons (Oct. through Apr.) 1968-73; 1983-88; 1993-98</p>
127 NAO transitions
Overall 76/127 transitions had DPI > 0 over four day period
69/127 + to – NAO transitions
49/69 DPI > 0 over four days (including transition and two days prior transition)
58/127 – to + NAO transitions
27/58 DPI > 0 over four days (including transition and two days prior transition)

Note: During cool season any random four days could yield a DPI > 0

4. Discussion

4.1 NAO/PNA and Northeast US Precipitation Correlations

Previous work on the relationship between precipitation and the NAO and PNA has focused on monthly and seasonal timescale. Rogers and van Loon (1979) noted that a positive NAO brought greater January precipitation to the majority of North America with the exception of the extreme southeast and eastern US, and Pacific Northwest. In a study of temperature and precipitation trends since 1980, Hurrell (1995) noted that because flow associated with synoptic-scale systems dictates areas of the greatest moisture transport and convergence, the influence of the NAO on the North Atlantic storm track is important in shaping regional precipitation anomalies. Leathers *et al.* (1991) looked at the relationship between monthly PNA indices and precipitation over the US. They found a negative correlation over the western US from October to January, and a negative correlation centered over the Ohio Valley from November to March. On a more regional scale, Bradbury *et al.* (2002) looked at the relationship between monthly winter precipitation in New England and the NAO and PNA. Their results suggest that there is no significant correlation between the monthly large-scale circulation anomalies and precipitation over New England.

The results presented in section 3.1 show a virtually zero correlation between daily large-scale circulation anomaly indices and precipitation amounts over the northeast US. Grouping the data into three seasons, the daily domain average precipitation was stratified by amount as defined by the DPI. For the majority of the fall, winter, and spring seasons (Figs. 3.2–3.27) the square of the correlation coefficients

remains nearly zero as the domain-average precipitation amounts become progressively larger. The one exception is the R^2 value of 0.4767 between the spring season NAO and Northeast domain average precipitation greater than 8.2 mm, or a DPI greater than 3 (Fig. 3.14). One possibility for such a high correlation is that this result could be the artifact of a small dataset, as only 24 cases had met the DPI parameters between 1954 and 1998.

The near zero correlations between daily large-scale circulation anomalies and precipitation amount over the northeast US suggest that there is little value in using the daily NAO/PNA index values to improve quantitative precipitation forecasts (QPF) over the northeast US within the context of the approach used in this thesis. These results also imply that forecasting trends in heavy precipitation over the Northeast during a specific phase of the NAO or PNA would be unsuccessful. However, these are preliminary results, and certain limitations should be considered with the conclusions drawn from their interpretation.

In calculating a daily domain-average precipitation value, it was assumed that precipitation was normally distributed over the northeast US domain on a daily time scale. However, on a daily time scale, precipitation events are rarely homogeneous across an area the size of the northeast US domain. For storms that take a coastal or southern track, precipitation amounts would be concentrated over the southern and eastern areas of the domain with northern and western areas possibly remaining dry. Even during precipitation events that encompass the entire domain, heavier precipitation amounts may be focused over elevated regions. This property of precipitation distribution might suggest the use of a smaller area in the correlation of precipitation

amount with the large-scale circulation anomaly indices. Though not presented, correlations between precipitation amount and large-scale circulation anomaly indices were calculated for smaller domains surrounding large metropolitan areas in the Northeast. Results from these calculations were similar to the results for the northeast US domain with R^2 values near zero. Another limitation in the interpretation of the correlation results is the calculation of the DPI. The calculation of a mean and standard deviation was based on the assumption that a Gaussian distribution would best fit the precipitation data. This assumption, however, would introduce the small probability of negative precipitation values, a probability that should not exist (Wilks 1995). Noting that precipitation is not normally distributed, Ropelewski *et al.* (1985) concluded that a skewed distribution would best fit precipitation data. They chose to fit their precipitation data to a Gamma distribution. Interpretation of the correlation between daily large-scale circulation anomaly indices and northeast US precipitation amount presented in chapter 3 should be conducted with the knowledge that our precipitation data were not fitted to a Gamma distribution. This limitation will need to be addressed in future research.

4.2 NAO/PNA Transitions

Statistics concerning northeast US precipitation events and transitions of the NAO were presented in section 3.1.3. The results showed a tendency for precipitation amounts exceeding a specific threshold to occur within a four-day period prior to and during an NAO transition. Four northeast US storms discussed in section 3.2 provide

evidence of both NAO and PNA transitions associated with large precipitation events. In the four case studies, NAO transitions were evenly split between positive-to-negative and negative-to-positive transitions. However, the results in section 3.1.3 show a significantly higher percentage of northeast US precipitation events associated with positive-to-negative NAO phase transitions rather than negative-to-positive transitions.

In each of the four case studies, the phase transition of the NAO/PNA occurred while the storm was within close proximity of the northeast US coast. Changes in the downstream 500 hPa geopotential height field associated with the event undoubtedly had an influence on the simultaneous transition of the NAO. While these results suggest a possible association between transient disturbances and NAO/PNA phase transitions, it is beyond the scope of this research project to delineate a cause-and-effect relationship between NAO/PNA transitions and northeast US precipitation events. Continuation of this research to include the PNA, a larger dataset of transitions for the NAO and PNA, and a greater number of individual case studies is necessary to address whether the occurrence of significant transient disturbances can result in the rearrangement of the planetary-scale flow pattern, or if rearrangements of the planetary-scale flow can lead to significant transient disturbances.

One of several issues to consider in the interpretation of our results on NAO transitions and northeast US precipitation events in section 3.1.3 would be the possibility that during any four-day period randomly selected over the cool season, a northeast US domain average precipitation amount could exceed a DPI of zero. To overcome the effects of this limitation, the inclusion of more cool-season NAO phase transitions is suggested. Another issue ignored in this research was the NAO phase transitions that

occurred without a precipitation event over the northeast US domain. One possible reason for this type of transition behavior is that storms tracked over eastern North America, but outside of the northeast US domain defined in this research. There were several cases identified by the author, but not introduced in this research, where storms that were associated with a NAO phase transition passed to the north of the northeast US domain.

4.3 NAO/PNA Case Studies

In this section a further analysis of the four cases studies, including the 12–14 March 1993 “Supertorm,” 24–26 January 2000 storm, 18–20 January 1996 “Meltdown,” and 5–9 January 1998 ice storm, is presented. For the three events that precipitation data were available (1993, 1996, and 1998) the daily event-averaged DPI values were 2.5, 1.5, and 2.7, respectively. Analysis of the 850 hPa low-level thermal advection patterns of the four cases shows the warm-air advection positioned in close proximity to the East Coast, ahead of the mean 850 hPa trough axis. A strong cold-air advection pattern was present on the backside of the mean 850 hPa trough in all but the 5–9 January 1998 ice storm (Figs. 3.65a,b and 3.66a,b).

The 24–26 January 2000 event had the strongest signal of 850 hPa warm air advection (Figs. 3.41a,b and 3.42a,b). Of the three events with precipitation data, the 5–9 January 1998 ice storm had the largest daily event-averaged DPI value, but one of the weaker 850 hPa warm air advection patterns (Figs. 3.65a,b and 3.66a,b). The 18–20 January 1996 “Meltdown” had a similarly weak 850 hPa warm-air advection pattern but

had the smallest daily event-averaged DPI value of the three events. The warm-air advection patterns for these two events were both weaker and located farther inland than the areas of warm-air advection for the 12–14 March 1993 “Superstorm” and 24–26 January 2000 events.

The coastal development and track of the 12–14 March 1993 and 24–26 January 2000 events are evident in the SLP maps (Figs. 3.29a,b and 3.40a,b). The precipitation total map for the 12–14 March 1993 “Superstorm” (Fig. 3.30) and an 18-hour radar loop of the 24–26 January event (not shown) complement the SLP figures with the heaviest precipitation totals and radar echoes concentrated along the Eastern Seaboard. While daily event-averaged DPI values are unavailable for the 24–26 January 2000 storm, the DPI values for the “Superstorm” are between the January 1996 and January 1998 storms. This finding would suggest that storms biased toward a general area of the domain (i.e., east over west) could have daily event-averaged DPI values comparable to storms that cover the entire domain with precipitation. The 300 hPa winds for the 12–14 March 1993 and 24–26 January 2000 events have an anomalously strong southerly component associated with meridionally oriented 45 to 50 m s^{-1} jet streaks located downstream of the 300 hPa trough axis (Figs. 3.33b, and 3.43b).

Surface low development and track for the 18–20 January 1996 and 5–9 January 1998 precipitation events is located farther north and west, respectively, than the two previous cases. Precipitation total maps for these events fit the surface low tracks with broad areas of moderate-to-large precipitation amounts over the Mid-Atlantic and Northeast during the 18–20 January 1996 storm, and an axis of heavy precipitation aligned southwest-to-northeast from Louisiana to Vermont for the 5–9 January 1998

event (Figs. 3.52 and 3.64). With the inland storm tracks the precipitation is more evenly distributed over the northeast US domain. Thus, the associated daily event-average DPI value would give a better representation of these precipitation events. Both precipitation events occurred in the presence of weak 300 hPa flow (Figs. 3.55a,b and 3.67a,b). Zonally oriented jet streaks are located north of the storms over northern Canada. The weak westerly 300 hPa flow associated with both storms is reflected in a strong anomalous easterly wind component over the northeast US.

The normal tendency of atmospheric variables, such as low-level air temperature, and upper-level winds, during the positive and negative phases the NAO and PNA have been well documented by others and discussed in chapter 1. The 12–14 March 1993 and 24–26 January 2000 precipitation events occurred during negative-to-positive NAO and PNA phase transitions. Over the northeast US, the transition to a positive NAO would imply rising heights, a more zonal flow pattern with an upper-level jet positioned over the North Atlantic, and anomalously warm low-level temperatures. However, the transition to a positive PNA over the Northeast would suggest lowering heights, a trough over the eastern US and anomalously cool low-level temperatures. The opposing effects of a positive NAO and PNA pattern imply that forecasting trends of these atmospheric variables from the described tendencies would be contradictory. After the 12–14 March 1993 “Superstorm” the positive PNA pattern dominated as a 500 hPa trough (Fig. 3.38a,b) and anomalously cold temperatures (Fig. 4.1a,b) remained over the eastern US. The North Atlantic jet, a signature feature of the positive NAO, had formed south of Greenland and Iceland (Fig. 4.2a,b). Conditions over the northeast US after the 24–26 January 2000 event also resembled a positive PNA pattern. A large 500 hPa (Fig.

3.47a,b) and 300 hPa (Fig. 4.3a,b) trough were positioned over the eastern US. The low-level temperature anomalies of the Northeast were slightly negative (Fig. 4.4a,b).

During the 18–20 January 1996 event the NAO and PNA transitioned from positive-to-negative. Over the northeast US, a negative NAO typically results in anomalously cold low-level temperatures with a less zonal flow pattern. A negative PNA pattern has the opposite effects on the northeast US with increased heights and anomalously warm temperatures. Conditions over the northeast US after the 18–20 January 1996 event matched the description of a negative PNA. The 500 hPa (Fig. 3.61a,b) and 300 hPa (Fig. 4.5a,b) flow pattern over the eastern US were zonal, with anomalously warm low-level temperatures (Fig. 4.6a,b).

The 5-9 January 1998 ice storm was associated with a positive-to-negative transition of the NAO and negative-to-positive transition of the PNA. Unlike the three previous cases, the resulting flow patterns of a positive PNA and negative NAO should bring a trough to the eastern US with anomalously cold temperatures. Conditions over the northeast US after the storm show a 500 hPa (Fig. 3.81a,b) and 300 hPa (Fig. 4.7a,b) trough over the eastern US. However, the low-level temperature anomalies over the Northeast are weakly positive (Fig. 4.8a,b).

4.4 Forecasting Results

The results presented in sections 3.1.1 and 3.1.2 would imply that the absence of a correlation between precipitation amount in the northeast US and the specific phase of the NAO or PNA strongly limits the potential for forecasting precipitation trends in

response to a specific phase of the NAO or PNA. Thus, any preconception that a negative NAO index is correlated with greater precipitation over the northeast US needs to be treated with great caution.

Another preliminary result that would be applicable to forecasting for the northeast US was the noted relationship between daily precipitation events and NAO phase transitions. Recognizing the association of precipitation events over the northeast US with NAO phase transitions provides forecasters with another tool in assessing the probability of the occurrence of a precipitation event. The potential linkage between NAO/PNA phase tendency and northeast US storminess implied by the preliminary results presented in this thesis needs to be researched further as there may eventually be forecast applications from the resulting findings.

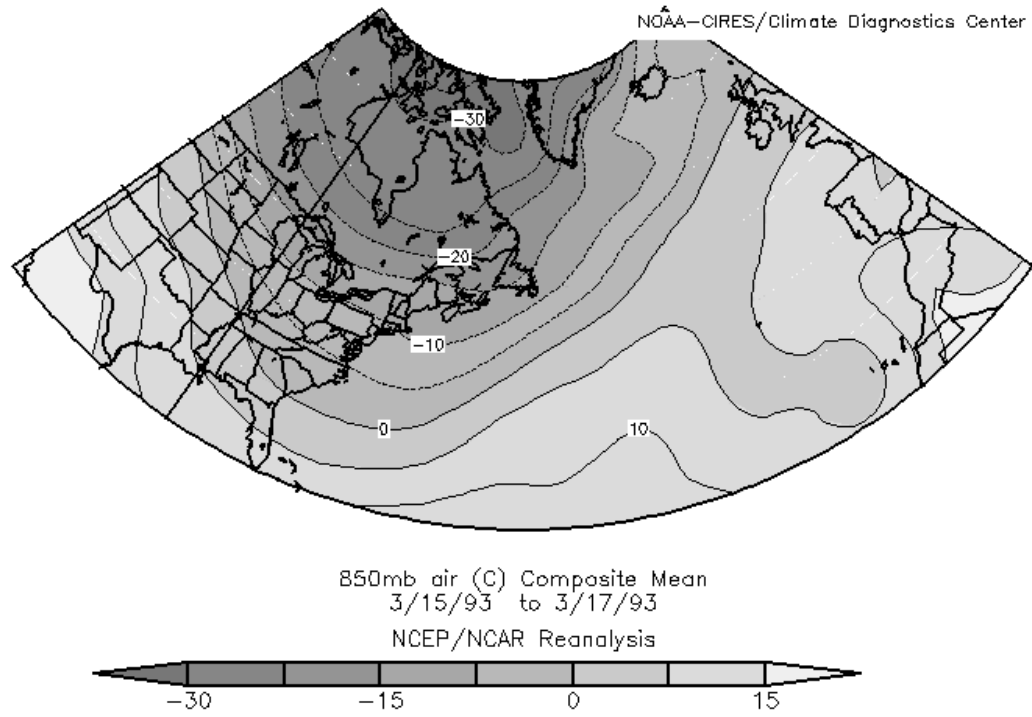


Fig. 4.1a. 850 mb temperature map (°C) for 15–17 March 1993.

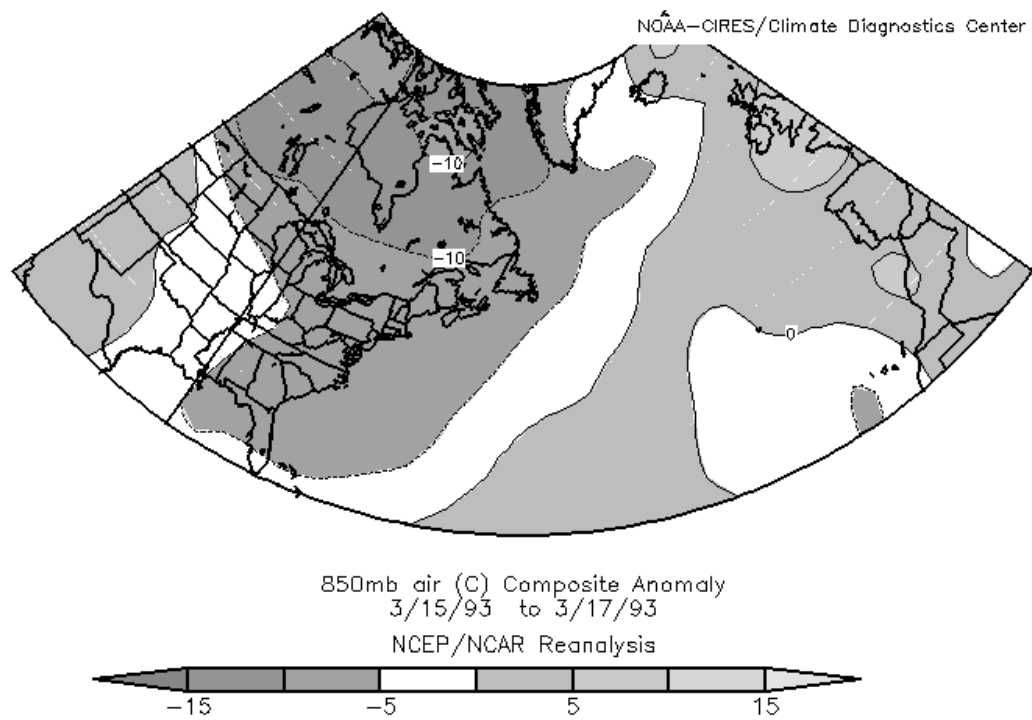


Fig. 4.1b. 850 mb temperature anomaly map (°C) for 15–17 March 1993.

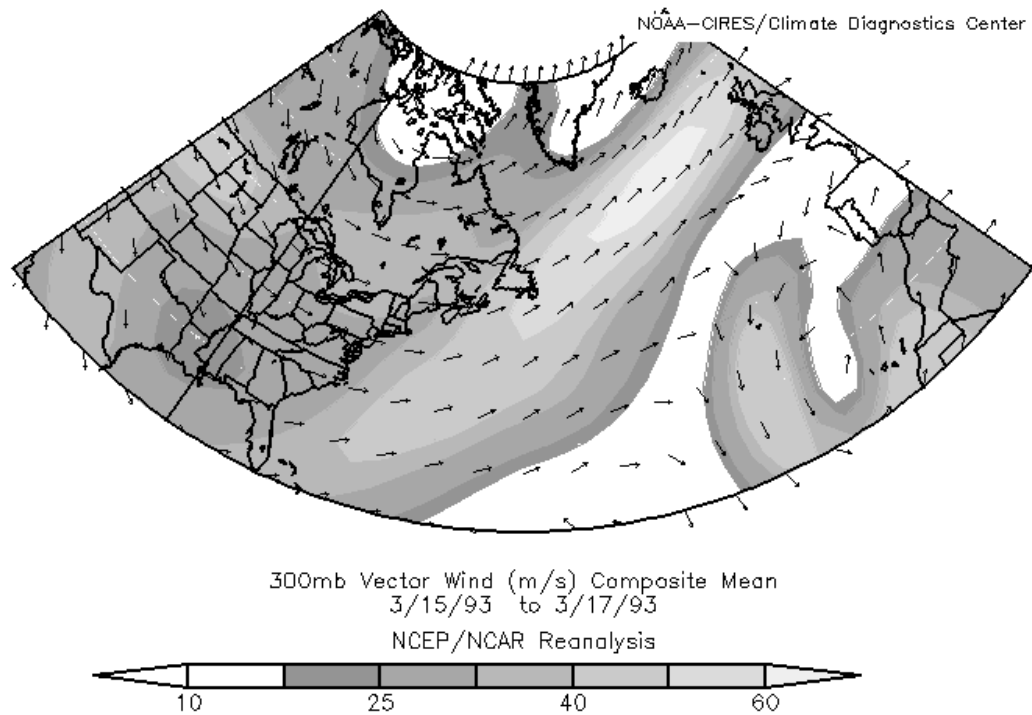


Fig. 4.2a. 300 hPa vector wind map (m s^{-1}) for 15–17 March 1993.

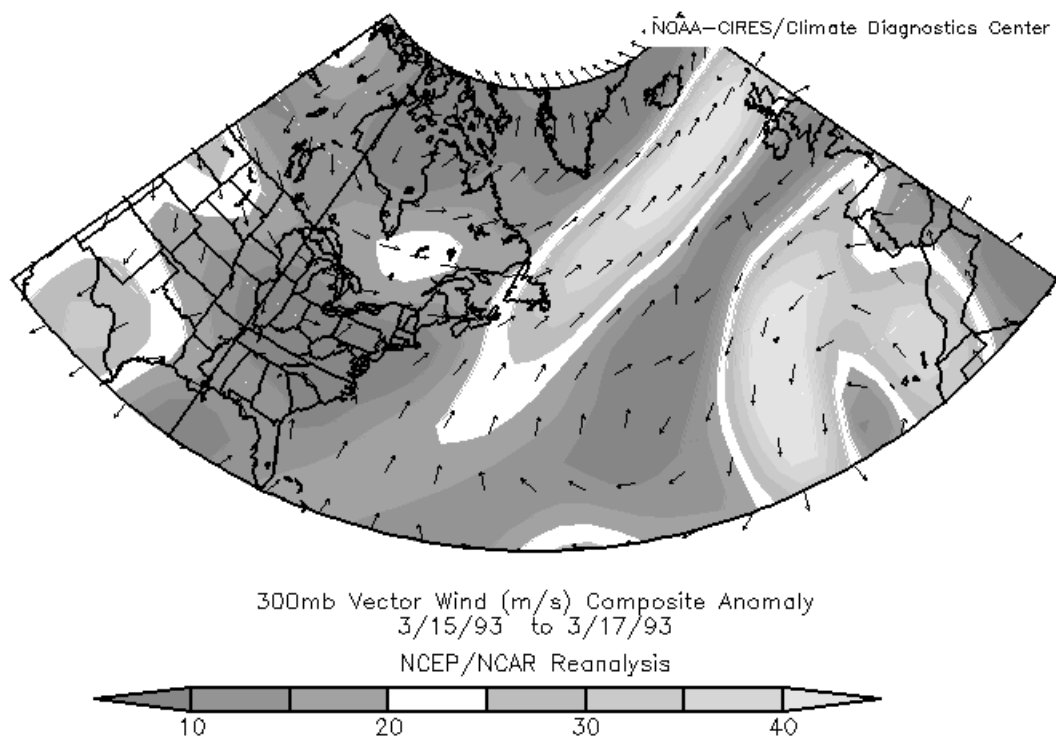


Fig. 4.2b. 300 hPa vector wind anomaly map (m s^{-1}) for 15–17 March 1993.

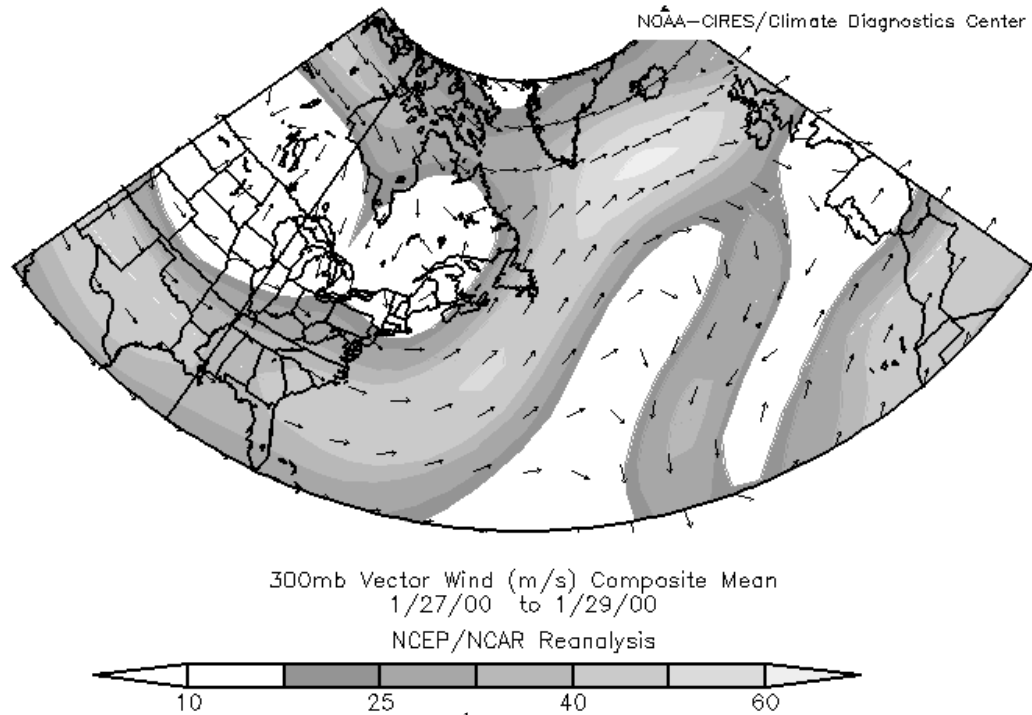


Fig. 4.3a. 300 hPa vector wind map (m s^{-1}) for 27–29 January 2000.

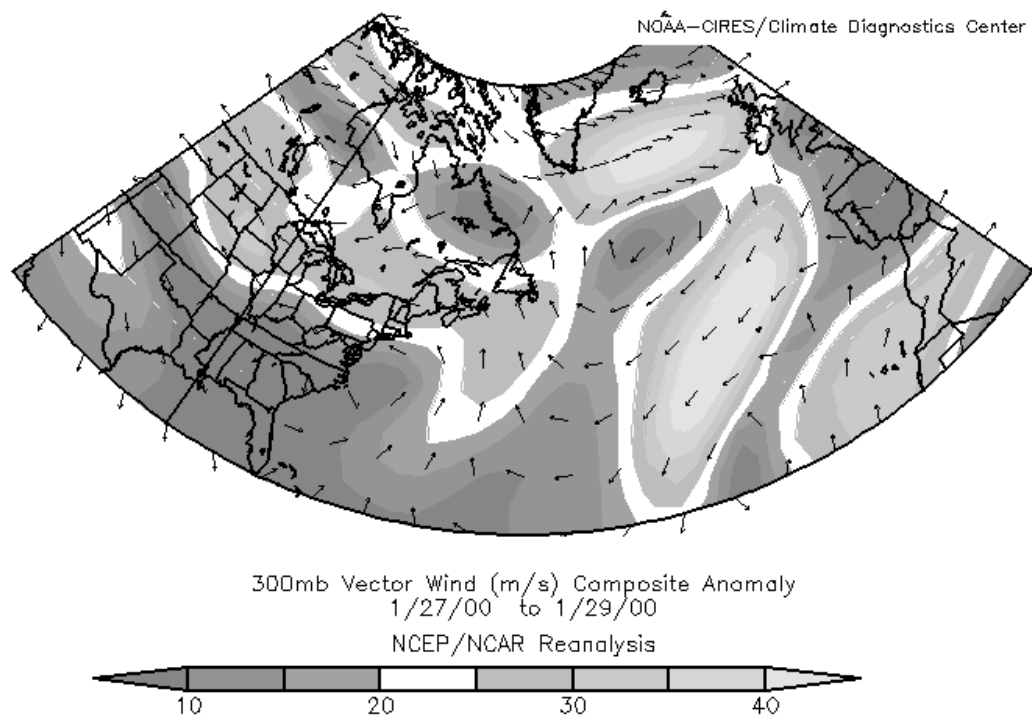


Fig. 4.3b. 300 hPa vector wind anomaly map (m s^{-1}) for 27–29 January 2000.

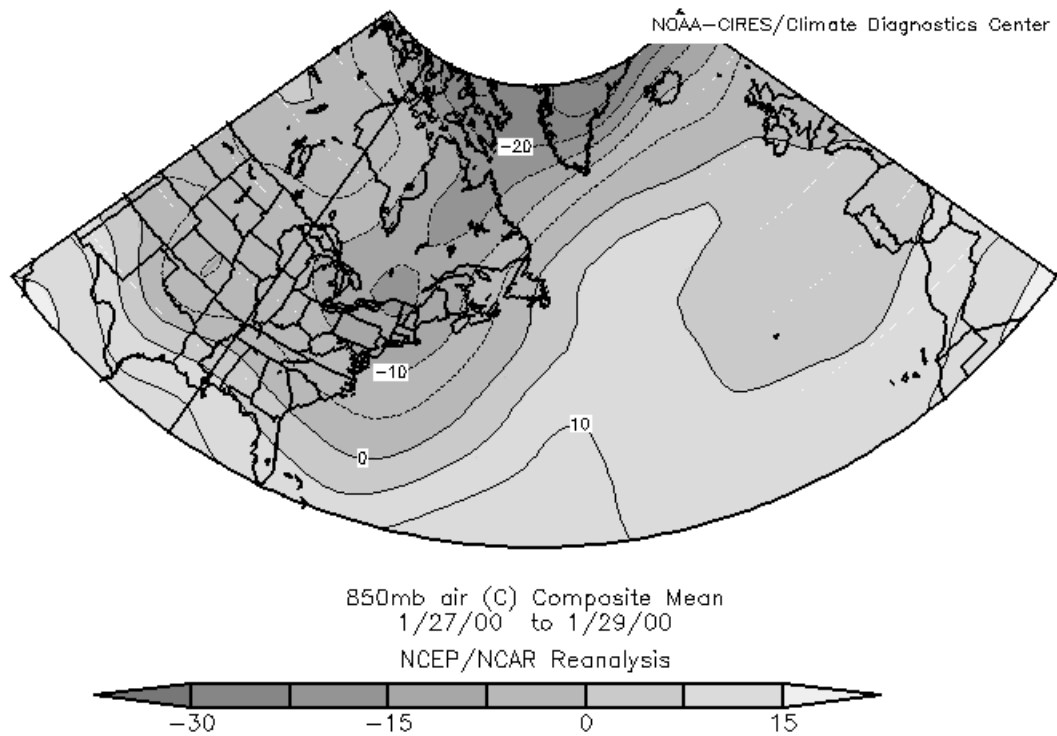


Fig. 4.4a. 850 mb temperature map ($^{\circ}\text{C}$) for 27–29 January 2000.

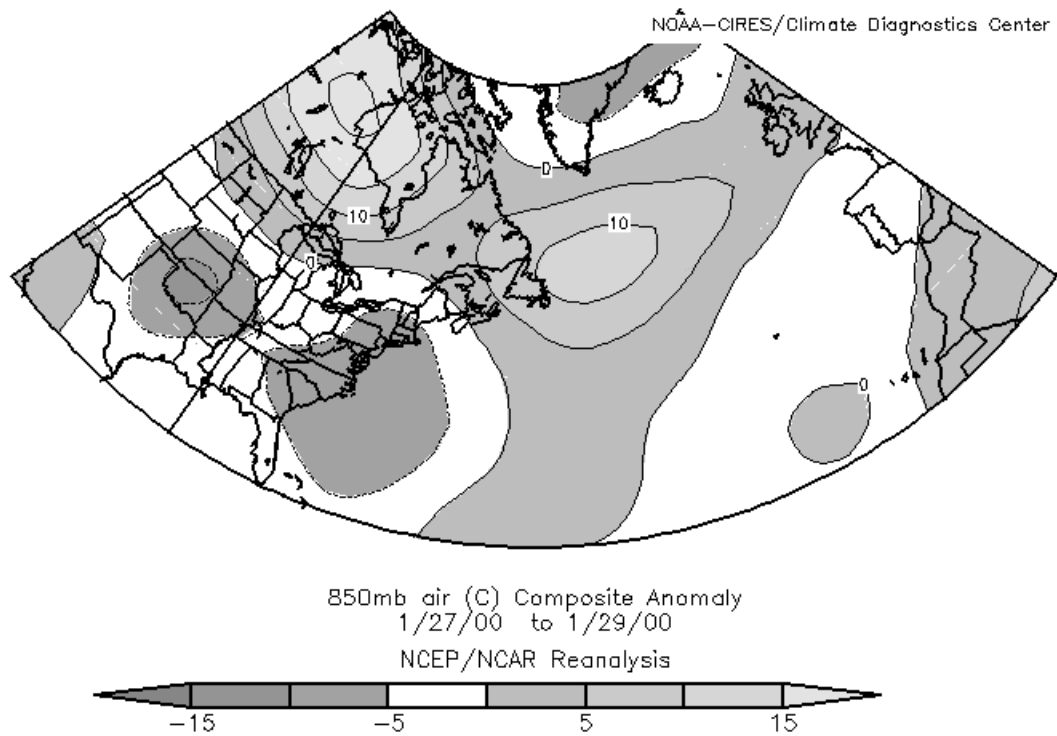


Fig. 4.4b. 850 mb temperature anomaly map ($^{\circ}\text{C}$) for 27–29 January 2000.

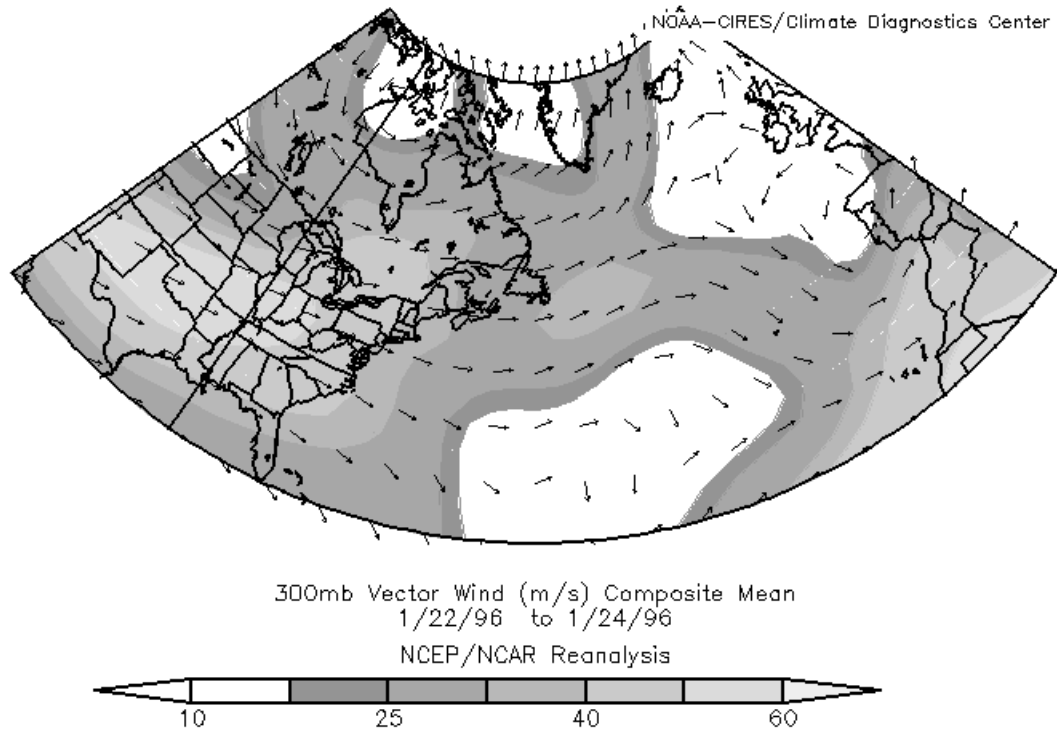


Fig. 4.5a. 300 hPa vector wind map (m s^{-1}) for 22–24 January 1996.

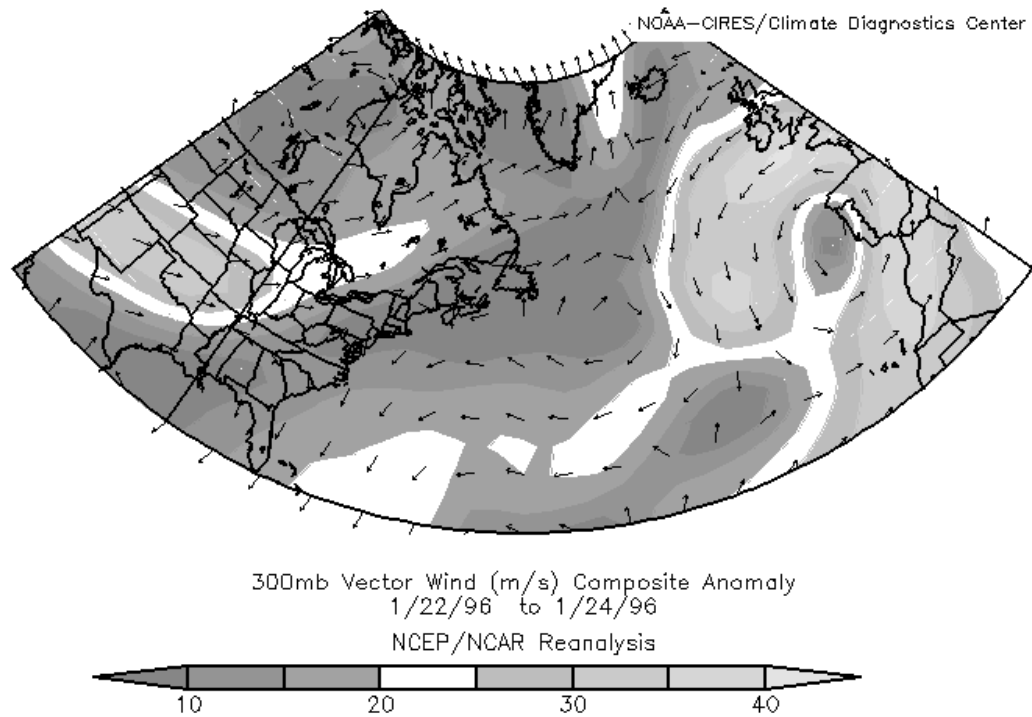


Fig. 4.5b. 300 hPa vector wind anomaly map (m s^{-1}) for 22–24 January 1996.

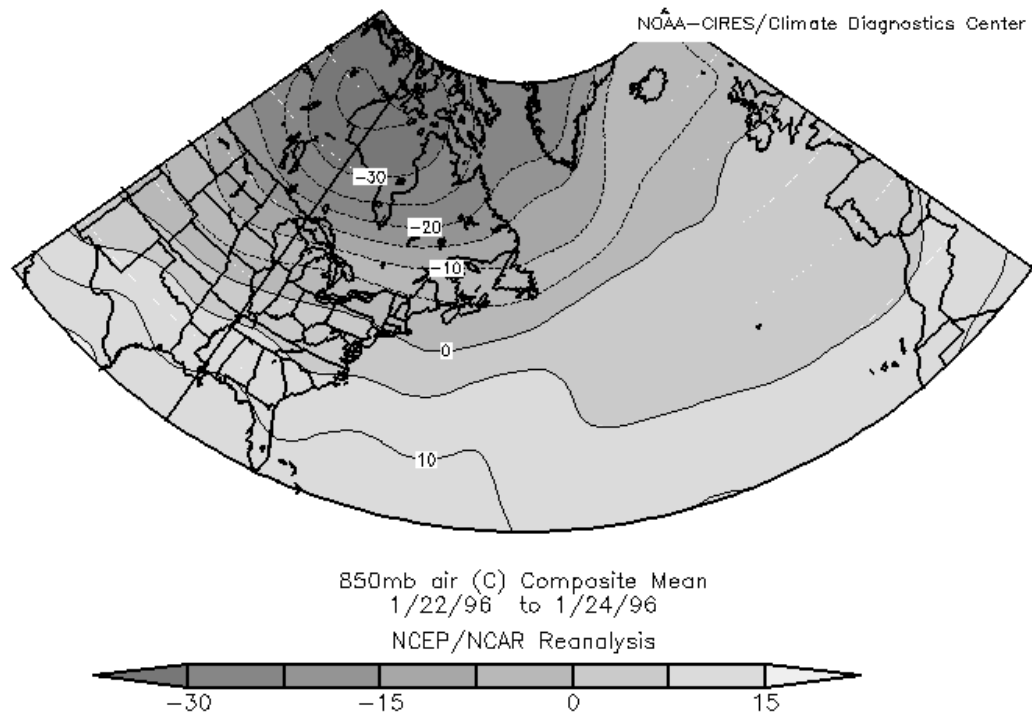


Fig. 4.6a. 850 mb temperature map ($^{\circ}\text{C}$) for 22–24 January 1996.

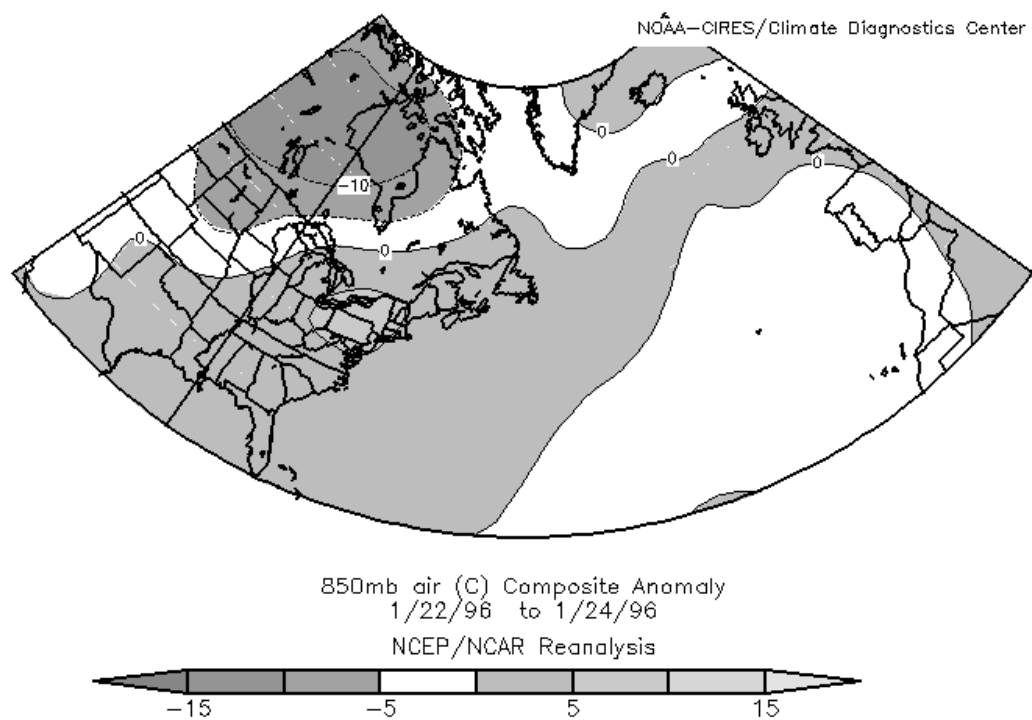


Fig. 4.6b. 850 mb temperature anomaly map ($^{\circ}\text{C}$) for 22–24 January 1996.

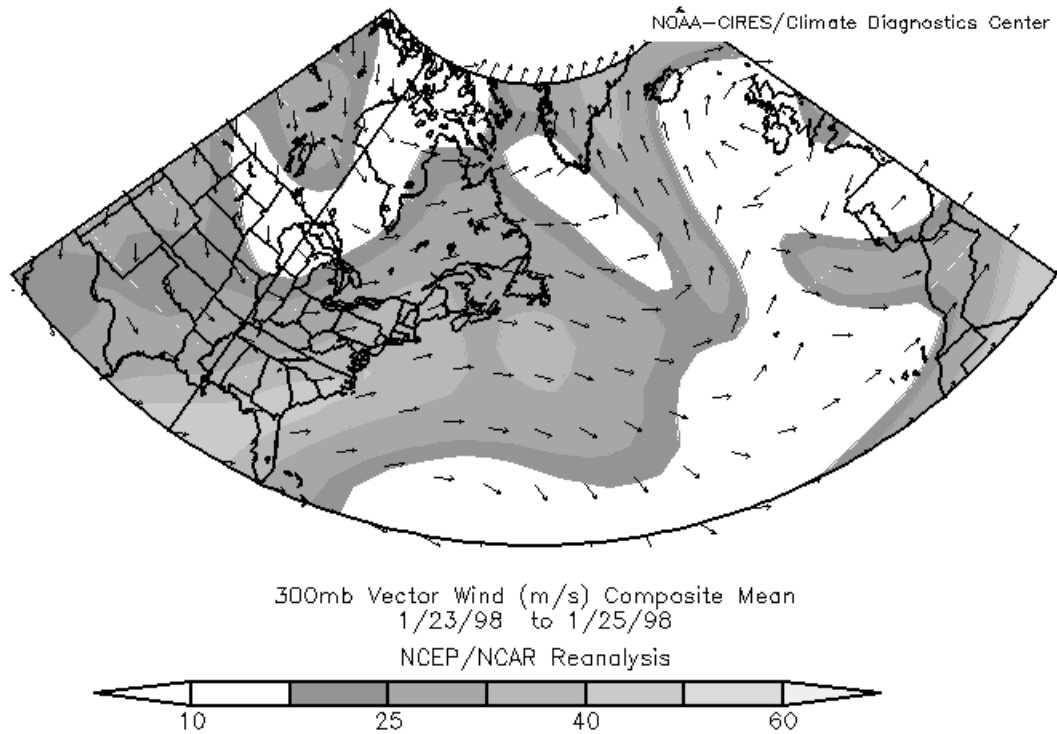


Fig. 4.7a. 300 hPa vector wind map (m s^{-1}) for 23–25 January 1998.

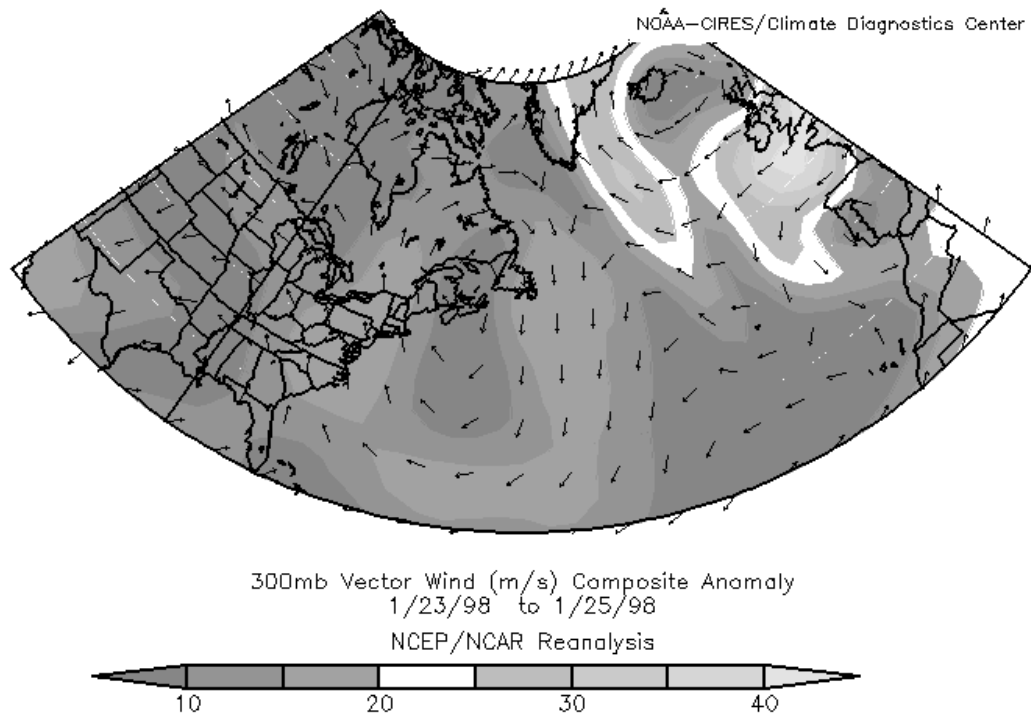


Fig. 4.7b. 300 hPa vector wind anomaly map (m s^{-1}) for 23–25 January 1998.

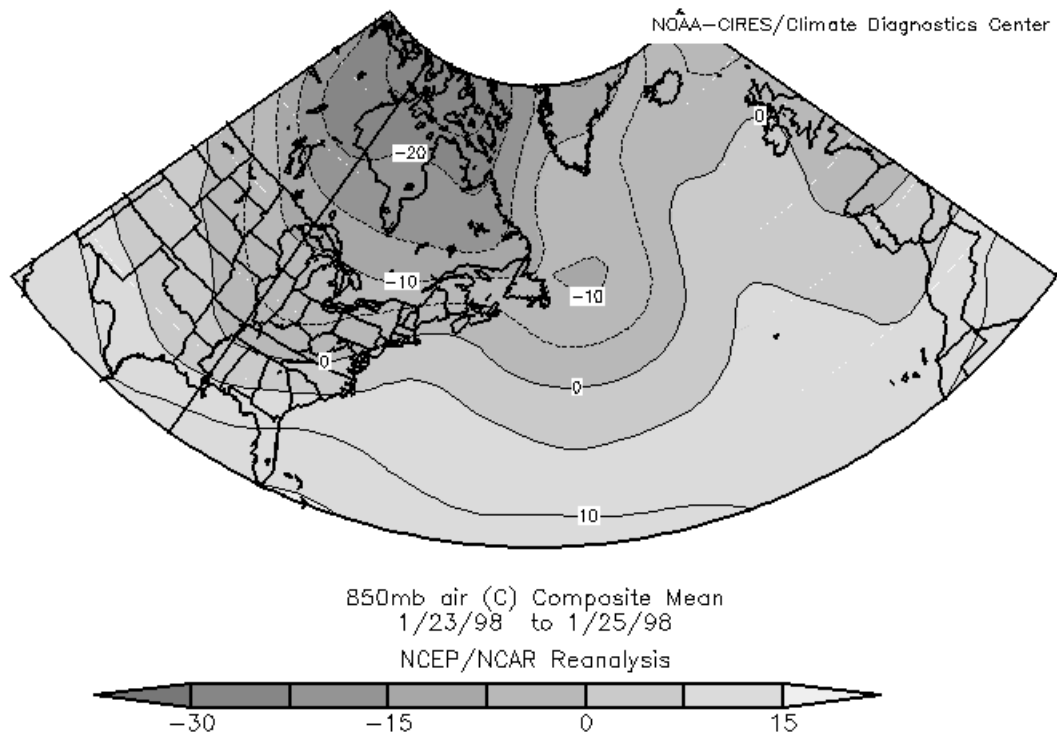


Fig. 4.8a. 850 mb temperature map ($^{\circ}\text{C}$) for 23–25 January 1998.

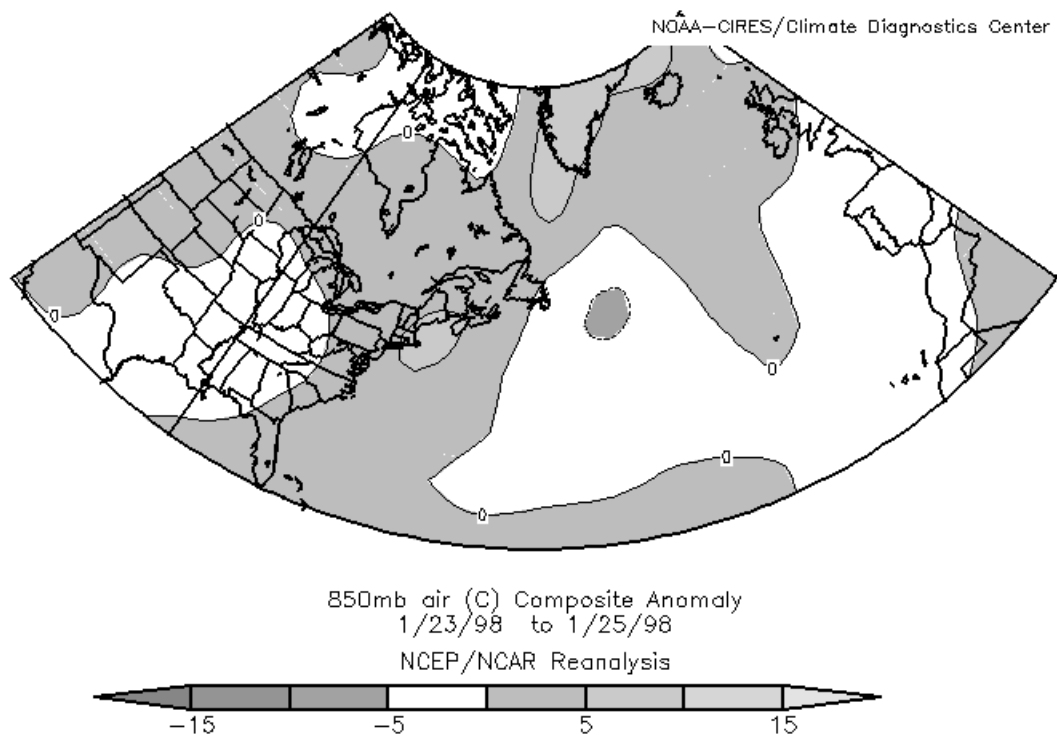


Fig. 4.8b. 850 mb temperature anomaly map ($^{\circ}\text{C}$) for 23–25 January 1998.

5. Conclusions and Suggestions for Further Research

The correlation between daily large-scale circulation anomalies and precipitation amount over the northeast US, the relationship between phase transitions of the daily value of the North Atlantic Oscillation (NAO) and Pacific North American (PNA) teleconnection indices and northeast US cool season precipitation events, and four case studies of significant northeast US precipitation events illustrating associated phase changes in the daily NAO/PNA indices were presented. In order to best compare the NAO and PNA to synoptic-scale precipitation events over the northeast US, a daily index of each was derived.

A preliminary attempt to calculate daily NAO indices from sea-level pressure (SLP) data at selected stations was abandoned in favor of a method that calculated the daily NAO and PNA indices from gridded 500 hPa geopotential height data. The daily NAO index was calculated from the NCEP/NCAR Reanalysis dataset by taking the difference of standardized 500 hPa geopotential height anomalies between two zonal domains over the North Atlantic as defined by the Climate Diagnostics Center. A similar method with four domains was used for calculating a daily PNA index. A daily climatology of the NAO and PNA indices was calculated for the period of 1954 to 2000.

A northeast US domain was defined from the NCEP Unified Precipitation Dataset (UPD) with the available precipitation data from the northeast US and its immediate borders. The Daily Precipitation Index (DPI) was created from the UPD data by calculating a standardized daily domain average precipitation value over the northeast US domain. Northeast US daily domain-average precipitation amounts of 2.5 mm, 4.4

mm, 6.3 mm, 8.2 mm, and 10.1 mm corresponded with DPI values of zero, one, two, three, and four, respectively. A daily climatology of the DPI index was calculated for the period 1954 to 1998.

The daily DPI was stratified into groups of greater than zero, one, two, three, and if necessary, four. Correlations between daily NAO/PNA indices and the stratified DPI data for three seasons (SON, DJF, MAM) revealed R^2 (correlation coefficient squared) values of nearly zero for all but a single correlation between the NAO and a DPI of greater than three for the MAM season. The R^2 value for DPI values greater than three during the MAM season was 0.477. This value implies that nearly 50% of the variance of domain-averaged precipitation greater than 8.2 mm over the northeast US domain during the MAM season can be explained by the NAO. A limitation in the analysis of the correlation results is that the calculation of the DPI was made under the assumption that precipitation is normally distributed. Ropelewski et al. (1985) and others, however, have noted that precipitation is not normally distributed, and is better fit by a Gamma distribution. It is recommended that future research address this concern.

A second statistical examination was performed for NAO phase transitions associated with precipitation events over the northeast US domain. The definition of an NAO phase transition established for this project states that the NAO had to change by one standard deviation in magnitude from negative-to-positive or positive-to-negative. The resulting phase had to last at least five days. In applying this definition to 18 cool seasons, 127 NAO phase transitions were identified. The precipitation event, considered to occur for any single day with a measured DPI value greater than zero, was associated with the NAO phase transition if it occurred within the two days prior to and during the

phase transition. Of the 127 NAO phase transitions, roughly 60% had an associated precipitation event. Nearly 65% of these were positive-to-negative NAO phase transitions. Over 70% of positive-to-negative NAO phase transitions had an associated precipitation event while only 47% of negative-to-positive NAO phase transitions had an associated precipitation event. These results imply a correlation between NAO phase transitions and precipitation events over the northeast US. It was noted, however, that any randomly selected four-day period during the cool season over the northeast US could contain a precipitation event meeting our criteria. To better understand the relationship between northeast US precipitation and the time tendency of the NAO, a greater number of both valid and null cases should be studied.

The four case studies of significant northeast US precipitation events presented in this research include: the 12–14 March 1993 “Superstorm,” the 24–26 January 2000 storm, the 18–20 January 1996 “Meltdown,” and the 5–9 January 1998 ice storm. The events were grouped according to the associated NAO transition with the negative-to-positive transition storms first, followed by the positive-to-negative transition storms second. Each of these storms was also associated with a PNA phase transition. The SLP, 850 hPa thermal advection pattern, and 300 hPa winds for each case were used to illustrate the storm development and track responsible for the associated DPI value. These fields were also used to identify characteristic features associated with the resultant phases of the NAO/PNA transitions. Trends in the 500 hPa geopotential height pattern were used to explore possible reasons for the associated NAO and PNA phase transitions.

The 12–14 March 1993 “Superstorm” and 24–26 January 2000 storm, both associated with negative-to-positive NAO and PNA phase transitions, tracked along the northeast US coast. The 18–20 January 1996 “Meltdown” and 5–9 January 1998 ice storm, both associated with a positive-to-negative NAO phase transition, and separate positive-to-negative and negative-to-positive PNA phase transitions, respectively, tracked farther inland over the northeast US. It was observed that the DPI values for the coastal storms were less representative of the precipitation distribution over the northeast US domain than the two events that tracked farther inland. It was also noted that for three of the cases where the resultant NAO and PNA phases succeeding the transitions were of the same sign and would result in interfering flow patterns over the northeast US, the resultant PNA pattern was dominant. Taken together, the results of the four case studies suggest that, unlike for the daily NAO/PNA indices, which show no apparent relationship with the DPI, there may be a relationship between NAO/PNA tendency and the DPI in the Northeast. It is left to future research to address cause and effect should the postulated relationship hold true for a much larger data sample.

The results of this research highlight the relationship between daily large-scale circulation anomalies and precipitation over the northeast US. The absence of a correlation between precipitation amount and daily NAO/PNA indices challenges the conventional wisdom that certain phases of the NAO and PNA are more conducive to greater precipitation amounts over the Northeast. Noted trends in the relationship between phase transitions of the NAO/PNA indices and northeast US precipitation events may also have a potential impact on improving precipitation forecasts over the northeast US. Further research based upon these preliminary results could lead to

forecasting applications instrumental in advancing the ability to forecast precipitation events for the Northeast.

REFERENCES

- Allen, R. A., R. Fletcher, J. Holmboe, J. Namias and H. C. Willett, 1940: Report on an Experiment on Five-day Weather Forecasting. *Pap. Phys. Oceanogr. Meteor.*, MIT/WHOI, **8**, 94.
- Ambaum, Maarten H. P., and B. J. Hoskins, 2002: The NAO Troposphere–Stratosphere Connection. *J. Climate*, **15**, 1969–1978.
- , B. J. Hoskins, and D. B. Stephenson, 2001: Arctic Oscillation or North Atlantic Oscillation?. *J. Climate*, **14**, 3495–3507.
- Angstrom, A., 1935: Teleconnections of Climate Changes in Present Time. *Geogr. Ann.*, **17**, 242–258.
- Appenzeller, C., J. Schwander, S. Sommer, and T. F. Stocker, 1998: The North Atlantic Oscillation and its Imprint on Precipitation and Ice Accumulation in Greenland. *Geophys. Res. Lett.*, **25**, 1939–1942.
- Barnston, A. G., and R. E. Livezey, 1987: Classification, Seasonality and Persistence of Low-Frequency Atmospheric Circulation Patterns. *Mon. Wea. Rev.*, **115**, 1083–1126.
- Blackmon, M. L., R. A. Madden, J. M. Wallace, and D. S. Gutzler, 1977: Geographical Variations in the Vertical Structure of Geopotential Height Fluctuations. *J. Atmos. Sci.*, **36**, 2450–2466.
- , Y. H. Lee, and J. M. Wallace, 1984: Horizontal Structure of 500 mb Height Fluctuations with Long, Intermediate, and Short Time Scales. *J. Atmos. Sci.*, **41**, 961–979.
- Bosart, L. F., G. J. Hakim, K. R. Tyle, M. A. Bedrick, W. E. Bracken, M. J. Dickinson, and D. M. Schultz, 1996: Large-scale Antecedent Conditions Associated with the 12–14 March 1993 cyclone (“Superstorm ‘93”) over Eastern North America. *Mon. Wea. Rev.*, **124**, 1865–1891.
- Bradbury, J. A., S. L. Dingman, and B. D. Keim, (Submitted to *Journal of American Water Resources* August, 2001): Relation of New England Hydroclimate to Large-scale Atmospheric Circulation Patterns.
- Crantz, D., 1765: *Historie von Grönland*. Barby und Leipzig. [Translation: *History of Greenland*, 2nd ed., 2 vols. London, 1820, see p. 42.]
- Dannmeyer, F., 1948: ZurFrage der Gegensatzlichkeit der kalten Winter in Gronland zu den warmen wintern in Deutschland. *Polarforsch.*, **2**, 29–30.

- Deser, C., 2000: On the Teleconnectivity of the “Arctic Oscillation”. *Geophys. Res. Lett.*, **27**, 779–782.
- DeWeaver, E., and S. Nigam, 2000: Do Stationary Waves Drive the Zonal – Mean Jet Anomalies of the Northern Winter?. *J. Climate*, **13**, 2160–2176.
- DeWeaver, E., and S. Nigam, 2000: Zonal – Eddy Dynamics of the North Atlantic Oscillation. *J. Climate*, **13**, 3893–3914.
- Dickinson, M. J., L. F. Bosart, W. E. Bracken, G. J. Hakim, D. M. Schultz, M. A. Bedrick, and K. R. Tyle, 1997: The March 1993 Superstorm Cyclogenesis: Incipient Phase Synoptic- and Convective-scale Flow Interaction and Model performance. *Mon. Wea. Rev.*, **125**, 3041–3072.
- Dickson, R. R., J. Namis, 1976: North American Influences on the Circulation and Climate of the North Atlantic Sector. *Mon. Wea. Rev.*, **104**, 1255–1265.
- , 1977: Winter 1976–77: A Comparison of circulation Statistics with Other Winters. *Proceedings of the Second Annual NOAA Climate Diagnostics Workshop*, pp. 7-1 to 7-12.
- Dole, R. M. 1986: Persistent Anomalies of the Extratropical Northern Hemisphere Wintertime Climate Circulation: Structure. *Mon. Wea. Rev.*, **114**, 178–207.
- , 1989: Life Cycles of Persistent Anomalies. Part I: Evolution of 500 mb Height Fields. *Mon. Wea. Rev.*, **117**, 177–211.
- Dove, H. W., 1839: Über die geographische Verbreitung gleichartiger Witterungserscheinungen. *Abh. Kön. Akad. Wiss. Berlin*, 1838, 287–415 (see p. 409).
- Esbensen, S. K., 1984: A Comparison of Intermonthly and Interannual Teleconnections in the 700 mb Geopotential Height Field during the Northern Hemisphere Winter. *Mon. Wea. Rev.*, **112**, 2016–2032.
- Exner, F. M., 1924. Monatliche Luftdruck- und Temperaturanomalien auf der Erde. *SitzBer. Akad. Wiss.*, **133**, 2a.
- Glowienka-Hense, R., 1990: The North Atlantic Oscillation in the Atlantic – European SLP. *Tellus*, **42A**, 497–507.
- Gyakum, J. R., and P. J. Roebber, 2001: The 1998 Ice Storm –Analysis of a Planetary-scale Event. *Mon. Wea. Rev.*, **129**, 2983–2997.
- Hann, J., 1890: Zur Witterungsgeschichte von Nord-Grönland, Westküste. *Meteor. Z.*, **7**, 109–115.

- Hart, R. E., and R. H. Grumm, 2001: Using Normalized Climatological Anomalies to Rank Synoptic-Scale Events Objectively. *Mon. Wea. Rev.*, **129**, 2426–2442.
- Herrera, R. G., D. G. Puyol, E. H. Martin, L. g. Presa, and P. R. Rodriguez, 2001: Influence of the North Atlantic Oscillation on the Canary Islands Precipitation. *J. Climate*, **14**, 3889–3903.
- Horel, J. D., 1981: A Rotated Principal Component Analysis of the Interannual Variability of the Northern Hemisphere 500 mb Height Field. *Mon. Wea. Rev.*, **109**, 2080–2092.
- Hurrell, J.W., 1995: Decadal Trends in the North Atlantic Oscillation Regional Temperatures and Precipitation. *Science*, **269**, 676–679.
- , and H. vanLoon, 1997: Decadal Variations in Climate Associated with the North Atlantic Oscillation. *Clim. Change*, **36**, 69–94.
- Kalnay, E., M. Kanamitsu, R. Kistler, W. Collins, D. Deaven, L. Gandin, M. Iredell, S. Saha, G. White, J. Woollen, Y. Zhu, A. Leetmaa, B. Reynolds, M. Chelliah, W. Ebisuzaki, W. Higgins, J. Janowiak, K.C. Mo, C. Ropelewski, J. Wang, R. Jenne, D. Joseph, 1996: The NCEP/NCAR 40-Year Reanalysis Project. *Bull. Amer. Meteor. Soc.*, **77**, 437–472.
- Kistler, R., E. Kalnay, W. Collins, S. Saha, G. White, J. Woollen, M. Chelliah, W. Ebisuzaki, M. Kanamitsu, V. Kousky, H. van den Dool, R. Jenne, M. Fiorino, 2001: The NCEP–NCAR 50–Year Reanalysis: Monthly Means CD–ROM and Documentation. *Bull. Amer. Meteor. Soc.*, **82**, 247–268.
- Klein, W. H., 1952: Some Empirical Characteristics of Long Waves on Monthly Mean Charts. *Mon. Wea. Rev.*, **80**, 203–219.
- , B. M. Lewis, C. W. Crockett and I. Enger, 1960: Application of Numerical Prognostic Heights to Surface Temperature forecasts. *Tellus*, **12**, 378–392.
- , 1965: Application of Synoptic Climatology and Short-range Numerical Prediction to Five-day Forecasting. U.W. Weather Bureau. Res. Pap. No. 46, 79–84.
- Kocin, P. J., P. N. Schumacher, R. F. Morales, and L. W. Uccellini, 1995: Overview of the 12–14 March 1993 Superstorm. *Bull. Amer. Meteor. Soc.*, **76**, 165–182.
- Lamb, P. J., and R. A. Peppler, 1987: North Atlantic Oscillation: Concept and an Application, *Bull. Amer. Meteor. Soc.*, **68**, 1218–1225.

- Langland, R. H., M. A., Shapiro, and R. Gelaro, 2002: Initial Condition Sensitivity and Error Growth of Forecasts of the 25 January 2000 East Coast Snowstorm. *Mon. Wea. Rev.*, **130**, 957–974.
- Leathers, D. J., D. R. Kluck, and S. Kroczyński, 1998: The Severe flooding Event of January 1996 across North-Central Pennsylvania. *Bull. Amer. Meteor. Soc.*, **79**, 785–797.
- , B. Yarnal, and M. A. Palecki, 1991: The Pacific/North American Teleconnection Pattern and United States Climate, Part I: Regional Temperature and Precipitation Associations. *J. Climate*, **4**, 517–528.
- Loewe, F., 1937: A Period of Warm Winters in Western Greenland and the Temperature See-saw between Western Greenland and Europe. *Quart. J. Roy. Meteor. Soc.*, **63**, 365–371.
- , 1966: The Temperature See-saw between Greenland and Europe. *Weather*, **21**, 241–246.
- Lorenz, E. N., 1951: Seasonal and Irregular Variations of the Northern Hemisphere Sea-level Pressure Profile. *J. Meteor.*, **8**, 52–59.
- Martin, D. E., 1953: Anomalies in the Northern Hemisphere 5-day Mean Circulation Patterns. Air Weather Service Rep. No. 105–100, 39pp.
- Meehl, G. A., and H. van Loon, 1979: The Seesaw in Temperatures between Greenland and Northern Europe. Part III: Teleconnections with Lower Latitudes. *Mon. Wea. Rev.*, **107**, 1095–1106.
- Nakamura, H., M. Tanaka, and J. M. Wallace, 1987: Horizontal Structure and Energetics of Northern Hemisphere Wintertime Teleconnection Patterns. *J. Atmos. Sci.*, **44**, 3377–3391.
- , and J. M. Wallace, 1990: Observed Changes in Baroclinic Wave Activity During the Life Cycles of Low-Frequency Circulation Anomalies. *J. Atmos. Sci.*, **47**, 1100–1116.
- Namias, J., 1951: The Great Pacific Anticyclone of the winter 1948–50: A Case Study in the Evolution of Climatic Anomalies. *J. Meteor.*, **8**, 251–261.
- , 1978: Multiple Causes of the North America Abnormal Winter 1976–77. *Mon. Wea. Rev.*, **106**, 279–295.
- O’Conner, J. T., 1969: Hemispheric Teleconnections of Mean Circulation Anomalies at 700 mb. ESSA Tech. Rep. WB–10, \$\$ pp.

- Portis, D. H., J. E. Walsh, M. E. Hamly, and P. J. Lamb, 2001: Seasonality of the North Atlantic Oscillation. *J. Climate*, **14**, 2069–2078.
- Renwick, J. A., and J. M. Wallace, 1995: Predictable Anomaly Patterns and the Forecast Skill of Northern Hemisphere Wintertime 500-mb Height Fields. *Mon. Wea. Rev.*, **123**, 2114–2131.
- Rogers, J.C., and H. van Loon, 1979: The Seesaw in Temperatures between Greenland and Northern Europe. Part II: Some Oceanic and Atmospheric Effects in Middle and High Latitudes. *Mon. Wea. Rev.*, **107**, 509–519.
- , 1981: Spatial Variability of Seasonal Sea Level Pressure and 500 mb Height Anomalies. *Mon. Wea. Rev.*, **109**, 2093–2106.
- , 1984: The Association between the North Atlantic Oscillation and the Southern Oscillation in the Northern Hemisphere. *Mon. Wea. Rev.*, **112**, 1999–2015.
- , 1997: North Atlantic Storm Track Variability and Its Association to the North Atlantic Oscillation and Climate Variability of Northern Europe. *J. Climate*, **10**, 1635–1647.
- Ropelewski, C. F., J. E. Janowiak, and M. S. Halpert, 1985: The Analysis and Display of Real Time Surface Climate Data. *Mon. Wea. Rev.*, **113**, 1101–1106.
- Saabye, H.E., 1942: *Brudstykker af en Dagbog holden i Grönland i Aarene 1770–1778*, H. Ostermann, Ed. *Medd. Grönland*, **129**, No. 2, (see pp. 45 and 103).
- Scherhag, R., 1936: Eine bemerkenswerte Klimaänderung über Nordeuropa. *Ann. Hydrogr.*, **64**.
- Serreze, M. C., F. Carse, R. G. Barry, J. C. Rogers, 1997: Icelandic Low Cyclone Activity: Climatological Features, Linkages with the NAO, and Relationships with Recent Changes in the Northern Hemisphere Circulation. *J. Climate*, **10**, 453–464.
- Stephenson, D. B., T. Raddatz, U. Ulbrich, U. Reading, U. Koeln, 2001: Long-Range Persistence in the North Atlantic Oscillation. EGS XXVI General Assembly, Nice, France.
- Thompson, David W. J., and J. M. Wallace, 1998: The Arctic Oscillation Signature in the Wintertime Geopotential Height and Temperature Fields. *Geophys. Res. Lett.*, **25**, 1297–1300.
- , and J. M. Wallace, 2000: Annular Modes in Extratropical Circulation. Part I: Month-to-Month Variability. *J. Climate*, **13**, 1000–1017.

- , J. M. Wallace, and G. C. Hegerl, 2000: Annular Modes in Extratropical Circulation. Part II: Trans. *J. Climate*, **13**, 1018–1036.
- , and J. M. Wallace, 2001: Regional Climate Impacts of the Northern Hemisphere Annular Mode. *Science*, **293**, 85–89.
- Uccellini, L. W., P. J. Kocin, R. S. Schneider, P. M. Stokols, and R. A. Dorr, 1995: Forecasting the 12–14 March 1993 Superstorm. *Bull. Amer. Meteor. Soc.*, **76**, 183–199.
- van Loon, H., and J. C. Rogers, 1978: The Seesaw in Winter Temperatures between Greenland and Northern Europe. Part I: General Description. *Mon. Wea. Rev.*, **106**, 296–310.
- Walker, G. T., 1924: Correlations in Seasonal Variations of Weather, IX. *Mem. Ind. Met. Dept.*, **24**, 275–332.
- , and E. W. Bliss, 1932: World Weather V. *Mem. Roy. Meteor. Soc.*, **4**, 53–84.
- Wallace, J. M., and D. S. Gutzler, 1981: Teleconnections in the Geopotential Height Field during the Northern Hemisphere Winter. *Mon. Wea. Rev.*, **109**, 784–811.
- , Y. Zhang, and K. Lau, 1993: Structure and Seasonality of Interannual and Interdecadal Variability of the Geopotential Height and Temperature Fields in the Northern Hemisphere Troposphere. *J. Climate*, **6**, 2063–2082.
- , 2000: North Atlantic Oscillation/Annular Mode: Two Paradigms – One Phenomenon. *Quart. J. Roy. Meteor. Soc.*, **126**, 791–805.
- , D. W. J. Thompson, and Z. Fang, 2000: Comments on “Northern Hemisphere Teleconnection Patterns during Extreme Phases of the Zonal – Mean Circulation”. *J. Climate*, **13**, 1037–1039.
- Zhang, F., C. Snyder, and R. Rotunno, 2002: Mesoscale Predictability of the “Surprise” Snowstorm of 24–25 January 2000. *Mon. Wea. Rev.*, **130**, 1617–1632.